In situ Fabrication of Metal Nanoparticle-Embedded Polymer Films: Optical Limiting and Bactericidal Applications

A Thesis Submitted for the Degree of

DOCTOR OF PHILOSOPHY

by

Shatabdi Porel

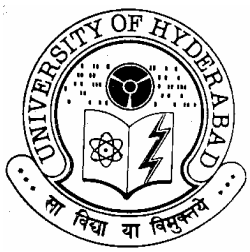

School of Chemistry
University of Hyderabad
Hyderabad 500 046
INDIA

July 2007

To

Grand-pa

(Late Dr. Abani Mohon Manji)

DECLARATION

I hereby declare that the matter embodied in this thesis is the result of investigations carried out by me in the School of Chemistry, University of Hyderabad, Hyderabad under the supervision of Prof. T. P. Radhakrishnan.

In keeping with the general practice of reporting scientific observations, due acknowledgements have been made wherever the work described is based on the findings of other investigators.

Shatabdi Porel

CERTIFICATE

This is to certify that the work described in this thesis entitled "***In situ* Fabrication of Metal Nanoparticle-Embedded Polymer Films: Optical Limiting and Bactericidal Applications**" has been carried out by Shatabdi Porel, under my supervision and the same has not been submitted elsewhere for any degree.

Prof. T. P. Radhakrishnan
(Thesis Supervisor)

DEAN
School of Chemistry
University of Hyderabad
Hyderabad 500 046

ACKNOWLEDGEMENTS

It is an immense pleasure to express my profound respect and a deep sense of gratitude to Prof. T. P. Radhakrishnan, supervisor and well wisher in my doctoral research work. It is needless to mention that without his constant guidance, encouragement and support, it would hardly be possible to come out with this thesis. His innovative thoughts supported by his commitments and dedication towards the research are highly admirable and motivating. His discipline and honesty for the research has paved a new path in my career. I am also indebted to him for the work-freedom he has given me during the last five years. His patience on listening me and his simplest but effective explanation to any research ideas, concepts and thoughts are greatly appreciable. I am also thankful to him for his warm and best possible support and guidance to solve my personal problems, whenever necessary.

I would like to thank the present and former Deans, School of Chemistry, University of Hyderabad, for their kind cooperation and providing necessary infrastructural facilities in the department. I thank all the faculty members of the school for their cooperation whenever required. The encouragement and support provided by the Non-teaching staff in the school is highly appreciable.

Financial assistance from UGC and CSIR, New Delhi for providing Research Fellowship as well as various instrumental facilities, are greatly acknowledged.

I am indebted to appreciate the academic support and encouragement provided by Prof. D. Narayana Rao (School of Physics, University of Hyderabad) and Prof. Aparna Duttagupta (School of Life Science, University of Hyderabad) throughout my doctoral research. Their contributions are truly significant to complete my research in interdisciplinary field. I am also thankful to them for their all time permission to use the necessary experimental facilities in their laboratory.

I would also like to express my sincere gratitude to Dr. Manjunath and Mr. Murthy for SEM (UOH), Dr. Ravi Chandra and Mr. Venkatesh (ARCI) for FESEM, and Dr. Singh (CCMB), Dr. Sreedhar and Dr. Hebalkar (IICT) for providing the TEM images, which constitute a major part of this thesis.

I am deeply indebted to all my teachers starting from my school to the university for their wonderful teaching and education throughout my academics. My special thanks to all my Professors in the Department of Chemistry, University of Burdwan, West Bengal, for their contribution in crossing the hurdle to enter into doctoral research.

It is indeed a pleasure to thank my seniors Dr. Prasad, Dr. Palash, Dr. Sonika, Dr. Subbalakshmi, Dr. Philip and Dr. Sharath for their cooperation whenever required. Thanks to Prakash, Abhijit, Rajesh, Ramesh and all M.Sc project students for their moral support and in maintaining a lively environment in the lab. I am thankful to Dr. Manoj, Dr. Prem, Dr. Srinivas, Dr. Shivakiran, Joseph, Chaitanya, Harsha, Venkatram, Santosh, Monoj and other friends from the laser lab for their help and cheerful support smile. I am also grateful to Monohar, Damodar, Chaitanya, Jacob and Ramakrishna from Prof. Duttagupta lab for their cooperation, support and the time they have spend with me for valuable discussions.

My special thanks to Abhik, Sunirban, Moloy, Saikat, Manab, Archan, Subhas who have passed their Academic, Moral and Personal support in my all state of emergencies forgetting their busy work schedule. I am also thankful to others from Bengali Samity in HCU, especially Dinubhai, Bks, Sandy, Rahulda, Prashant, Aniruddha, Bhaswati, Arindam, Anindita, Rumpa, Baru, Bipul, Utpal, Suparna, Naba, Ghata, Poti, Tapto and Ghona.

My parents – my beloved ‘Maa o Bapi’, without whom, I would not have reached to this stage of my life. They have always proved to be a great source of encouragement throughout my life. Especially my mother, who has sacrificed a lot to build up my career and to provide me this platform. My special thanks to my Uncle, Barid-kaku for his constant support and to my mother-in-law and others for giving me a peaceful environment to complete my research work.

As far as entering into the doctoral research is concerned, a great source of my inspiration is my grandfather. His moral support and encouragement had led me to mould myself as a researcher. I am very much proud to dedicate my thesis in his honor.

Last but not the least, my adorable Husband, without his support and patience, I wouldn’t be able to complete a single phase of my research. His affection plays a vital role for the successful completion of my research.

Shatabdi Porel

COMMON ABBREVIATIONS

AFM	atomic force microscopy
CFU	colony forming unit
DMSO	dimethyl sulfoxide
ED	electron diffraction
EDXS	energy dispersive X-ray spectroscopy
FESEM	field emission scanning electron microscopy
fs	femtosecond
GW	gigawatt
kDa	kilo Dalton
LB	Luria-Bertani
μm	micrometer
M_w	average molecular weight
NLO	nonlinear optical
ns	nanosecond
PVA	poly(vinyl alcohol)
PS	polystyrene
RPM	revolutions per minute
RSA	reverse saturable absorption
SA	saturable absorption
SEM	scanning electron microscopy
SPR	surface plasmon resonance
STM	scanning tunneling microscopy
t	time
T	temperature
TEM	transmission electron microscopy
TW	terawatt
XPS	X-ray photoelectron spectroscopy

CONTENTS

Scope

Advances in nanoscience and nanotechnology are closely linked to the development of new methods for the synthesis and assembly of nanostructures. Development of environment-friendly procedures and control of particle size, shape and organization are important contemporary issues. The 'bottom-up' approaches to metal nanoparticle synthesis are mostly based on the colloidal route. However, assembly of nanoparticles in matrices such as polymer films is of major interest in several optical, nonlinear optical and sensor applications, especially those requiring large area coverage and flexible design. Nanoparticle-polymer composite films afford superior versatility in their design and fabrication, and hence are emerging as important candidates to meet several challenging demands of modern technology. This thesis envisages the development of a simple and environment-friendly approach to the in situ synthesis of metal nanoparticles inside polymer films, enabling the variation of particle size, shape and size/shape distribution by control of the composition of the films and parameters related to the thermal treatment. Such a procedure would also be significant in the context of the current debates on potential health hazards of free and inhalable nanoparticles. The potential utility of these metal nanoparticle-polymer composites fabricated in the form of supported or free-standing thin films, in optical limiting and antibacterial applications are explored.

In this chapter we present an appraisal of the uniqueness of nanomaterials (Sec. 1.1), followed by a brief sketch of the historical perspective (Sec. 1.2). An overview of nanoscopy is presented in Sec. 1.3, since the revolutionary developments in the field of microscopy has been critical for the emergence of nanoscience and nanotechnology as we know it today. Some general classifications of nanomaterials are listed in Sec. 1.4, and the experimental methods for their synthesis are discussed in Sec. 1.5. This is followed by a brief discussion of the range of properties that show dramatic variation from the bulk state (Sec. 1.6) and applications of the unique properties and functions of nanostructures (Sec. 1.7). Sec. 1.8 and 1.9 present an overview of two topics of special interest in this thesis, namely optical limiting and antibacterial applications. The layout of the thesis is outlined in Sec. 1.10.

1.1. Uniqueness of Nanomaterials

Materials play a vital role in our daily lives and activities, and influence considerably the evolution of our culture and civilization. Materials can be classified based on their function (structural/engineering, electronic, magnetic, optical/nonlinear

optical) as well as their composition (metals/alloys, semiconductors, ceramics, glasses, polymers and molecular materials). The properties of materials and hence their applications are largely defined by the chemical composition and atomic/molecular organization. Traditionally, particle size of materials is of relevance only in some very specific or technical contexts such as characterization using X-ray diffraction (where the diffraction lines broaden for small particles), solubility (the dissolution becoming easier for smaller particles), sintering and processing (rate increasing with decreasing size).

The current interest in materials in the nano size domain arises due to novel physical phenomena and attributes they exhibit and unique applications they can be deployed in. The extensive range of methodologies through which they can be fabricated, has also considerably enhanced the excitement about nanomaterials. At the nanometric size, novel physics can appear due to the confinement of electrons or excitons; surface effects related to plasmons, adsorption and chemical reactivity become pronounced. Mechanical properties of materials and role of defects can be considerably modified in nanoparticulate matter. Unusual effects can crop up at times, such as polymorphic structures which are metastable in the bulk materials becoming stabilized in the nanometric range. Even though there is considerable discussions and debate about where the nano-domain begins, it is judicious to avoid explicit use of dimension; a good example of this approach may be found in the report from the Royal Society on nanoscience and technology.[1] In a broad sense, nanoscience can be defined as the study of phenomena and manipulation of materials at atomic, molecular and supramolecular level, where properties differ significantly from those at a larger scale.[2]

Nanomaterials cover the diverse range of materials we have referred above, in terms of their functions and compositions. Another unique aspect is the range and breadth of areas which contribute to the growth of nanomaterials and are influenced by nanoscience and nanotechnology. Chemistry plays a crucial role in the synthesis of nanomaterials and assembly of nanostructures through the so called ‘soft methods’ and novel properties at nanoscale can alter significantly chemical reactivity and enhanced catalytic process. Physics at the nanoscale is a subject in its own right and a whole host of devices are emerging based on such physics. Growth in the field of nanobiology is opening up new vistas in the understanding of sub-cellular structures and areas such as targeted drug delivery systems and biosensors. The concept of miniaturizations is at the

heart of emerging technologies. Nanomaterials are beginning to play a major role in industries such as textiles, paints/coating and catalysis. They are also being increasingly used in agriculture, for example in soil remediation using magnetic nanoparticles and water remediation using carbon nanotubes, and in tackling environmental problems. Development of better diagnosis and therapy systems (for example gold nanoparticles for the cancers/tumors) and possible futuristic applications of nanorobots are promising avenues in nanomedicine.

Over a last few years, the potential impact of introducing nanotechnologies and nanomaterials into the market has received considerable attention. Critical questions have been raised about ethical and legal implications such as those related to patenting. For the case of patenting under the US law, an invention may not be patentable where the sole element of novelty is a difference in size.[3] On the other hand, the Royal Society has recommended in the year 2004 that the chemical in the form of nanoparticles/nanotubes should be treated as new substance and assigned a new Chemical Abstract Service (CAS) Registry number.[1] The enormous capital input for research and development and increasing investments in the industry has fuelled serious debates about the long-term impact of nanotechnology. One of the major concerns raised is the potential health and environment risks associated with it. An interesting case concluded recently is the world-wide competition and the new warning symbol proposed for potential hazards due to nanomaterials.[4] Despite the tremendous societal benefits offered by nanotechnology, fingers have been pointed at possible negative impacts on the health of workers, consumers and above all the environment. Currently there is little information available concerning the risks and several investigations are aimed at unraveling the toxicological aspects of nanomaterials.

The different aspects discussed above clearly show that nanomaterials form a unique subject for fundamental investigations and novel applications.

1.2. Historical Perspective

The discussions in the previous section indicate that nanostructures, nanomaterials and phenomenona at the nanoscale are likely to provide critical solutions to a wide range of technological problems in the current century. However,

nanomaterials have been in use for quite some time. A striking example from the ancient past is the Lycurgus cup, believed to be from the 4th century A.D. The chalice has a dark greenish tint under reflected lighting, but appears red when illuminated from behind; this is attributed to the optical responses of gold nanoparticles dispersed throughout the glass. Similar phenomena are also featured in the stained glass windows in the 10th century's cathedrals which utilized mostly, nanoparticles of coinage metals such as copper, silver and gold. These were indeed, not systematic scientific experiments with the metals fabricated in the nanometer size regime. It is generally agreed that Michael Faraday conducted the first careful experimentation on 'activated gold', in the year 1857. He synthesized gold colloid by the reduction of gold chloride using phosphorous in CS_2.[5]

In 1905, Albert Einstein provided a quantitative theory for the colloidal state, using the picture of 'big atoms' subjected to Brownian motion. Significant contributions of Mie,[6] Debye[7] and several others provided the foundation for understanding the physical behavior of nanoparticles. Preparation of monolayers of molecules at air-water interface by Langmuir in 1932 and their transfer to suitable substrates by Blodgett in 1938, were further landmark events in the slow progress of materials at the nanoscale. The exciting possibilities in the field of nanoscience and technology were described most eloquently by the visionary exposition by Richard Feynmann at the annual meeting of the American Physical Society at Caltech in 1959, through his famous lecture, 'There's plenty of room at the bottom'. Revolutionary developments witnessed in the field of microscopy during the last quarter of the last century were the critical factors that triggered the avalanche of activities occurring in this field currently.

1.3. Advent of Nanoscopy

As noted above, several decades have passed since metal colloids were first synthesized through systematic procedures. A range of techniques have been employed to characterize nanomaterials. They include powder X-ray diffraction, small angle X-ray scattering, dynamic light scattering, Brunauer-Emmett-Teller gas absorption surface area measurement and pore structure analysis (BET methods), X-ray photoelectron and a range of other spectroscopies. However, lack of appropriate sophisticated analytical

techniques for the detailed characterization and visualization of nanomaterials and nanostructures have hampered in-depth understanding of nanoscience and effective utilization of nanotechnology.

Development of electron microscopy in the 1930's made it possible to go beyond the limitations of optical microscopy and image features with dimensions well below micrometers. However it is the advent of scanning tunneling microscopy (STM) and atomic force microscopy (AFM) in the 1980's that really opened up for the first time, the possibility of visualizing materials at the atomic scale. High resolution electron microscopy is also now added to this repertoire for imaging at the atomic level. It is now possible to not only 'see' atoms, but also to manipulate them in desired fashions. Since the development of nanoscience and nanotechnology are intimately connected to the advent of modern nanoscopy, we provide a brief overview of the salient aspects of the electron and scanning probe microscopies.

1.3.1. *Electron Microscopy*

The first practical transmission election microscope (TEM) was built by Albert Prebus and James Hillier in 1938 using concepts developed by Max Knoll and Ernst Ruska in 1931. TEM was developed because of the limited image resolution of light microscopes, imposed by the wavelength of visible light. Use of electron beams with considerably smaller wavelengths should provide much higher resolution. The wavelength of the electron beam can be tuned by controlling the accelerating voltage. A high-voltage electron beam is partially transmitted through a very thin sample (~ 100 nm); the areas which do not allow the beam to pass lead to an image which is magnified using appropriate magnetic lenses and recorded by a fluorescent screen or charge-coupled device (CCD) based camera. Modern high voltage instruments, high resolution TEM (HRTEM) provide Angstrom resolution enabling efficient and accurate imaging of nanostructures. The electron beam can also be used to record diffraction from selected areas of the samples allowing fingerprinting of the periodic atomic lattice structures. This is referred to as selected area electron diffraction (SAED).

The first, true scanning electron microscope (SEM) was developed by Zworykin *et al* in 1942 and the first commercial SEM, Cambridge Scientific Instruments Mark I,

was available in 1965. In a scanning electron microscope, a finely focused electron beam sweeps across the surface of the specimen giving a wide range of signals including secondary or backscattered electrons. These signals vary according to differences in the surface topography and composition, allowing imaging of structures down to nanometer sizes. Important features of SEM are its capability to examine objects at low as well as high magnification; extraction of 3-dimensional information of the specimen images, and the feasibility of studying nonconducting samples by applying a thin coating of conducting film. Energy dispersive X-ray scattering (EDXS) allows the mapping of elemental composition with high spatial resolution.

1.3.2. *Scanning Probe Microscopy*

The scanning tunneling microscope (STM) was discovered by Gerd Binnig and Heinrich Rohrer in 1981. In STM, a weak current tunneling between a fine probe tip and a conducting surface is monitored; the tip is mechanically connected to the scanner, an XYZ positioning device using piezoelectric materials. The sample is positively or negatively biased so that a small current, the 'tunneling current' flows if the tip is sufficiently close to the sample surface. This feeble tunneling current is amplified and measured. With the help of the tunneling current the feedback electronics keeps the distance between tip and sample constant. If the tunneling current exceeds its preset value, the distance between tip and sample is increased, if it falls below this value, the feedback decreases the distance. The tip is scanned line by line above the sample surface following the topography of the sample; it is possible to image surface features down to atomic resolution.

The restriction in the case of STM imaging to samples with conducting surface is circumvented in the design of the atomic force microscope (AFM) by Gerd Binnig, Calvin Quate and Christoph Gerber in 1986. When the sample is moved using a piezo scanner, a fine probe tip resting in close proximity of the sample surface monitors the weak forces of interaction with the features on the surface. The resulting tiny deflections of the tip are detected using an optical system consisting of a laser beam, reflecting mirror in the back of the probe tip and a position sensitive detector. AFM allows the 3-dimensional imaging of surface features with nanometer resolution. Developments in AFM technology allow imaging in contact and dynamic force or

tapping (non contact) modes and exploitation of a wide range of forces including electrostatic, magnetic, friction and viscoelastic.[8]

1.4. Classifications of Nanomaterials

In view of the wide range of nanostructures and nanomaterials that are known today, it is very difficult to make a general and unique classification scheme. Several terminologies are commonly used to describe nanostructured materials; some of the terms encountered often are: cluster, colloid, nanoparticle, nanocrystal, quantum dot.[9] Although these terms are not very precisely defined, some general meanings are as follows. Cluster usually means a collection of units (atoms/molecules) surrounded by a ligand shell which makes it stable, isolable and soluble in an appropriate medium. Colloid is a stable liquid suspension having particles with size typically < 1 μm. Nanoparticles are solid particles with sizes upto a few hundred nanometers; they could be polycrystalline or single crystalline. If the nanoparticle is single crystal in nature, then it is termed a nanocrystal and if it exhibits confinement effect due to size in three dimensions, it is called a quantum dot.

A crystal consists of a periodic arrangement of specific repeating units (atoms, ions or molecules). The individual repeat units have quantized electronic structure, while the crystal has continuous band structure resulting from overlap and combination of the wave functions of the repeating units. When the crystal size decreases to the nanometer regime (~ 1 - 100 nm), the electronic band starts getting quantized and assumes a character intermediate between that of the crystals and its building units. The nanocrystals thus exhibit novel properties which differ from that of both the bulk and the atomic/molecular units; strong dependence on the size, shape and mode of assembly also emerges. Precise control over size and shape can lead to control over their physical properties and chemical reactivities. Because of their unique electronic structure, nanocrystals can be used as novel building blocks for the assembly and patterning of future nanodevices.

Based on the growth habit and morphology, nanostructure can be classified as 2, 1 and 0-dimensional.[10] Plates and discs with polygonal shape are 2-dimensional structures; rods, cylinders and wires are examples of 1-dimensional structures (e.g.

nanorods and nanowires of metals and semiconductors, carbon nanotubes); isotropic spheres, icosahedrons and cubes can be classified as 0-dimensional (e.g. spherical particles of metals and semiconductors, C_{60}) (Fig. 1.1). Several novel nanostructure have been reported which fall outside the ambit of these general classifications. Some of these interesting structures include L-shaped or V-shaped bipods, T-shaped tripods and multipods appearing as kinetically controlled intermediate states in the assembly of the regular building blocks.[11]

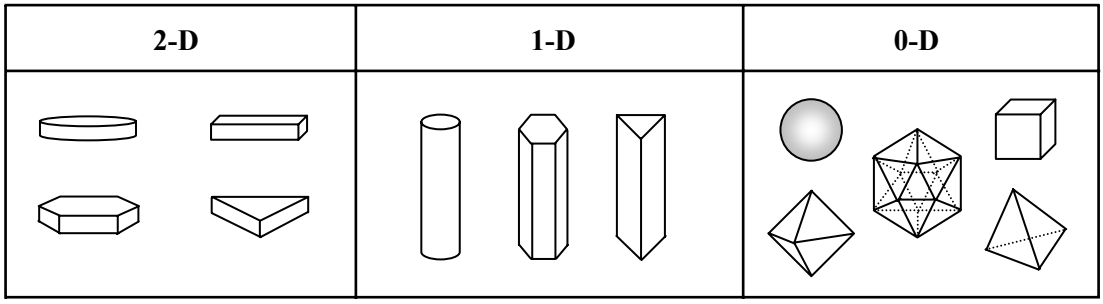

Figure 1.1. *Classification of nanostructures based on growth habit and morphology (Figure adapted from Ref. 10).*

Assemblies of nanocrystals or superlattice structures build up using basic nano building blocks can also be achieved by chemical interparticle interactions or binding mediated by linker groups. Slow evaporation of a solution of highly monodisperse nanocrystals leads to highly ordered 3-dimensional closed packed structure built through van der Waals interaction. The symmetry of the superlattice structures is closely dependent on the size, shape and interparticle interaction. For example, assembly of spherical nanoparticles with shorter or longer interparticle distances (imposed by the chain length of the capping agent) leads to cubic or hexagonal packed superlattices respectively.[12]

1.5. Nanomaterials: Synthesis

The various approaches to the synthesis of nanomaterials can be broadly grouped into "top-down/break-down" and "bottom-up/build up" methods. In the top-down approach, large objects are broken down to give smaller features down to the

nanolevel, for example by mechanical techniques (e.g. machining, grinding, polishing), laser-beam processing and lithographic techniques. In the bottom-up approach, atomic or molecular building blocks are assembled into nanostructures; examples include colloid formation, induced-assembly and self-assembly. Top-down techniques have been developed for production of nanomaterials at the industrial scale but optimization of the process to produce well-defined nanostructures remain difficult; the size limits that can be reached in these techniques are still larger than those obtained through bottom-up approaches. Bottom-up techniques on the other hand can provide extremely small structures with superior control over size, shape,[13] and even organization.[14] Current efforts are likely to lead ultimately to a solution of the problem of large scale production capability.[15]

We discuss below, some of the bottom-up synthesis approaches to three important classes of nanomaterials based on metals, semiconductors and ceramics. Special emphasis is placed on metal nanoparticles as they are of particular interest to the work presented in this thesis.

1.5.1. *Metals*

The different procedures are based on two general approaches to the conversion of precursor to metal atoms followed by the controlled aggregation of the atoms (Fig. 1.2). The first one employs different sources of external energy whereas the other methods use specific reducing agents.

The first group of method include the use of irradiation (UV, near-IR), sonochemistry, radiolysis, thermolysis, laser ablation and nucleation from vapor. UV or near IR irradiation causes the photochemical reduction of the precursor where the reaction rate can be controlled by light intensity.[16] UV irradiation in presence of micelles or seeds facilitates synthesis along with control of size and shape.[17] Presence of an ultrasonic field can provide control on the rate of precursor reduction and control over nanoparticle size. It can also be used for the synthesis of nanoparticles within the pores of silica and for the synthesis of bimetallic nanoparticles.[18] Radiolysis has been used to synthesize metallic/bimetallic nanoparticles and control their size and size distribution.[19] Thermolysis of organometallic complexes, mostly metal carbonyl

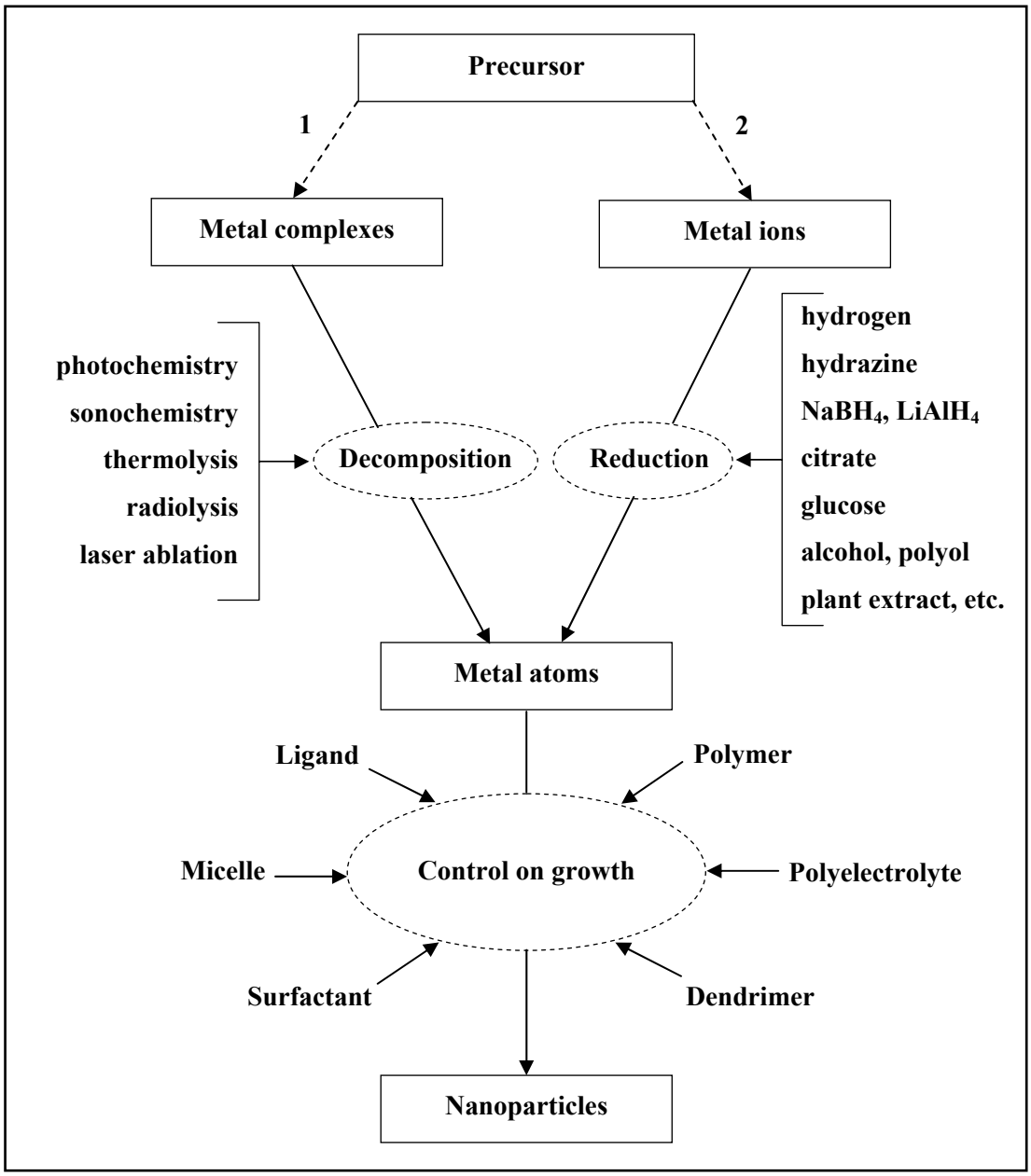

Figure 1.2. *Schematic diagram illustrating some of the bottom-up protocols for the synthesis of metal nanoparticles.*

complexes can produce uniform-sized metal nanocrystals.[20] Thermolysis of crude preparations of Brust's gold nanoparticles led to an increase of the particle sizes and this size evolution was discussed on the basis of a thermodynamic model.[21] Laser ablation

is another technique of nanoparticles synthesis that has been used under various conditions whereby size control can be induced by laser irradiation.[22] Sputtering of nanoparticles give flexibility to the synthesis of uniformly distributed metal clusters and permits the fabrication of composite films of various metals and dielectric materials.[23]

In the second set of approach to metal nanoparticles synthesis, metal salts are usually reduced in the presence of a suitable protecting agent. Reducing agents such as molecular hydrogen, hydrazine, $NaBH_4$, $LiAlH_4$, citrate, ascorbic acid, glucose, alcohols or some naturally occurring materials such as protein/enzyme and plant extract is added to a solution of the metal salt.[24] An easily oxidized solvent may function both as the electron donor and the dispersing medium. Alcohols and ethers have been used extensively for this purpose.[25] Nanoparticles tend to agglomerate in order to reduce the surface free energy, and therefore, it is necessary to protect them using ligands, surfactants or dendrimers. Phosphine, phosphine oxide, thiols, amines, carboxylates, cyclodextrin, citrate, quaternary ammonium salts, PAMAM dendrimers etc have been used for this purpose. Reaction media such as supercritical fluid or ionic liquid are used to facilitate efficient isolation of nanoparticles. Ionic liquids with suitable functional groups can also act as reducing and/or stabilizing agents, allowing the reactions to occur at room temperature.[26] The well-known Brust biphasic method of synthesis uses thiol ligands that strongly bind gold due to the soft character of Au and S.[27] In an alternate strategy, the metal salt is reduced in microemulsion, copolymer micelles or reversed micelles.[28] In this technique, the micelles function as nanoreactors, where the size of the particles can be controlled by the concentrations employed and the micelle size. Although the size of nanoparticles cannot be controlled very preciously in such synthesis, it is possible to narrow the size distribution by controlling the reaction conditions. Functionalized polymers and polyelectrolytes[29] have also been used extensively in the synthesis of nanoparticles. The most commonly used polymers for the stabilization of nanoparticles include poly(*N*-vinyl-2-pyrrolidone) (PVP) and poly(ethylene glycol) (PEG).[30] Poly(vinyl alcohol) (PVA) is also used in some cases.[31] Assembly of nanoparticles inside polymer matrices is also of considerable interest. Although there are several ways to fabricate nanoparticle-polymer composites,[32] the following approaches are quite common. *In situ* synthesis of the nanoparticles in the polymer matrix is achieved by reduction of the metal salts dissolved with the polymer in solution or in a film.[33] Films can also be cast using a mixture of preformed

nanoparticles and the polymer.[34] In plasma deposition technique, metals are evaporated on to heated polymer surface and impregnated in the film, or metals and polymers are evaporated and collected on a substrate.[35] Polymerization around the nanoparticles has also been used to produce metal-polymer nanocomposite.[36] The sol-gel method regularly used for metal-oxide nanoparticles synthesis can also be used to synthesize metal nanoparticles inside a solid medium. Modified sol-gel monomers are used to stabilize the metal salts before the reduction step and to cap and prevent coagulation of the metal sol after reduction, through gel formation, drying, and aging.[37] Synthesis inside solid matrices is especially significant from the point of view of potential health hazards of inhalable nanoparticles.[38]

1.5.2. *Semiconductors*

Decomposition of molecular precursors in presence of coordinating solvent (e.g. tri-n-octylphosphine oxide, TOPO) at relatively high temperatures[39] and RF magnetron sputtering in a glass matrix[40] are a couple of common approaches used to synthesize semiconductor nanocrystals. A popular method for the synthesis of nanocrystals of materials such as CdS, CdTe and Ag_2S makes use of mixed reverse micelles.[41] Micellar solutions containing the metal ion (Cd^{2+}, Ag^{+}) and S^{2-} or Te^{2-} are mixed together and the formation of the semiconductor phase occurs inside the nanoreactors. The nanocrystals can be extracted or isolated from the micelles as powders and re-dispersed in appropriate solvents for further processing. Metal-sulphide nanocrystals can also be formed inside confined spaces, using H_2S gas as the source of sulfur and the metal ions confined in a variety of host matrices; which may be soft (microemulsions, liquid crystals, polymer solutions), semi-rigid (gels, Langmuir-Blodgett monolayer films, polymer thin films) or hard (zeolites, mesoporous materials, layered solids).[42] Sol-gel process is also commonly used for the synthesis of semiconductor nanocrystals.[43]

1.5.3. *Ceramics*

Ceramics based on oxides such as MgO, CaO, Al_2O_3, SiO_2, ZnO, TiO_2, NiO, Fe_2O_3 and Cr_2O_3 can be synthesized as nanosized particles by a variety of methods. Mechanochemical methods,[44] aerosol methods including gas condensation techniques,[45]

spray pyrolysis,[46] and thermochemical or flame decomposition of metal-organic precursors[47] are some of the most commonly used procedures. Reverse micelles[48] and sol-gel[49] are also frequently employed for the synthesis of metal oxide nanoparticles. Synthesis using micelles follows the methodology discussed in the case of metal nanoparticles. Sol-gel process is typically used to prepare metal oxides via hydrolysis of metal alkoxides in an alcoholic medium to the corresponding hydroxide. Removal of water via condensation followed by gelation leads to a dense porous gel, a polymeric structure having interconnected 3-dimensional framework. Removal of solvent from the gel and further heat treatment causes the formation of metal oxide nanoparticles. Precipitation from solutions is another simple and common procedure to prepare oxide nanoparticles.[50] It involves the precipitation of the relevant metal hydroxide from an aqueous solution of the precursor salt by addition of a suitable base (NaOH or NH_4OH), followed by filtration, washing and calcinations to form the metal oxide nanopowder. Metal oxide nanoparticles are also obtained by electric arc discharge in an oxygen atmosphere.[51]

1.6. Nanomaterials: Properties

Properties of materials are generally governed by the chemical composition and atomic/molecular/ionic structure and organization. In the nanoscopic world however, the physical and chemical properties are strongly dependent on the size, shape and interparticle separation and assembly of the nanoparticles; for example color and solubility as well as thermal, chemical (catalytic), mechanical, magnetic, electrical, nonlinear optical and antibacterial properties, are significantly different compared to their bulk counterparts. Properties and applications of materials are intimately related to each other. However, for convenience of presentation, we outline first, the conceptual aspects of the properties of nanomaterials in this section and then discuss the application possibilities in the following section (Sec. 1.7).

Many of the special properties of nanomaterials are related to the very high surface area/volume ratio arising as a result of the ultrasmall sizes. For bulk materials, the surface atoms are a negligible part of the total number of atoms. The smaller the particle, higher the proportion of surface atoms. This would be clear from an estimation

of the surface area/volume ratio for spherical particle. If the radius is r, surface area/volume = $4\pi r^2/[4\pi r^3/3] = 3/r$. This means that the surface area/volume ratio is inversely proportional to the radius for spherical particles. The ratio increases by a factor of 10^7 when a 1 cm radius particle is broken down into 1 nm radius particles. The impact of this effect can be understood from the fact that 1g gold nanoparticles having 1 nm radius would have a surface area of ~ 155 m^2 **!**

1.6.1. *Color*

Bulk metals are usually opaque and the smooth surfaces of some metals have a shiny luster due to the reflection of light. If the metal particles reach nanodimensions, they can develop genuine color. For example, bulk silver is shiny white ('silvery'), while silver nanoparticles with sizes in the range of 5 - 10 nm are yellow in color. Gold nanoparticles can exhibit a range of colors due to absorption in the range, 500 nm to near IR depending on the particle size/shape.[52] Even more dramatic variation of color is observed in the emission from semiconductor nanoparticles. For example Si and CdSe can be prepared in nanoparticulate forms emitting colors in the wide spectrum of visible range.[53, 54, 55] The origin of the phenomenon of light absorption by the metallic nanoparticles was explained by Mie[6] in terms of the coherent oscillation of the conduction band electrons induced by the interacting electromagnetic field; this is commonly known as Mie theory. According to Mie theory,[56, 57] for very small spherical particles of radius, R (where R<< λ, wavelength of light), the extinction cross-section can be expressed as

$$C_{ext} = \frac{24\pi^2 R^3 \varepsilon_m^{3/2}(\lambda)}{\lambda} \frac{\varepsilon''(\lambda)}{[\varepsilon'(\lambda) + 2\varepsilon_m(\lambda)]^2 + \varepsilon''^2(\lambda)} \quad \ldots (1.1)$$

where, $\varepsilon = \varepsilon'(\lambda) + i\varepsilon''(\lambda)$ is the wavelength dependent, complex dielectric function of the nanoparticle material and ε_m is the dielectric constant of the surrounding medium. Eq. 1.1 shows that at the wavelength for which $\varepsilon' = -2\varepsilon_m$, C_{ext} will be maximum. In this condition, the electromagnetic field of the radiation induces a resonant coherent dipolar oscillation of free electrons across the nanoparticle. This oscillation is known as surface plasmon resonance (SPR) (Fig. 1.3). For silver, copper and gold this resonance occurs at the visible frequencies. The SPR of metal electrons results in a strong enhancement of absorption and scattering of electromagnetic radiation. The wavelength, intensity and

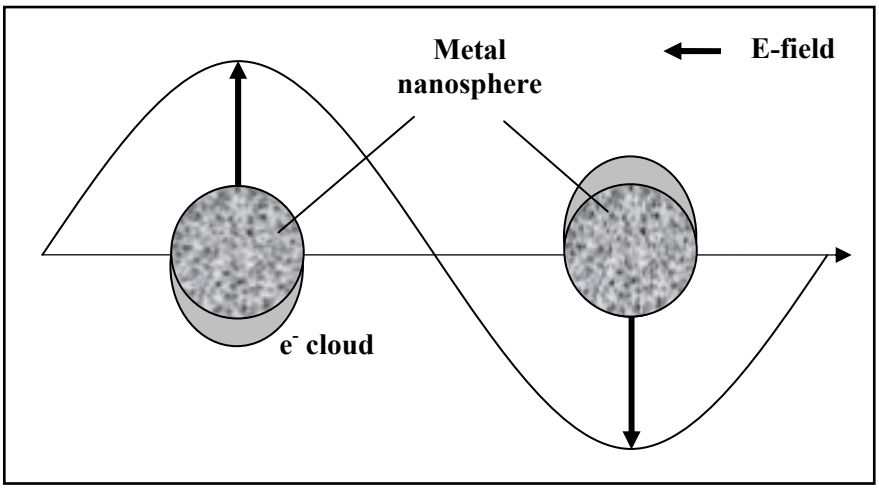

Figure 1.3. *Schematic representation of interaction of the electromagnetic field of light with metal nanospheres (Figure adapted from Ref. 57).*

the width of SPR spectra depends on the metal composition, size and shapes of nanoparticles, dielectric properties of the surrounding medium and interparticle interactions.[58]

Variation of the wavelength of light absorption and emission[54] with size of the semiconductor nanocrystals arises as a result of quantum confinement[59] of the conduction electron. This is particularly significant when typical exciton delocalization lengths are larger than the diameter of the nanocrystals. The particle-in-a-box picture shows that the quantized energy level and therefore the energy gaps between them would scale inversely with the square of the box size. This explains the red shift of the absorption/emission with increasing particle size.

1.6.2. *Solubility*

Bulk metals and semiconductors are generally insoluble in common organic solvents and water. However, in the nanoparticulate form they are soluble in several solvents including water. For example, gold nanoparticles capped with stabilizers are soluble in water and organic solvents such as alcohols, acetone, acetonitrile.[60] The increased solubility of nanomaterials is related to the enhanced interaction of the surface atoms with the solvent molecules, modulated by the capping agents present.

1.6.3. *Chemical (Catalytic)*

The large surface area/volume ratios and the unique binding sites of nanoparticles make them better heterogeneous catalysts. The adsorption characteristics and thermodynamics are also considerably modified in the nanomaterials. More importantly, deliberate tailoring of nanoparticle size, shape and surface composition or structure enables tuning of the catalytic properties.[61] For example, single component semiconductor nanoparticles exhibit relatively poor photocatalytic efficiency since the majority of the photogenerated charge carriers undergo recombination.[62] Semiconductor-metal composite nanoparticles on the other hand, facilitate charge rectification (i.e., directing the flow of electrons and holes) and improve the photocatalytic efficiency. Deposition of a noble metal on semiconductor nanoparticles has been shown to maximize the efficiency of photocatalytic reactions.[63]

1.6.4. *Mechanical*

Metal nanocrystals often exhibit high strength as compared to the bulk. For example, nanocrystalline copper with a narrow grain size distribution (~ 2 - 3 nm), exhibits tensile yield strength approximately an order of magnitude higher than that of conventional μm-grained copper.[64]

In several applications, ceramics are preferred over metals because of their superior chemical resistance, hardness and wear resistance; higher melting temperature, low density and reduced cost. However, the use of ceramics is often hampered by their brittleness, especially at low temperatures. The limitation can be overcome by reducing the grain sizes. The traditional brittle ceramic materials (e.g. Al_2O_3, TiO_2, ZrO_2, ZnO etc.) can be made ductile in nature by making them nanocrystalline.[65] The ceramic nanocrystals can be deformed superplastically at modest temperatures and then heat-treated at higher temperatures for strengthening. Superplasticity and ductility refer to the capability of polycrystalline materials to undergo extensive tensile deformation without necking or fracture. The great interest of this property stems from the fact that brittle fracture is a technical barrier in the use of ceramics in load-bearing applications.

1.6.5. *Magnetic*

In the case of ferromagnet or ferrimagnet, the magnetic moment can be enhanced by reducing the size. If the cluster size is smaller than the critical sizes for magnetic domains, then the magnetic anisotropy energy is much smaller than the thermal energy. This makes the cluster behave like paramagnetic species. In the absence of external magnetic field, the net magnetization in any direction would then be zero. As the magnetic field is applied, the cluster develops a magnetic moment and responds to the applied field independently; the moments can be quite large, of the order of thousands of Bohr magnetons. The applied field would tend to align the giant magnetic moments but thermal energy would always try to randomize them. If the thermal energy is lower than the magnetic anisotropy energy, then the cluster can show spontaneous magnetization. This phenomenon of enhanced magnetization called superparamagnetism, is observed in several nanomaterials.[66]

1.6.6. *Electrical*

In bulk metals the collective motion of electrons (current, I) and the applied voltage (V), which induces it are related linearly and described by Ohm's law, V = RI, where R is the resistance of the material. The electrical transport properties become size-dependent in the nanoscopic size regime. The $I - V$ characteristics of quantum dots are not linear. In order to tunnel an electron onto a nanoparticle, it is necessary to overcome a charging energy $E_C = e^2/2C$, where C is the capacitance of the particle; this phenomenon is called the Coulomb blockade. In such a situation, the $I - V$ graph shows a staircase structure, indicating that the injection of an additional electric charge into a nanocrystal that is already charged by an electron is prevented by the Coulombic repulsion between the two electrons.[67]

1.6.7. *Nonlinear Optical*

Nanoparticles exhibit characteristic size and shape-dependent electronic structure leading to unique optical and nonlinear optical (NLO) responses. The optical nonlinearity of metal nanoparticles in dielectrics is of special interest because of their

high polarizability and ultra fast responses. The strong electric fields associated with the nanocrystal surfaces can play a significant role in producing enhanced NLO effects. Second-harmonic generation (SHG) has been used as an optical probe of electronic properties of metal nanoparticles of varying shape, size, composition, and spatial organization.[68] The arrays of gold nanoparticles can be characterized by SHG microscopy, which delivers the high contrast images due to enhancement of the electric field.[69] The electric properties or electro-optics effects of polar nanoparticles are also an interesting subject to examine.[70] The SPR energy states of metal nanoparticles can facilitate multiphoton excitations and hence nonlinear absorptions. As this thesis presents several studies of optical limiting application of metal nanoparticle, more details on this topic are presented later.

1.7. Nanomaterials: Applications

Nanoscience and technology are extremely vibrant and fast growing areas of research and development today. Therefore the numbers of applications of nanomaterials are increasing steadily. It is impossible to review them exhaustively. Based on the various properties discussed in Sec. 1.6, we list below a small section of applications of nanomaterials in different fields. In each case a few examples are provided, to impart a flavor of the nature of applications. We follow this up with details of two specific areas of application (Sec. 1.8 and 1.9) that are relevant to the work presented in this thesis.

1.7.1. *Colorants*

Nanoparticles have found a wide range of applications from fabrics colorants to paint whiteners. From 10th Century AD onwards nanoparticles have been employed as colorants in stained glass windows. Nanoparticles of desired color can be fabricated by suitable size/shapes variations designed based on theoretical calculations.[71] Simple size-tuning in the case of semiconductors[55] and changes of shape anisotropy in the case of nanoparticles of metals such as gold[52] are commonly employed to dramatically modify the optical properties. Efficient absorption in the UV region by TiO_2 nanoparticles make them useful in protecting human skin from harmful UV rays.

1.7.2. *Sensors*

Plasmonic metal nanoparticles have great potential for chemical and biological sensor applications, due to their sensitive spectral response to the local environment around the nanoparticle surface. The strong scattering or absorption of the metal nanoparticles helps in the efficient monitoring of optical signals. Surface enhanced Raman scattering (SERS) is often used in sensing applications. The detection of heavy metal ions is very important for biomedical and industrial applications. Functionalization of nanoparticles with ligands that bind selectively to heavy metal ions facilitates nanoparticle aggregation in presence of specific ions, leading to shifts in the absorption spectrum and concomitant color changes. This provides a powerful optical method for sensing.[72] Colorimetric techniques have been developed for DNA detection using gold and silver nanocrystals.[73] Exposure to vapors, such as methanol, ethanol, propanol, hexane, pentane, toluene etc changes the conductivity of functionalized metal nanoparticles. Measurement of changes in the current at a fixed applied voltage is a convenient method for vapor sensing by the nanoparticles.[74] Conductivity changes of palladium nanowires are exploited in sensing hydrogen gas.[75] Metal oxide nanoparticles are efficient gas sensors and find applications in a number of areas including environment monitoring, healthcare, and automobiles.[2, 76]

1.7.3. *Catalysts*

Transition metal nanoparticles are efficient catalysts and are often supported on suitable substrates for enhanced stability, reusability and broader scope of applications.[77] Palladium is one of the most popular catalysts in modern organic synthesis and widely used for a wide range of synthetic transformations. Beyond its well-known early applications in hydrogenation reactions,[78] palladium has gained enormous relevance in various coupling reactions such as Heck, Stille, Suzuki, Sonogashira and Buchwald-Hartwig reactions.[79] Many products could be synthesized by this methodology for the first time or in a much more efficient way than before. Palladium catalysis provides high reaction rate and high turnover numbers (TON) and often affords high selectivity and yields. Palladium nanoparticles stabilized by block copolymer micelles or phosphine dendrimer, or supported by silica shows high activity

and recyclability for reactions leading to C-C and C-X (X = Heteroatom) bond formation.[80] Bulk gold is chemically inert and has generally been found to be poorly active as a catalyst. However, when size is reduced to ~ 10 nm, it turns out to be amazingly active for reactions such as CO oxidation, especially at low temperature.[81]

Bi-metallic nanoparticles in the form of core-shell structures often show improved catalytic activity over the individual counterparts or their physical mixtures.[82] Since catalytic reactions occur only on the surface of the nanoparticles, the core of the nanoparticle is essentially unused; this could turned out to be very wasteful if the whole nanoparticle is constituted of expensive metals like Pd or Pt. Synthesis of core-shell nanoparticles having a cheap metal as the core and a noble metal as the shell turns out to be economical, without compromising the catalytic activity.[83] Additional factors like modulation of the shell surface activity by the core material could also be significant.

Nanoparticles of semiconductors like TiO_2 are important photocatalysts for decomposition of harmful organic pollutants.[84] Several metal oxides are catalysts for industrial applications such as oxidation-reduction reactions and hydrogen generation; they also act as supports for metal catalysts. In the nanoparticle form, they show enhanced catalytic activity.[85]

1.7.4. *Coating and Structural Materials*

It is well-known that surface properties such as wear resistance, friction and corrosion resistance of materials can be improved without changing the properties of the bulk material, by providing thin film coatings. Coatings by nanostructured materials can enhance wear protection of cutting tools and reduce the friction in sliding parts. Superhard nanocomposites such as nanocrystalline-$(Ti_{1-x}Al_x)N$/amorphous-Si_3N_4 show superior cutting performance compared to conventional, hard coatings with $(Ti_{1-x}Al_x)N$, commonly used for dry machining.[86] Nanoparticles, chain aggregates of carbon nanoparticles or carbon nanotubes have been used as reinforcements to improve the mechanical properties of matrix composites.[87] Addition of silica nanoparticles to polypropylene polymer matrix led to an increase of both Young's modulus and impact strength; addition of powder silica did not have such favorable impact on the mechanical properties of the polymer.[88] The mechanical properties of nanoparticle

chain aggregates are important in the manufacture of composite materials such as reinforced rubber, fabrication of sensor films and nanoparticle catalyst films. Measurement of the nanomechanical properties and the mechanism of enhancement due to nanoparticle chain aggregates are of great current interest,[89] because of their potential application to deformable electronic surfaces. The change in mechanical property by the incorporation of nanomaterials in the required matrix is highly relevant for biomedical application such as bone tissue engineering.[90]

1.7.5. *Magnetic Materials*

High-density magnetic data storage arrays provide a major technological driving force for the exploration of magnetic nanoparticles. They have been used as functional elements in magneto-optical switches,[91] and magnetically controllable single electron transistor devices.[92] Magnetic nanoparticles have found use in photonics crystals[93] and as toxic waste remediators for decomposing a variety of chemicals in ground water including halogenated alkenes.[94] They are also used to remove heavy metals.[95] The suspension of magnetic nanoparticles (ferrofluids) has enormous number of applications starting from friction-reducing lubricant in automobiles to medicine for cancer therapy. Magnetic nanocrystals are used in the drug delivery applications; the appropriate biochemical entity bound to magnetic nanocrystals; can be steered into regions of the body where they are required using applied magnetic fields.[96]

1.7.6. *Electronics*

Nanowires and single molecule conductors are critical components required for the miniaturization of electronic systems and devices. Nanoparticles behaving as quantum dots are extremely important in future nanoelectronics because they enable single-electron storage and tunneling. It has been shown that 17 nm palladium particles behave like bulk material at room temperature, following Ohm's law, but as quantum dots at liquid helium temperature, exhibiting a measurable value of Coulomb gap.[97] Studies on 1.4 nm gold clusters have shown typical Coulomb blockade behavior even at room temperature.[98] Therefore, these particles behave as single electron transistors whereas normal transistor unit on a silicon wafer works with ~10^4 electrons per action.

1.7.7. *Photonics*

Nanophotonics is a rapidly growing field of research holding considerable promise for wide range areas including communication, computation, information technology, biology and medicine. Surface plasmon of metal nanoparticles can be exploited in many applications such as subwavelength optics, data storage, light generation, microscopy and bio-photonics.[99] Promising developments in optoelectronics has greatly increased the demand for new nonlinear optical materials in recent years. The optical nonlinearity of metal nanoparticles can be utilized in applications such as optical switching.[100]

1.7.8. *Health and Medicine*

Nanoparticles are ideal for probing biological systems such as cells and their constituent organelles having sizes upto micrometers.[101, 102] Tunable surface chemistry facilitates the coating, functionalization and integration of nanoparticles with a host of biomolecular moieties.[103] These phenomena open up a range of applications in molecular biology and biomedicine, such as drug[96, 104] and gene[105] delivery, tissue engineering,[101, 106] protein and DNA sensing[73, 107] and detection based diagnostics[108] and biological/biomedical imaging.[57, 109] Nanomaterials can also be used in purification of drinking water. Magnetic nanoparticles and nanoporous materials such as zeolites and attapulgite have been used to absorb toxic heavy metals, organic pollutants and bacteria from water.[94, 95, 110]

1.8. Optical Limiting: Concepts and Materials

Advances in the field of lasers have led to revolutionary changes in many fields of science and technology. Power flux densities from 10^{12} to 10^{19} W cm^{-2} can be obtained using short focused pulses of laser with pulse widths in the range nanosecond to femtosecond. High-power lasers find use not only in academic research, but also in several industrial and military applications. Semiconductor and solid-state lasers are portable, compact and efficient, and hence of special interest in the realm of laser weaponry. With the advent of such high power laser sources operating over wide

ranges of wavelengths and pulse durations, the necessity for protection of sensors, optical components and human eyes from laser inflicted damages has increased enormously over the last few years. In this context, optical limiters which can display decreasing transmittance at high intensities (power per unit area) and fluence (energy per unit area) have received significant attention. In an ideal optical limiter, the transmittance change abruptly at some critical input intensity or threshold and therefore exhibits an inverse dependence on the intensity; the output is thus clamped at a certain value (Fig. 1.4). If this value is below the minimum that can damage the particular equipment, the optical limiter becomes an efficient safety device. The limiting threshold ($I_{1/2}$) of the material is defined as the input intensity/fluence at which the transmittance reduces to half of the linear transmittance.[111] An optical limiter can clamp the output intensity/fluence over a wide range of input intensity/fluence, but may breakdown after certain value, most probably due to the material damage, and exhibit increased transmittance again. The threshold upto which the material can provide effective limiting is called the damage threshold and the ratio of damage threshold to the limiting threshold is called the dynamic range of the optical limiter.[111] Desirable attributes of an effective optical limiter are (i) low limiting threshold and high optical damage threshold and stability, leading to a large dynamic range, (ii) sensitive broadband response to long and short pulses, (iii) fast response time, and (iv) high linear transmittance, optical clarity, and robustness (i.e. resistance to damage/degradation with time due to humidity, temperature etc).[112]

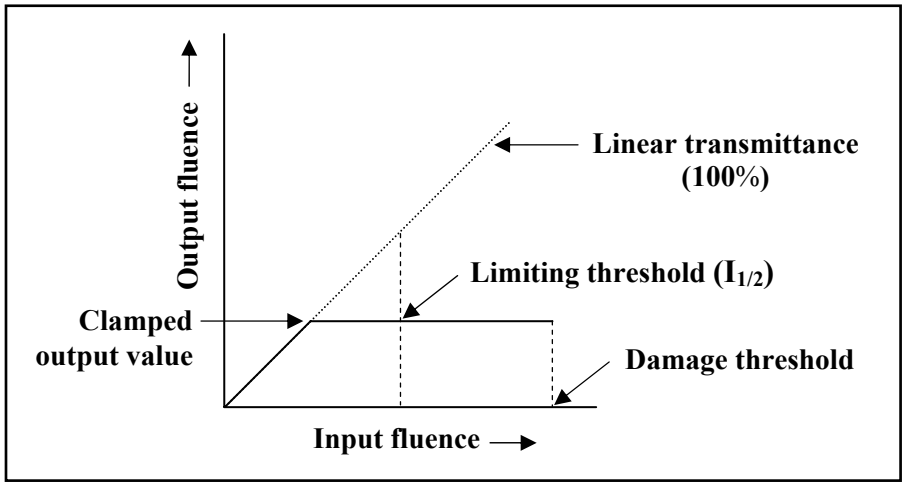

Figure 1.4. *Schematic representation of the behavior of an ideal optical limiter.*

1.8.1. *Processes Leading to Optical Limiting*

Optical limiting can be achieved by various nonlinear optical mechanisms. The most common ones are mostly by nonlinear refraction effecting self-focusing, self-defocusing, induced aberration, induced scattering, induced refraction etc and nonlinear absorption mediated by excited state absorption (ESA), reverse saturable absorption (RSA), free-carrier absorption (FCA), two-photon absorption (TPA) and multiphoton absorption.[113, 114] Fig. 1.5 shows a classification of the various mechanisms that can lead to optical limiting broadly based on energy spreading and energy absorbing modes.

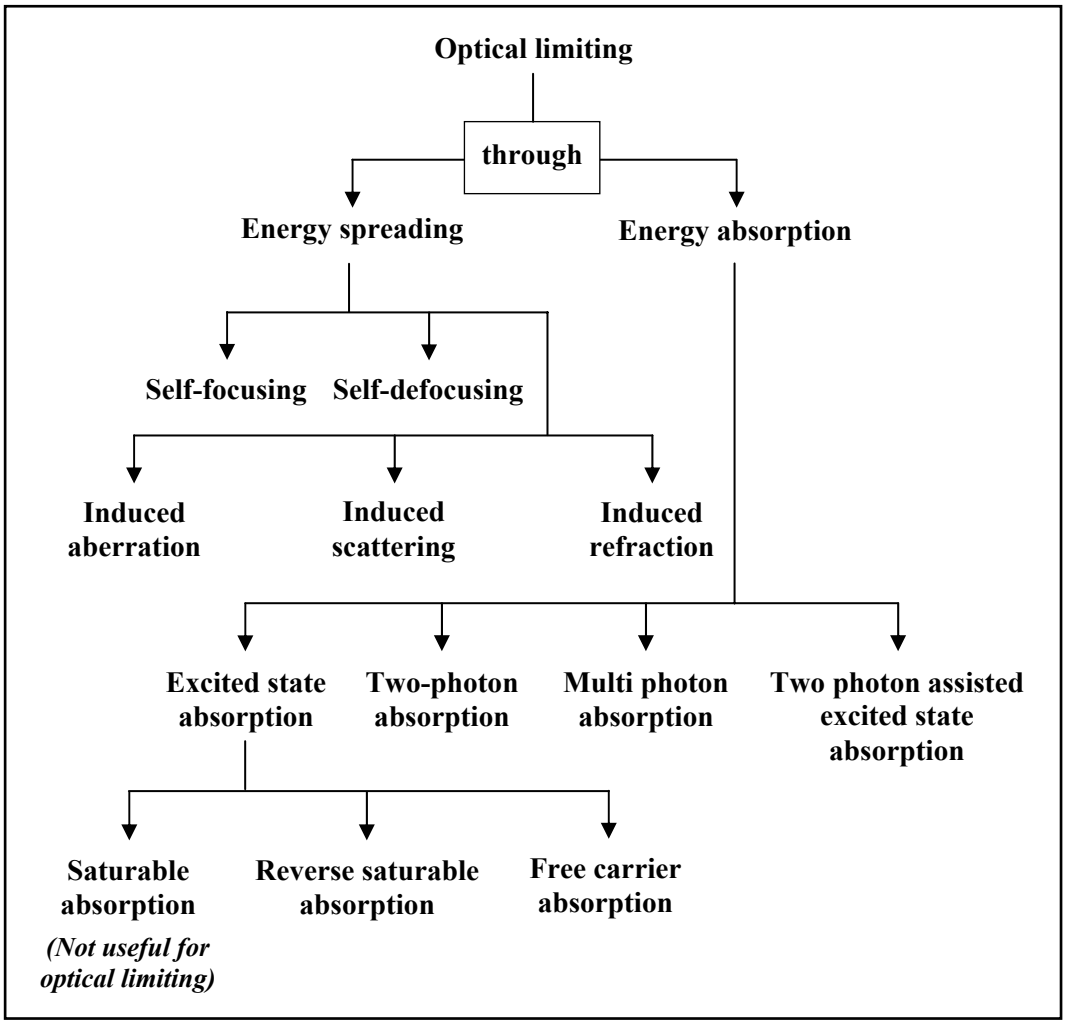

Figure 1.5. *Schematic representation of the various mechanisms responsible for optical limiting.*

1.8.2. *Energy-spreading type Optical Limiters*

The key requirement for energy-spreading type of materials is to place an aperture or pinhole in front of a detector or the target where the laser light is directed. The limiting of the detected laser beam is based on the change in the spatial energy distribution of the transmitted beam. With the increase of input laser intensity/fluence, a larger fraction of the incident laser energy is spread out to a wider solid-angle range; as a result the fraction passing through the aperture will decrease accordingly. In these cases, the observed limiting behavior depends not only on the input laser intensity and the nonlinear medium, but also on the pinhole size and the geometric configuration of the optical system for a given device. For most of this type of materials, thermally induced refractive index changes play a key role. Typical effects operating in energy-spreading type of optical limiting materials are schematically shown in Fig. 1.6. In all these cases the size of the aperture is chosen in such a way that when the input fluence is very low, the laser beam transmitted through the medium can totally pass through the aperture without any blocking. In the case self-focusing (Fig. 1.6a) and self-defocusing (Fig. 1.6b), when the input fluences are high, the detected energy is significantly reduced due to the energy spreading in the aperture plane. Fig. 1.6c represents the mechanism based on induced aberration. It is well known that induced refractive index change is a function of the local intensity distribution of the laser beam inside the nonlinear medium. An irregular spatial distribution of local light intensity can lead to random refractive index changes at high intensity levels, causing severe aberration influences on the wavefront of the transmitted laser beam. By keeping a small pinhole in the focal plane of a focusing lens, the portion of the laser energy passing to the detector can be decreased as the induced aberration becomes larger.[115, 116] Fig. 1.6d and 1.6e show optical limiting based on laser-induced intensity dependent scattering and refraction. In the case of induced scattering, the limiting medium is a system of linearly absorbing particles randomly distributed in a transparent host material. For weak input intensity, the temperature and refractive index changes of the particles due to light absorption in the system are negligible, whereas for strong input intensity, the absorption-induced heating of the particles is no longer negligible. Each particle forms an individual heating center and the medium becomes highly inhomogeneous resulting in considerable part of the energy spreading out into a wider spatial range and only a small fraction passing through the aperture.[117] In the case of induced refraction, the

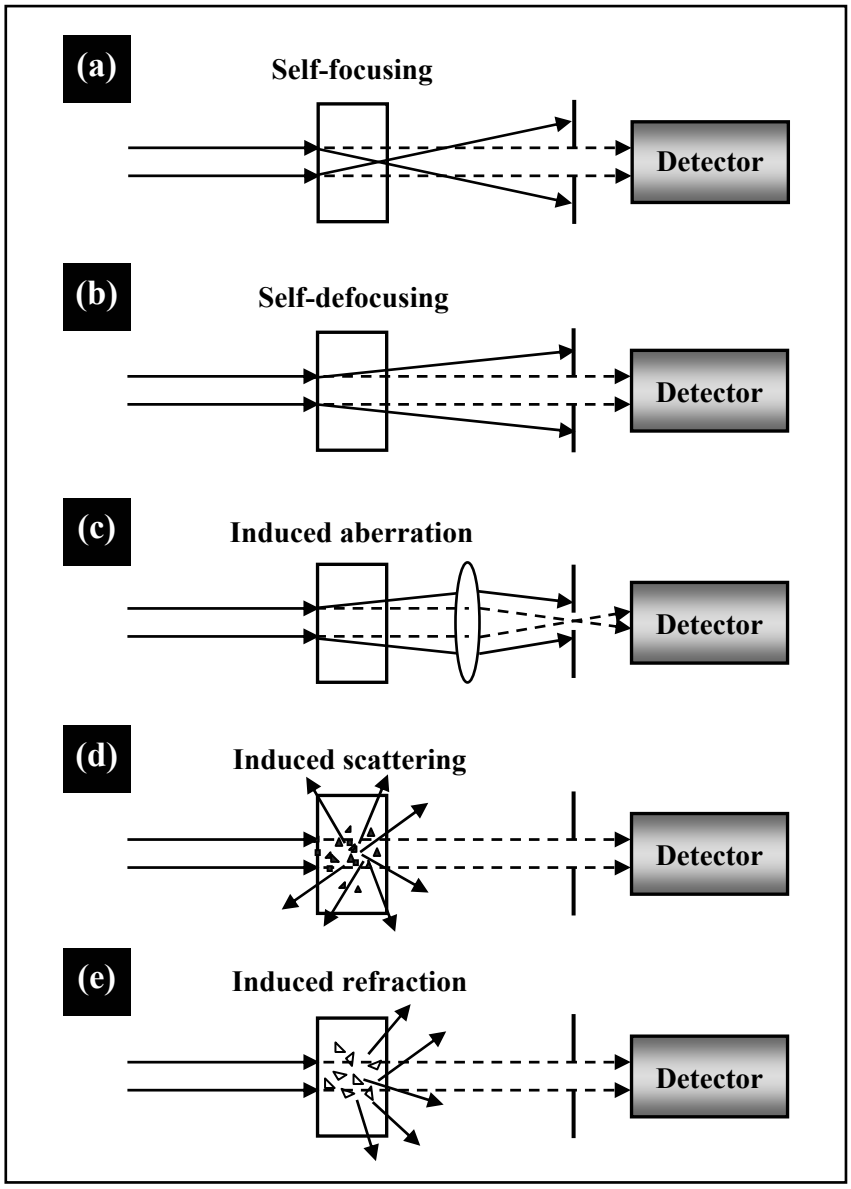

Figure 1.6. *Schematic illustration of energy-spreading type optical limiters (Figure adapted from Ref. 115).*

medium is composed of two microscopic components that have the same static refractive index but are in different phase (e.g. liquid and solid mixture). If one component is transparent and the other absorbs the incident laser beam, the selective heating, makes the whole system inhomogeneous at the boundary between the two components.[115] Although, all energy-spreading type of optical limiting are featured

using an aperture, in some experimental cases no aperture is used; in the latter case, the limited sensitive area of the detector plays the role of an aperture.

Although all these mechanisms lead to slow temporal response, the opto-thermal effect-induced refractive index change is considered to be important for optical limiting. Even though impurities or external particles cause only small residual linear absorption in transparent and non-resonantly absorptive medium, this small absorption is strong enough to create remarkable thermally induced refractive index changes at higher input laser intensity. The induced refractive index change will be significant for a resonant and linearly absorbing medium even at low input intensity.

1.8.3. *Energy-absorption type Optical Limiters*

Nonlinear absorption is another mechanism employed for optical limiting. In this case no aperture or pinhole is necessary, and the optical limiting relies on the fact that the transmittivity of nonlinear absorbing media decreases when the input laser intensity increases. At sufficiently high intensities, the probability of a material absorbing more than one photon or an excited molecule (or electron in the case of, say, semiconductors) being elevated to a higher-lying excited state before relaxing to ground state can be greatly enhanced. The optical limiting devices based on this mechanism can be called the energy-absorption type of optical limiters and the various processes leading to optical limiting are listed below.

Excited State Absorption (ESA)

When the incident intensity is well above the saturation intensity, then the excited state can become significantly populated. If the excited state has a high density of states near to it (as in the case of a semiconductor), the excited electron can rapidly make a transition to these states before it decays back to the ground state. There could also be a number of higher-lying states which are coupled with these intermediate states, for which the energy differences are in near-resonance with the incident photon energy. In such a case, before the electron completely relaxes to the ground state, it may experience absorption that promotes it to a higher-lying state. This process is called excited state absorption. This process is observable when the incident intensity is

sufficient enough to deplete the ground state significantly.

Fig. 1.7 represents the ESA mechanism for nonlinear absorption, usually called five-level model, referring to five distinct electronic states.[116] Absorption of an incident photon promotes an electron to the first excited singlet state, S_1, from which one of the following can happen: (i) the electron can relax back to ground state by radiative or nonradiative transition, with rate constant k_f, (ii) it can undergo spin flip transition to a triplet state T_1 (intersystem crossing) with rate constant, k_{isc}, or (iii) the material can

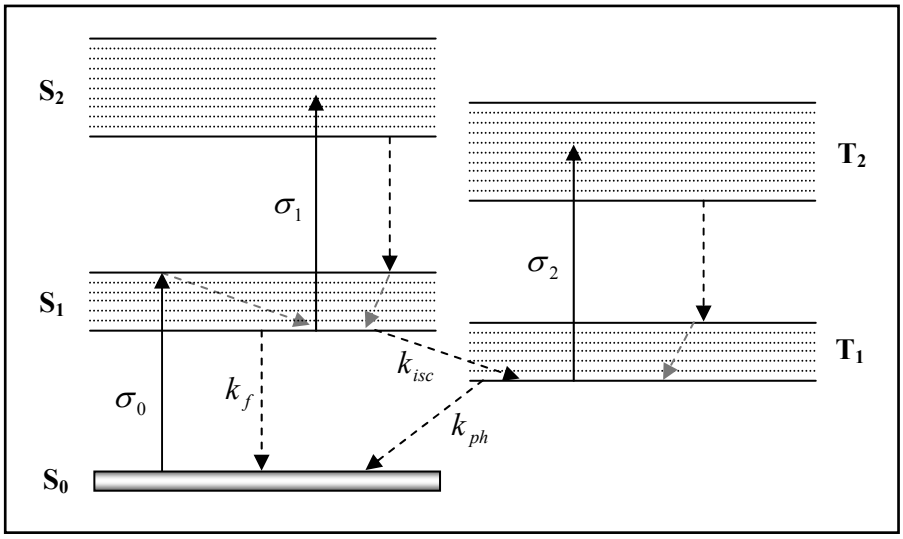

Figure 1.7. *Schematic energy level diagram for the excited state absorption (ESA).*

absorb another photon, promoting the electron to a higher-lying singlet state, S_2 from which it can relax back to the first excited singlet state. Electron in the lowest triplet state has two options: (i) it can relax back to the ground state by another spin flip transition, leading to phosphorescence, with rate constant k_{ph}, or (ii) the material can absorb another photon, promoting the electron to a higher-lying triplet state T_2, from which it can relax back to T_1.

If the absorption cross-section of the excited state is smaller than that of the ground state, the transmission of the system will be increased when the system is strongly excited. This process is called saturable absorption (SA) which is similar but more complex than that of saturation of absorption occurring in simple two-level systems. On the other hand, if the absorption cross-section of the excited state is larger

than that of the ground state, the system will be less transmissive when excited; since this phenomenon is opposite to that of saturable absorption, it is called reverse saturable absorption (RSA). Free carrier absorption (FCA) has similar characteristics as RSA. Among these three nonlinear processes RSA and FCA contribute to optical limiting and hence are discussed further below.

Reverse Saturable Absorption (RSA)

Materials showing RSA show enhanced absorption as the input optical intensity/fluence is increased.[118] Such a nonlinear optical response is exhibited when materials have weak ground state absorption over some spectral range and strong excited state absorption in the same wavelength range. Reverse saturable absorbers are of special interest since (i) they display large nonlinear attenuation while maintaining high linear transmittance; (ii) energy is absorbed and converted to heat and not spread as in nonlinear refractive or scattering media, making the limiting process more reliable and useful in fast (highly convergent) optical systems and (iii) materials with prompt singlet excited-state absorption and long-lived triplet-state absorption may be effectively used for optical limiting of a wider range of pulse widths (sub-picosecond to microsecond duration).

A simple model of sequential one-photon absorption in a two-step process[115, 116] can be used to explain RSA as shown schematically in Fig. 1.8. 1, 2 and 3 are the

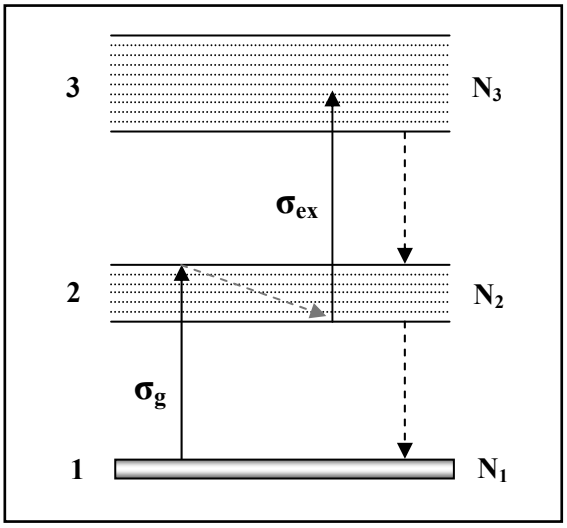

Figure 1.8. *Schematic energy level diagram for reverse saturable absorption (RSA).*

ground, first and higher-lying excited states respectively, N_1, N_2 and N_3 the respective populations and σ_g and σ_{ex}, the absorption cross-sections for the ground and excited states respectively. If the material has resonant linear absorption for the incident laser, excitation of a definite population to state 2 occurs, followed by further transition from state 2 to 3 via further photon absorption. Probability of the latter transition depends on N_2, σ_{ex} and the incident intensity, I; N_2 is determined by N_1, σ_g and I. With increase in the intensity, N_2 increases continuously and hence the sequential one-photon absorption from state 2 to 3 becomes significant provided $\sigma_{ex} >> \sigma_g$. Under steady state conditions,

$$\frac{dI}{dz} = -\sigma_g (N_1 - N_2) I - \sigma_{ex} N_2 I \quad \text{... (1.2)}$$

In the simplest situation, it can be assumed that $N_1 \rangle\rangle N_2, N_3 \approx 0$ and $N_1 \approx N$ where N is the total population of the absorbing species. If $N_2 \approx b\sigma_g N$, where b is a proportionality constant, the attenuation of the light inside the medium,

$$\frac{dI}{dz} = -\sigma_g NI - b\sigma_g \sigma_{ex} NI^2 \quad \text{... (1.3)}$$

$$\frac{dI}{dz} = -\alpha_0 I - \beta' I^2 \quad \text{... (1.4)}$$

The linear and nonlinear absorption coefficient α_0 and β' are defined as

$$\alpha_0 = \sigma_g N \quad \text{... (1.5)}$$

$$\beta' = b\sigma_g \sigma_{ex} N \quad \text{... (1.6)}$$

The solution of Eq. 1.4 gives the intensity of the light at a distance, z inside the medium,

$$I(z) = \frac{I_0 e^{-\alpha_0 z}}{1 + (1 - e^{-\alpha_0 z}) \dfrac{\beta'}{\alpha_0} I_0} \quad \text{... (1.7)}$$

where I_0 is the input intensity incident on the medium. If the linear absorption is small, then $e^{-\alpha_0 z} \approx 1 - \alpha_0 z$, transmittivity,

$$T(I_0) = \frac{I}{I_0} = \frac{T_0}{1 + \beta' z I_0} \quad \text{... (1.8)}$$

Here $T_0 = e^{-\alpha_0 z}$ is the linear transmittivity of the material for low input intensity. $T(I_0)$ is the intensity dependent transmittivity of the same material at high input intensity.

This simplest quantitative description of RSA explains how the transmittivity decreases with increasing input intensity.

Free Carrier Absorption (FCA)

Absorption of photons with energy greater than the band gap will promote electrons to the conduction band, where they become free carriers. With sufficiently high intensities, there is a high probability for them to absorb more photons although they are still in the conduction band. This can lead to nonlinear absorption. Once free carriers are generated in semiconductors, they may experience phonon-assisted absorption to higher lying states in the conduction band.

Two-photon Absorption (TPA)

Two-photon absorption (TPA) involves a transition from ground state 1 of a material to a higher-lying state 2 by the simultaneous absorption of two photons via an intermediate virtual state, as schematically shown in Fig. 1.9.

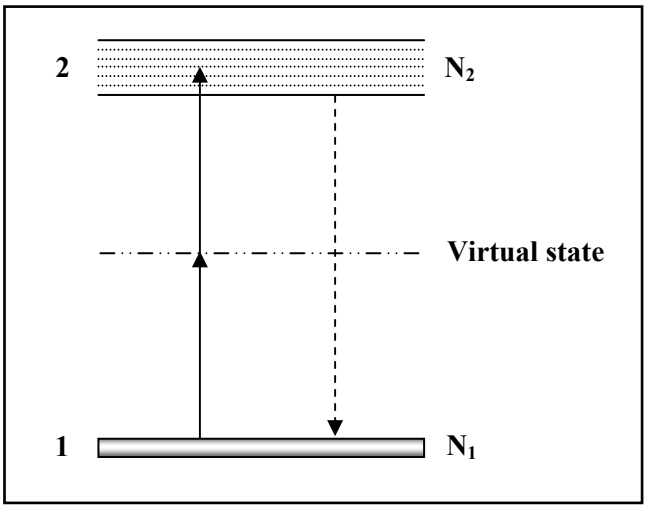

Figure 1.9. *Schematic energy level diagram for two-photon absorption (TPA).*

In this case, the attenuation of the incident light is described by

$$\frac{dI}{dz} = -\alpha_0 I - \beta I^2 \qquad \ldots (1.9)$$

where α_0 and β are the linear and two-photon absorption coefficient respectively.

Three-photon and multiphoton absorption involves a transition from the ground state to a higher-lying state by the simultaneous absorption of three or more photons via multiple number of virtual states.

Two-photon Assisted Excited State Absorption

When TPA is particularly strong in a material, it can lead to significant population of a two-photon allowed state. Often there are allowed transitions from this state to higher-lying states of the system, i.e. when excited with ultrashort laser pulses, ESA can ensue from the two-photon excited state. Attenuation of the laser intensity can be written as

$$\frac{dI}{dZ} = -\alpha_0 I - \beta I^2 - \sigma N I \qquad \ldots (1.10)$$

where α_0 and β are the linear and TPA absorption coefficient and σ is the ESA cross-section.

1.8.4. *Materials for Optical Limiting*

A wide variety of materials have been studied as potential candidates for optical limiting based on different processes. Nonlinear materials with higher sensitivity and negligible linear absorption are prime targets for development and incorporation into optical systems. Particular attention is focused on optical limiters for pulsed lasers in the visible and near infrared range, in view of their importance for eye protection.[119] Colloidal suspensions provide optical limiting in the UV to near IR range, using scattering mechanisms.[120] Several dye molecules are useful in the visible band because of nonlinear absorption and refraction. The most extensively studied systems are phthalocyanines,[121] porphyrins[122] and fullerenes and their derivatives[123] in which long-lived triplet excited state can be produced conveniently. Liquid crystals are another class of materials studied in the visible to mid IR region; they cause optical limiting via refraction and TPA.[124] Another system studied is bacteriorhodopsin.[125] Photorefractive materials,[126] photonic band gap materials,[127] nonlinear absorbers doped in xerogels and sol-gel films,[128] glasses,[129] filters,[130] organic/ inorganic clusters[131] and layered systems[132] have been reported to show efficient optical limiting properties.

Over the last few years, semiconductor nanoparticles and carbon nanotubes,[133] as well as metal nanoparticles[134] have emerged as promising candidates for optical limiting in the nanosecond and picosecond regime. Semiconductor quantum dots,[135] metal nanoparticles,[136] carbon nanostructures,[137] fullerene functionalized polymers,[138] and organometallics[139] have been reported to show optical limiting of femtosecond laser pulses. Optical limiting properties of metal nanoparticle-embedded polymer thin films in the nanosecond and femtosecond regimes will be the subject of some of the studies presented in this thesis.

1.9. Antibacterials: A Brief Overview

A microorganism or microbe is a living organism which is microscopic in size i.e. typically few micrometers along the largest dimensions. Microorganisms can be bacteria, fungi, archaea or protists, but not prions or viruses which are non-living. An antimicrobial is a substance which can kill or inhibit the growth and reproduction of microbes. When the antimicrobial substance is effective only against bacteria, it is called an antibacterial. The action of these substances can be bactericidal (killing) or bacteriostatic (inhibition of growth and reproduction).

1.9.1. *Bacteria*

Bacteria are the simplest, most diverse and widespread group of microbes on earth. The structural differences of bacteria lie in the organization of a key component of the cell wall, peptidoglycan, which is one of the most essential parts for survival of most bacteria. Gram-negative bacteria (*Escherichia coli, Salmonella* etc.) possess only a thin peptidoglycan layer (~ 2 - 3 nm) between the cytoplasmic membrane and the outer membrane; in contrast, gram-positive bacteria (*Bacillus, Listeria, Staphylococcus* etc) lack the outer membrane but have a peptidoglycan layer that is ~ 30 nm thick.[140]

Bacteria can inhabit practically all environments where liquid water is available and temperature is below 140^{o}C; they can quickly adapt and respond to new environments and environmental stresses. Some of the bacteria can make spores, which are reproductive structures adapted for dispersion and survival over extended periods of

time in adverse conditions. They reproduce by binary fission. Under optimal conditions they can grow extreme rapidly and the population can be doubled within few minutes. The standard bacterial growth curve is shown in Fig. 1.10 consisting of four phases: (i) lag phase when growth is slow while bacteria adapt to the food and nutrients

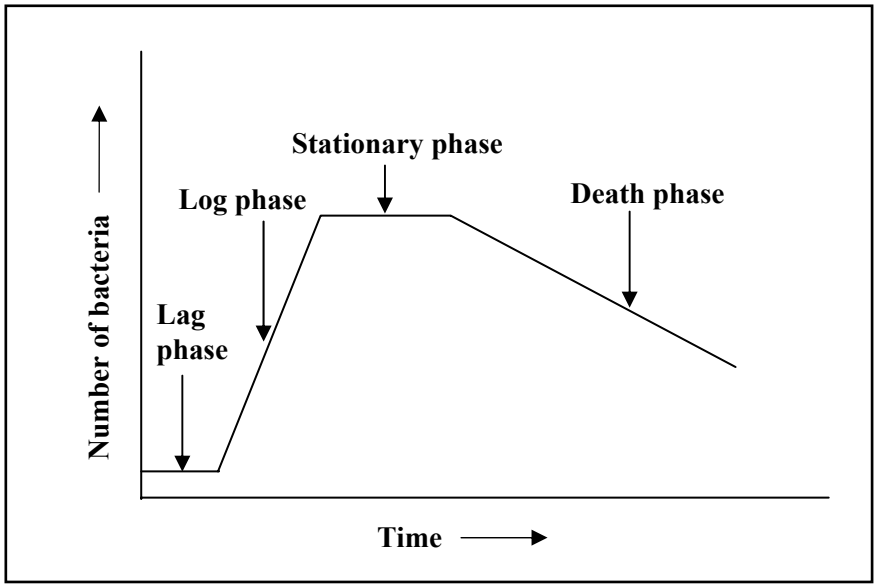

Figure 1.10. *Bacterial growth curve showing the four phases of growth versus time.*

in their new habitat, (ii) log phase in which metabolic machinery is operative and exponential growth occurs, (iii) stationary phase where the bacteria start competing for the dwindling food and nutrients causing the growth rate to reduce and the number of bacteria to stabilize, (iv) death phase in which the toxic waste products built up and depleted food lead to death of bacteria. The number of viable bacteria present in a sample can be measured indirectly by a method named 'plate counts', where the sample is diluted by nontoxic diluent (e.g. water) before plating/spreading. If plated on a suitable medium (usually nutrient agar surface), each viable unit grows and forms a colony. The count of colonies is expressed as the number of colony forming units (CFU); it provides an estimate of the viable number of bacteria present in the original sample. Although the majority of bacteria are harmless or even benefit a host in different ways, a few are pathogenic, invading other organisms and causing various diseases.

1.9.2. *Antibiotics*

Antibiotics are generally used to treat bacterial diseases such as cholera, syphilis, plague, tuberculosis, anthrax, leprosy and many more. Some antibiotics are bactericidal, whereas others are merely bacteriostatic allowing the host's immune system to eradicate them. Originally all antibiotics were based on formulations derived from living organisms, penicillin being the classic example; however synthetic molecules such as sulfonamides are quite common now. It has been known for long that heavy metal such as mercury, lead, copper and silver as well as their ionic salts can exhibit strong antibacterial activity.

Misuse or excessive use of antibiotics has led to the emergence of antibiotic-resistant pathogens.[141] For example infections due to *Staphylococcus aureus* used to be treated with penicillin in the mid-nineteenth century. But at present nearly all strains of these bacteria are resistant to penicillin and even a few other antibiotics. The genes coding for antibiotic resistance is transferred between bacteria via plasmids, making it possible for bacteria which were never exposed to an antibiotic to acquire resistance from those that have been already exposed. Even though bacteria have not been able to develop resistance against heavy metals and their salts, most of these are unsuitable for treating infectious deceases because of their high toxicity to other living organisms including humans.

Recently, different types of materials have been used as antimicrobial/ antibacterial agents, such as ampiphilic polymers,[142] or synthetic mimics of naturally occurring antibacterial peptides,[143] microbe-repelling anti-adhesive polymers,[144] and polymeric/composite materials loaded with slow releasing biocides such as heavy metals,[145] antibiotics,[146] small molecule biocides,[147] halogen species,[148] etc.

1.9.3. *Efficacy of Silver*

Silver-based materials are popular antibacterial because of their potent efficacy,[149] ease of fabrication, low toxicity towards mammalian cells[150] and low provocation of microbial resistance.[151] Compounds containing both ionic silver (Ag^{+})[152] and metallic silver (Ag^{0})[153] exhibit antimicrobial activity. They can be used to reduce

infections in burn treatment[154] and arthroplasty[155] and to prevent bacteria colonization on prostheses,[156] catheters,[157] vascular grafts,[158] dental materials,[159] stainless steel materials,[160] and even human skin.[161] Silver-containing materials can be employed to eliminate microorganisms on textile fabrics[162] and for water treatment.[163]

Silver nanoparticles have emerged as one of the most popular agents for bactericidal applications.[164, 165] Contrary to bactericide effects of ionic silver, the antimicrobial activity of colloid silver particles are influenced by the dimensions of the particles; the smaller the particles, greater the antimicrobial effect.[165, 166] Colloidal silver nanoparticles,[166, 167, 168, 169] as well as embeddings in polymers,[170] foams,[171] fibers[172] and textiles[173] have been extensively used as antibacterial agents. Silver nanoparticles also exhibit potent cytoprotective activity towards HIV infected cells.[174]

1.9.4. *Bactericidal Mechanism of Silver Nanoparticles*

The bactericidal effect of silver on micro-organisms is very well known; however, the mechanism involved in bactericidal action is only partially understood. It is the subject of extensive investigations currently. It is generally believed that the silver nanoparticles provide slow and controlled supply of silver ions which actually participate in the bactericidal process. The electrostatic attractive interaction due to surface charges of the nanoparticles and bacteria is also implicated in the antibacterial activity. It has been shown that the bacterial cells get damaged after treatment with metal nanoparticles, the formation of 'pits' in the cell wall of the bacteria has been suggested to lead to the antibacterial activity.[168] It has also been reported that nanoparticles enter the bacterial cell and presumably get attached to the DNA.[165] A recent study suggests that the enhanced activity of nanoparticles is due to their large surface area/volume ratio and the improved surface interaction that facilitates specific binding to cell membrane (generally to the sulfur-containing proteins) causing greater permeability of the membrane culminating in bactericidal action.[169] Whatever the details of mechanism, silver nanoparticles have clearly been demonstrated to be useful and effective in antibacterial applications.

1.10. Layout of the Thesis

The main objectives of this thesis are the development of a simple and environment-friendly *in situ* process for generating metal nanoparticles inside polymer films and exploration of their utility in different applications. We merge the advantages of the chemical route to nanoparticles, environment-friendly reagents, and the stabilization of the particles in a polymer matrix, in the fabrication of nanoparticle-embedded polymer film using appropriate precursors and polymers. The polymer we have chosen in our study, poly(vinyl alcohol) (PVA) can serve multiple functions as, reducing agent for the precursor metal ions, stabilizer for the nanoparticles and the matrix for homogeneous distribution and immobilization. The specific metals we have chosen in our studies are silver, gold and palladium, based on the fact that the hydroxyl group on PVA can reduce the corresponding cations. The protocol we have developed is generally carried out in aqueous medium and provides a convenient route to supported as well as free-standing films of the nanoparticle-embedded polymer; fabrication of the latter involves the use of a sacrificial layer of polystyrene (PS). The free-standing films are not only useful from an application point of view, but also facilitate direct imaging in a transmission electron microscope. The process we have developed facilitates the variation of particle size, shape and size/shape distribution by control of the composition of the films and parameters related to the thermal treatment. The nanocomposite materials fabricated are found to have efficient optical power limiting capability and reusable antibacterial application. This thesis is organized in five chapters. The uniqueness and significance of nanomaterials are introduced in this chapter along with an overview of the historical perspective including the crucial role of microscopy in the development of nanotechnology. The classifications, different methods of the synthesis, special properties and multidisciplinary applications of nanomaterials are already discussed in the previous sections of this chapter. The salient features of the subsequent chapters are summarized below.

Chapter 2

This chapter presents the details of the methodology we have developed for the *in situ* generation of metal nanostructures inside polymer films. The chapter is specifically focused on silver nanoparticles formed in PVA films. The nanoparticles are

generated by the reduction of silver nitrate *in situ* inside the film, through thermal treatment; PVA acts simultaneously as the reducing agent and stabilizer for the nanoparticle formation and facilitates homogenous nucleation. A simple and efficient protocol for the fabrication of free-standing films is also demonstrated. The silver/polymer ratio, time and temperature of thermal treatment are shown to exert a strong influence on the size of the nanoparticles and the size distribution. Fine-tuning these parameters can provide homogeneous and narrow distributions around small particle sizes typically, 2 - 3 nm. The films fabricated are characterized using spectroscopy and microscopy. Nonlinear absorption and optical limiting properties of the supported and free-standing silver nanoparticle-embedded PVA films are investigated using Z-scan studies in the nanosecond and femtosecond regimes. These studies revealed strong responses in the thin films which are comparable or superior to those reported for silver colloids earlier. Antibacterial application of the reusable composite films is presented in the last part of this chapter.

Chapter 3

Extension of the methodology developed in Chapter 2 to the fabrication of gold nanoplates embedded in PVA films is presented in this chapter. A range of polygonal shapes are realized by optimizing the gold/polymer ratio and the reaction conditions. Infrared spectroscopy allowed us to investigate the chemistry occurring in the polymer film leading to the formation of the gold nanostructure. Optical limiting application of the supported Au-PVA film studied using femtosecond pulse laser is also presented in this chapter. An assortment of studies including the synthesis of gold nanopyramids, green synthesis of gold nanocrystals and the real time monitoring of the *in situ* growth of gold nanodomes, are collected in the last part of this chapter.

Chapter 4

This chapter describes the studies of palladium nanowire formation inside PVA films. Crystallization of the precursor, potassium palladium (II) chloride as nanowires inside the film and the influence of its concentration on the morphology of the nanostructures formed are discussed. The precursor nanowires are reduced to palladium nanowires by the polymer under mild thermal annealing. The chemical reaction

occurring *in situ* inside the polymer films, including byproduct formation, are investigated through spectroscopy together with microscopy and electron diffraction. The overall process can be described as a novel case of crystal-to-crystal transformation at the nanoscopic level. Optical limiting studies of the nanowires-embedded polymer thin films are discussed. In the last part of the chapter, general utility of the present approach to nanowire fabrication is demonstrated using preliminary explorations carried out on gold in PVA.

Chapter 5

The final chapter presents an overview of the various investigations presented in the thesis and highlights the salient achievements of the *in situ* synthesis methodology we have developed for the fabrication of metal nanoparticle-polymer composite films. The highlights of the work include : (i) the simple, convenient and general fabrication protocol developed for the synthesis of metal nanoparticles, (ii) use of bio-compatible and bio-degradable polymer and aqueous medium for the fabrication process, (iii) the *in situ* generation of nanocrystals in polymer films using the matrix itself as the reagent, leading to free-standing or supported films with embedded nanoparticles, (iv) control over size, shape and size/shape distribution of the nanoparticles, (v) orientational ordering of nanoplates and nanowires without the help of special templates or linker molecules, (vi) monitoring of the reaction occurring inside the polymer thin films using spectroscopic and microscopic tools, (vii) optical limiting capability of the silver, gold and palladium nanoparticle-polymer composite thin films and the unambiguous estimation of the nonlinear refractive index and nonlinear optical susceptibility of the nanoparticles without the substrate contribution through the use of free-standing films and (viii) the efficient bactericidal application of reusable silver nanoparticle-polymer composite films.

The current protocol opens up a wide range of possibilities for the fabrication of supported/free-standing metal or semiconductor nanoparticle-embedded polymer films. Organized assembly of the nanostructures inside the polymer matrix may be achieved by fine-tuning our protocol or mechanical manipulation of the films. Exploration of further applications of the composite films in areas including catalysis and opto-electronics are some of the important directions for further work.

References

1. Nanoscience and nanotechnologies: opportunities and uncertainties, The Royal Society & The Royal Academy of Engineering, London, 2004.
2. Pitkethly, M. J. *Nanotoday* **2004**, 20.
3. Bleeker, R. A.; Troilo, L. M.; Ciminello, D. P. *Materialstoday* **2004**, 44.
4. Winners of nanotechnology hazard symbol contest announced (January 24, 2007). http://www.nanowerk.com/news/newsid=1326.php
5. Faraday, M. *Phil. Trans. Royal Soc. London* **1857**, *147*, 145.
6. (a) Mie, G. *Ann. Phys*. **1908**, *25*, 377; (b) Mie, G. *Physik. Z.* **1908**, *8*, 769.
7. Debye, P. *Ann. Physik* **1909,** *30*, 57.
8. Gerber, C; Lang, H. P. *Nature Nanotechnol* **2006**, *1*, 3.
9. Klabunde, K. J. *Nanoscale Materials in Chemistry*, John Wiley: New York, 2001.
10. Retello, V. *Nanoparticles: Building Blocks for Nanotechnology*, Kluwer Academic / Plenum Publishers: New York, 2004.
11. (a) Jun, Y.; Lee, S.-M.; Kang, N.-J.; Cheon, J. *J. Am. Chem. Soc.* **2001**, *123*, 5150; (b) Lee, S.-M.; Jun, Y.; Cho, S.-N.; Cheon, J. *J. Am. Chem. Soc.* **2002**, *124*, 11244; (c) Milliron, D. J.; Hughes, S. M.; Cui, Y.; Manna, L.; Li, J.; Wang, L.-W.; Alivisatos, A. P. *Nature* **2004**, *430*, 190.
12. (a) Murray, C. B.; Kagan, C. R.; Bawendi, M. G. *Science* **1995**, *270*, 1335; (b) Wang, Z. L. *Adv. Mater.* **1998**, *10*, 13; (c) Li, M.; Schnablegger, H.; Mann, S. *Nature* **1999**, *402*, 393; (d) Wang, Z. L. *J. Phys. Chem. B* **2000**, *104,* 1153.
13. (a) Peng, X.; Manna, L.; Yang, W.; Wickham, J.; Scher, E.; Kadavanich, A.; Alivisatos, A. P. *Nature* **2000**, *404*, 59; (b) Lisiecki, I. *J. Phys. Chem. B* **2005**, *109,* 12231; (c) Burda, C.; Chen, X.; Narayanan, R.; El-Sayed, M. A. *Chem. Rev.* **2005**, *105*, 1025.
14. Wang, Z. L. *Adv. Mater.* **1998**, *10*, 13.
15. (a) Masala, O.; Seshadri, R. *Annu. Rev. Mater. Res.* **2004**, *34*, 41; (b) Liu, S.; Zhang, Z.; Han, M. *Anal. Chem.* **2005**, *77*, 2595.
16. (a) Niidome, Y.; Hori, A.; Sato, T.; Yamada **,** S. *Chem. Lett.* **2000**, *29*, 310; (b) Mallik, K.; Mandal, M.; Pradhan, N.; Pal, T. *Nano Lett.* **2001**, *1*, 319; (c) Giuffrida, S.; Condorelli, G. G.; Costanzo, L. L.; Fragala, I. L.; Ventimiglia, G.; Vecchio, G. *Chem. Mater.* **2004,** *16*, 1260.
17. (a) Mössmer, S.; Spatz, J. P.; Möller, M.; Aberle, T.; Schmidt, J.; Burchard, W. *Macromolecules* **2000**, *33*, 4791; (b) Sau, T. K.; Pal, A.; Jana, N. R.; Wang, Z. L.; Pal, T. *J. Nanopart. Res.* **2001**, *3*, 257.
18. (a) Mizukoshi, Y.; Okitsu, K.; Maeda, Y.; Yamamoto, T. A.; Oshima, R.; Nagata, Y. *J. Phys. Chem. B* **1997**, *101*, 7033; (b) Prozorov, T.; Prozorov, R.; Koltypin, Yu.; Felner, I.; Gedanken, A. *J. Phys. Chem. B.* **1998**; *102*, 10165; (c) Pol, V. G.; Gedanken, A.; Calderro-Moreno, J. *Chem. Mater.* **2003**, *15*, 1111.
19. (a) Henglein, A.; Meisel, D. *Langmuir* **1998**, *14*, 7392; (b) Henglein, A. *J. Phys. Chem. B.*

2000, *104*, 1206; (c) Doudna, C. M.; Bertino, M. F.; Blum, F. D.; Tokuhiro, A. T.; Lahiri-Dey, D.; Chattopadhyay, S.; Terry, J. *J. Phys. Chem. B.* **2003**, *107*, 2966.

20. (a) Park, S.-J.; Kim, S.; Lee, S.; Khim Z. G.; Char, K.; Hyeon, T. *J. Am. Chem. Soc.* **2000**, *122*, 8581; (b) Teranishi, T.; Hasegawa, S.; Shimizu, T.; Miyake, M. *Adv. Mater.* **2001**, *13*, 1699; (c) Puntes, V. F.; Krishnan, K. M.; Alivisatos, A. P. *Science* **2001**, *291*, 2115.
21. Shimizu, T.; Teranishi, T.; Hasegawa, S.; Miyake, M. *J. Phys. Chem. B* **2003**, *107*, 2719.
22. (a) Mafumé, F.; Kohno, J.-y.; Takeda, Y.; Kondow, T. *J. Phys. Chem. B* **2002**, *106*, 7575; (b) Sylvestre, J.-P.; Kabashin, A. V.; Sacher, E.; Meunier, M.; Luong, J. H. T. *J. Am. Chem. Soc.* **2004**, *126*, 7176; (c) Zeng, H.; Cai, W.; Li, Y.; Hu, J.; Liu, P. *J. Phys. Chem. B.* **2005**, *109*, 18260; (d) Amendola, V.; Polizzi, S.; Meneghetti, M. *J. Phys. Chem. B.* **2006**, *110*, 7232.
23. (a) Birtcher, R. C.; McCormick, A. W.; Baldo, P. M.; Toyoda, N.; Yamada, I.; Matsuo, J. *NIM Phys. Res. B* **2003**, *206*, 851; (b) Armelao, L.; Barreca, D.; Bottaro, G.; Gasparotto, A.; Tondello, E.; Ferroni, M.; Polizzi, S. *Chem. Mater.* **2004**, *16*, 3331; (c) Chung, B.-X.; Liu, C.-P. *Mater. Lett.* **2004**, *58*, 1437.
24. (a) Turkevitch, J.; Stevenson, P. C.; Hillier, J. *Discuss. Faraday Soc*. **1951**, *11*, 55; (b) Turkevich, J.; Kim, G. *J. Macromol. Sci. -Chem.* **1970**, *169*, 873; (c) Bönnemann, H.; Brijoux, W.; Brinkmann, R.; Fretzen, R.; Joussen, T.; Köppler, R.; Korall, B.; Neiteler, P.; Richter, J. *J. Mol. Catal.* **1994,** *86*, 129; (d) Mukherjee, P.; Ahmad, A.; Mandal, D.; Senapati, S.; Sainkar, S. R.; Khan, M. I.; Parishcha, R.; Ajaykumar, P. V.; Alam, M.; Kumar, R.; Sastry, M. *Nano Letters* **2001**, *1*, 515; (e) Shankar, S. S.; Ahmad, A.; Pasricha, R.; Sastry, M. *J. Mater. Chem.* **2003**, *13***,** 1822; (f) Shankar, S. S.; Ahmad, A.; Sastry, M. *Biotechnol. Prog.* **2003**, *19*, 1627; (g) Shankar, S. S.; Rai, A.; Ankamwar, B.; Singh, A.; Ahmad, A.; Sastry, M. *Nat. Mater.* **2004**, *3*, 482; (h) Burt, J. L.; Gutiérrez-Wing, C.; Miki-Yoshida, M.; José-Yacamán, M. *Langmuir* **2004**, *20*, 11778; (i) Chandran, S. P.; Chaudhary, M.; Pasricha, R.; Ahmad, A.; Sastry, M. *Biotechnol. Prog.* **2006**, *22*, 577.
25. (a) Hirai, H.; Nakao, Y.; Toshima, N. *J. Macromol. Sci. -Chem.* **1979,** *A13*, 727; (b) Wang, Y.; Ren, J.; Deng, K.; Gui, L.; Tang, Y. *Chem. Mater.* **2000,** *12*, 1622.
26. (a) Shah, P. S.; Hanrath, T.; Johnston, K. P.; Korgel, B. A. *J. Phys. Chem. B* **2004**, *108*, 9574; (b) Bhatt, A. I.; Mechler, Á.; Martina, L. L.; Bond, A. M. *J. Mater. Chem.* **2007**, *17*, 2241; (c) Zhu, J.; Shen, Y.; Xie, A.; Qiu, L.; Zhang, Q.; Zhang, S. *J. Phys. Chem. C* **2007**, *111,* 7629.
27. (a) Brust, M.; Walker, M.; Bethell, D.; Schiffrin, D. J.; Whyman, R. J. *J. Chem. Soc. Chem. Commun.* **1994**, 801; (b) Brust, M.; Fink, J.; Bethell, D.; Schiffrin, D. J.; Kiely, C. J. *J. Chem. Soc. Chem. Commun*. **1995**, 1655.
28. (a) Petit, C.; Lixon, P.; Pileni, M. P. *J. Phys. Chem.* **1993**, *9*, 12974; (b) Taleb, A.; Petit, C.; Pileni, M. P. *Chem. Mater.* **1997**, *9*, 950; (c) Wu, M.-L.; Chen, D.-H.; Huang, T.-C. *Langmuir* **2001,** *17,* 3877; (d) Xu, S.; Zhou, H.; Xu, J.; Li, Y. *Langmuir* **2002,** *18,* 10503; (e) Salzemann, C.; Brioude, A.; Pileni, M-P. *J. Phys. Chem. B* **2006,** *110,* 7208.
29. (a) Mayer, A. B. R.; Mark, J. E. *Pure Appl. Chem.* **1997**, *A34*, 2151; (b) Mayya, K. S.; Schoeler, B.; Caruso, F. *Adv. Funct. Mater.* **2003**, *13*, 183; (c) Choi, W. S.; Koo, H. Y.;

Park, J.-H.; Kim, D.-Y. *J. Am. Chem. Soc.* **2005***, 127*, 16136.

30. (a) Huang, H. H.; Ni, X. P.; Loy, G. L.; Chew, C. H.; Tan, K. L.; Loh, F. C.; Deng, J. F.; Xu, G. Q. *Langmuir* **1996,** *12,* 909; (b) Pastoriza-Santos, I,; Liz-Marzán, L. M. *Langmuir* **2002,** *18,* 2888; (c) Yin, B.; Ma, H.; Wang, S.; Chen, S. *J. Phys. Chem. B* **2003,** *107,* 8898; (d) Chen, M.; Xing, Y. *Langmuir* **2005,** *21,* 9334.
31. (a) Korchev, A. S.; Bozack, M. J.; Slaten, B. L.; Mills, G. *J. Am. Chem. Soc.* **2004**, *126*, 10; (b) Wu, W.-T.; Wang, Y.; Shi, L.; Pang, W.; Zhu, Q.; Xu, G.; Lu, F. *J. Phys. Chem. B* **2006**, *110,* 14702.
32. (a) Ziolo, R. F.; Giannelis, E. P.; Weinstein, B. A.; O'Horo, M. P.; Gamguly, B. N.; Mehrota, V.; Russel, M. W.; Huffman, D. R. *Science* **1992**, *257*, 219; (b) Jordan, R.; West, N.; Chou, Y.-M.; Nuyken, O. *Macromolecules* **2001**, *34*, 1606.
33. (a) Selvan, S. T.; Spatz, J. P.; Klock, H.-A.; Möller, M. *Adv. Mater*. **1998**, *10*, 132; (b) Southward, R. E.; Boggs, C. M.; Thompson, D. W.; St. Clair, A. K. *Chem. Mater.* **1998**, *10*, 1408; (c) Zhou, Y.; Yu, S.; Wang, C.; Zhu, Y.; Chen, Z. *Chem. Lett.* **1999**, 677; (d) Zhang, Z.; Han, M. *J. Mater. Chem.* **2003**, *13*, 641; (e) Korchev, A. S.; Bozack, M. J.; Slaten, B. L.; Mills, G. *J. Am. Chem. Soc.* **2004**, *126*, 10.
34. (a) Mbhele, Z. H.; Salemane, M. G.; van Sittert, C. G. C. E.; Nedeljkovic´, J. M.; Djokovic´, V.; Luyt, A. S. *Chem. Mater.* **2003**, *15*, 5019; (b) Feng, Q.; Dang, Z.; Li, N.; Cao, X. *Mater. Sci. Eng.* **2003**, *B99*, 325.
35. (a) Sayo, K.; Deki, S.; Hayashi, S. A. *Eur. Phys. J. D* **1999**, *9*, 429; (b) Heilmann, A. *Polymer Films with Embedded Metal Nanoparticles*; Springer-Verlag: New York, 2002.
36. (a) Lee, J.; Sundar, V. C.; Heine, J. R.; Bawendi, M. G.; Jensen, K. F. *Adv. Mater*. **2000**, *12*, 1102; (b) Teichroeb, J. H.; Forrest, J. A. *Phys. Rev. Lett.* **2003**, *91*, 016104; (c) Raula, J.; Shan, J.; Nuopponen, M.; Niskanen, A.; Jiang, H.; Kauppinen, E. I.; Tenhu, H. *Langmuir* **2003**, *19*, 3499.
37. (a) Bharathi, S.; Fishelson, N.; Lev, O. *Langmuir* **1999**, *15,* 1929; (b) Kobayashi, Y.; Correa-Duarte, M. A.; Liz-Marzán L. M. *Langmuir* **2001**, *17,* 6375*;* (c) Cheng, S.; Wei, Y.; Feng, Q.; Qiu, K.-Y.; Pang, J.-B.; Jansen, S. A.; Yin, R.; Ong, K. *Chem. Mater.* **2003,** *15,* 1560.
38. Warheit, D. B.; Laurence, B. R.; Reed, K. L.; Roach, D. H.; Reynolds, G. A. M.; Webb, T. R. *Toxicol. Sci.* **2004**, *77*, 117.
39. Murray, C. B.; Norris, D. J.; Bawendi, M. G. *J. Am. Chem. Soc.* **1993**, *115*, 8706.
40. (a) Potter, B. G.; Simmons, H. *Phys. Rev. B* **1991**, *43*, 2234; (b) Paula, A. M.; Barbosa, L. C.; Cruz, C. H. B.; Alves, O. L.; Sanjurjo, J. A.; Cesar, C. L. *Appl. Phys. Lett.* **1996**, *69*, 357; (c) Msumoto, Y.; Sonobe, K. *Phys. Rev. B* **1997**, *56*, 9734.
41. (a) Pileni, M. P. *J. Phys. Chem.* **1993**, *97*, 6961; (b) Pileni, M. P. *Langmuir* **1997**, *13*, 3266.
42. (a) Wang, Y.; Herron, N. *J. Phys. Chem.* **1987**, *91*, 257; (b) Cassagneau, T.; Hix, G. B.; Jones, D. J.; Maireles-Torres, P.; Rhomari, M.; Roziere, J. *J. Mater. Chem.* **1994**, *4*, 189; (c) Choi, K. M.; Shea, K. J. *J. Phys. Chem.* **1994**, *98*, 3207; (d) Moffitt, M.; Eisenberg, A. *Chem. Mater.* **1995**, *7*, 1178; (e) Urquhart, R. S.; Furlong, D. N.; Gengenbach, T.; Geddes, N. J.; Grieser, F. *Langmuir* **1995**, *11*, 1127; (f) Agger, J. R.; Anderson, M. W.; Pemble, M.

E.; Terasaki, O.; Nozue, Y. *J. Phys. Chem. B* **1998**, *101*, 3345.

43. (a) Zelner, M.; Minti, H.; Reisfeld, R. *Chem. Mater.* **1997**, *9,* 2541; (b) Kovtyukhova, N. I.; Buzaneva, E. V.; Waraksa, C. C.; Martin, B. R.; Mallouk, T. E. *Chem. Mater.* **2000**, *12,* 383.
44. (a) Zeng, D.; Hampden-smith, M. J. *Chem. Mater.* **1992**, *4*, 968; (b) Ding, J.; Mico, W. F.; McCormick, P. G.; Street, R. *Appl. Phys. Lett.* **1995**, *67*, 3804; (c) Ding, J.; Tsuzuki, T.; McCormick, P. G. *Nanostructure. Mater.* **1997**, *8*, 739.
45. (a) El-Shall, M. S.; Slack, W.; Vann, W.; Kane, D.; Hanely, D. *J. Phys. Chem.* **1994**, *98*, 3067; (b) Huh, M. Y.; Kim, S. H.; Ahn, J. P.; Park, J. K.; Kim, B. K. *Nanostructure. Mater.* **1999**, *11*, 211.
46. (a) Kodas, T. T. *Adv. Mater.* **1989**, *6*, 180; (b) Janackovic, D.; Jokanovic. V.; Kostic-Gvozdenovic, L.; Uskokovic, D. *Nanostructure. Mater.* **1998**, *10*, 341.
47. (a) Lindackers, D.; Janzen, C.; Rellinghaus, B.; Wassermann, E. F.; Roth, P. *Nanostructure. Mater.* **1998**, *10*, 1247; (b) Skanadan, G.; Chen, Y.-J.; Glumac, N.; Kear, B. H. *Nanostructure. Mater.* **1999**, *11*, 149.
48. (a) Herrig, H.; Hempelmann, R. *Mater. Lett.* **1996**, *27*, 287; (b) Wang, J.; Lee, S. E.; Ng, S. C.; Gan. L. M. *Mater. Lett.* **1997**, *30*, 119.
49. (a) Hench, L. L.; West, J. K. *Chem. Rev.* **1990**, *90*, 33; (b) Chandler, C. D.; Roger, C.; Hampden-smith, M. J. *Chem. Rev.* **1993**, *93*, 1205; (c) Avnir, D. *Acc. Chem. Res.* **1995**, *28*, 328.
50. (a) Rao, R. M.; Rao, K.; Prasada, A. V.; Komameni, S. *Mater. Lett.* **1996**, *1*, 463; (b) Qian, Z.; Shi, J. L. *Nanostructure. Mater.* **1998**, *10*, 235.
51. (a) Chang, R. P. H.; Lauerhaas, J. M.; Marks, T. J.; Pernisz, U. C. *U S Patent* 5962132, **1999**; (b) Needham, S. A.; Calka, A.; Wang, G.; Peleckis, G.; Liu, H. *J. Mater. Chem.* **2006**, *16*, 4488.
52. (a) Kim, F.; Song, J. H.; Yang, P. *J. Am. Chem. Soc.* **2002**, *124*, 14316; (b) Eustis, S.; El-Sayed, M. A. *Chem. Soc. Rev.* **2006**, *35*, 209.
53. Veinot, J. G. C. *Chem. Commun.* **2006**, 4160.
54. Li, L. S.; Hu, J. T.; Yang, W. D.; Alivisatos, A. P. *Nano Lett.* **2001**, *1*, 349.
55. Dabbousi, B. O.; Rodriguez-Viejo, J.; Mikulec, F. V.; Heine, J. R.; Mattoussi, H.; Ober, R.; Jensen, K. F.; Bawendi, M. G. *J. Phys. Chem. B* **1997**, *101,* 9463.
56. Liz-Marzán, L. M. *Materialstoday* **2004**, *7*, 26.
57. Jain, P. K.; El-Sayed, I. H.; El-Sayed, M. A. *Nanotoday* **2007**, *2*, 18.
58. (a) Mulvaney, P. *Langmuir* **1996,** *12,* 788; (b) Hohenester, U.; Krenn, J. *Phys. Rev. B* **2005**, *72*, 195429.
59. (a) Marcus, M. A.; Flood, W.; Stiegerwald, M.; Brus, L.; Bawendi, M. *J. Phys. Chem.* **1991**, *95*, 1572; (b) Brus, L. E.; Szajowski, P. F.; Wilson, W. L.; Harris, T. D.; Schuppler, S.; Citrin, P. H. *J. Am. Chem. Soc.* **1995**, *117*, 2915; (c) Chen, C. C.; Herhold, A. B.; Johnson, C. S.; Alivisatos, A. P. *Science* **1997**, *276*, 398; (d) Shim, M.; Guyot-Sionnest, P. *Phys. Rev. B* **2001**, *6424*, 245342.
60. (a) Johnson, S. R.; Evans, S. D.; Brydson, R. *Langmuir* **1998**, *14*, 6639; (b) Chen, S.;

Murray, R. W. *Langmuir* **1999**, *15*, 682; (c) Selvakannan, P. R.; Mandal, S.; Phadtare, S.; Pasricha, R.; Sastry, M. *Langmuir* **2003**, *19,* 3545; (d) Ganguli, M.; Jayachandran, K. N.; Maiti, S. *J. Am. Chem. Soc.* **2004**, *126*, 26.

61. (a) Kamat, P. V. *J. Phys. Chem. B* **2002**, *106,* 7729; (b) Narayanan, R.; El-Sayed, M. A. *J. Phys. Chem. B* **2005**, *109,* 12663.
62. Kamat, P. V. *Chem. Rev.* **1993**, *93*, 267.
63. (a) Bard, A. J. *J. Phys. Chem.* **1982**, *86*, 172; (b) Bard, A. J.; Fox, M. A. *Acc. Chem. Res.* **1995**, *28*, 141.
64. Youssef, K. M.; Scattergood, R. O.; Murty, K. L.; *App. Phys. Lett.* **2005**, *87*, 091904.
65. (a) Karch, J; Birringer, R; Gleiter, H. *Nature* **1987**, *330*, 556; (b) Hahn, H; Aberback, R. S. *J. Am. Ceram. Soc.* **1991**, *74*, 2918; (c) Yoshimura, M.; Ohji, T.; Sando, M.; Niihara, K. *Mat Res Innovat* **1998**, *2,* 83; (d) Koch, C. C.; Morris, D. G.; Lu, K. L.; Inoue, A. *Mater. Res. Bull.* **1999**, *24*, 54.
66. (a) Victora, R. H.; Falicov, L. M. *Phys. Rev. B* **1985**, *31*, 7335; (b) Khanna, S. N.; Linderoth, S. *Phys. Rev. Lett.* **1991**, *67*, 742; (c) Blugel, S. *Phys. Rev. Lett.* **1992**, *68*, 851; (d) Kosaka, W.; Tozawa, M.; Hashimoto, K.; Ohkoshi, S.-i. *Inorg. Chem. Commun.* **2006**, *9*, 920; (e) Mitra, S.; Mandal, K. *Mater. Manufac. Proc.* **2007**, *22*, 444; (f) Binns, C.; Baker, S. H.; Louch, S. *J. Mag. Mag. Mater.* **2007**, 312, 379.
67. (a) Shin, M.; Lee, S.; Park, K. W.; Lee, E.-H. *J. App. Phys.* **1998**, *84*, 2974; (b) Vorojtsov, S.; Baranger, H. U. *Phys. Rev. B* **2005**, *72*, 165349; (c) Sordan, R.; Balasubramanian, K.; Burghard, M.; Kern, K. *App. Phys. Lett.* **2005**, *87*, 013106.
68. (a) Malvezzi, A. M.; Allione, M.; Patrini, M.; Stella, A.; Cheyssac, P.; Kofman, R. *Phys. Rev. Lett.* **2002**, *89*, 087401; (b) McMahon, M. D.; Lopez, R.; Haglund, Jr. R. F. *Phys. Rev. B* **2006**, *73*, 041401.
69. Tsuboi, K. *App.Phys. Lett.* **2006**, *88*, 103102.
70. (a) Zhivkov, A. M.; Zande, B. M. I. v. d.; Stoylov, S. P. *Colloids and Surfaces A: Physicochem. Eng. Aspects* **2002**, *209*, 299; (b) Stoylov, S. P. *Colloids and Surfaces B: Biointerfaces* **2007**, *56*, 50.
71. (a) Pileni, M. P. *New J. Chem.* **1998**, *22*, 693; (b) Kelly, K. L.; Coronado, E.; Zhao, L. L.; Schatz, G. C. *J. Phys. Chem. B* **2003**, *107,* 668.
72. (a) Kim, Y.; Johnson, R. C.; Hupp, J. T. *Nano Lett.* **2001***, 1*, 165; (b) Obare, S. O.; Hollowell, R. E.; Murphy, C. J. *Langmuir* **2002**, *18,* 10407.
73. Chen, Y.; Aveyard, J.; Wilson, R., *Chem. Commun.* **2004**, 2804.
74. Evans, S. D.; Johnson, S. R.; Cheng, Y. L.; Shen T. *J. Mater. Chem.* **2000**, *10*, 183.
75. Favier, F.; Walter, E. C.; Zach, M. P.; Benter, T.; Penner, R. M. *Science* **2001**, *293*, 2227.
76. Franke, M. E; Koplin, T. J; Simon, U. *Small* **2006**, *2*, 36.
77. (a) Heerbeek, R. v.; Kamer, P. C. J.; Leeuwen, P. W. N. M. v.; Reek, J. N. H. *Chem. Rev.* **2002**, *102,* 3717; (b) Roucoux, A.; Schulz, J.; Patin, H. *Chem. Rev.* **2002**, *102,* 3757.
78. (a) Kidambi, S.; Bruening, M. L. *Chem. Mater.* **2005**, *17*, 301; (b) Vasylyev, M. V.; Maayan, G.; Hovav, Y.; Haimov, A.; Neumann, R. *Org. Lett.* **2006**, *8*, 5445; (c) Rossi, L.

M.; Silva, F. P.; Vono, L. L. R.; Kiyohara, P. K.; Duarte, E. L.; Itri, R.; Landers, R.; Machado, G. *Green Chemistry* **2007**, *9*, 379.

79. (a) Reetz, M. T.; Westermann, E. *Angew. Chem. Int. Ed.* **2000**, *39*, 165; (b) Li, Y.; El-Sayed, M. A. *J. Phys. Chem. B* **2001**, *105*, 8938; (c) Rahim, E. H.; Kamounah, F. S.; Frederiksen, J.; Christensen, J. B. *Nano Lett.* **2001**, *1*, 499; (d) Rocaboy, C.; Gladysz, J. A. *New J. Chem.* **2003**, *27*, 39; (e) Pittelkow, M.; Moth-Poulsen, K.; Boas, U.; Christensen, J. B. *Langmuir* **2003**, *19*, 7682; (f) Narayanan, R.; El-Sayed, M. A. *J. Phys. Chem. B* **2004**, *108*, 8572; (g) Garcia-Martinez, J. C.; Lezutekong, R.; Crooks, R. M. *J. Am. Chem. Soc*. **2005**, *127*, 5097; (g) Bhattacharya, S.; Srivastava, A.; Sengupta, S. *Tetrahedron Lett.* **2005**, *46*, 3557.

80. (a) Kogan, V.; Aizenshtat, Z.; Popovitz-Biro, R.; Neumann, R. *Org. Lett.* **2002**, *4*, 3529; (b) Kim, S. W.; Kim, M.; Lee, W. Y.; Hyeon, T. *J. Am. Chem. Soc*. **2002**, *124*, 7642; (c) Bedford, R. B.; Singh, U. G.; Walton, R. I.; Williams, R. T.; Davis, S. A. *Chem. Mater.* **2005***, 17*, 701; (d) Astruc, D.; Lu, F.; Aranzaes, J. R. *Angew. Chem. Int. Ed.* **2005**, *44*, 7852; (e) Wu, L.; Li, B.-L.; Huang, Y.-Y.; Zhou, H.-F.; He, Y.-M.; Fan, Q.-H. *Org. Lett.* **2006**, *8*, 3605; (f) Beletskaya, I. P.; Kashin, A. N.; Litvinov, A. E.; Tyurin, V. S.; Valetsky, P. M.; Koten, G. v. *Organometallics* **2006**, *25,* 154; (g) Cho, J. K.; Najman, R.; Dean, T. W.; Ichihara, O.; Muller, C.; Bradley, M.; *J. Am. Chem. Soc.* **2006**, *128*, 6276.

81. (a) Haruta, M.; Date, M. *Appl. Catal. A* **2001**, *222*, 427; (b) Bond, G. C. *Gold Bulletin* **2001**, *34*, 117; (c) Bulushev, D. A.; Yuranov, I;. Suvorova, E. I.; Buffat, P. A.; Kiwi-Minsker, L. *Journal of Catalysis* **2004**, *224*, 8.

82. (a) Scott, R. W. J.; Datye, A. K.; Crooks, R. M. *J. Am. Chem. Soc.* **2003**, *125*, 3708; (b) Scott, R. W. J.; Wilson, O. M.; Oh, S.-K.; Kenik, E. A.; Crooks, R. M. *J. Am. Chem. Soc.* **2004**, *126*, 15583.

83. Son, S. U.; Jang, Y.; Park, J.; Na, H. B.; Park, H. M.; Yun, H. J.; Lee, J.; Hyeon, T. *J. Am. Chem. Soc.* **2004**, *126*, 5026.

84. Ilisz, I.; Dombi, A.; Mogyorosi, K.; Dekany, I. *Colloids and Surfaces A: Physicochem. Eng. Aspects* **2004**, *230*, 89; (b) Zhu, H. Y.; Li, J.-Y.; Zhao, J.-C.; Churchman, G. J. *Applied Clay Science* **2005**, *28*, 79.

85. (a) Koper, O.; Lagadic, I.; Volodin, A.; Klabunde, K. J. *Chem. Mater.* **1992**, *4*, 323; (b) Koper, O. B.; Lagadic, I.; Volodin, A.; Klabunde, K. J. *Chem. Mater.* **1997**, *9,* 2468; (c) Klabunde, K. J.; Mohs, C. *Chemistry of Advanced Materials*, Interrante, L. V.; Hampden-Smith, M. J. (editors), Wiley-VCH, New York, 1998, Chap. 7. p. 317

86. Koch, C. C. *J. Mater. Sci.* **2007**, *42*, 1403.

87. (a) Naser, J.; Riehemann, W.; Ferkel, H. *Mater. Sci. Eng.* **1997**, *A234-236*, 467; (b) Pecharromán, C.; Esteban-Betegón, F.; Bartolomé, J. F.; Richter, G. ; Moya, J. S. *Nano Lett.* **2004***, 4*, 747; (c) Bandyopadhyaya, R.; Rong, W.; Friedlander, S. K. *Chem. Mater.* **2004**, *16,* 3147; (d) Hasan, M. M.; Zhou, Y.; Mahfuz, H.; Jeelani, S. *Mater. Sci. Eng.* **2006**, *A429*, 181; (e) Liff, S. M.; Kumar, N.; McKinley, G. H. *Nature Mater.* **2007**, *6*, 76.

88. Garcia, M.; Vliet, G. v.; Jain, S.; Schrauwen, B. A. G.; Sarkissov, A.; Zyl, W. E. v.; Boukamp, B. *Rev. Adv. Mater. Sci.* **2004**, 6, 169.

89. (a) Rong, W.; Pelling, A. E.; Ryan, A.; Gimzewski, J. K.; Friedlander, S. K.; *Nano Lett.* **2004**, *4*, 2287; (b) Rong, W.; Ding, W.; Ma1dler, L.; Ruoff, R. S.; Friedlander, S. K. *Nano Lett.* **2006**, *6*, 2646.
90. Horch, R. A.; Shahid, N.; Mistry, A. S.; Timmer, M. D.; Mikos, A. G.; Barron, A. R. *Biomacromolecules* **2004**, *5*, 1990.
91. (a) Menéndez, J. L.; Bescós, B.; Armelles, G.; Serna, R.; Gonzalo, J.; Doole, R.; Petford-Long, A. K; Alonso, M. I. *Phys. Rev. B* **2002**, *65*, 205413; (b) Shemer, G.; Markovich, G. *J. Phys. Chem. B* **2002**, *106*, 9195.
92. Fiete, G. A.; Zarand, G.; Halperin, B. I.; Oreg, Y. *Phys. Rev. B* **2002**, *66*, 024431.
93. Xu, X.; Friedman, G.; Humfeld, K. D.; Majetich, S. A.; Asher, S. A. *Chem. Mater.* **2002**, *14*, 1249.
94. Elliott, D. W.; Zhang, W.-X. *Environ. Sci. Technol.* **2001**, *35*, 4922
95. Ponder, S. M.; Darab, J. G.; Mallouk, T. E. *Environ. Sci. Technol.* **2000**, *34*, 2564.
96. (a) Pedro, T.; Maria del Puerto, M.; Sabino, V.-V.; Teresita, G.-C.; Carlos J., S. *J. Phys. D: Applied Physics* **2003**, *36*, R182; (b) Jurgons, R.; Seliger, C.; Hilpert, A.; Trahms, L.; Odenbach, S.; Alexiou, C. *J. Phys.: Condens. Matter* **2006**, *18*, S2893; (c) Yunpeng, B.; Bao, T.; Shizhen, C.; Yu, C.; Zhaolong, L. *Macromol.r Rapid Commun.* **2006**, *27*, 2107.
97. Bezryadin, A.; Dekker, C.; Schmid, G. *Appl. Phys. Lett.* **1997**, *71*, 1273.
98. Chi, L. F.; Hartig, M.; Drechsler, T.; Schwaack, T.; Seidel, C.; Fuchs, H; Schmid, G. *Appl. Phys. A.*, **1998**, *A66*, 187.
99. Barnes, W. L.; Dereux, A.; Ebbesen, T. W. *Nature* **2003**, *424*, 824.
100. (a) Inouye, H.; Tanaka, K.; Tanahashi, I.; Hattori, T.; Nakatsuka, H. *Jpn. J. Appl. Phys.* **2000,** *39*, 5132; (b) Venkatram, N.; Kumar, R. S. S.; Rao, D. N.; Medda, S. K.; De, S.; De, G. *J. Nanosci. Nanotechnol.* **2006**, *6*, 1990.
101. Salata, O. V. *J. Nanobiotechnol.* **2003**, *2*, 3.
102. Whitesides, G. M. *Nat. Biotechnol.* **2003**, *21*, 1161.
103. Katz, E.; Willner, I. *Angew. Chem. Int. Ed.* **2004**, 43, 6042.
104. Psciotti, G. *Drug Delivery* **2004**, *11*, 169.
105. Suh, J.; Wirtz, D.; Hanes, J. *Proc. Natl. Acad. Sci. USA* **2003**, *100*, 3878.
106. Berry, C. C.; Dalby, M. J.; McCloy, D.; Affrossman, S. *Biomaterials* **2005**, *26*, 4985.
107. Bailey, R. C.; Nam, J.-M.; Mirkin, C. A.; Hupp J. T. *J. Am. Chem. Soc.* **2003**, *125*, 13541.
108. (a) Alivisaos, P. *Nat. Biotechnol* **2004**, *22*, 47; (b) Haes, A. J.; Hall, W. P.; Chang, L.; Klein, W. L.; Duyne, R. P. V. *Nano Lett.* **2004**, *4*, 1029; (c) Rosi, N. L.; Mirkin, C. A. *Chem. Rev.* **2005**, *105*, 1547.
109. (a) Wang, Y.; Xie, X.; Wang, X.; Ku, G.; Gill, K. L.; O'Neal, D. P.; Stoica, G.; Wang, L. V. *Nano Lett.* **2004**, *4*, 1689; (b) El-Sayed, I. H.; Huang, X.; El-Sayed, M. A. *Nano Lett.* **2005**, *5*, 829.
110. Court, E. B.; Daar, A. S.; Persad, D. L.; Salamanca-Buentello, F.; Singer, P. A. *Materialstoday* **2005**, *8*, 14.
111. Hagan, D. J.; Van Stryland, E. W.; Wu, Y. Y.; Wei, T. H.; Sheik-Bahae, M.; Said, A.; Mansour, K.; Young, J.; Soileau, M. J. *Materials for Optical Switches, Isolators, and*

Limiters; Proceedings of SPIE, Vol. 1105; SPIE: Bellingham, WA, 1989; p 103.
112. Van Stryland, E. W.; Soileau, M. J.; Ross, S.; Hagan, D. J. *Nonlinear Optics* **1999**, *21*, 29.
113. Tutt, L. W.; Boggess, T. F. *Prog. Quant. Elcetron.* **1993**, *17*, 299.
114. (a) Boggess, T. F.; Moss, S. C.; Boyd, I. W.; Smirl, A. L. *Opt. Lett*. **1984**, *9*, 291; (b) Ji, W.; Kukaswadia, A. K.; Feng, Z. C.; Tang, S. H. *J. Appl. Phys.* **1994**, *75*, 3340.
115. He, G .S.; Liu, S. H. *Physics of Nonlinear Optics*, World Scientific Publishing Co. Pte. Ltd.: Singapore, 1999.
116. Sutherland, R. L. *Handbook of Nonlinear Optics*, Marcel Dekker Inc.: New York, 1996.
117. (a) Khoo, I. C.; Michael, R. R.; Finn, G. M. *Appl. Phys. Lett.* **1988**, *52*, 2108; (b) Tian, J.-G.; Zhang, C.; Zhang, G.; Li, J. *App. Opt.* **1993**, *32*, 6628.
118. (a) Reddy, K. P. J. *Curr. Sci.* **1991**, *61*, 520; (b) Kim, S.; McLaughlin, D.; Potasek, M. *Phys. Rev. A* **2000**, *61*, 025801; (c) Lepkowicz, R.; Koyakov, A.; Hagan, D. J.; Strylabd, E. W. V. *J. Opt. Soc. Am. B* **2002**, *19*, 94.
119. Wood, G. L.; Mott, A. G.; Sharp, E. J. *Proc. SPIE* **1992**, *2*, 1692; (b) Hollins, R. C. *Nonlinear Optics*, **2001**, *27*, 1.
120. (a) Lawson, C. M.; Euliss, G. W.; Michael, R. R. *Appl. Phys. Lett.* **1991**, *58*, 2195; (b) Micheal, R. R.; Lawson, C. M. *Opt. Lett.* **1992**, *17*, 1055; (c) Durand, O.; Grolier-Mazza, V.; Frey, R. *Opt. Lett.* **1998**, *23*, 1471; (d) Fougeanet, F.; Riehl, D. *Nonlin. Opt.* **1999**, *21*, 435; (e) Hernandez, F. E.; Shensky, W.; Cohanoschi, I.; Hagan, D. J.; Strylabd, E. W. V. *Appl. Opt.* **2002**, *41*, 1103.
121. (a) Messier, J.; Kajzar, F.; Prasad, P. *Organic molecules for Nonlinear Optics and Phtotonics*, Series E, applied Science, Vol 194, Kluwer Academic Publishers: New York, 1991; (b) Shirk, J. S.; Pong, R. G. S.; Bartoli, F. J.; Snow, A. W. *Appl. Phys. Lett.* **1993**, *63*, 1880.
122. Kiran, P. P.; Srinivas, N. K. M. N.; Reddy, D. R.; Maiya, B. G.; Sandhu, A. S.; Dharmadhikari, A.; Kumar, G .R.; Rao, D. N. *Opt. Commun.* **2002**, *202*, 347.
123. (a) Taheri, B.; Liu, H.; Jassemnejad, B.; Appling, D.; Powell, R. C.; Song, J. J. *Appl. Phys. Lett.* **1996,** *68*, 1317; (b) Sun, Y-P.; Riggs, J. E.; Liu, B. *Chem. Mater.* **1997,** *9*, 1268; (c) Ma, B.; Riggs, J. E.; Sun, Y.-P. *J. Phys. Chem. B* **1998**, *102*, 5999.
124. (a) Khoo, I. C.; Wood, M. V.; Lee, M.; Guenther, B. D. *Opt. Lett.* **1996**, *21*, 1625; (b) Ono, H.; Kawatsuki, N. *Opt. Commun.* **1997**, *139*, 60.
125. Rao, D. N.; Yelleswarapu, C. S.; Kothapalli, S. R.; Rao, D. V. G. L. N. *Optics Express* **2003**, *11*, 2848.
126. Rao, D. N.; Kiran, P. P. *Nonlinear Optics* **2001**, *27*, 347.
127. Scalora, M.; Dowling, J. P.; Bowden, C. M.; Blemer, M. J. *Phys. Rev. Lett.* **1994**, *73*, 1368.
128. (a) Bentivegna, F.; Canve, M.; Georges, P.; Brun, A.; Chaput, F.; Malier, L.; Boilot, J. C. *Appl. Phys. Lett.* **1993**, *62*, 1721; (b) Schell, J.; Brinkmann, D.; Ohlmann, D.; Honerlage, B.; Levy, R.; Joucia, M.; Rehspringer, J. L.; Serughetti, J.; Bovier, C. *J. Chem. Phys.* **1998**, *108*, 8599.
129. Bindra, K. S.; Oak, S. M.; Rustagi, K. C. *Opt. Commun.* **1996**, *124*, 452.
130. Fischer, G. L.; Boyd, R. W.; Moore, T. R.; Sipe, J. E. *Opt. Lett.* **1996**, *21*, 1643.

131. (a) Shi, S.; Ji, W.; Tang, S. H.; Lang, J. P.; Xin, X. Q. *J. Am. Chem. Soc.* **1994**, *116*, 3615; (b) Low, M. K. M.; Hou, H.; Zheng, H.; Wong, W.; Jin, G.; Xin, X.; Ji, W. *Chem. Commun.* **1998**, 505.

132. (a) Herbert, C. J.; Cpinski, W. S.; Malcuit, M. S. *Opt. Lett.* **1992**, *17*, 1037; (b) Kahn, L. M. *Phys. Rev. B* **1996**, *53*, 1429.

133. (a) Sun, X.; Yu, R. Q.; Xu, G. Q.; Hor, T. S. A.; Ji, W. *Appl. Phys. Lett.* **1998**, *73*, 3632; (b) Sun, Y.-P.; Riggs, J. E.; Henbest, K. B.; Martin, R. B. *J. Nonlinear Opt. Phy. & Mater.* **2000**, *9*, 481; (c) Venkatram, N.; Rao, D. N.; Akundi, M. A.; *Opt. Express* **2005**, *13*, 867; (d) Venkatram, N.; Kumar, R. S. S.; Rao, D. N. *J. App. Phys.* **2006**, *100*, 074309.

134. (a) Qu, S.; Zhao, C.; Jiang, X.; Fang, G.; Gao, Y.; Zeng, H.; Song, Y.; Qiu, J.; Zhu, C.; Hirao, K. *Chem. Phys. Lett.* **2003**, *368*, 352; (b) Shen, H.; Cheng, B. L.; Lu, G. W.; Guan, D. Y.; Chen, Z. H.; Yang, G. Z. *J. Phys. D: Appl. Phys.* **2006**, *39*, 233; (c) Martin, R. B.; Meziani, M. J.; Pathak, P.; Riggs, J. E.; Cook, D. E.; Perera, S.; Sun, Y.-P. *Opt. Mater.* **2007**, *29*, 788.

135. (a) He, J.; Mi, J.; Li, H.; Ji, W. *J. Phys. Chem. B* **2005**, *109*, *41*, 19184; (b) Gong, H.-M.; Wang, X.-H.; Du, Y.-M.; Wang, Q.-Q. *J. Chem. Phys.* **2006**, *125*, 024707.

136. (a) Kyoung, M.; Lee, M. *Opt. Comm.* **1999**, *171*, 145; (b) Elim, H. I.; Yang, J.; Lee, J.-Y. *Appl. Phys. Lett.* **2006**, *88*, 083107; (c) Liu, T.-M.; Tai, S.-P.; Yu, C.-H.; Wen, Y.-C.; Chu, S.-W. *Appl. Phys. Lett.* **2006**, *89*, 043122.

137. Neto, N. M. B.; Mendonca, C. R.; Misoguti, L.; Zilio, S. C. *Appl. Phys. B* **2004**, *78*, 1.

138. (a) Kamanina, N.; Putilin, S.; Stasel'ko, D. *Synth. Metals* **2002**, *127*, 129; (b) Tong, R.; Wu, H.; Li, B.; Zhu, R.; You, G.; Qian, S.; Lin, Y.; Cai, R. *Physica B* **2005**, *366*, 192.

139. Vestberg, R.; Westlund, R.; Eriksson, A.; Lopes, C.; Carlsson, M.; Eliasson, B.; Glimsdal, E.; Lindgren, M.; Malmström, E. *Macromolecules* **2006**, *39*, 2238.

140. (a) Murray, R. G. E.; Steed, P; Elson, H. E. *Can. J. Microbiol.* **1965**, *11*, 547; (b) Shockman, G. D.; Barret, J. F. *Annu. Rev. Microbiol.* **1983**, *37*, 501.

141. Kyriacou, S. V.; Brownlow, W. J.; Xu, X.-H. N. *Biochemistry* **2004**, *43*, 140.

142. (a) Tashiro, T. *Macromol. Mater. Eng.* **2001**, *286*, 63; (b) Ilker, M. F.; Nüsslein, K.; Tew, G. N.; Coughlin, B. E. *J. Am. Chem. Soc.* **2004**, *126*, 15870; (c) Lee, S. B.; Koepsel, R. R.; Morley, S. W.; Matyjaszewski, K.; Sun, Y.; Russell, A. J. *Biomacromolecules* **2004**, *5*, 877; (d) Ilker, M. F.; Schule, H.; Coughlin, E. B. *Macromolecules* **2004**, *37*, 694; (e) Dizman, B.; Elasri, M. O.; Mathias, L. *J. Appl. Polym. Sci.* **2004**, *94*, 635; (f) Kuroda, K.; DeGrado, W. F. *J. Am. Chem. Soc.* **2005**, *127*, 4128; (g) Alasino, R. V.; Ausar, S. F.; Bianco, I. D.; Castagna, L. F.; Contigiani, M.; Beltramo, D. M. *Macromol. Biosci.* **2005**, *5*, 207.

143. (a) Liu, D.; DeGrado W. F. *J. Am. Chem. Soc.* **2001**, *123*, 7553; (b) Tew, G. N.; Liu, D.; Chen, Bi.; Doerksen, R. J.; Kaplan, J.; Carroll, P. J.; Klein, M. L.; DeGrado, W. F. *Proc. Natl. Acad. Sci. U.S.A.* **2002**, *99*, 5110; (c) Tang, H.; Doerksen, R. J.; Tew, G. N. *Chem. Commun.* **2005**, *12*, 1537.

144. (a) Desai, N. P.; Hossainy, S. F.; Hubbell, J. A. *Biomaterials* **1992**, *12*, 417; (b) Lin, J.; Murthy, S. K.; Olsen, B. D.; Gleason, K. K.; Klibanov, A. M. *Biotechnol. Lett.* **2003**, *25*, 1661; (c) Ignatova, M.; Voccia, S.; Gilbert, B.; Markova, N.; Cossement, D.; Gouttebaron,

R.; Jerome, R.; Jerome, C. *Langmuir* **2006**, *22*, 255.

145. (a) Tsukada, M.; Arai, T.; Colonna, G. M.; Boschi, A.; Freddi, G. *J. Appl. Polym. Sci.* **2003**, *89*, 638; (b) Ho, C. H.; Tobis, J.; Christina, S.; Thoman R.; Tiller, J. C. *Adv. Mater.* **2004**, *16*, 957; (c) Cioffi, N.; Torsi, L.; Ditaranto, N.; Tantillo, G.; Ghibelli, L.; Sabbatini, L.; Bleve-Zacheo, T.; D'Alessio, M.; Zambonin, P. G.; Traversa, E. *Chem. Mater.* **2005**, *17*, 5255; (d) Weickmann, H.; Tiller, J. C.; Thomann, R.; Muelhaupt, R. *Macromol. Mater. Eng.* **2005**, *290*, 875; (e) McDonnell, A. M. P.; Beving, D.; Wang, A.; Chen, W.; Yan, Y. *Adv. Funct. Mater.* **2005**, *15*, 336.

146. (a) Kohnen, W.; Kolbenschlag, C.; Keiser, S. T.; Jansen, B. *Biomaterials* **2003**, *24*, 4865; (b) Changez, M.; Koul, V.; Dinda, A. *Biomaterials* **2004**, *26*, 2095; (c) Maeyama, R.; Kwon, I. K.; Mizunoe, Y.; Anderson, J. M.; Tanaka, M.; Matsuda, T. *J. Biomed. Mater. Res.* **2005**, *75A*, 146; (d) Dizman, B.; Elasri, M. O.; Mathias, L. J. *Biomacromolecules* **2005**, *6*, 514.

147. (a) Gerrard, J. J.; Annable, J. A.; Moore, J. *Surf. Coat. Int., Part B* **2005**, *88*, 83; (b) Iconomopoulou, S. M.; Voyiatzis, G. A. *J. Controlled Release* **2005**, *103*, 451.

148. (a) Sun, Y.; Sun, G. *Macromolecules* **2002**, *35*, 8909; (b) Chen, Y.; Worley, S. D.; Kim, J.; Wei, C. I.; Chen, T. Y.; Santiago, J. I.; Williams, J. F.; Sun, G. *Ind. Eng. Chem. Res.* **2003**, *42*, 280; (c) Sun, Y.; Sun, G. *Ind. Eng. Chem. Res.* **2004**, *43*, 5015.

149. (a) Friedenthal, H. *Biochem. Z.*, **1919**, *94*, 47; (b) Feng, Q. L.; Wu, J.; Chen, G. Q.; Cui, F. Z.; Kim, T. N.; Kim, J. O. *J. Biomed. Mater. Res.* **2000**, *52*, 662.

150. (a) Hollinger, M. A. *Crit. Rev. Toxicol.* **1996**, *26*, 255; (b) Gosheger, G.; Hardes, J.; Ahrens, H.; Streitburger, A.; Buerger, H.; Erren, M.; Gunsel, A.; Kemper, F. H.; Winkelmann, W.; von Eiff, C. *Biomaterials* **2004**, *25*, 5547.

151. (b) Brady, M. J.; Lisay, C. M.; Yurkovetskiy, A. V.; Sawan, S. P. *Am. J. Infect. Control* **2003**, *31*, 208; (b) Percival, S. L.; Bowler, P. G.; Russell, D. *J. Hosp. Infect.* **2005**, *60*, 1.

152. (a) Butkus, M. A.; Edling, L.; Labare, M. P. *J. Water Supply Res. Technol-Aqua* **2003**, *52*, 407; (b) Chen, S. P.; Wu, G. Z.; Zeng, H. Y. *Carbohydr. Polym.* **2005**, *60*, 33.

153. (a) Zhang, L. Z.; Yu, J. C.; Yip, H. Y.; Li, Q.; Kwong, K. W.; Xu A. W.; Wong, P. K. *Langmuir* **2003**, *19*, 10372; (b) Park, S. J.; Jang, Y. S. *J. Colloid Interface Sci.* **2003**, *261*, 238; (c) Lee, D.; Cohen, R. E.; Rubner, M. F. *Langmuir* **2005**, *21*, 9651; (d) Taylor, P. L.; Ussher A. L.; Burrell, R. E. *Biomaterials* **2005**, *26*, 7221; (e) Shanmugam, S.; Viswanathan, B.; Varadarajan, T. K. *Mater. Chem. Phys.* **2006**, *95*, 51.

154. (a) Ulkur, E.; Oncul, O.; Karagoz, H.; Yeniz, E.; Celikoz, B. *Burns* **2005**, *31*, 874; (b) Parikh, D. V.; Fink, T.; Rajasekharan, K.; Sachinvala, N. D.; Sawhney A. P. S.; Calamari, T. A.; Parikh, A. D. *Text. Res. J.* **2005**, *75*, 134.

155. Alt, V.; Bechert, T.; Steinrücke, P.; Wagener, M.; Seidel, P.; Dingeldein, E.; Domann, U.; Schnettler, R. *Biomaterials* **2004**, *25*, 4383.

156. Gosheger, G.; Hardes, J.; Ahrens, H.; Streitburger, A.; Buerger, H.; Erren, M.; Gunsel, A.; Kemper, F. H.; Winkelmann, W.; Eiff, Ch. *Biomaterials* **2004**, *25*, 5547.

157. (a) Rupp, M. E.; Fitzgerald, T.; Marion, N.; Helget, V.; Puumala, S.; Anderson, J. R.; Fey, P. D. *Am. J. Infect. Control* **2004**, *32*, 445; (b) Samuel, U.; Guggenbichler, J. P. *Int. J.*

Antimicrob. Agents **2004**, *23S1*, S75.
158. Strathmann, M.; Wingender, J. *Int. J. Antimicrob. Agents* **2004**, *24*, 36.
159. Ohashi, S.; Saku, S.; Yamamoto, K. *J. Oral Rehabil.* **2004**, *31*, 364.
160. Bosetti. M.; Masse`, A.; Tobin, E.; Cannas, M. *Biomaterials* **2002**, *23*, 887.
161. (a) Gauger, A.; Mempel, M.; Schekatz, A.; Schafer, T.; Ring, J.; Abeck, D. *Dermatology* **2003**, *207*, 15; (b) Lee, H. J.; Jeong, S. H. *Text. Res. J.* **2005**, *75*, 551.
162. (a) Yuranova, T.; Rincon, A. G.; Bozzi, A.; Parra, S.; Pulgarin, C.; Albers, P.; Kiwi, J. *J. Photochem. Photobiol. A* **2003**, *161*, 27; (b) Jeong, S. H.; Yeo, S. Y.; Yi, S. C. *J. Mater. Sci.* **2005**, *40*, 5407.
163. Chou, W.-L.; Yu, D.-G.; Yang, M.-C. *Polym. Adv. Technol.* **2005**, *16*, 600.
164. (a) Klueh, U.; Wagner, V.; Kelly, S.; Johnson, A.; Bryers, J. D. *J. Biomed. Mater. Res.* **2000,** *53,* 621; (b) Sun, R. W.-Y.; Chen, R.; Chung, N. P.-Y.; Ho, C.-M.; Lin, C.-L. S.; Che, C.- M. *Chem. Commun.* **2005**, 5059; (c) Tian, J.; Wong, K. K. Y.; Ho, C.-M.; Lok, C.-N.; Yu, W.-Y.; Che, C.-M.; Chiu, J.-F.; Tam, P. K. H. *ChemMedChem* **2006**, *2*, 129.
165. Morones, J. R.; Elechiguerra, J. L.; Camacho, A.; Holt, K.; Kouri, J. B.; Ramírez, J. T.; Yacaman, M. J. *Nanotechnology* **2005**, *16*, 2346.
166. Baker, C.; Pradhan, A.; Pakstis, L.; Pochan, D. J.; Shah, S. I. *J. Nanosci. Nanotechnol.* **2005**, *5*, 244.
167. (a) Aymonier, C.; Schlotterbeck, U.; Antonietti, L.; Zacharias, P.; Thomann, R.; Tiller, J. C.; Mecking, S. *Chem. Commun.* **2002**, 3018; (b) Jeong, S. H.; Hwang, Y. H.; Yi, S. C. *J. Mater. Sci.* **2005**, *40*, 5413; (c) Zeng, F.; Hou, C.; Wu, S.; Liu, X.; Tong, Z.; Yu, S. *Nanotechnology* **2007**, *18*, 055605.
168. Sondi, I.; Salopek-Sondi, B. *J. Colloid Interface Sci.* **2004**, *275*, 177.
169. Gogoi, S. K.; Gopinath, P.; Paul, A.; Ramesh, A.; Ghosh, S. S.; Chattopadhyay, A. *Langmuir* **2006***, 22,* 9322.
170. (a) Kim, J.-W.; Lee, J.-E.; Ryu, J.-H.; Lee, J.-S.; Kim, S.-J.; Han, S.-H.; Chang, I.-S.; Kang, H.-H.; Suh, K.-D. *J. Polym. Sci.: Part A: Polym. Chem.* **2004**, *42*, 2551; (b) Kumar, R.; Howdle, S.; Münstedt, H. *J. Biomed. Mater. Res.* **2005,** *75B*, 311; (c) Hong, K. H.; Park, J. L.; Sul, I. H.; Youk, J. H.; Kang, T. J. *J. Polym. Sci.: Part B: Polym. Phys.* **2006**, *44*, 2468; (d) Li, Z.; Lee, D.; Sheng, X.; Cohen, R. E.; Rubner, M. F. *Langmuir* **2006**, *22,* 9820; (e) Yu, H.; Xu, X.; Chen, X.; Lu, T.; Zhang, P.; Jing, X. *J. Appl. Polym. Sci.* **2007**, *103*, 125.
171. Jain, P.; Pradeep, T.; *Biotech. Bioengg.* **2005**, *90*, 59.
172. Chou, W.-L.; Yu, D.-G.; Yang, M.-C. *Polym. Adv. Technol.* **2005,** *16,* 600.
173. (a) Lee, H. J.; Yeo, S. Y.; Jeong, S. H. *J. Mater. Sci.* **2003**, *38*, 2199; (b) Tarimala, S.; Kothari, N.; Abidi, N.; Hequet, E.; Fralick, J.; Dai, L. L. *J. App. Polym. Sci.* **2006**, *101*, 2938.
174. Sun, R. W.-Y.; Chen, R.; Chung, N. P.-Y.; Ho, C.-M.; Lin, C.-L. S.; Che, C.-M. *Chem. Comm.* **2005**, *40*, 5059.

Scope

We present in this chapter, our investigations of silver nanoparticles generated in situ inside poly(vinyl alcohol) film through thermal treatment, the polymer serving simultaneously as the reducing agent and stabilizer for the nanoparticle formation. A simple and efficient protocol for the fabrication of free-standing films is also demonstrated. Spectroscopy and microscopy studies show that the silver/polymer ratio and the time and temperature of thermal treatment can be used effectively to fine-tune the size and density of nanoparticles in these composite films. Homogeneous and narrow distributions around small particle sizes (2 - 3 nm) can be achieved under optimal conditions. Nonlinear optical studies using Z-scan measurements indicate that these nanoparticle-embedded polymer films are potentially efficient optical limiters. Bactericidal application of reusable silver nanoparticle-polymer composite films is also presented in this chapter.

2.1. Introduction

Synthesis and assembly of nanoparticles are central themes in nanomaterials science and technology. Environment-friendly procedures are highly desirable[1] and methods which allow control of particle size and shape are extremely useful. Even though metal nanoparticles are often synthesized in colloidal solutions,[2] their solid composites in polymer or glassy matrices are in demand in various device applications.[3,4] The common approaches to such materials include casting of films from a mixture of preformed nanoparticles and polymer,[5] plasma deposition techniques[6] and *in situ* growth.[3, 7, 8] The latter mode of synthesis inside solid matrices is of interest in the context of the current debate on potential health hazards of inhalable nanoparticles.[9] Free-standing thin films are useful for device applications, and have been fabricated at the air-water interface[10] and through layer-by-layer assembly;[11] however, preformed nanoparticles were used in both cases. The methodology we have developed combines the advantages of the chemical reduction route to metal nanoparticles, environment-friendly reagents and the stabilization of the particles in a polymer matrix, in the fabrication of silver nanoparticle-embedded polyvinyl alcohol (PVA) films. Optimal concentrations and thermal treatment for short periods of time are shown to lead to a homogeneous *in situ* generation of 2 - 3 nm diameter particles. A simple procedure involving a sacrificial layer[12] of polystyrene (PS) is used to obtain free-standing Ag-

PVA films. This strategy facilitated the monitoring of particle size directly in a TEM, without the need for microtoming. To the best of our knowledge, ours was the first report of *in situ* fabrication leading to free-standing polymer film incorporating silver nanoparticles. Further, the small sizes and narrow distributions achieved under such mild conditions and short processing time are very significant. Our methodology opens up a wide range of possibilities in terms of the choice of metals, polymers and particle growth conditions and the feasibility of further mechanical or optical manipulations.[13] We have investigated the optical limiting capability of these nanoparticle-embedded polymer films in the nanosecond and femtosecond regimes. In addition, we have found that the Ag-PVA films can be used as an efficient bactericidal agent, in repeated action cycles. The reusable films could be monitored using spectroscopy and microscopy to investigate possible changes after bactericidal action.

2.2. A New Fabrication Protocol

The steps involved in the fabrication are shown in Fig. 2.1. The procedure used to prepare films, with different Ag/PVA weight ratios, x is as follows. 5.3 mg or 8.1 mg or 10.8 mg of silver nitrate ($AgNO_3$) dissolved in 0.5 ml water was mixed with a solution of 120 mg of poly(vinyl alcohol), PVA (Fluka, average molecular weight, M_w = 15 kDa, % hydrolysis = 87-89) in 0.6 ml water to prepare the three different compositions, x = 0.028, 0.042 and 0.058. In each case, the solution mixture was diluted by adding 2.0 ml more of water and stirred for 10 min at room temperature (27 - 30^oC). The solution was always protected from light. Millipore purified water was used in all operations.

Glass/quartz plates were cleaned by sonication in isopropyl alcohol, methanol and finally acetone for 10 min each. A few drops of a solution of polystyrene, PS (M_w = 280 kDa) in toluene (1 g in 8 ml) was spin coated on the glass substrate using a standard photoresist spinner at 1,000 RPM for 10 sec. Two such layers were coated in succession and the coated plate was air-dried. On top of the polystyrene coating, the $AgNO_3$-PVA solution was spin coated at 6,000 RPM for 10 sec. A second layer was coated similarly. Alternately, the $AgNO_3$-PVA solution was spin coated directly on quartz substrates without the polystyrene film, and used for optical studies.

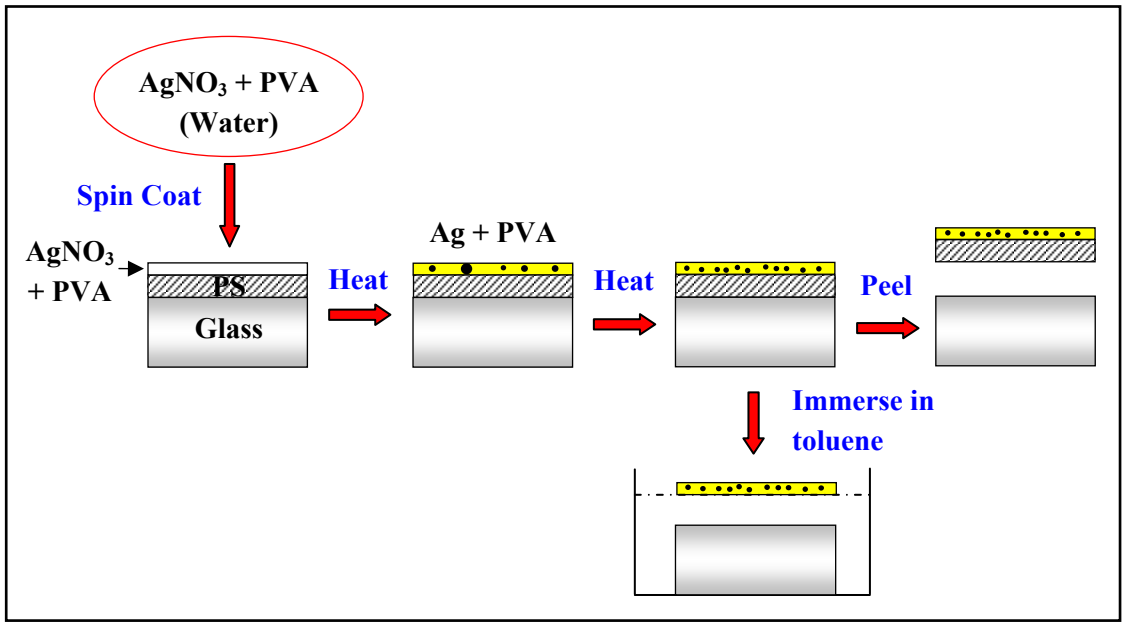

Figure 2.1. *Schematic representation of the fabrication procedure for Ag-PVA and Ag-PVA/PS films.*

Since the thermal properties of the polymers are relevant for the in situ nanoparticle synthesis, we have examined them using differential scanning calorimetry (DSC). PVA film showed a glass transition with onset at 92°C and melting transition with peak at 191°C; these are consistent with values expected for partially hydrolyzed PVA (Fig. 2.2a).[14] The thermal behavior of PVA is retained in PVA/PS film; pure PS shows melting peak at 209°C (Fig. 2.2b). These data suggest that the PVA film is likely to be in a soft (but not molten) state during the thermal treatment carried out for the formation of metal nanoparticles in the temperature range of 50 - 150°C, as described below.

Silver nanoparticles were generated *in situ,* inside the polymer film by heating the $AgNO_3$-PVA films in a hot air oven under ambient atmosphere. Different conditions of heat treatment were explored with temperatures, T = 50 - 110°C and times, t = 5 - 60 min. PVA acts simultaneously as the reducing agent,[15] stabilizer for the nanoparticles and the matrix for homogeneous distribution and immobilization. The films obtained are fully transparent with no visible coloration; however when larger amounts of silver are involved, the films appear yellow. Interestingly, the photostability

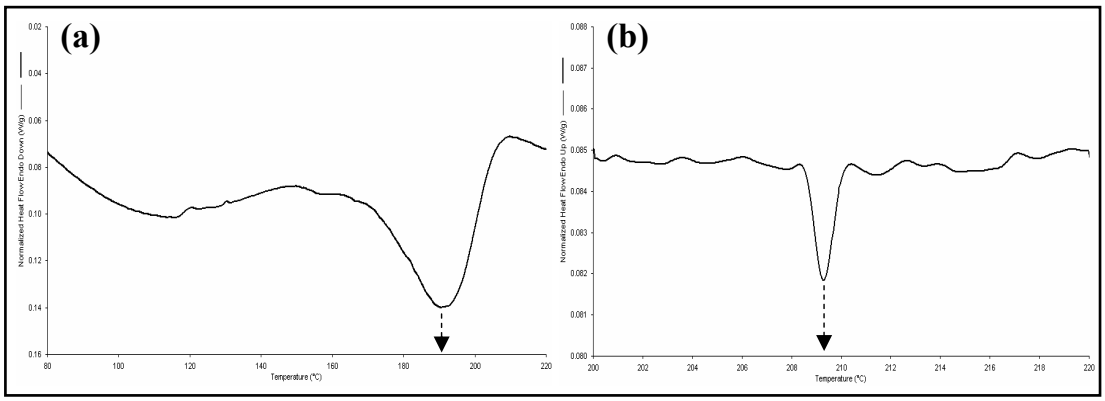

Figure 2.2. *Differential scanning calorimetry (DSC) plots of (a) PVA film (scan rate = 10°C/min) and (b) PS (scan rate = 3°/min) used in the nanoparticle-polymer composite fabrication.*

of $AgNO_3$-PVA and Ag-PVA films are considerably enhanced with respect to that of colloidal mixtures of $AgNO_3$ and PVA. After the thermal treatment, the Ag-PVA/PS on glass could be peeled off to give free-standing films. Alternately, the glass substrate with Ag-PVA/PS was immersed in toluene whereupon the PS layer dissolved and the floating freestanding Ag-PVA film could be isolated (inset of Fig. 2.3). The thickness of the individual layers was examined by SEM imaging of the cross section image of the Ag-PVA/PS film. The film was sandwiched between two glass plates and held vertically to examine the cross section. The thickness of the PS and PVA layers are ~ 3 - 6 μm and 400 - 500 nm respectively as seen from the SEM image (Fig. 2.3). EDXS was used to confirm the presence of silver in the Ag-PVA layer.

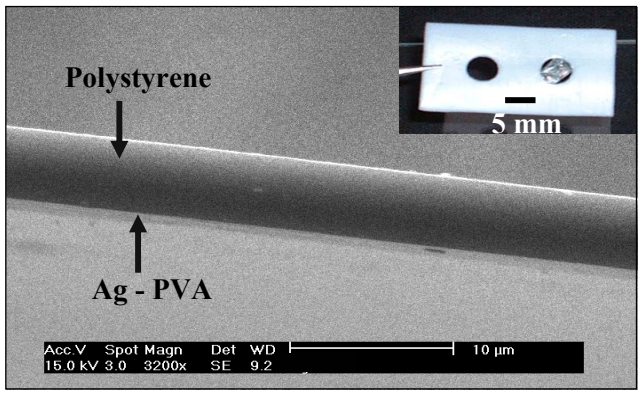

Figure 2.3. *SEM image of the cross-section of Ag-PVA/PS film. Inset shows the Ag-PVA free-standing film on a teflon support; the empty hole shows the contrast.*

2.3. Size Tuning of the Nanoparticles

We envisaged that the Ag/PVA ratio, x as well as the temperature and time of thermal treatment would have significant influence on the size and size distribution of the silver nanoparticles formed inside the polymer films. As noted in the fabrication procedure, these parameters were varied and the films obtained were investigated using spectroscopy and microscopy to observe the size variation of silver nanoparticles inside the polymer films.

Absorption spectra of Ag-PVA films with different values of x (0.028, 0.042 and 0.058), heated at T = 90°C for different lengths of time, t are shown in Fig. 2.4. The spectra were deconvoluted using Gaussian functions to extract the features of the surface plasmon resonance (SPR) peak accurately, avoiding errors due to broad absorption appearing deep in the UV region. The variation of intensity, peak maximum

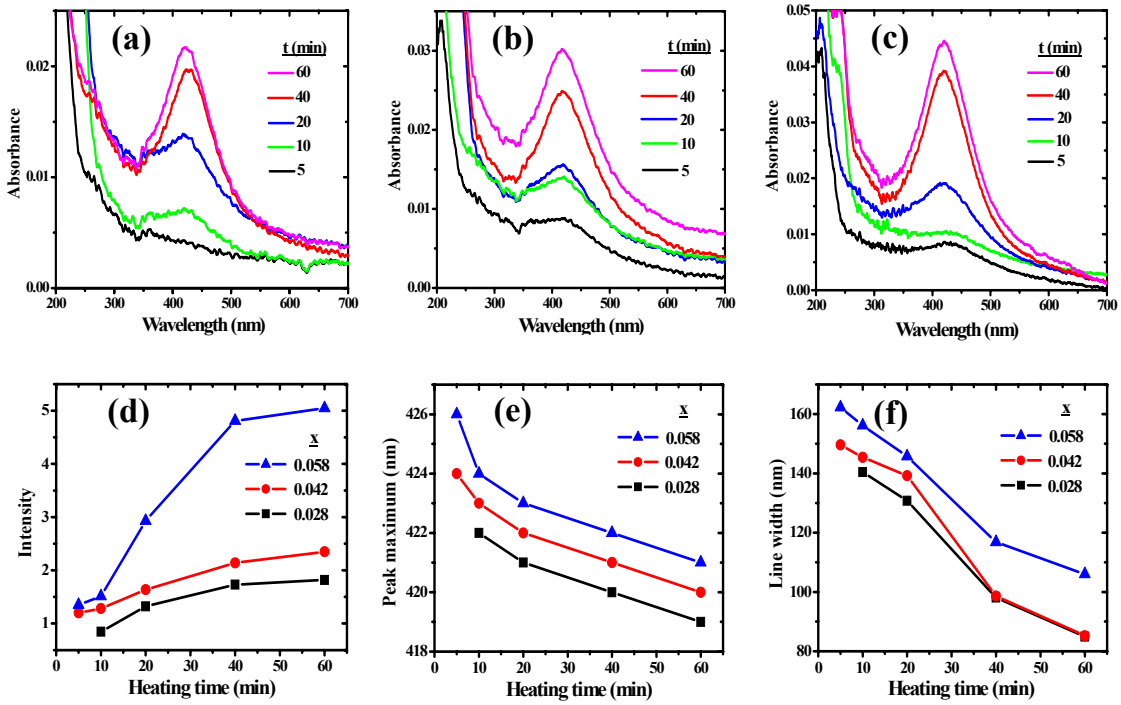

Figure 2.4. *Absorption spectra of Ag-PVA films with x = **(a)** 0.028, **(b)** 0.042 and **(c)** 0.058, heated at T = 90°C for different periods of time, t. Variation of **(d)** intensity, **(e)** peak maximum and **(f)** line width of the absorption spectra in (a), (b), and (c), with heating time.*

and line width for different compositions are shown in Fig. 2.4. The intensity plots show that the nanoparticle production increases with time and saturates in about an hour; the progress is very prominent at the highest Ag/PVA ratio. The small but steady blue shift of the peaks with heating time indicates decrease of the particle size.[16] We found that our observations are quite reproducible and supported by TEM studies discussed below. The marked line width reduction reflects the increasing monodispersity of the size. Fig. 2.5 represents the SPR spectra of Ag-PVA films with x = 0.028 and 0.042 heated at different temperatures for 1 h; considerable enhancement in the peak intensity is observed at higher temperature. It is important to note that, an earlier study of silver nanoparticles in polymers[17] reported a broad size distribution (10 - 60 nm) and suggested possible increase of size with heating time. No supporting microscopy evidence was provided, however.

For the TEM studies, a small piece of Ag-PVA/PS film peeled off the glass substrate was placed on a 100 mesh copper grid and the PS layer was dissolved out by dipping the grid for 3 - 5 min in toluene taken in a petri dish. The thin film samples were directly examined at an accelerating voltage of 100kV. The Ag-PVA films showed the formation of smaller particles, tighter size distribution and size decrease with heating time, fully consistent with the plasmon absorption data. Fig. 2.6 shows TEM images of the roughly spherical silver nanoparticles in PVA matrix obtained by heating the films (x = 0.042) at 90^{o}C. The histograms illustrate the increase in particle density (average number of particles in unit area of the film), decrease in the mean diameter (d_{mean}) and narrowing of the size distribution with increasing heating time. Film heated for 60 min shows very small particles (d_{mean} = 2.6 nm) and a tight

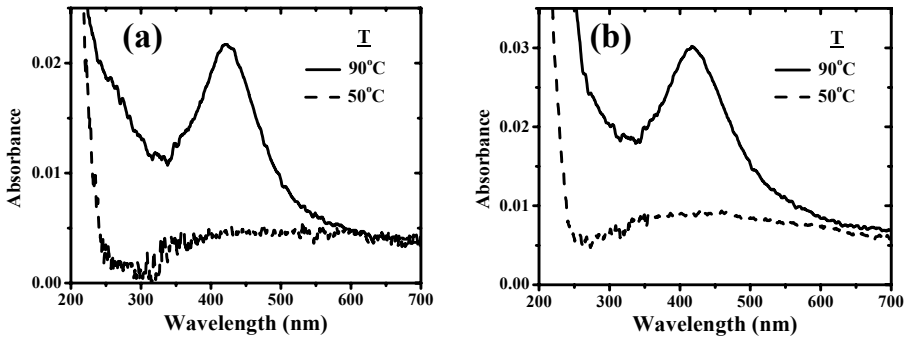

Figure 2.5. *Absorption spectra of Ag-PVA films with x = **(a)** 0.028 and **(b)** 0.042 heated at different temperatures, T for t = 60 min.*

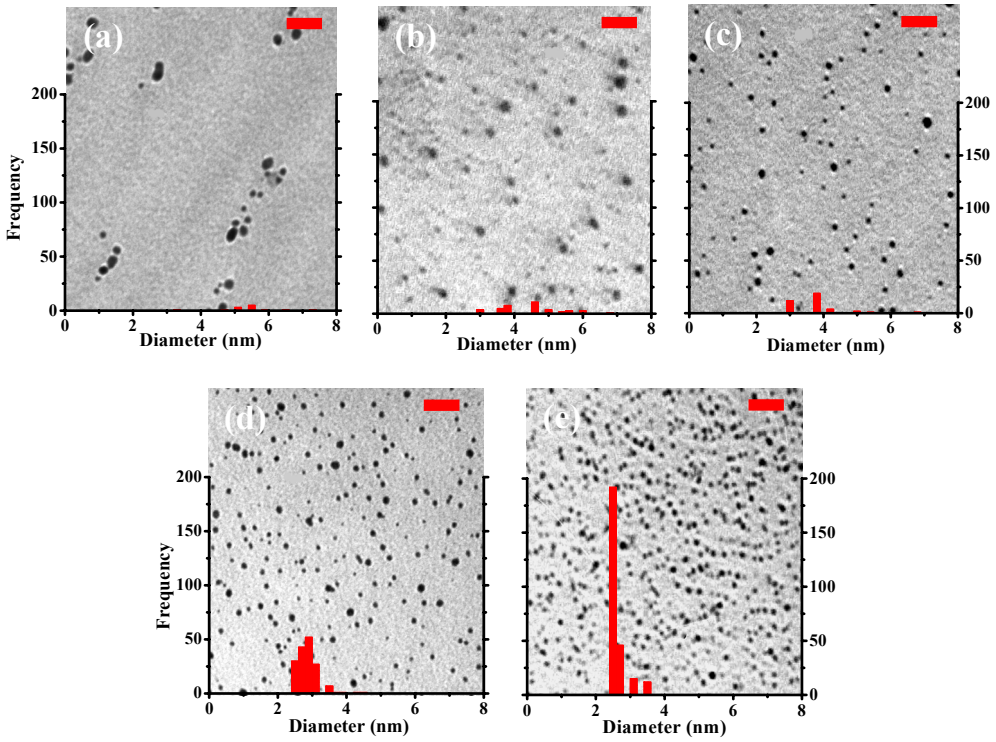

Figure 2.6. *TEM images of Ag-PVA films (x = 0.042) heated at T = 90°C for t =* ***(a)*** *5,* ***(b)*** *10,* ***(c)*** *20,* ***(d)*** *40,* ***(e)*** *60 min (scale bar = 20 nm). Mean diameters (standard deviation) are : (a) 5.4 (0.9), (b) 4.5 (1.0), (c) 3.8 (0.8), (d) 2.8 (0.3) (e) 2.6 (0.2) nm. The histograms show the particle size distribution in the image area.*

distribution (σ = 0.2 nm). Other Ag/PVA compositions (x = 0.028 and 0.058) show similar trends, at T = 90°C with different heating times, t = 5 - 60 min, but the average size increases and size distribution broadens with concentration (Fig. 2.7). Temperature also provides control on the particle size. In the case of x = 0.042, very few particles with variable sizes are formed at 50°C when heated for 60 min. But uniformly small particles (d_{mean} = 2.1 (0.2) nm) are obtained at 110°C (Fig. 2.8). For x = 0.028, nanoparticles do not form at 50°C even after heating for 60 min (Fig. 2.9). Gradual decrease in size is obtained for x = 0.028, 0.058 with increasing T. Interestingly, the Ag/PVA = 0.058 film heated at 110°C for 60 min showed appreciable ordering of the nanoparticles. If the heating temperature is sufficiently high and the Ag/PVA ratio moderate, uniform silver nanoparticles can be generated in very short time. For example, Fig. 2.10 shows that, uniform nanoparticles can be generated when x = 0.042 and T = 110°C even at t = 10 min. Fig. 2.11 shows the electron diffraction patterns

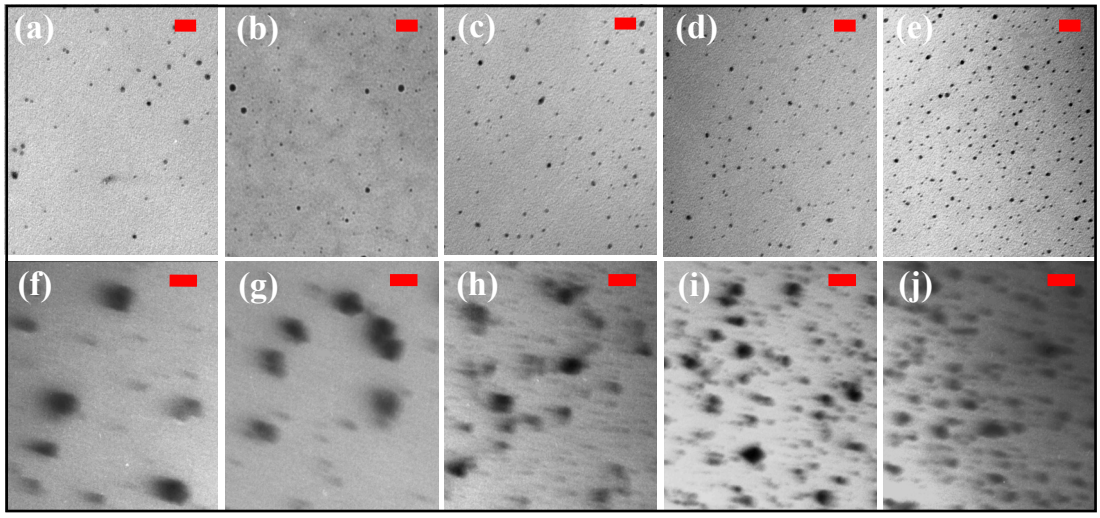

Figure 2.7. *TEM images of Ag-PVA films heated at T = 90°C, with x = 0.028 for t = **(a)** 5, **(b)** 10, **(c)** 20, **(d)** 40, **(e)** 60 min. **(f)** – **(j)** are similar images for x = 0.058 (scale bar = 20 nm).*

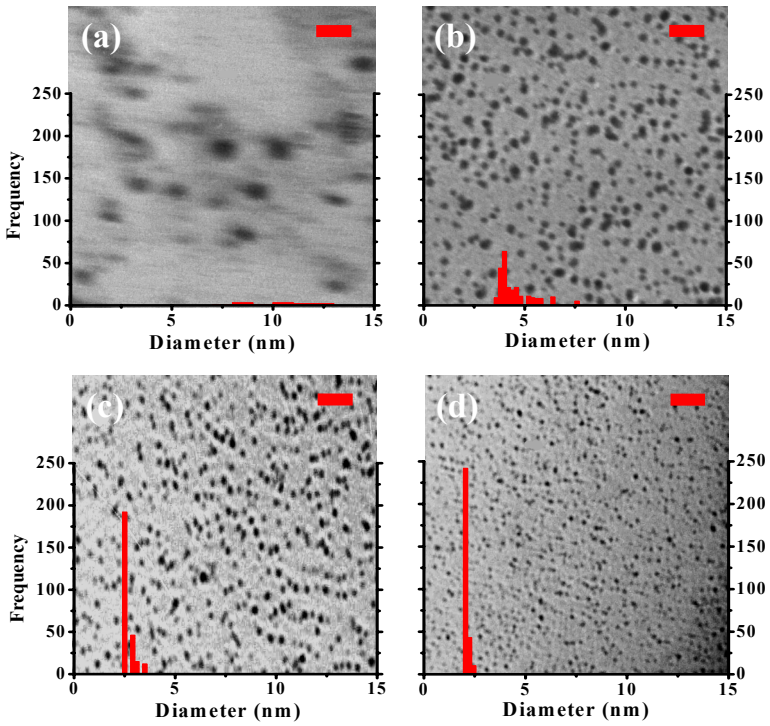

Figure 2.8. *TEM images of Ag-PVA films (x = 0.042) heated for t = 60 min at T = **(a)** 50, **(b)** 70, **(c)** 90, **(d)** 110°C (scale bar = 20 nm). Mean diameters (standard deviation) are : (a) 10.2 (1.7), (b) 4.5 (0.8), (c) 2.6 (0.2), (d) 2.1 (0.2) nm. The histograms show the particle size distribution in the image area.*

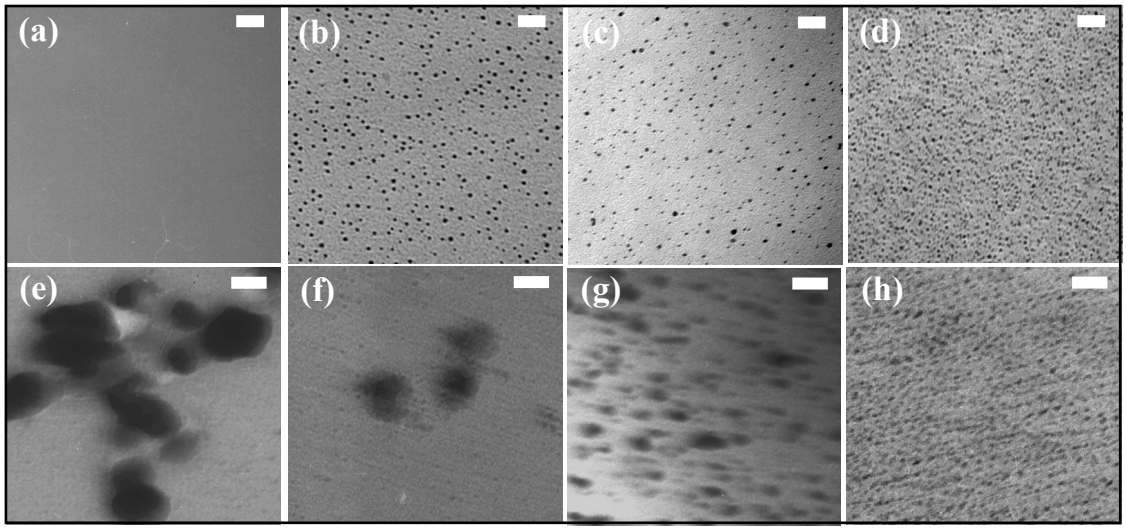

Figure 2.9. *TEM images of Ag-PVA films with x = 0.028 heated for t = 60 min at T = **(a)** 50, **(b)** 70, **(c)** 90, **(d)** 110°C. **(e)** – **(h)** are similar images for x = 0.058 (scale bar = 20 nm).*

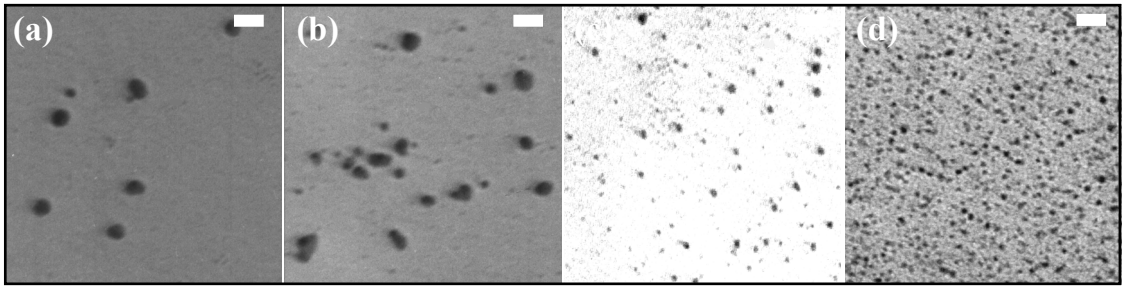

Figure 2.10. *TEM images of Ag-PVA films with x = 0.042 heated for t = 10 min at T = **(a)** 50, **(b)** 70, **(c)** 90, **(d)** 110°C (scale bar = 20 nm).*

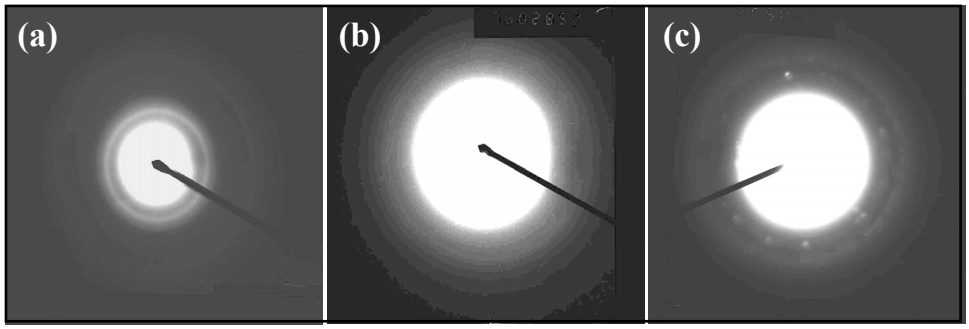

Figure 2.11. *Electron diffraction images of Ag-PVA films **(a)** x = 0.042, T = 110°C, t = 10 min, **(b)** x = 0.042, T = 110°C, t = 60 min and **(c)** x = 0.058, T = 90°C, t = 60 min.*

recorded for selected Ag-PVA films. The ring patterns can be indexed to fcc silver, providing final evidence for the formation of silver nanoparticle inside the PVA matrix.

The change in the particle density and size distribution with time, and more markedly with temperature of heating appears to result from the varying extent of chemical reduction as well as a digestive ripening process. Digestive ripening observed earlier with gold nanoparticles[15] has been reported recently for silver nanoparticles as well.[18] Longer heating time and higher temperatures lead to greater progress of reaction and faster rates respectively. The concomitant decrease in the polymer viscosity possibly facilitates higher ion/atom mobility and homogeneous nucleation. The small sizes obtained suggest that the PVA matrix effectively suppresses particle aggregation.

These studies on Ag-PVA system illustrate the simple *in situ* process we have developed for the fabrication of free-standing metal nanoparticle-embedded polymer film and the control it provides on the particle size and size distribution.

2.4. Optical Limiting

Noble metal nanoparticles exhibit characteristic size and shape dependent electronic structure leading to unique optical and nonlinear optical (NLO) properties. These attributes find application in a wide range of fields including electronics,[19] photonics,[20] plasmonics[21] and sensing.[22] The plasmon absorption of metals such as copper, silver, gold and palladium occur in the UV-visible region of the spectrum. Multiphoton excitations in this energy range and further excited state absorptions can be exploited to elicit NLO responses from these nanomaterials. From a materials point of view, it is advantageous to embed the metal nanoparticles in thin polymer films for optical and nonlinear applications.[23] The polymer matrix serves not only as a medium to assemble the nanoparticles and stabilize them against aggregation, but with its characteristic mechanical properties should be uniquely suited for device applications.

Optical power limiting, a phenomenon to which a range of processes including nonlinear absorption and nonlinear scattering can contribute (Sec 1.8), is an important area of application where metal nanoparticles are promising candidates.[24, 25] Optical limiters are ideally suited for the protection of human eyes and devices from damages that can be inflicted by high energy lasers. Extensive studies have been reported on

optical limiting in the nanosecond and picosecond time scales using metal nanoparticles.[25] Nonlinear absorption in the nanosecond regime, of Ag/Au-PVA films typically 100 μm thick, has also been reported.[26] Thermal effects may play a significant role in the optical limiting process at these time scales. Optical limiting of femtosecond pulses, involving higher input power in the terawatt (TW) regime and likely to be dominated by purely electronic responses, have been explored relatively less; some of the materials that have been investigated include semiconductor quantum dots,[27] silver and gold nanocrystals,[28, 29] carbon nanostructures,[30] fullerene functionalized polymers,[31] and organometallics.[32]

We present first, Z-scan measurements and optical limiting studies in the nanosecond time scale, on silver nanoparticle-embedded poly(vinyl alcohol) film layered over polystyrene (Ag-PVA/PS) and supported on glass. These experiments demonstrated that films typically a few micrometers thick show characteristics comparable to colloidal silver with path lengths of a few millimeters. We have also investigated the nonlinear absorption/refraction and optical limiting of femtosecond laser pulses by Ag-PVA coated directly on glass and more importantly, as free-standing films with the tri-layer structure, PVA/Ag-PVA/PVA. The films with optimal concentrations of Ag show efficient responses and are quite stable against the high energy laser irradiation. Unlike the case with nanosecond laser pulses, the high intensities associated with the femtosecond laser pulses can cause the substrates on which the films are coated to produce their own nonlinear responses. Open and closed aperture Z-scan experiments on the free-standing films allowed unambiguous estimation of the nonlinear absorption cross sections and nonlinear refraction due to the nanoparticles without the complications arising from the contribution of the glass substrate. Ag-PVA film shows large nonlinear absorption (β = 2.2 cm GW^{-1}) and nonlinear refractive index ($n_2 = 1.20\times10^{-12}$ esu). Significantly, the n_2 dominated by electronic responses has a positive sign; experiments in the nanosecond domain revealed contrasting behavior, with negative nonlinearity possibly arising due to thermal contributions. The Ag-PVA films show nearly 90% linear transmission coupled with efficient optical limiting for femtosecond pulses; the free-standing nature of these composite films is a significant development from the point of view of device applications.

2.4.1. *Studies on Supported Ag-PVA/PS Film in the Nanosecond Regime*

The films were fabricated as discussed in Sec. 2.2. All the studies were carried out on Ag-PVA/PS films with x = 0.058, prepared by heating at T = 90^{o}C for t = 60 min.

Nonlinear absorption of the films supported on glass was studied using the open aperture Z-scan technique. The second harmonic beam (532 nm) of an Nd:YAG laser (6 ns, 10 Hz) was employed in f/24 geometry.[33] Laser beam was focused on the sample using a lens of 60 mm focal length; the beam waist was 20 μm at focus leading to peak fluences in the range 0.18 - 1.7 J cm^{-2} which could be varied using calibrated neutral density filters. The transmitted output was collected using a calibrated fast photodiode (FND 100) and processed using a data acquisition system consisting of a boxcar avarager, ADC and computer. The sample position was moved along the Z-axis using a computer-controlled translation stage; repeated scans were used to ensure reproducibility of the data. The films were stable at all the intensities we report below. The experimental setup is shown in the Fig. 2.12; the aperture is removed for the open aperture Z-scan experiment.

Optical limiting capability was studied keeping the sample at the focus in f/24 geometry. The input energy was varied using calibrated neutral density filters and the

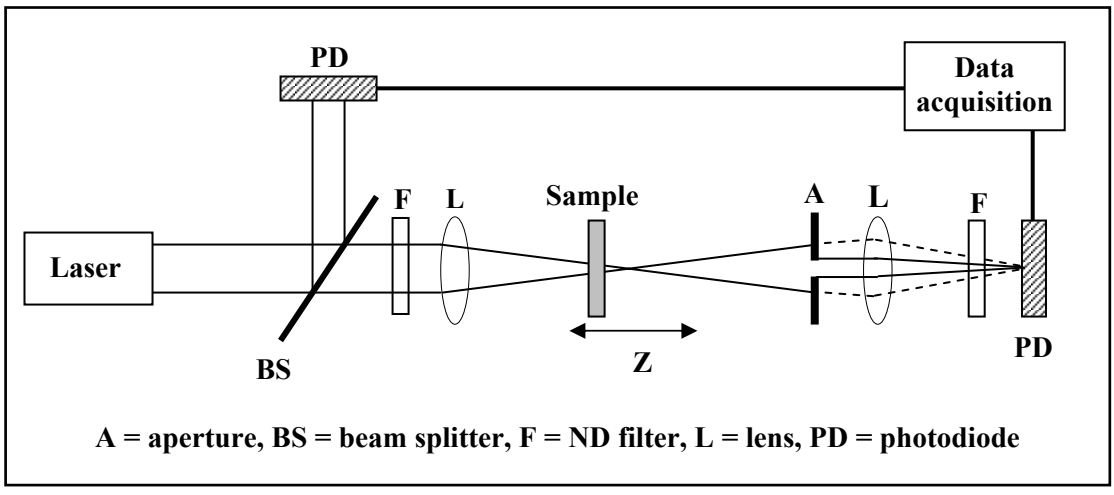

Figure 2.12. *Schematic diagram of the experimental setup for the Z-scan and optical limiting studies.*

output was measured as noted above. The optical limiting curve was drawn as output fluence versus input fluence. Each experimental point is an average of 64 laser pulses.

Ag-PVA/PS films ~ 5 μm thick, with a linear transmission of 84% at low laser intensities, show strong reverse saturable absorption at higher intensities (Fig. 2.13a). Plot of the output fluence versus the input fluence (Fig. 2.13b) shows appreciable optical limiting with a threshold ($I_{½}$)[34] (Sec. 1.8) of 0.83 J cm^{-2} and output clamped at 0.35 J cm^{-2}. The dynamic range estimated[32] from the damage and limiting thresholds is approximately 2. Ag-PVA films without PS showed similar behavior, however the damage threshold was lower. It is significant that this first report of optical limiting with silver nanoparticle-embedded polymer thin films indicates thresholds which are comparable or superior to those obtained earlier[35] for silver nanoparticles in colloidal medium with 1 - 2 mm path lengths.

In order to gain insight into the nonlinear absorption of the Ag-PVA/PS film, we have investigated the response of the individual polymer layers and their combinations: PS, PVA, Ag-PVA, and Ag-PVA/PS. PVA does not show any nonlinear absorption. The Z-scans for the other films at two different input intensities are shown in Fig. 2.14. PS shows a weak reverse saturable absorption (RSA) at the lower input intensity, which is enhanced slightly at the higher intensity. Ag-PVA film on the other hand exhibits

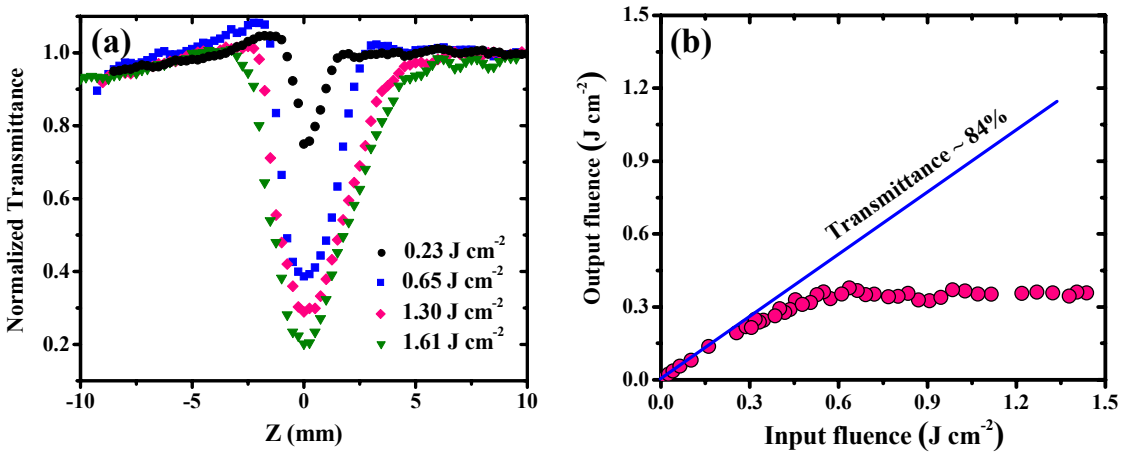

Figure 2.13. ***(a)*** *Open aperture Z-scan traces at different input fluences,* ***(b)*** *Output versus input fluence plot of Ag-PVA/PS film on glass substrate for nanosecond laser pulses.*

RSA and saturable absorption (SA) respectively at the two intensities. The appreciable RSA of Ag-PVA/PS at the low input intensity is further enhanced at the higher intensity. These observations clearly indicate a non-additive behavior in the nonlinear response of Ag-PVA/PS films. PS does not show any electronic absorption in the visible region but has an absorption peak at 270 nm. The absorption at high laser intensities observed in the Z-scan curve (Fig. 2.14a, d) suggests possible two-photon absorption by PS. Different processes are known to lead to optical limiting behavior in metal nanoparticles (Sec. 1.8). The films containing silver nanoparticles show plasmon absorption with a peak at ~ 420 nm (Fig. 2.4c); a weak absorption occurs at 532 nm, the wavelength of the laser used. The RSA in Ag-PVA films may be attributed to excitations from the plasmon band to the free carrier band of the silver nanoparticles; at higher input intensities, fast decay of the free carriers to the plasmon band can lead to the observed SA (Fig. 2.14b, e). It is likely that the free carrier band of Ag-PVA overlaps with the absorption band of PS so that in the case of Ag-PVA/PS a channel of

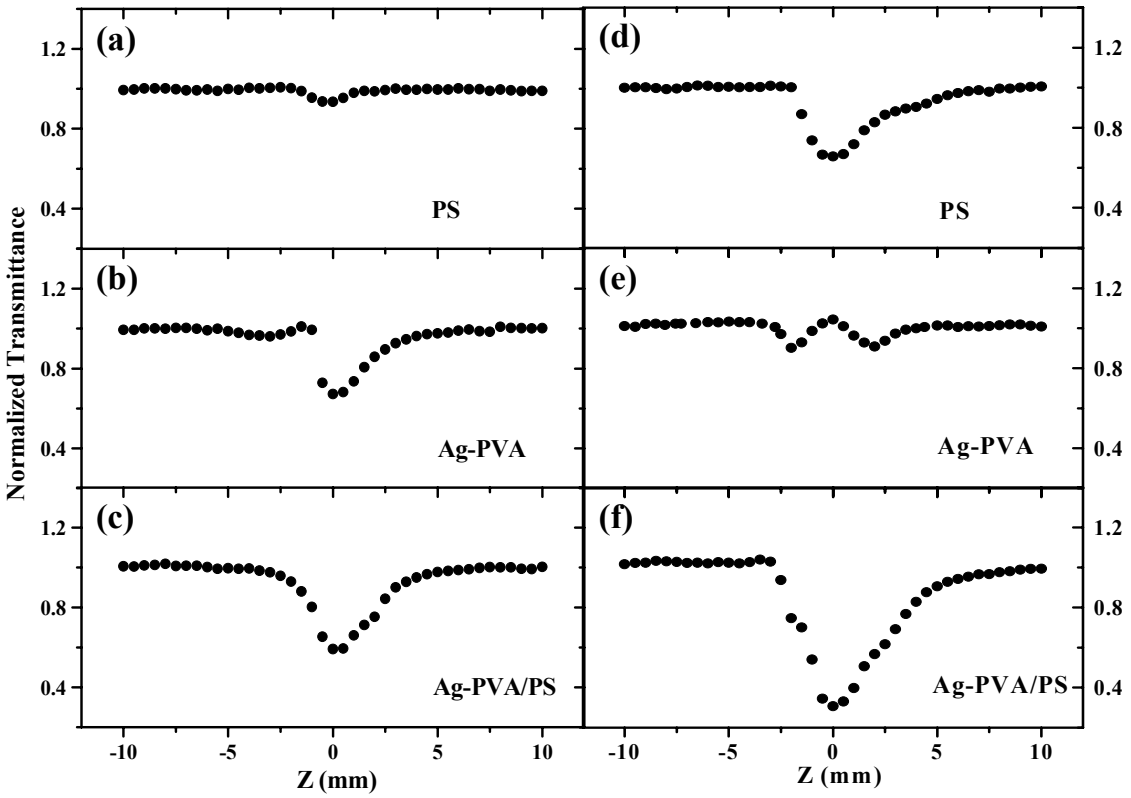

Figure 2.14. *Open aperture Z-scan traces of PS, Ag-PVA and Ag-PVA/PS films at input intensities of* ***(a, b, c)*** *0.11 GW cm^{-2} and* ***(d, e, f)*** *0.24 GW cm^{-2}.*

energy transfer to PS is opened up leading to strong absorption by the silver nanoparticles and enhanced RSA in the multilayer system (Fig. 2.14c, f).

2.4.2. *Studies on Supported and Free-standing Ag-PVA Films in the Femtosecond Regime*

The film fabrication procedure and the polymer used in the synthesis of these Ag-PVA films are slightly different from those described in Sec. 2.2. Therefore we discuss first, the fabrication protocol, followed by the details of spectroscopy, microscopy and nonlinear optical studies. The linear and nonlinear absorption and optical limiting characteristics of the supported and free-standing films are presented along with details of the analysis.

Required weight of silver nitrate ($AgNO_3$) dissolved in 1.0 ml water was mixed with 0.4 ml of a solution of poly(vinyl alcohol) (PVA; Aldrich, M_w = 13 - 23 kDa, % hydrolysis = 86) in water (2.4 g PVA in 8 ml water) to prepare different compositions designated using the Ag/PVA weight ratio, x (e.g. 5.5 mg of $AgNO_3$ gives x = 0.029). The solution mixture was stirred for 5 min at 27 - 30^oC. Millipore purified water was used in all operations. The glass substrate was cleaned by sonication using the methodology described earlier. The substrate required for fabricating free-standing films of Ag-PVA and samples for TEM studies was prepared by spin-coating a few drops of a solution of polystyrene, PS (average molecular weight = 280 kDa) in toluene (1 g PS in 8 ml toluene) on glass, using a photoresist spinner, at 1,000 RPM for 10 sec followed by drying in a hot air oven at 85 - 90^oC for 15 - 20 min. Three kinds of $AgNO_3$-PVA films were prepared for the current study, by spin-coating at 6,000 RPM for 10 sec: (i) $AgNO_3$-PVA solution on glass substrate, (ii) $AgNO_3$-PVA solution on PS/glass substrate, and (iii) PVA, $AgNO_3$-PVA and PVA solutions in succession on PS/glass substrate (Fig. 2.15); the first two are similar to those described in Sec. 2.2, but the third one is new. The film coated plates were heated in a hot air oven at T = 130^oC for t = 60 min to generate the silver nanoparticles *in situ* inside the PVA matrix. Sample prepared using procedure (i) is referred in the following discussion as Ag-PVA film on glass. Samples from procedures (ii) and (iii) were immersed in toluene taken in a petri dish to dissolve the PS layer and release free films. The free Ag-PVA film obtained via procedure (ii) was used directly for TEM imaging. We refer to the film obtained via

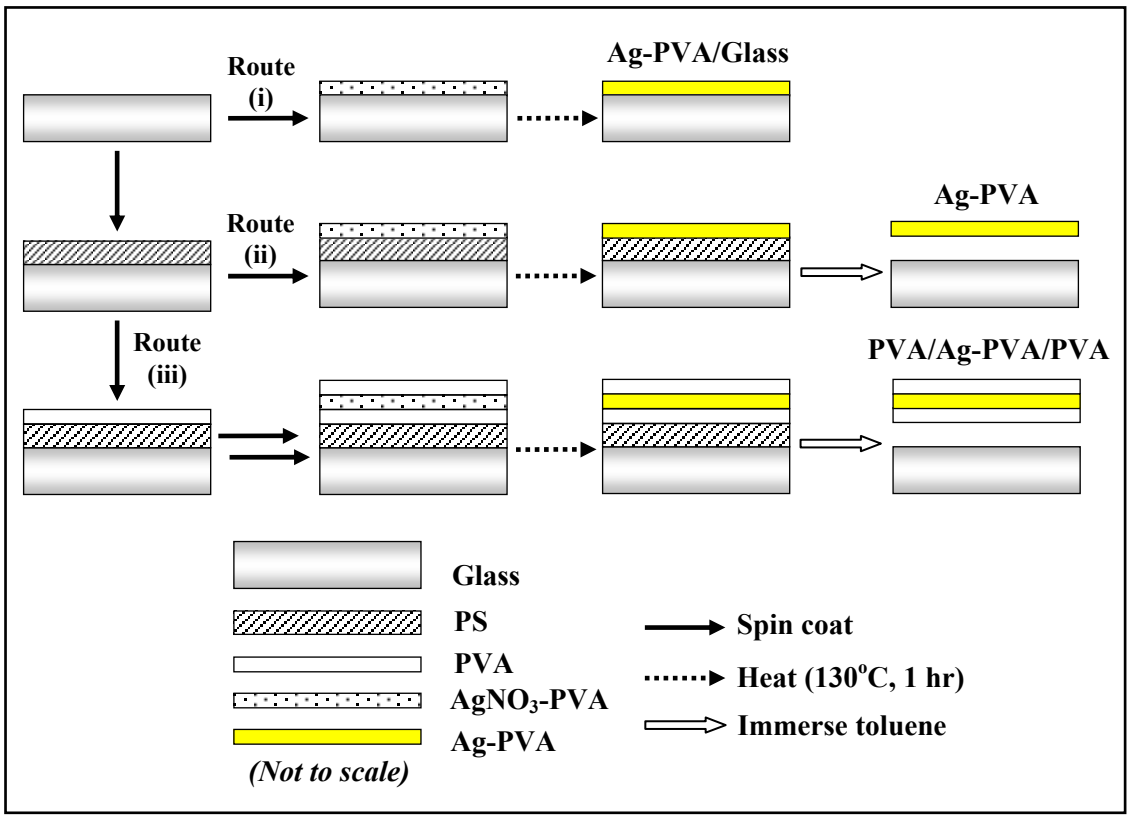

Figure 2.15. *Schematic representation of the fabrication procedures used in the studies discussed in Sec. 2.4.2. Route (ii) is same as that presented in Fig. 2.1.*

procedure (iii) as free-standing Ag-PVA or PVA/Ag-PVA/PVA film. Thickness of the films was measured using a profilometer are as follows: Ag-PVA (on glass) ~ 0.5 μm; Ag-PVA/PS (on glass) ~ 5.5 μm; free-standing PVA/Ag-PVA/PVA ~ 10 μm.

Ag-PVA films spin-coated on glass substrate were fabricated with four different compositions (x = 0.029, 0.058, 0.087, 0.116). Absorption spectra of the Ag-PVA films coated on glass as well as free-standing films were recorded. Fig. 2.16 shows the spectra recorded for the films coated on glass. The intensity of the plasmon peak increases with increasing silver content. TEM images of Ag-PVA films prepared following procedure (ii) described above and placed directly on a 100 mesh copper grid were obtained using an accelerating voltage of 120 kV. The images are shown in Fig. 2.17. A uniform distribution of silver nanoparticles is observed with particle sizes ranging from 5 - 10 nm. The density of particles increases with the value of x.

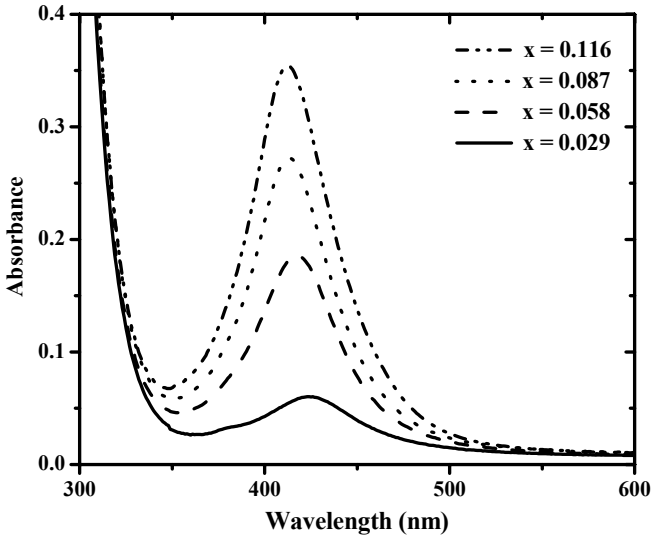

Figure 2.16. *Absorption spectra of Ag-PVA films on glass, with x = **(a)** 0.029, **(b)** 0.058, **(c)** 0.087 and **(d)** 0.116 heated at T = 130^{o}C for t = 60 min.*

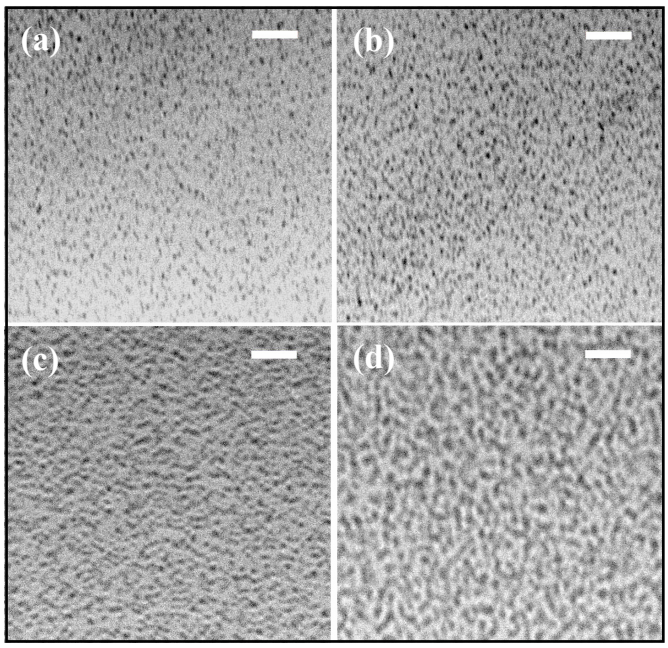

Figure 2.17. *TEM images of the Ag-PVA films with x = **(a)** 0.029, **(b)** 0.058, **(c)** 0.087 and **(d)** 0.116 heated at T = 130^{o}C for t = 60 min (scale bar = 100 nm).*

Nonlinear optical studies used Ti:Sapphire laser (800 nm, ~110 fs, 1 kHz) as the excitation source. Frequency doubled Nd:YAG laser (532 nm, 6 ns, 10 Hz) was used in

the control experiments. Open and closed aperture Z-scan measurements were carried out by moving the sample across the focus of the laser beam using a computer-controlled translation stage; the scans were repeated several times to ensure reproducibility of the data. Femtosecond (nanosecond) pulse laser was focused using a lens of 80 mm (60 mm) focal length; the beam waist was 27.1 μm (13.5 μm) at focus leading to peak intensity in the range 0.15 - 1.73 TW cm^{-2} (0.03 - 0.28 GW cm^{-2}) i.e. fluences in the range 0.02 - 0.19 J cm^{-2} (0.18 - 1.7 J cm^{-2}). The input intensity could be varied using calibrated neutral density filters; closed aperture experiments used an aperture of diameter 1 mm or 2 mm after the sample. The transmitted output was collected using a calibrated fast photodiode (FND 100) and processed using a data acquisition system consisting of a lock-in amplifier or boxcar averager, ADC and computer; the setup is same as that shown in Fig. 2.12. The films were stable at all the intensities reported in the experiments. Optical limiting studies were carried out using f/40 geometry (using 8 cm focal length lens and a beam diameter of 0.2 cm) with the femtosecond pulse laser in the same input fluence/intensity range as noted above.

We have carried out the nonlinear optical studies on the films with different compositions, but have focused more on the films with x = 0.029 and 0.058, since they showed superior damage thresholds compared to the films with higher content of silver. Plots of the transmittance versus scan position for the open aperture Z-scan studies using the femtosecond pulse laser are shown in Fig. 2.18. Control experiment on glass and plain PVA coated on glass showed weak nonlinear absorption, possibly resulting from the large (~ 1 mm) interaction length of glass involved, since both show nearly identical response (Fig. 2.19); it is also shown that PVA on glass has no absorption in the region corresponding to the plasmon absorption of silver. With comparable and higher input laser power, Ag-PVA films coated on glass exhibit strong nonlinear absorption. Films with x > 0.06 show perceptible damage at input intensity exceeding ~ 1.3 TW cm^{-2}. Earlier studies on silver nanoparticles in the form of suspensions and doped in glass matrices indicated saturable absorption;[36] this could be due to larger lifetimes of the surface plasmon state in these environments. We have attempted to fit the Z-scan curves of the Ag-PVA films using models for nonlinear absorption. However the fitting was not very satisfactory, possibly because of the non-negligible effect of the glass substrate at these high laser powers. Results of the optical limiting experiments are collected in Fig. 2.20. The films show high linear transmittance

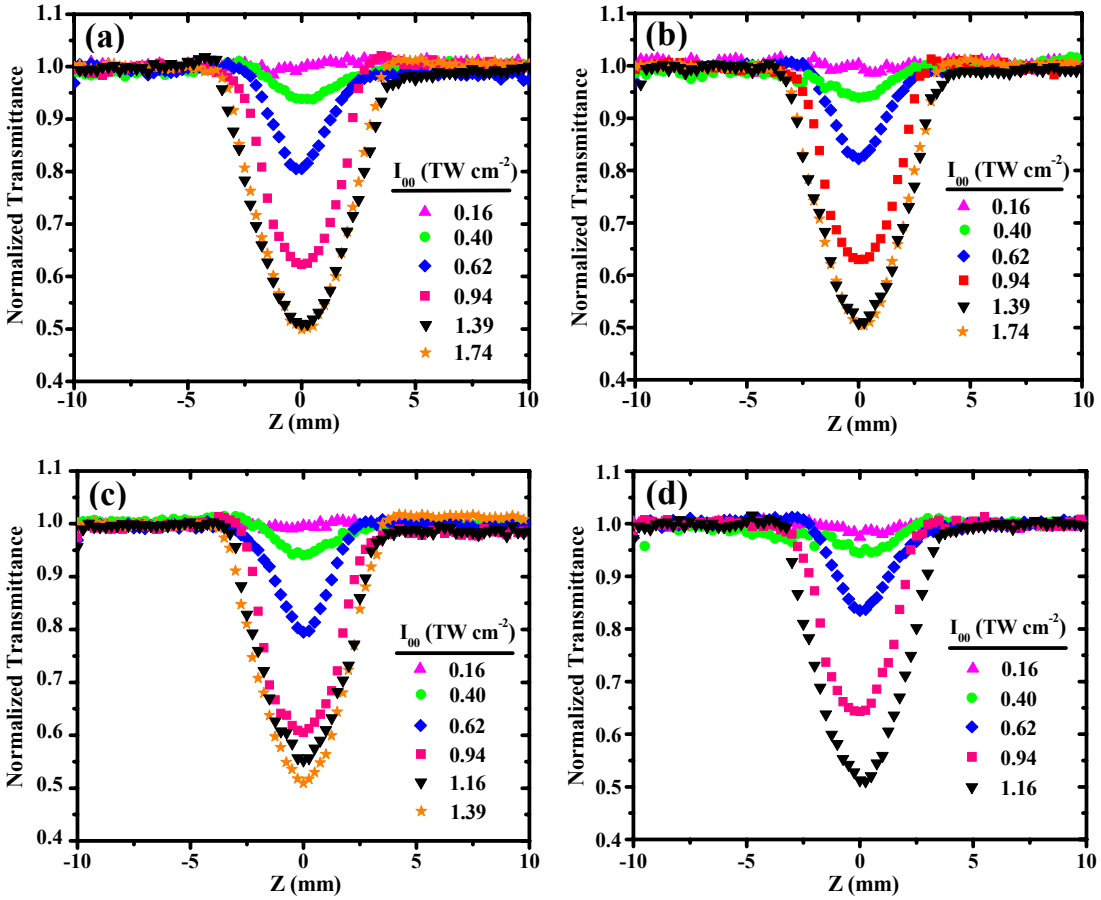

Figure 2.18. *Open aperture Z-scan traces of Ag-PVA films on glass, with x = **(a)** 0.029, **(b)** 0.058, **(c)** 0.087 and **(d)** 0.116, for different input intensities (I_{00}) of femtosecond laser pulses.*

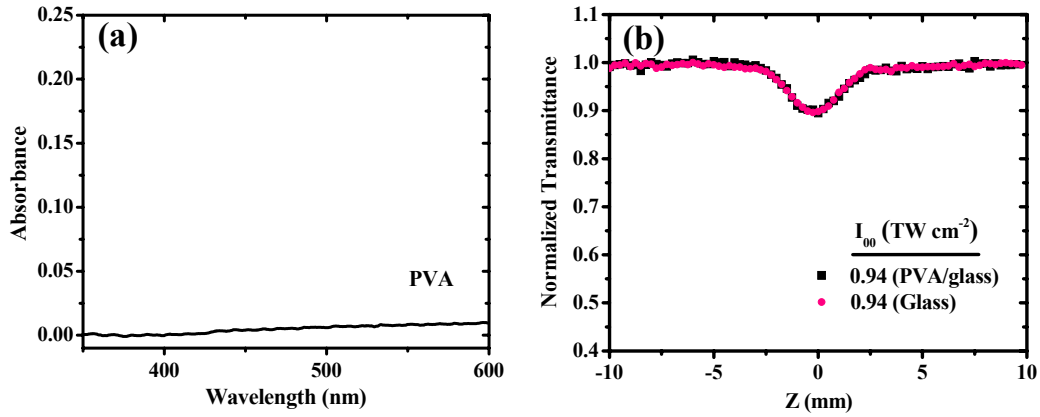

Figure 2.19. ***(a)** Electronic absorption spectrum of PVA coated on glass. **(b)** Open aperture Z-scan traces of glass and PVA on glass.*

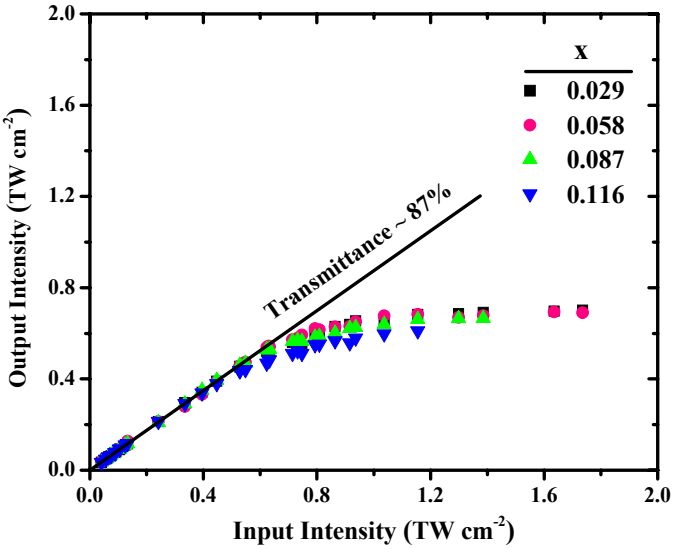

Figure 2.20. *Output versus input intensity plots of Ag-PVA films on glass with different values of x, for femtosecond laser pulses.*

(~87%) at low laser intensity. The plots of output versus input intensity indicate appreciable optical limiting with a threshold ($I_{½}$) of 1.62 TW cm^{-2} and output clamped at 0.70 TW cm^{-2}. The dynamic range is ~ 1.1 for the films with x = 0.029 and 0.058. The ability of these polymer films to sustain high laser power is of practical interest. Once again films with higher x are found to have lower damage threshold and hence dynamic range.

The contribution to optical limiting, from nonlinear refraction was assessed using closed aperture Z-scan experiments with the femtosecond pulses on the Ag-PVA films coated on glass with x = 0.029 and 0.058. The transmittance values are normalized and divided by the corresponding values in the open aperture experiment so as to reveal the effect of nonlinear refraction alone (Fig. 2.21). The reduced transmittance before focus and increased transmittance after focus indicate that Ag-PVA possesses positive nonlinearity for refraction in the femtosecond regime. Thermal buildup would typically lead to negative nonlinearity; the positive nonlinearity of the films observed even with 1 kHz repetition rate, therefore suggests that the responses are dominated by electronic effects. As in the case of the open aperture Z-scan curves, theoretical fitting of the closed aperture data is not dependable; the value of nonlinear refractive index obtained is comparable to that of glass alone.

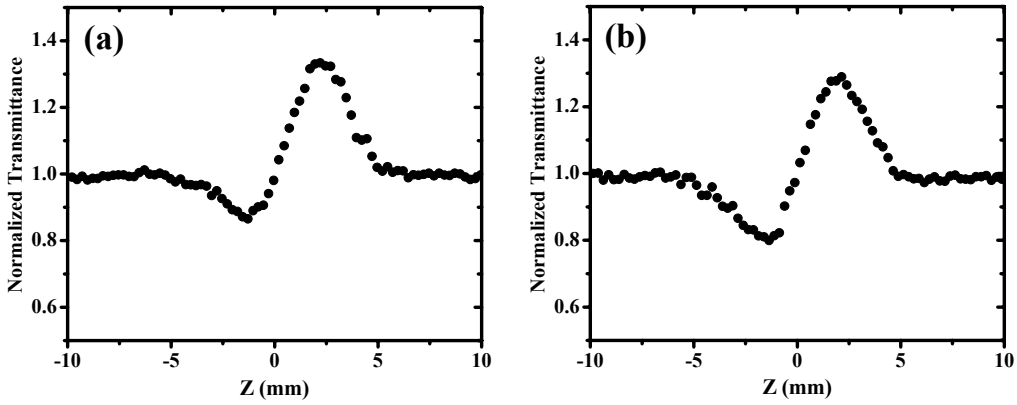

Figure 2.21. *Closed aperture Z-scan traces of Ag-PVA films on glass, with x = **(a)** 0.029 and **(b)** 0.058, for femtosecond laser pulses with input intensity, I_{00} = 0.62 TW cm^{-2}. The transmittance is normalized and divided by the corresponding open aperture values.*

We have carried out some parallel experiments using nanosecond laser pulses, which revealed interesting contrast with the nonlinear response for femtosecond pulses. Open and closed aperture Z-scan experiments were carried out on pure PVA on glass as well as Ag-PVA films on glass with the two lower compositions (Fig. 2.22). PVA film did not show any detectable nonlinear absorption or refraction with the nanosecond pulses. Ag-PVA films however showed appreciable nonlinear absorption (as seen earlier with Ag-PVA/PS films (Sec. 2.4.1) and the closed aperture experiment clearly revealed a negative nonlinearity. The latter is a consequence of resonant absorption at 532 nm and considerable thermal effects operative with the longer laser pulses in the nanosecond regime. These experiments reaffirm that the strong positive nonlinear response of Ag-PVA films to femtosecond laser pulses arises primarily due to electronic effects. However, as noted above, the Z-scan experiments on the films supported on glass substrates do not permit an accurate evaluation of the nonlinear susceptibility of the Ag-PVA films. The reason for this is the following: the glass substrate, in spite of its weaker nonlinear susceptibility compared to Ag-PVA, is a couple of orders of magnitude thicker than the polymer film and hence exerts a comparable or even overwhelming impact on the total nonlinear response for the femtosecond pulses.

In order to unambiguously demonstrate the nonlinear absorption, quantitatively estimate the nonlinear susceptibility and project the potential advantage from the point

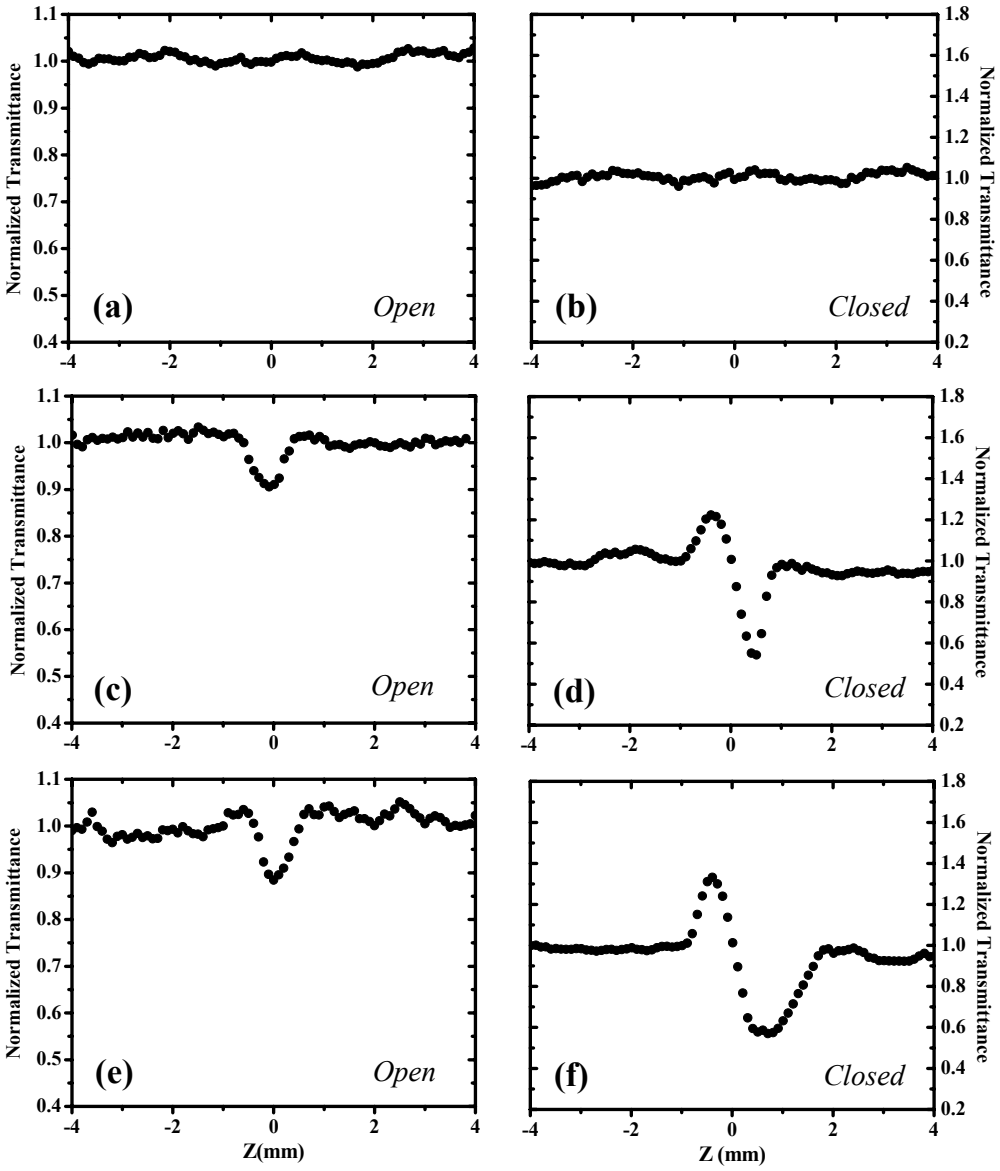

Figure 2.22. *Open and closed aperture Z-scan traces of:* ***(a, b)*** *PVA on glass and Ag-PVA films on glass with* ***(c, d)*** *x = 0.029 and* ***(e, f)*** *x = 0.058, for nanosecond laser pulses with input intensity, I_{00} = 0.58 GW cm^{-2}. The transmittance values in the closed aperture plots have been normalized and divided by the corresponding open aperture values.*

of view of device applications, we have fabricated free-standing films of Ag-PVA having no glass substrate and carried out the nonlinear optical studies on them. As noted earlier, these films were fabricated by successively spin coating PVA, $AgNO_3$-

PVA and PVA and generating the Ag nanoparticles by thermal treatment. Photographs of the ~ 10 μm thick free-standing films are shown in Fig. 2.23. The larger thickness of these films precluded direct TEM imaging. Electronic absorption spectra of the free-standing films are shown in Fig. 2.24a; the plasmon absorption peaks are quite similar to those observed in the supported films suggesting that the nanoparticles are similar in size. Data from the open aperture Z-scan experiments using femtosecond laser pulses are provided in Fig. 2.24. Pure PVA film of comparable thickness (~ 10 μm) does not show any nonlinear absorption (Fig. 2.24b), once again proving that the weak absorption seen in Fig. 2.19b is due to the glass substrate. On the other hand, the free-standing films of Ag-PVA show appreciable nonlinear absorption similar to that observed in the glass supported films (Fig. 2.18a, b). The data were fit to the equation for the transmittivity $T(z)$ taking into account the spatial extent of a Gaussian beam,[37]

$$T(z) = \frac{\ln[1+\beta \mathrm{LI}_{00}(z_0^2/(z_0^2+z^2))]}{\beta \mathrm{LI}_{00}(z_0^2/(z_0^2+z^2))} \qquad \ldots (2.1)$$

z_0 is the Rayleigh range for the beam with intensity I_{00} at focus, L is the thickness of the film and β is a gross nonlinear absorption coefficient. The value of β is found to increase linearly with I_{00} with a small but nonzero intercept (Fig. 2.25), suggesting that it is likely to arise from an association of two and three photon absorptions leading to reverse saturable absorption.[38] At the highest input fluence of 1.22 TW cm^{-2} we have studied, the value of β is found to be 2.0 and 2.2 cm GW^{-1} respectively for films with x = 0.029 and 0.058. The plots of output versus input intensity (Fig. 2.26) from the optical limiting studies indicate a limiting threshold ($I_{½}$) of 1.4 TW cm^{-2}, output

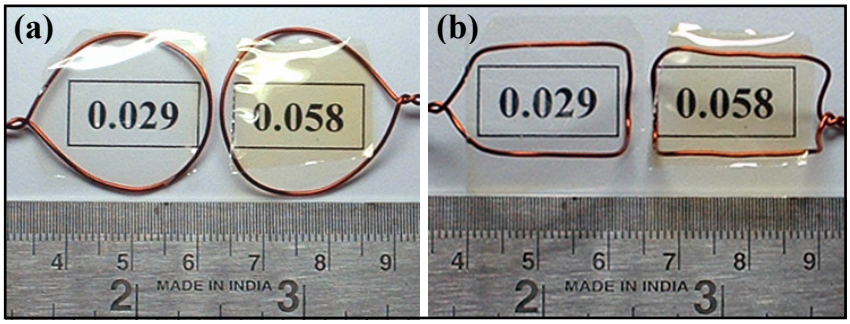

Figure 2.23. *Photographs of free-standing films of Ag-PVA (PVA/Ag-PVA/PVA); transparency of the films is demonstrated by placing them on wire frames* ***(a)*** *directly on and* ***(b)*** *~ 1 cm above, a paper, on which the corresponding value of x is printed.*

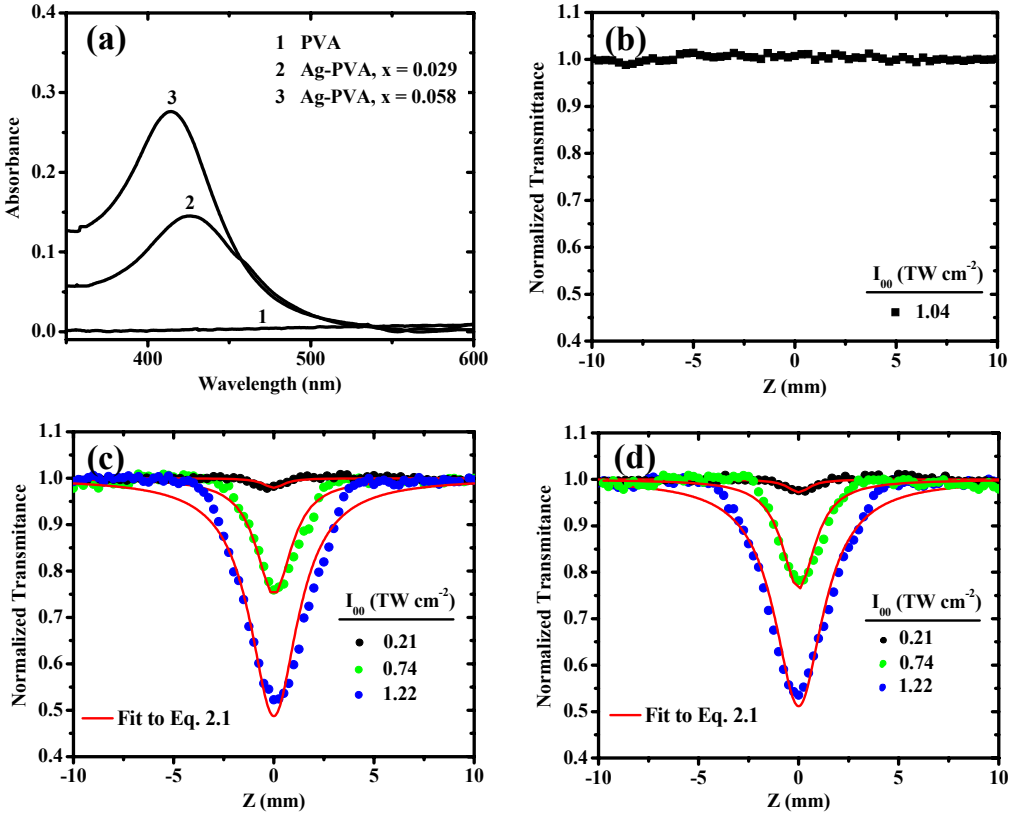

Figure 2.24. ***(a)*** *Absorption spectra of free-standing PVA and Ag-PVA films. Open aperture Z-scan traces of free-standing* ***(b)*** *PVA film and Ag-PVA films with x =* ***(c)*** *0.029 and* ***(d)*** *0.058, for different input intensities (I_{00}) of femtosecond laser pulses. Theoretical fitting of the data to Eq. 2.1 are shown in (c) and (d).*

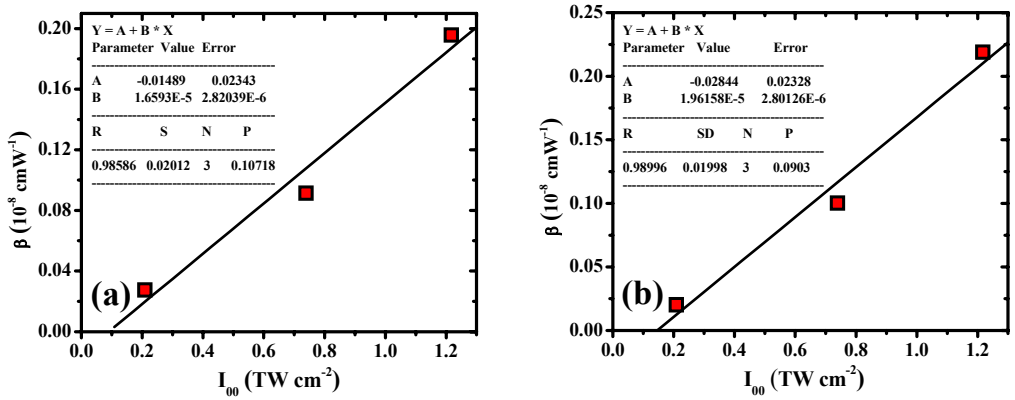

Figure 2.25. *Variation of the nonlinear absorption coefficient, β with input intensity (with femtosecond pulse laser) for free-standing Ag-PVA films x =* ***(a)*** *0.029 and* ***(b)*** *0.058. Fitting data are shown in the inset.*

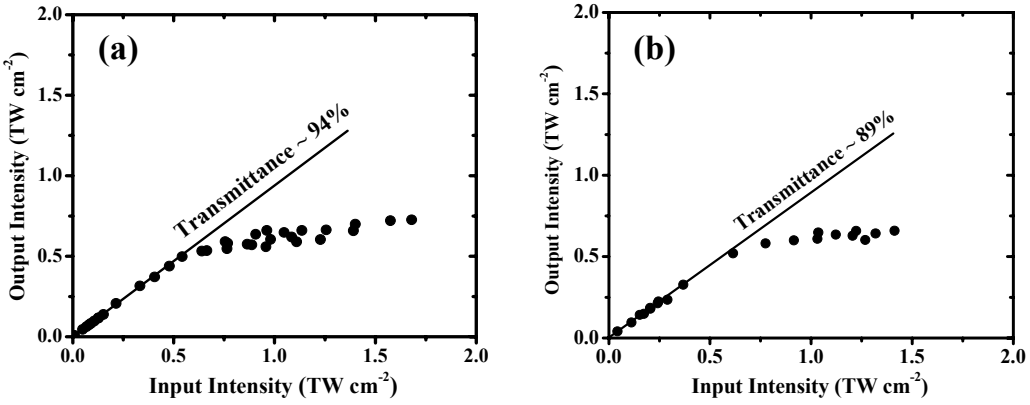

Figure 2.26. *Output versus input intensity plots of free-standing Ag-PVA films with x = **(a)** 0.029 and **(b)** 0.058, for femtosecond laser pulses.*

clamped at 0.70 TW cm^{-2} and dynamic range of ~ 1.2 for the film with x = 0.029; similar characteristics are observed in the case of x = 0.058 as well. It may be noted that the linear transmittance of the free-standing films are higher than that of the glass supported ones; transparency of the film with x = 0.029 is quite significant. Closed aperture Z-scan experiments using femtosecond laser pulses on the free-standing films of Ag-PVA confirm that they exhibit positive nonlinearity (Fig. 2.27). More importantly, these Z- scan traces allow the direct estimation of the nonlinear refractive index, n_2 and the real part of the third order susceptibility, $\chi^{(3)}$ of the Ag-PVA films. The data were fitted to the equation,[39]

$$T(z) = 1 - \frac{4\Delta\varphi_0 (z/z_0)}{[1+(z/z_0)^2][9+(z/z_0)^2]} \quad \ldots (2.2)$$

where $\Delta\varphi_0$ is the phase change. The value of $\Delta\varphi_0$ extracted from the data analysis for Ag-PVA films with x = 0.029 and 0.058 are very similar, –0.39 and –0.41 respectively. The nonlinear refractive index and susceptibility, n_2 and real part of the nonlinear susceptibility, $\mathrm{Re}\,\chi^{(3)}$ were estimated from the phase change, $\Delta\varphi_o$ as follows. The nonlinear refractive index, γ (in m^2/W) is given by:

$$\gamma(\mathrm{m}^2/\mathrm{W}) = |\Delta\varphi_o| / (2\pi/\lambda) I_{oo} L_{eff} \quad \ldots (2.3)$$

where λ is the wavelength of the laser used (800 nm), I_{oo} is the laser intensity at focus and L_{eff} is defined as:

$$L_{eff} = [1 - e^{-\alpha L}]/\alpha \approx L \quad \ldots (2.4)$$

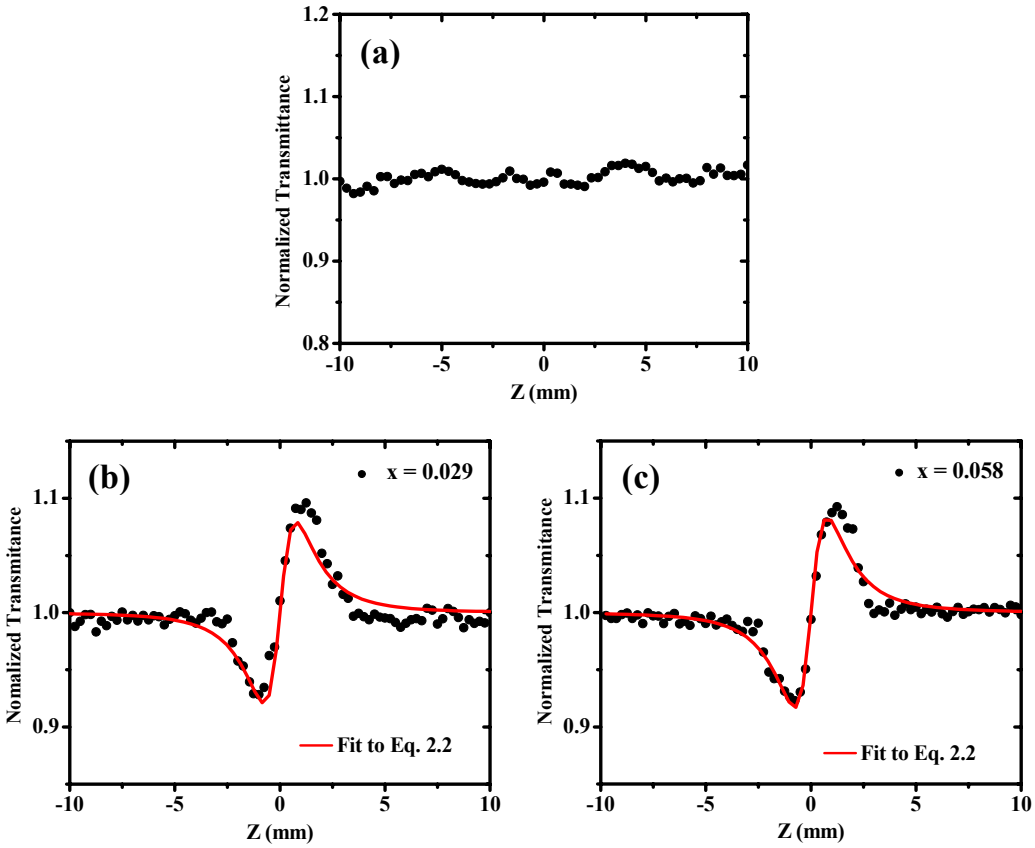

Figure 2.27. *Closed aperture Z-scan traces of free-standing (a) PVA film and Ag-PVA films with x = (b) 0.029 and (c) 0.058, for femtosecond laser pulses with input intensity, I_{00} = 0.14 TW cm^{-2}. The transmittance is normalized and divided by the corresponding open aperture values. Theoretical fitting of the data to Eq. 2.2 are shown in (b) and (c).*

where α is the linear absorption coefficient at λ and L is the thickness of the sample; the approximation is valid when the value of α is negligible as is the case with our films. Nonlinear refractive index, n_2 (in esu) is related to γ by:

$$n_2(\text{esu}) = (cn_o\gamma)/40\pi \quad \ldots (2.5)$$

where c is the velocity of light and n_o is the linear refractive index. n_o was determined using the Brewster angle technique. $\text{Re}\chi^{(3)}$ is obtained using the relation:

$$\text{Re}\chi^{(3)}(\text{esu}) = n_0 n_2(\text{esu})/3\pi \quad \ldots (2.6)$$

The values of n_o, n_2 and $\text{Re}\chi^{(3)}$ obtained for the free-standing films with the compositions, x are collected in table 2.1.

Table 2.1 The values of linear refractive index (n_0), nonlinear refractive index (n_2) and susceptibility (Re $\chi^{(3)}$) for the Ag-PVA free-standing films with compositions, x.

x	n_0	n_2 (10^{-12} esu)	Re $\chi^{(3)}$ (10^{-11} esu)
0.029	1.53	1.13	1.84
0.058	1.53	1.20	1.95

Based on the fabrication procedure, the active layer of Ag-PVA in the free-standing PVA/Ag-PVA/PVA films is likely to be ~ 1 μm thick. Even though SEM and TEM images of the film cross sections support this, in spite of several attempts we were unable to establish the thickness of the Ag-PVA layer unambiguously with corroborating elemental composition or electron diffraction data. Therefore, we have used the full thickness (10 μm) of the PVA/Ag-PVA/PVA films in the estimation of n_2 and $\chi^{(3)}$ even though the contribution of the PVA layer is negligible. It should be noted that, the value of γ is inversely related to the thickness, L (Eqs. 2.3, 2.4). Hence the values we report in Table 2.1, are likely to be the lower bounds for these materials. It is notable that, even then they are comparable to the nonlinear susceptibility reported[26] for silver nanoparticles in colloidal films on silicon substrates. The free-standing films which exhibit strong nonlinear response and optical limiting capability are highly advantageous from an application point of view.

2.5. Antibacterial Application

Antibacterial efficacy of silver is known for a long time.[40] Among heavy metals which are antibacterial, silver is the most popular one because of its activity against a wide spectrum of prokaryotes while being relatively harmless to eukaryotes. In recent years, there has been considerable interest in employing nanometric silver particles as antibacterial agents in several applications.[41] Silver nanoparticles have been used in the colloidal state[42, 43] as well as in the form of embeddings in polymers,[44] foams,[45] fibers[46] and textiles.[47] The ultrasmall dimensions lead to large surface area/volume ratio and hence enhanced activity; it is also likely to facilitate specific binding to cell membrane leading to the bactericidal action.[41]

Several methods have been developed for the bottom-up synthesis of silver nanoparticles through soft chemical protocols.[48] Colloidal silver was directly used in several antibacterial applications reported. Fabrication of polymer composites of the nanoparticles however, is highly desirable since it facilitates: (i) coating of surfaces of varying size and shape, (ii) controlled release of the metal atoms/ions or even restriction of the bactericidal action to contact-killing, (iii) reuse and perhaps regeneration, and (iv) monitoring of the bactericidal agent through successive action cycles. The methodology we have developed for the fabrication of silver nanoparticle-embedded poly(vinyl alcohol) film discussed in Sec. 2.2, is not only very simple and safe to implement, but also likely to prove economically viable. As noted earlier, highlights of the method include the use of aqueous medium for the fabrication process, deployment of the bio-compatible and bio-degradable polymer itself as the reducing agent, mild thermal annealing for generating the metal and *in situ* generation of the nanoparticles inside the polymer matrix which serves as the stabilizer as well.

Among the several avenues where antibacterial find utility, purification of drinking water is one of the most critical and important. The antibacterial agent used should be non-toxic to humans at the concentrations being used, effective against a wide range of pathogens and cheap and easy to fabricate. One of the efficient and convenient ways to deploy the agent in a domestic setting would be as a coating on stirring devices. The methodology we have developed for the fabrication of silver nanoparticle embedded polymer film is unique and meets all these demands. The experiments discussed below establish that the bactericidal agent (Ag-PVA film) can be used efficiently and repeatedly in several action cycles, allowing simultaneously, its monitoring using spectroscopy and microscopy.

Fabrication of the Ag-PVA Films

The Ag-PVA films were fabricated following the general procedure discussed in the earlier sections. Aqueous solutions with appropriate concentrations of silver nitrate and poly(vinyl alcohol) were mixed (Ag/PVA ratio, x = 0.1) and either spin coated on quartz plates or dip coated on glass rods for carrying out the different kinds of studies discussed below. They were subjected to mild thermal annealing at, T = 130^{o}C for t = 60 min, whereupon the nanoparticles were generated in the film. The Ag-PVA films were characterized by plasmon absorption and TEM imaging. The silver content in the

films used in all antibacterial study is < 0.1 mg. Films prepared with the three different types PVA (PVA(I), PVA(II), PVA(III)) were used in these studies.

The antibacterial studies are conducted in aqueous medium. Hence the choice of the specific PVA used in terms of its average molecular weight (M_w) and the extent of hydrolysis (% hydrolysis) is very critical, since these parameters influence its solubility in water. We have examined three PVA polymer which are available commercially (Aldrich), having M_w and % of hydrolysis respectively: (I) 16 kDa, 98%, (II) 31-50 kDa, 98-99% and (III) 87-146 kDa, 99+%. PVA with % of hydrolysis ≥ 98% alone were chosen since they showed low solubility in water at room temperature. This also implied that the aqueous solutions of PVA had to be prepared in water at 60-70^{o}C, and then cooled to room temperature (~30^{o}C) before mixing with the solution of silver nitrate.

Antibacterial action of Ag-PVA was examined on *Escherichia coli* (NCIM No. 2931, ATCC No. 25922); control experiments were conducted in all cases. The effective concentration of silver used in all the experiments is < 6 ppm. Approximately 10^7 - 10^8 CFU of *E. coli* was inoculated in 15 ml Luria-Bertani (LB) broth. Ag-PVA film coated on 6 cm^2 quartz plate was immersed in this and shaken at 37^{o}C for 10, 30 and 60 min in different runs; the plate was removed immediately after the run. Following this, the bacterial growth was monitored for up to 12 h by measuring the optical density at 600 nm. The main results are collected in Fig. 2.28. Fig. 2.28a - c shows that, when the films are shaken in the broth for 10 min, the bacterial growth suppression is more effective with Ag-PVA(II) and Ag-PVA(III). However, when shaken for 30 min or more, the effective inhibition of bacterial growth is achieved with Ag-PVA(I) and Ag-PVA(III). Ag-PVA(III) produces the maximum bacterial growth inhibition at 10 h. Based on the strongest effects observed, we have chosen Ag-PVA(III) for further antibacterial experiments discussed below. The main aspect investigated in the following experiments is the reusability of the Ag-PVA films; three types of situations were studied.

1. *Bacteria introduced in LB Broth*

Approximately 10^7 - 10^8 CFU of *E. coli* was inoculated in 15 ml LB broth. Ag-PVA(III) film coated on a 6 cm^2 quartz plate was immersed in this and shaken at 37^{o}C

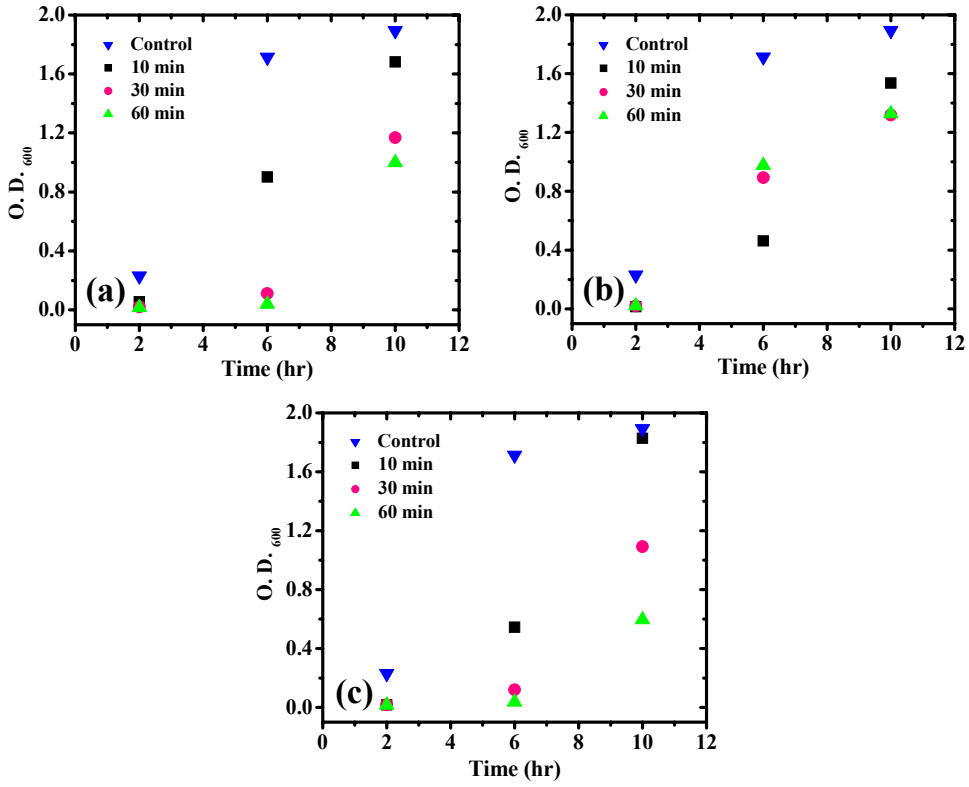

Figure 2.28. *Bacterial growth reflected in the increase of optical density (at 600 nm) of the bacterial suspension (in LB broth) with time; control, samples treated with the films* ***(a)*** *Ag-PVA(I)* ***(b)*** *Ag-PVA(II) and* ***(c)*** *Ag-PVA(III) for different periods of times, 10, 30 and 60 min.*

for 30 min; the plate was immediately removed. Following this, the bacterial growth was monitored for up to 12 h by measuring the optical density at 600 nm. The main results collected in Fig. 2.29 indicate effective inhibition of bacterial growth for up to 8 h in the first two uses of the film and for up to 4 h in the third use of the same film. The changes in the absorption spectra after the reuses are shown in the Fig. 2.30; it is interesting to note that the change in intensity upto third reuse is < 10%. We have examined the film morphology before and after the reuses, using atomic force microscopy (Fig. 2.31). The films show formation of pits, typically ~ 30-100 nm in diameter from the second reuse onwards. This could be a cause behind the degradation of antibacterial activity. We have carried out control experiments in which LB broth alone was used with no bacteria inoculated. The films were found to be unaffected after multiple reuses.

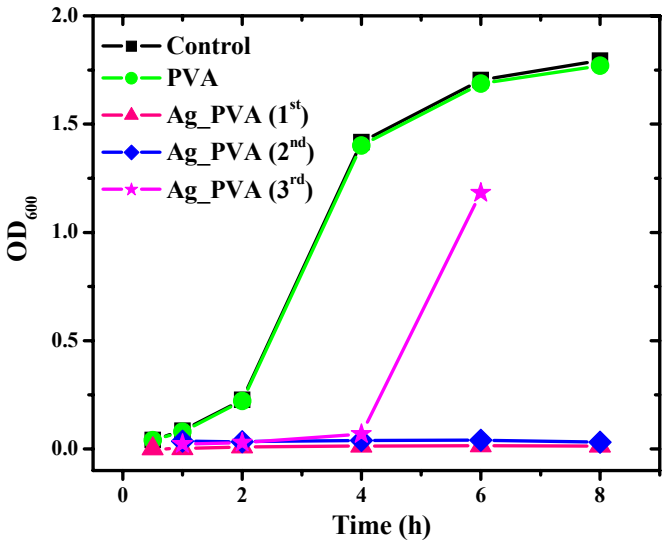

Figure 2.29. *Bacterial growth reflected in the increase of optical density (at 600 nm) of the bacterial suspension (in LB broth) with time; control, sample treated with PVA film, and samples treated with one Ag-PVA(III) film in multiple uses are shown.*

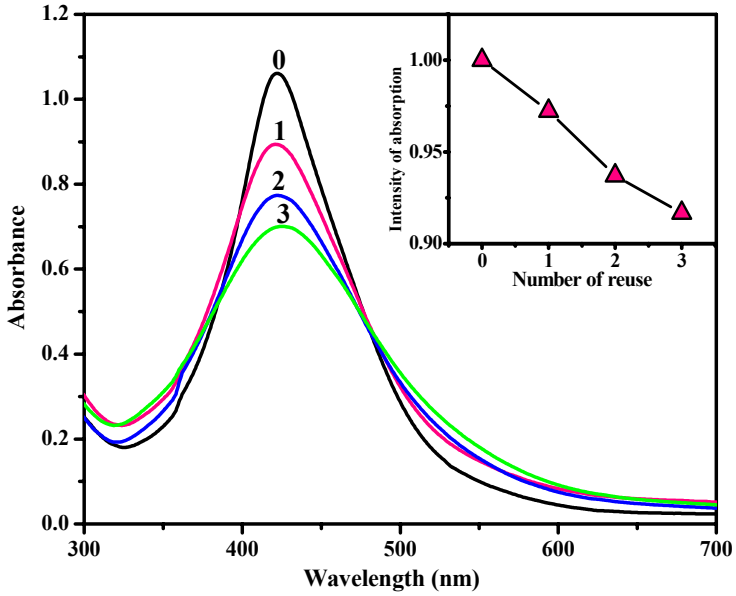

Figure 2.30. *Absorption spectra of the same Ag-PVA(III) film before and after multiple uses for 30 min each in the bacterial suspension (in LB broth). Inset shows the integrated intensity in each case, normalized to the starting value.*

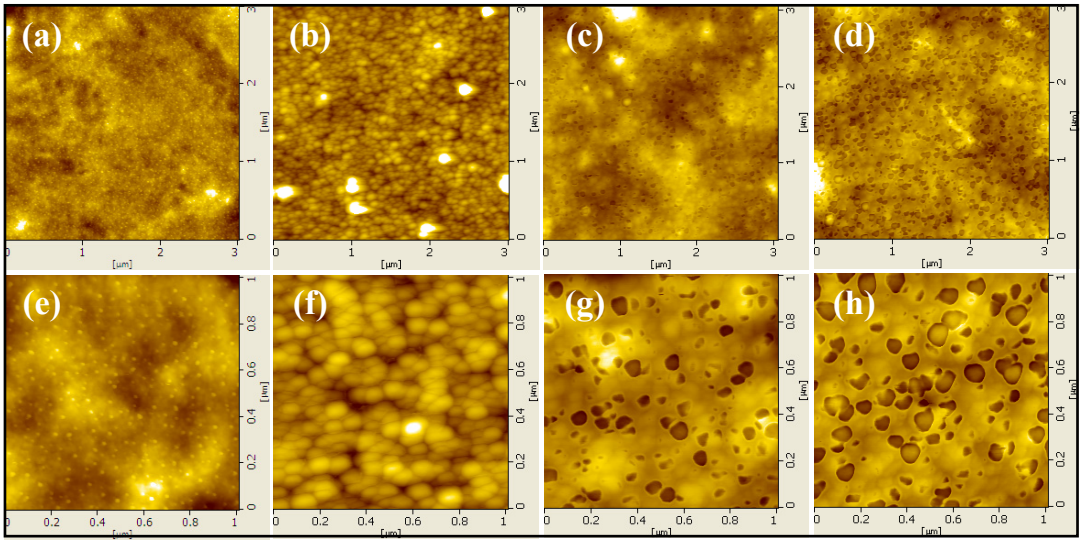

Figure 2.31. *AFM images of the same Ag-PVA(III) film* ***(a)*** *before use and after use for 30 min each in the bacterial suspension (in LB broth)* ***(b)*** *first* ***(c)*** *second and* ***(d)*** *third time. Magnified images of the same films are shown in* ***(e), (f), (g)*** *and* ***(h)*** *respectively.*

2. *Bacteria Introduced in Ultrapure Water*

In the previous experiments, we have used very large concentrations (CFU/ml) of bacteria, which are typically much higher than that encountered in typical drinking water. In spite of this, we have observed the bactericidal action of Ag-PVA films. We have now considered slightly lower concentration of bacteria. Approximately 10^5 CFU of *E. coli* was inoculated in 15 ml of ultrapure water (Millipore). Ag- PVA(III) film coated on a 6 cm^2 quartz plate was immersed in this and shaken at 37^{o}C for 15 min. The test was repeated using the same film 20 times in new samples of bacteria-containing water. Subsequent to each treatment, the water sample was plated on LB agar petri plates and incubated for 12 h at 37^{o}C. The bacterial colonies formed were observed under a microscope. Control sample of water showed > 450 bacterial colonies whereas not a single colony was detected in the experimental samples from up to the 20th reuse of the Ag-PVA film (Fig. 2.32). Absorption spectra of the film were monitored throughout the experiment. Selected spectra of the films upto twenty reuse are collected in the Fig. 2.33. There is very little variation of the spectrum and its intensity observed even after twenty reuses. The AFM images of the film surface show no appreciable change through the multiple uses (Fig. 2.34). The lower concentration of

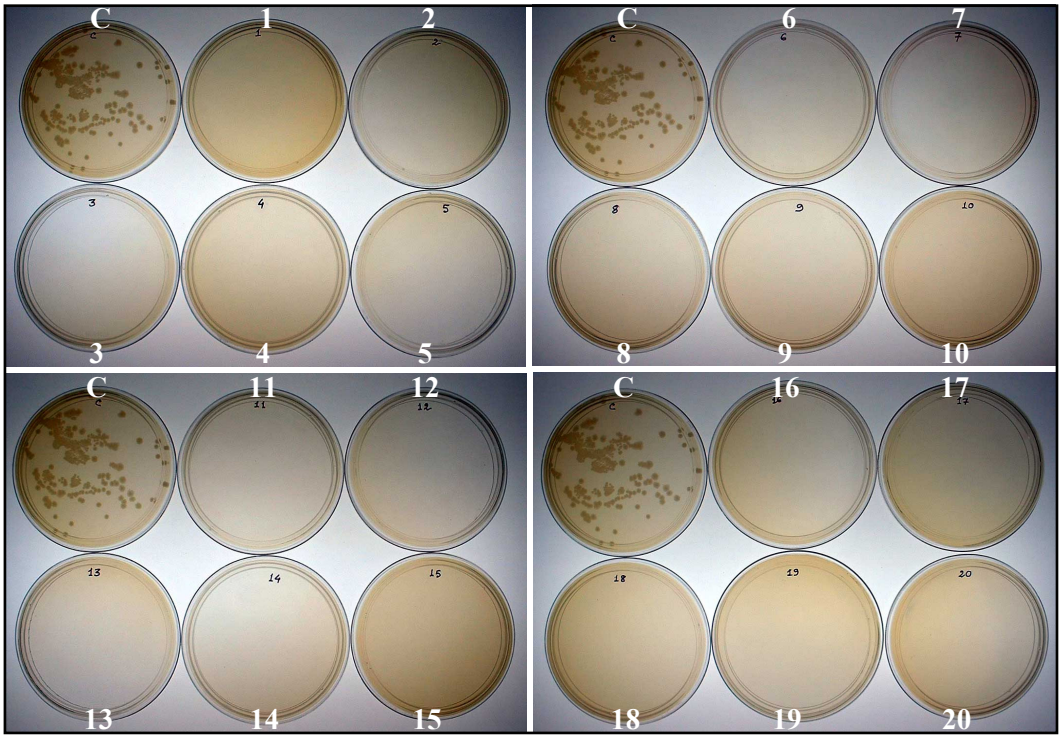

Figure 2.32. *Photographs of petri plates (after 12 h incubation) spread with ultrapure water samples containing E. coli. (10^5 CFU); untreated (C) and treated for 15 min with the same Ag-PVA(III) film in multiple uses (1 - 20) are shown.*

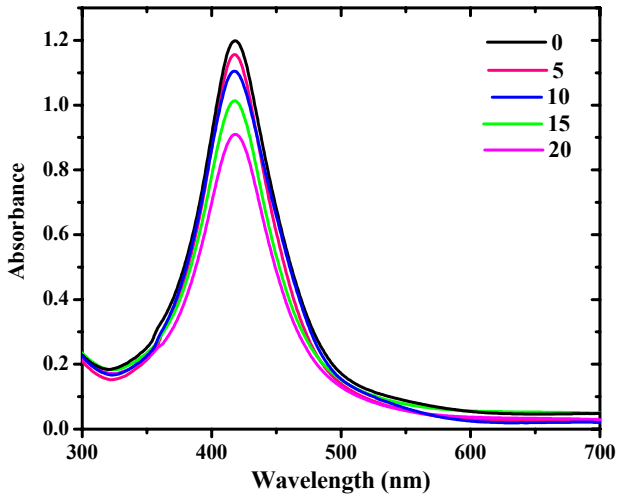

Figure 2.33. *Absorption spectra of the Ag-PVA(III) films before and after multiple uses for 15 min each in ultrapure water samples containing 10^5 CFU of E. coli (the number of uses are indicated on the plot).*

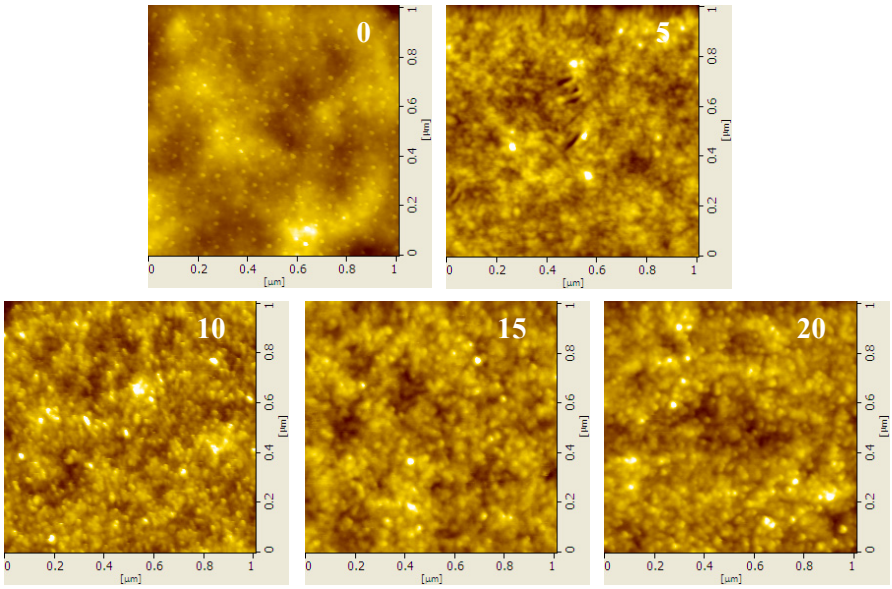

Figure 2.34. *AFM images of the Ag-PVA(III) film before and after multiple uses for 15 min each in ultrapure water samples containing 10^5 CFU of E. coli (the number of uses are indicated on the images).*

bacteria present in this study and the absence of LB broth and bacteria growth process therein, might be the reasons for the film morphology remaining unaffected. This experiment shows that even with fairly large bacterial concentrations, Ag-PVA film is very effective as reusable antibacterial agent for water purification.

3. *Ordinary Tap Water*

Ordinary tap water (possibly containing a range of nonpathogenic and pathogenic bacteria) was treated by stirring with Ag-PVA(III) coated glass rods for 5 min at 37°C. With 15 ml fresh samples of water, the test was repeated 21 times using the same rod. The effective concentration of silver present in the films, in these experiments is ~ 0.4 ppm. While the control showed a bacterial count of ~ 250 CFU/ml, the 5 min treated ones showed tremendous reduction; the sample subjected to the 20th reuse of the same rod showed ≤ 30CFU/ml (Fig. 2.35). Similar results were obtained with a single treatment of ~ 200 - 250 ml water (Fig. 2.36).

The different experiments described above demonstrate the antibacterial capability of silver nanoparticles in Ag-PVA(III) film. The mechanism behind the

Figure 2.35. *Photographs of petri plates spread with ordinary tap water - 15 ml each of untreated sample (C) and samples treated for 5 min with the same Ag-PVA(III) film coated glass rod in multiple uses upto 21 times – and incubated for 12 h.*

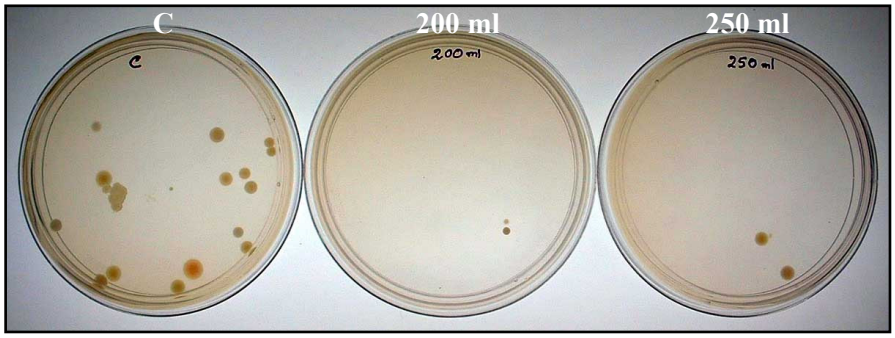

Figure 2.36. *Photographs of petri plates spread with ordinary tap water - untreated sample (C) and 200 ml and 250 ml samples treated for 5 min each with Ag-PVA(III) film coated on glass rod - and incubated for 12 h.*

bactericidal action is not fully clear at the moment. Two general possibilities can be considered: (i) bacteria coming into contact with the silver nanoparticles inside the Ag-PVA film and (ii) silver leaching out from the film into the bacterial medium. The spectroscopy and microscopy experiments suggest that the Ag-PVA films are strongly

affected only when inserted in the LB broth containing large initial concentrations of bacteria (10^7-10^8 CFU) which grow further during incubation. In view of the pit formation observed, leaching of silver from the film is quite possible; particle aggregation may also occur. The pit formation could facilitate contact of bacteria with the nanoparticles inside the film. In the case of water samples with lower concentration of bacteria (10^5 CFU), even though the films are intact, bactericidal action is still observed. The minor decrease in the absorption spectral intensities suggests that the nanoparticles are mildly affected. One possibility is that the films swell when submerged in the aqueous medium allowing bacterial contact with the nanoparticles; particle aggregation may result from this. Another possibility is that the film swelling induces controlled leaching of the nanoparticles and consequent bactericidal action.

2.6. Summary

We have describe in this chapter, a simple and convenient protocol that we have developed for the *in situ* generation of silver nanoparticles inside poly(vinyl alcohol) film, leading to glass-supported or free-standing nanoparticle-embedded films. Plasmon absorption spectra and TEM images of the films were used to characterize the nanoparticle size and distribution, which are shown to be strongly influenced by the metal/polymer ratio and parameters of the thermal treatment. Ag-PVA films with immobilized and size-tuned metal nanoparticles are found to be attractive candidates for optical limiting application. ~ 5 μm thick Ag-PVA/PS film, exhibit optical limiting characteristics (in the nanosecond time scale), comparable to that of colloidal silver with path length of the order of 1 - 2 mm! Nonlinear optical studies using femtosecond pulse laser revealed appreciable nonlinear absorption and optical limiting capability in free-standing PVA/Ag-PVA/PVA films. The positive nonlinearity observed is relatively rare and of potential utility in fabricating devices with graded nonlinear refractive indices. The free-standing nature of the films facilitated unambiguous estimation of the nonlinear refractive index and susceptibility which are comparable to those reported earlier for supported films. The different types of Ag-PVA films with their polymeric constitution and embedded silver nanoparticles are promising candidates for the development of novel optical power limiting devices. The silver nanoparticle-polymer composite films are found to have a very different application as well - as antibacterial

agent for purification of water. The easy fabrication procedure, convenience of developing as a coating material and effective bactericidal action in solution medium with the efficient reuse capability are very significant aspects. The facility to monitor to bactericidal agent between multiple uses is likely to prove very beneficial from the point of view of further explorations. These composite materials can be developed as effective antimicrobial coating for a variety of general and biomedical applications.

References

1. Raveendran, P.; Fu, J.; Wallen, S. L. *J. Am. Chem. Soc.* **2003**, *125*, 13940.
2. (a) Daniel, M. C.; Astruc, D. *Chem. Rev.* **2004**, *104*, 293; (b) Pileni, M. P. *New J. Chem.* **1998**, 693.
3. Korchev, A. S. ; Bozack, M. J.; Slaten, B. L.; Mills, G. *J. Am. Chem. Soc.* **2004**, *126*, 10.
4. Inouye, H.; Tanaka, K.; Tanahashi, I.; Hattori, T.; Nakatsuka, H. *Jpn. J. Appl. Phys.* **2000**, *39*, 5132.
5. (a) Mbhele, Z. H.; Salemane, M. G.; van Sittert, C. G. C. E.; Nedeljković, J. M.; Djoković, V.; Luyt, A. S. *Chem. Mater.* **2003**, *15*, 5019; (b) Feng, Q.; Dang, Z.; Li, N.; Cao, X. *Mater. Sci. Eng.* **2003**, *B99*, 325.
6. (a) Heilmann, A. *Polymer Films with Embedded Metal Nanoparticles*, Springer Verlag, 2002; (b) Zdunek, K. *Surf. Coatings Tech.* **2007**, *201*, 4813.
7. Zhang, Z.; Han, M. *J. Mater. Chem.* **2003**, *13*, 641.
8. (a) Southward, R. E.; Boggs, C. M.; Thompson, D. W.; St. Clair, A. K. *Chem. Mater.* **1998**, *10*, 1408; (b) Zhou, Y.; Yu, S.; Wang, C.; Zhu, Y.; Chen, Z. *Chem. Lett.* **1999**, 677.
9. Warheit, D. B.; Laurence, B. R.; Reed, K. L.; Roach, D. H.; Reynolds, G. A. M.; Webb, T. R. *Toxicol. Sci.* **2004**, *77*, 117.
10. Lim, M. H.; Ast, D. G. *Adv. Mater.* **2001**, *13*, 718.
11. Jiang, C. Y.; Markutsya, S.; Tsukruk, V. V. *Adv. Mater.* **2004**, *15*, 157.
12. Mamedov, A. A.; Kotov, N. A. *Langmuir* **2000**, *16*, 5530.
13. Matsuda, S.; Ando, S. *Polym. Adv. Tech.* **2003**, *14*, 458.
14. (a) *Concise Polymeric Materials Encyclopedia*, (Ed.) J. C. Salamone, CRC Press, Boca Raton, 1999, p. 1338; (b) H.; Huang, L.; Gu, Ozaki, Y. *Polymer*, **2006**, *47*, 3935.
15. Longenberger, L.; Mills, G. *J. Phys. Chem.* **1995**, *99*, 475.
16. (a) Prasad, B. L. V.; Stoeva, S. I.; Sorensen, C. M.; Klabunde, K. J. *Chem. Mater.* **2003**, *15*, 935; (b) Stoeva, S.; Klabunde, K. J.; Sorensen, C. M.; Dragieva, I. *J. Am. Chem. Soc.* **2002**, *124*, 2305.
17. Fritzsche, W.; Porwol, H.; Wiegand, A.; Bornmann, S.; Köhler, J. M. *Nanostruct. Mater.* **1998**, *10*, 89.
18. (a) Smetana, A. B.; Klabunde, K. J.; Sorensen, C. M.; Ponce, A. A.; Mwale, B. *J. of Phys. Chem. B* **2006**, *110*, 2155. (b) Smetana, A. B.; Klabunde, K. J.; Sorensen, C. M. *J. of Coll. Inter. Sci.* **2005**, *284*, 521.
19. (a) Gudiksen, M. S.; Lauhon, L. J.; Wang, J.; Smith, D. C.; Lieber, C. M. *Nature* **2002**, *415*, 617; (b) Li, Y.; Wu, Y.; Ong, B. S. *J. Am. Chem. Soc.* **2005**, *127*, 3266.
20. (a) De, S.; Pal, A.; Pal, T. *Langmuir* **2000**, *16*, 6855; (b) Zhang, X.; Sun, B.; Friend, R. H.; Guo, H.; Nau, D.; Giessen, H. *Nano Lett.* **2006**, *6*, 651.
21. (a) Kang, Y.; Erickson, K. J.; Taton, T. A. *J. Am. Chem. Soc.* **2005**, *127*, 13800; (b) Sönnichsen, C.; Reinhard, B. M.; Liphardt, J.; Alivisatos, A. P. *Nature Biotechnol.* **2005**, *23*, 741; (c) Wang, H.; Halas, N. J. *Nano Lett.* **2006**, *6*, 2945.

22. (a) Wohltjen, H.; Snow, A. W. *Anal. Chem.* **1998**, *70*, 2856; (b) Kim, Y.; Johnson, R. C.; Hupp, J. T. *Nano Lett.* **2001**, *1*, 165; (c) Zamborini, F. P.; Leopold, M. C.; Hicks, J. F.; Kulesza, P. J.; Malik, M. A.; Murray, R. W. *J. Am. Chem. Soc.* **2002**, *124*, 8958; (d) Obare, S. O.; Hollowell, R. E.; Murphy, C. J. *Langmuir* **2002**, *18*, 10407; (e) Krasteva, N.; Besnard, I.; Guse, B.; Bauer, R. E.; Mu1llen, K.; Yasuda, A.; Vossmeyer, T. *Nano Lett.* **2002**, *2*, 551; (f) Lee, K.; El-Sayed, M. A. *J. Phys. Chem. B* **2006**, *110*, 19220.

23. (a) Stepanov, A. L. *Technical Physics*, **2004**, *49*, 143; (b) Takele, H.; Greve, H.; Pochstein, C.; Zaporojtchenko, V.; Faupel, F. *Nanotechnology* **2006**, *17*, 3499.

24. (a) Sun, Y.; Riggs, J. E. *Int. Rev. Phys. Chem.* **1999**, *18*, 43; (b) Sun, Y.; Riggs, J. E.; Rollins, H. W.; Guduru, R. *J. Phys. Chem. B* **1999**, *103*, 77; (c) Sun, Y.; Riggs, J. E.; Henbest, K. B.; Martin, R. B. *J. Nonlin. Opt. Phys. Mater.* **2000**, *9*, 481; (d) Qu, S.; Song, Y.; Liu, H.; Wang, Y.; Gao, Y.; Liu, S.; Zhang, X.; Li, Y.; Zhu, D. *Opt. Comm.* **2002**, *203*, 283; (e) Nair, A. S.; Suryanarayanan, V.; Pradeep, T.; Thomas, J.; Anija, M.; Philip, R. *Mater. Sci. Engg. B, Solid State Mater. Adv. Techn.* **2005**, *B117*, 173; (f) Sun, W.; Dai, Q.; Worden, J. G.; Huo, Q. *J. Phys. Chem. B* **2005**, *109*, 20854; (g) Wang, G.; Sun, W. *J. Phys. Chem. B* **2006**, *110*, 20901.

25. (a) Qu, S.; Zhao, C.; Jiang, X.; Fang, G.; Gao, Y.; Zeng, H.; Song, Y.; Qiu, J.; Zhu, C.; Hirao, K. *Chem. Phys. Lett.* **2003**, *368*, 352; (b) Shen, H.; Cheng, B. L.; Lu, G. W.; Guan, D. Y.; Chen, Z. H.; Yang, G. Z. *J. Phys. D: Appl. Phys.* **2006**, *39*, 233; (c) Martin, R. B.; Meziani, M. J.; Pathak, P.; Riggs, J. E.; Cook, D. E.; Perera, S.; Sun, Y.-P. *Opt. Mater.* **2007**, *29*, 788.

26. Karthikeyan, B.; Anija, M.; Philip, R. *Appl. Phys. Lett.* **2006**, *88*, 053104.

27. (a) He, J.; Mi, J.; Li, H.; Ji, W. *J. Phys. Chem. B* **2005**, *109*, 19184; (b) Gong, H.-M.; Wang, X.-H.; Du, Y.-M.; Wang, Q.-Q. *J. Chem. Phys.* **2006**, *125*, 024707.

28. (a) Kyoung, M.; Lee, M. *Opt. Comm.* **1999**, *171*, 145; (b) Elim, H. I.; Yang, J.; Lee, J.-Y. *Appl. Phys. Lett.* **2006**, *88*, 083107.

29. Liu, T.-M.; Tai, S.-P.; Yu, C.-H.; Wen, Y.-C.; Chu, S.-W. *Appl. Phys. Lett.* **2006**, *89*, 043122.

30. Neto, N. M. B.; Mendonca, C. R.; Misoguti, L.; Zilio, S. C. *Appl. Phys. B* **2004**, *78*, 1.

31. (a) Kamanina, N.; Putilin, S.; Stasel'ko, D. *Synth. Metals* **2002**, *127*, 129; (b) Tong, R.; Wu, H.; Li, B.; Zhu, R.; You, G.; Qian, S.; Lin, Y.; Cai, R. *Physica B* **2005**, *366*, 192.

32. Vestberg, R.; Westlund, R.; Eriksson, A.; Lopes, C.; Carlsson, M.; Eliasson, B.; Glimsdal, E.; Lindgren, M.; Malmström, E. *Macromolecules* **2006**, *39*, 2238.

33. Kiran, P. P.; De, G.; Rao, D. N. *IEE Proc. Circuits Devices Syst.* **2003**, *150*, 559.

34. Hagan, D. J.; Van Stryland, E. W.; Wu, Y. Y.; Wei, T. H.; Sheik-Bahae, M.; Said, A.; Mansour, K.; Young, J.; Soileau, M. J. *SPIE – Materials for Optical Switches, Isolators, and Limiters* **1989**, *1105*, 103.

35. (a) Sun, Y.; Riggs, J. E.; Rollins, H. W.; Guduru, R. *J. Phys. Chem. B* **1999**, *103*, 77; (b) Ispasoiu, R. G.; Balogh, L.; Varnavski, O. P.; Tomalia, D. A.; Goodson, T. *J. Am. Chem. Soc.* **2000**, *122*, 11005.

36. Ganeev, R. A.; Ryasnyansky, A. I. *Appl. Phys. B* **2006**, *84*, 295.

37. Boggess, T. F.; Bohnert, K.; Mansour, K.; Moss, S. C.; Boyd, I. W.; Smirl, A. L. *IEEE J. Quantum Electron.* **1986**, *QE-22*, 360.
38. Guo, S.; Xu, L.; Wang, H. T.; You, X. Z.; Ming, N. B. *Optik* **2003**, *114*, 58.
39. Sheik-Bahae, M.; Said, A. A.; Wei, T.–H.; Hagan, D. J.; van Stryland, E. W. *IEEE J. Quantum Electron.* **1990**, *26*, 760.
40. (a) Friedenthal, H. *Biochem. Z.* **1919**, *94*, 47; (b) Feng, Q. L.; Wu, J.; Chen, G. Q.; Cui, F. Z.; Kim, T. N.; Kim, J. O. *J. Biomed. Mater. Res.* **2000**, *52*, 662.
41. (a) Klueh, U.; Wagner, V.; Kelly, S.; Johnson, A.; Bryers, J. D. *J. Biomed. Mater. Res.* **2000**, *53,* 621; (b) Sun, R. W.-Y.; Chen, R.; Chung, N. P.-Y.; Ho, C.-M.; Lin, C.-L. S.; Che, C.-M. *Chem. Commun.* **2005**, 5059; (c) Morones, J. R.; Elechiguerra, J. L.; Camacho, A.; Holt, K.; Kouri, J. B.; Ramírez, J. T.; Yacaman, M. J. *Nanotechnology* **2005,** *16*, 2346; (d) Tian, J.; Wong, K. K. Y.; Ho, C.-M.; Lok, C.-N.; Yu, W.-Y.; Che, C.-M.; Chiu, J.-F.; Tam, P. K. H. *ChemMedChem* **2006**, *2*, 129.
42. (a) Aymonier, C.; Schlotterbeck, U.; Antonietti, L.; Zacharias, P.; Thomann, R.; Tiller, J. C.; Mecking, S. *Chem. Commun.*, **2002**, 3018; (b) Jeong, S. H.; Hwang, Y. H.; Yi, S. C. *J. Mater. Sci.* **2005**, *40*, 5413; (c) Baker, C.; Pradhan, A.; Pakstis, L.; Pochan, D. J.; Shah, S. I. *J. Nanosci. Nanotechnol.* **2005**, *5*, 244; (d) Zeng, F.; Hou, C.; Wu, S.; Liu, X.; Tong, Z.; Yu, S. *Nanotechnology* **2007**, *18*, 055605.
43. Gogoi, S. K.; Gopinath, P.; Paul, A.; Ramesh, A.; Ghosh, S. S.; Chattopadhyay, A. *Langmuir* **2006***, 22,* 9322.
44. (a) Kim, J.-W.; Lee, J.-E.; Ryu, J.-H.; Lee, J.-S.; Kim, S.-J.; Han, S.-H.; Chang, I.-S.; Kang, H.-H.; Suh, K.-D. *J. Polym. Sci.: Part A: Polym. Chem.* **2004**, *42*, 2551; (b) Kumar, R.; Howdle, S.; Münstedt, H. *J. Biomed. Mater. Res.* **2005**, *75B*, 311; (c) Hong, K. H.; Park, J. L.; Sul, I. H.; Youk, J. H.; Kang, T. J. *J. Polym. Sci.: Part B: Polym. Phys.* **2006**, *44*, 2468; (d) Li, Z.; Lee, D.; Sheng, X.; Cohen, R. E.; Rubner, M. F. *Langmuir* **2006**, *22,* 9820; (e) Yu, H.; Xu, X.; Chen, X.; Lu, T.; Zhang, P.; Jing, X. *J. Appl. Polym. Sci.* **2007**, *103*, 125.
45. Jain, P.; Pradeep, T. *Biotech. Bioengg.* **2005**, *90*, 59.
46. Chou, W.-L.; Yu, D.-G.; Yang, M.-C. *Polym. Adv. Technol.* **2005**, *16,* 600.
47. (a) Lee, H. J.; Yeo, S. Y.; Jeong, S. H. *J. Mater. Sci.* **2003**, *38*, 2199; (b) Tarimala, S.; Kothari, N.; Abidi, N.; Hequet, E.; Fralick, J.; Dai, L. L. *J. App. Polym. Sci.* **2006**, *101*, 2938.
48. (a) Taleb, A.; Petit, C.; Pileni, M. P. *Chem. Mater.* **1997**, *9,* 950; (b) Raveendran, P.; Fu J.;, Wallen, S. L. *J. Am. Chem. Soc.* **2003**, *125*, 13940; (c) Callegari, A.; Tonti, D.; Chergui, M. *Nano Lett.* **2003***, 3*, 1565; (d) Panáček, A.; Kvítek, L.; Prucek, R.; Kolář, M.; Večeřová, R.; Pizúrová, N.; Sharma, V. K.; Nevěčná, T.; Zbořil, R. *J. Phys. Chem. B* **2006**, *110,* 16248.

Scope

Shapes of nanoparticles can have significant influence on their properties and hence, applications. In the course of our efforts to fabricate metal nanoparticles in situ inside polymer films, we have observed that gold forms nanoplates with different polygonal shapes inside the polymer matrix without the help of special templates or linker molecules. The gold nanoplates are generated in poly(vinyl alcohol) film through thermal treatment, the polymer serving as the reducing agent and stabilizer for the nanoparticle formation and enforcing preferential orientation of the plates. The rare pentagon as well as the more commonly observed hexagon, triangle and square/ rectangle are obtained by tuning the gold/polymer ratio and the time and temperature of fabrication. We have also investigated the optical limiting capability of the gold nanoplates-embedded polymer thin films. An assortment of preliminary studies on the synthesis of gold nanopyramids, real time monitoring of the in situ growth of gold nanodomes inside polymer films and green synthesis of gold nanocrystals are discussed.

3.1. Introduction

Properties of nanocrystals are strongly influenced by their size, shape and assembly. Synthesis that enables control over these attributes and generates novel nanostructures are of fundamental interest. The most common approaches for the synthesis of metal nanoparticles are usually based on the colloidal route and the size and shape control are often rendered through the choice of capping agents or seeding protocols. We envisaged that the growth of nanoparticles inside anisotropic environments such as thin solid polymer films would be a simple and convenient approach to gain enhanced control of nanoparticle shape. As discussed in the previous chapter, such *in situ* fabrications offer additional advantages such as the production of free-standing films[1] for device applications, the possibility of further optical and mechanical manipulations,[2] preclusion of potential health hazards of inhalable nanoparticles,[3] and through judicious choice of the polymer, environmentally safe synthesis[4] without the requirement of additional reducing/stabilizing agents.

Gold nanoparticles in a wide range of shapes have been reported; these include triangle,[5] square/cube,[6] hexagon,[7] rod[8] and tadpole.[9] Even though there is a report of faceted nanocrystals with a few possessing pentagonal faces,[10] a route to regular

pentagonal gold nanoplates is conspicuously absent. Many methods are available for the synthesis of gold nanocrystals,[11] including those carried out inside confined spaces;[12] however, selective formation of several shapes by small variations in a single process are rare.[7] Addressing the latter question, we have explored the *in situ* synthesis of gold nanoparticles in spin-cast poly(vinyl alcohol) films through mild thermal treatment, following the general methodology we have developed (Sec. 2.2).[13] This approach is found to provide facile control on the particle shape leading to triangular, square/rectangular, pentagonal and hexagonal nanoplates and several other shapes and patterns. Significantly, the nanoplates show preferential orientation in the thin films. The fabrication of Au-PVA films allowed us to explore the chemistry occurring inside the polymer matrix, using infra-red spectroscopy. The Au-PVA combination appears to be a rich source of novel nanostructures.

3.2. Shape Tuning of the Nanoplates

The gold-polymer composite films were fabricated using the following procedure. Different weights (3.6 mg, 7.2 mg, 14.4 mg, 21.6 mg, 32.4 mg) of hydrogen tetrachloroaurate (III) trihydrate ($HAuCl_4$, $3H_2O$) (Aldrich) dissolved in 0.5 ml water was mixed with a solution of 90 mg of poly(vinyl alcohol), PVA (Aldrich, average molecular weight = 13 - 23 kDa, % hydrolysis = 86) in 0.3 ml water to prepare the five different compositions which are designated using the Au/PVA weight ratios (x), 0.02, 0.04, 0.08, 0.12, 0.18 respectively. The solution mixture was diluted by adding 0.3 ml more of water and mixed properly. Cleaning of glass/quartz plates and spin coating the polystyrene (PS) layers on the glass substrate followed the methodology discussed in Sec. 2.2. The $HAuCl_4$-PVA solutions were spin-coated on glass or quartz substrates directly or with a pre-coating of PS at 6,000 RPM for 10 sec. The thickness of the Au-PVA and PS layers were measured using a profilometer and found to be ~ 0.5 and ~ 4.0 μm respectively. The film coated plates were placed in a closed stainless steel chamber and heated in a standard oil bath at different temperatures, T = 100 - 170^{o}C and times, t = 5 - 60 min. A few different heating rates were also explored. Following the protocol mentioned in Fig. 2.1, the Au-PVA/PS films can be peeled off as free-standing films or PS layer could be dissolved in toluene to release the Au-PVA free-standing film. Fig. 3.1 shows the free-standing films which could be directly examined in a TEM.

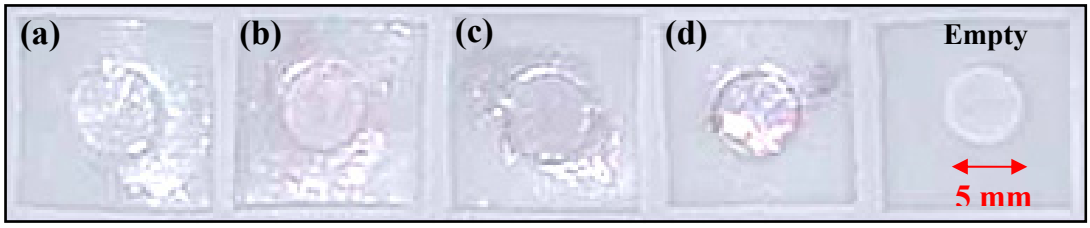

Figure 3.1. *Photographs of Au-PVA free-standing films on teflon supports; with x, T (°C) and t (min) :* ***(a)*** *0.04, 170, 5,* ***(b)*** *0.08, 130, 30,* ***(c)*** *0.12, 100, 60 and* ***(d)*** *0.18, 100, 60. The empty hole shows the contrast.*

The Au-PVA films coated on quartz substrates were used for the absorption spectroscopy study. The *in situ* formation of gold nanoparticles in the PVA film is demonstrated by the emergence of the surface plasmon resonance absorption. As we show from the TEM studies, the particle sizes are in the range ~ 10 - 90 nm; therefore in addition to plasmon absorption, there could be a contribution from scattering, in the spectra,[14] making the term extinction spectra more appropriate. However, for the sake of consistency with the rest of the thesis we continue to use the term, absorption spectra. The spectra recorded for the Au-PVA films shown in Fig. 3.1, are collected in Fig. 3.2. The peak intensities show that the nanoparticle production increases with increasing

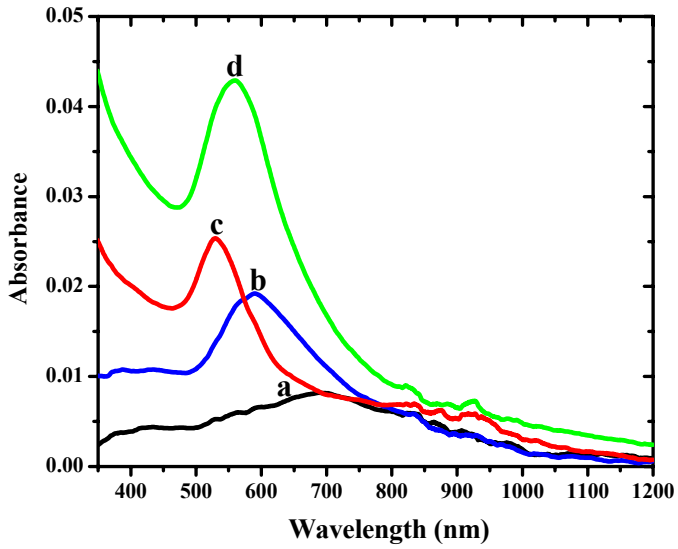

Figure 3.2. *Absorption spectra of Au-PVA films with x, T (°C) and t (min) : (a) 0.04, 170, 5; (b) 0.08, 130, 30; (c) 0.12, 100, 60 and (d) 0.18, 100, 60.*

value of x and the absorption maxima are blue-shifted in parallel, from (a) to (c); (d) is slightly red-shifted with respect to (c). A weak near infra-red absorption is also observed in all the cases.

TEM studies were carried out on thin film samples prepared following the same methodology described in Sec 2.3, with various Au/PVA compositions and thermal treatments. In most cases, the Au particles generated are found to have plate morphology with preferential orientation parallel to the substrate. This is probably promoted by the thin film nature of the polymer matrix. The shapes and sizes of the nanoplates are found to be sensitive to the value of x, temperature, T and time, t of heating. When both the concentration and temperature are low, no particles are formed, whereas when both are high, a mixture of plates with different shapes is obtained. Careful control of these factors led to the enrichment (~ 70 - 80%) of specific polygonal shapes. Fig. 3.3 illustrates the prominent polygonal nanoplates obtained and the conditions favoring their formation. Regularity is observed in the evolution of the shape; pentagon, hexagon, triangle and square/rectangle are formed with increasing concentration, decreasing temperature and increasing heating time. The rationale behind the observed sequence is not clear. The density of particles is commensurate with the concentration. The perfect regular pentagons deserve special mention. To the best of our knowledge, exclusive formation of pentagonal nanoplates of gold or any other metal was not reported earlier; pentagonal forms have been found only in mixtures with other morphologies,[15] in twin structures[16] or faceted crystals[10] and as tubes.[17] The restricted growth allowed by the solid polymer matrix appears to be the critical factor promoting pentagonal plate formation in the present case. The size of the polygons shows sequential variation; the sides of the pentagons, hexagons, triangles and squares/ rectangles are in the range, 70 - 85, 20 - 35, 15 - 45 and 10 - 25 nm respectively. These are notably smaller than the sizes of polyhedral gold nanocrystals reported earlier[5-9] ranging from 200 - 500 nm. The plate morphology of the nanocrystals in the PVA matrix is revealed by the slightly tilted crystals found occasionally in the films. The thickness of these plates is ~ 5 - 8 nm (Fig. 3.4). The aspect ratios range from 15 - 2.

The absorption spectra for the Au-PVA films (Fig. 3.2) are consistent with the TEM observations. The peak intensities scale with the density of particles. The absorption maxima are blue-shifted with decreasing size, from pentagon to hexagon to

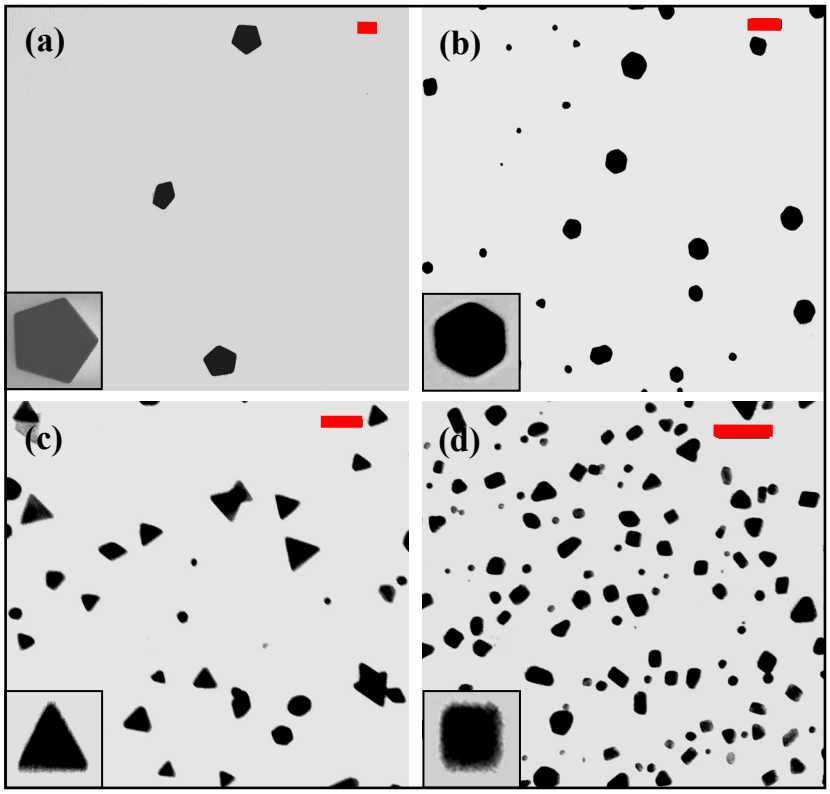

Figure 3.3. *TEM images of Au-PVA films with polygonal nanoplates generated under different conditions. The x, T (^{o}C) and t (min) are indicated in that order in parenthesis: (a) pentagons (0.04, 170, 5); (b) hexagons (0.08, 130, 30); (c) triangles (0.12, 100, 60) and (d) squares/rectangles (0.18, 100, 60) (scale bar = 50 nm). Inset shows enlarged view of a single nanoplate with the dominant shape in each case.*

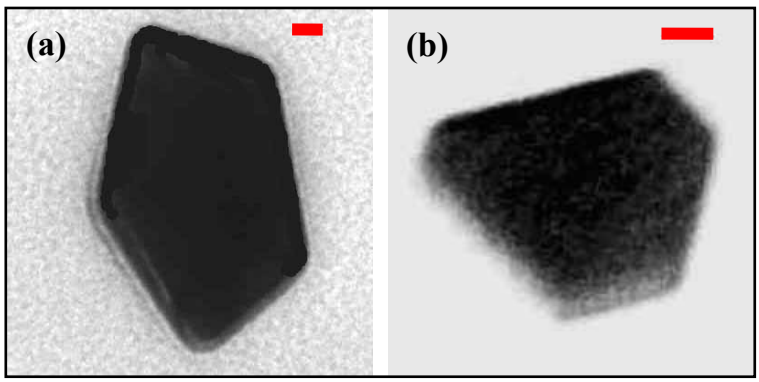

Figure 3.4. *TEM images of gold pentagon and truncated triangle found in tilted orientation in the Au-PVA film (scale bar = 10 nm).*

triangle; the red shift with square/rectangle could be attributed to the admixture of larger size triangles. The observed weak near infra-red absorption is the consequence of the moderate aspect ratios.

Under specific conditions, a range of other shapes and patterns are observed in the gold plates generated in the polymer matrix (Fig. 3.5); Table 3.2 presents the complete list of composition and fabrication conditions for different Au-PVA films and the morphologies of gold nanostructures observed in each case. Examples illustrated in Fig. 3.6 show beautiful stress patterns in a collection of different shapes and what looks like a conglomerate of polygons. It is likely that the uniform stress imposed by the polymer

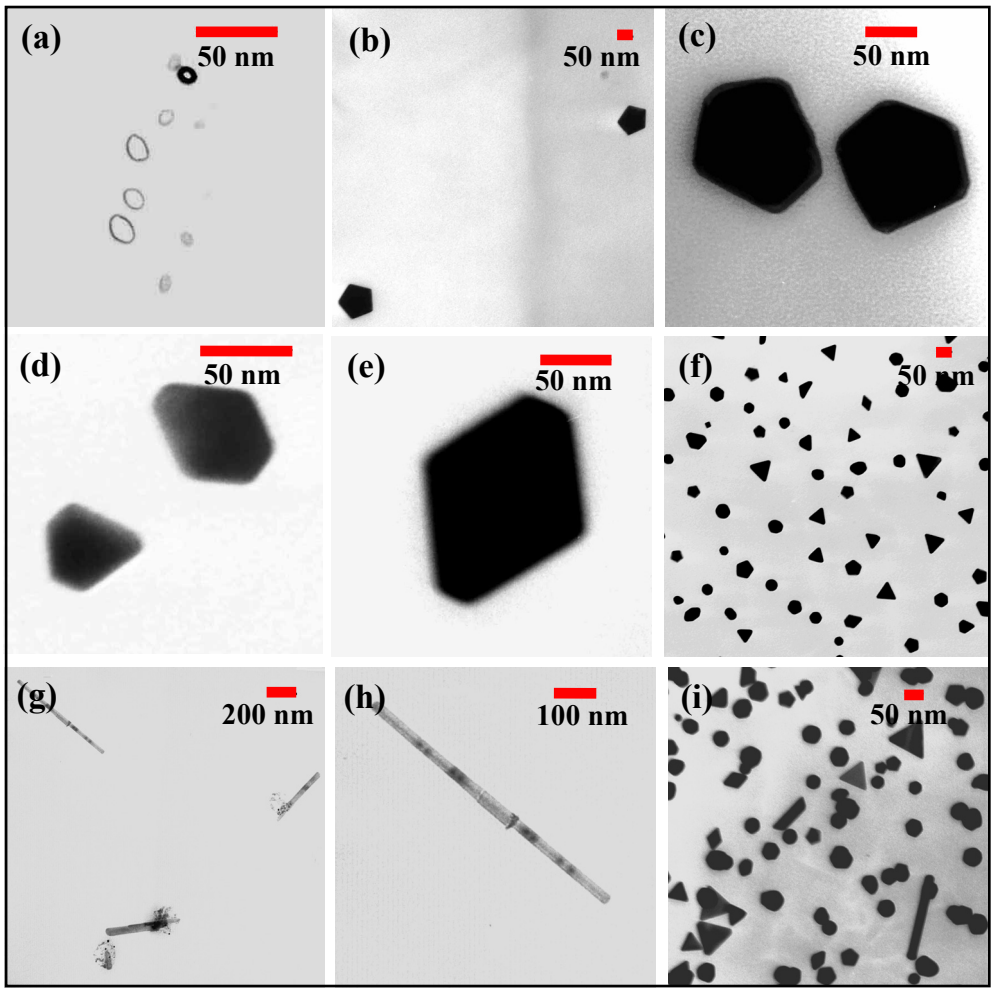

Figure 3.5. *TEM images of the Au-PVA films with a range of shapes. The fabrication conditions corresponding to each image is given in Table 3.2.*

Table 3.2. Composition and fabrication conditions of Au-PVA films and the shape/ morphology of Au nanoplates/nanoparticles observed in these films.

Au/PVA ratio (x)	T (^{o}C), t (min)	Shape/morphology	Figure number for TEM image
0.02	100, 2*	Rings	3.6 (a)
	170, 5	Regular pentagons	3.6 (b)
0.04	100, 2*	Irregular truncated pentagons	3.6 (c)
	100, 60	Twinned structures with stress patterns	3.7 (c), (d), (e)
	130, 60	Triangles with stress patterns	3.7 (a), (b)
	170, 5	Regular pentagons	3.4 (a)
0.08	100, 2*	Irregular pentagons, hexagons	3.6 (d), (e)
	130, 30	Regular hexagons	3.4 (b)
	130, 60	Hexagons to circular with stress patterns	3.7 (f)
0.12	100, 30*	Long needles	3.6 (g), (h)
	100, 60	Regular triangles	3.4 (c)
	130, 60	Triangles, pentagons	3.6 (f)
0.18	100, 60	Squares, rectangles	3.4 (d)
	130, 60	Mixed polygons	3.6 (i)

* The films were heated from room temperature (27 - 30^{o}C) to the designated temperature over ~3 h and held at that temperature for the time specified. In other cases, the samples were placed in the chamber heated to the designated temperature and then held at that temperature for the time specified.

matrix causes the symmetric buckling of the ultrathin gold plates.[18] Electron diffraction from several single nanoplates were examined (Fig. 3.7). The patterns can be indexed to fcc gold with a dominant (111) face.

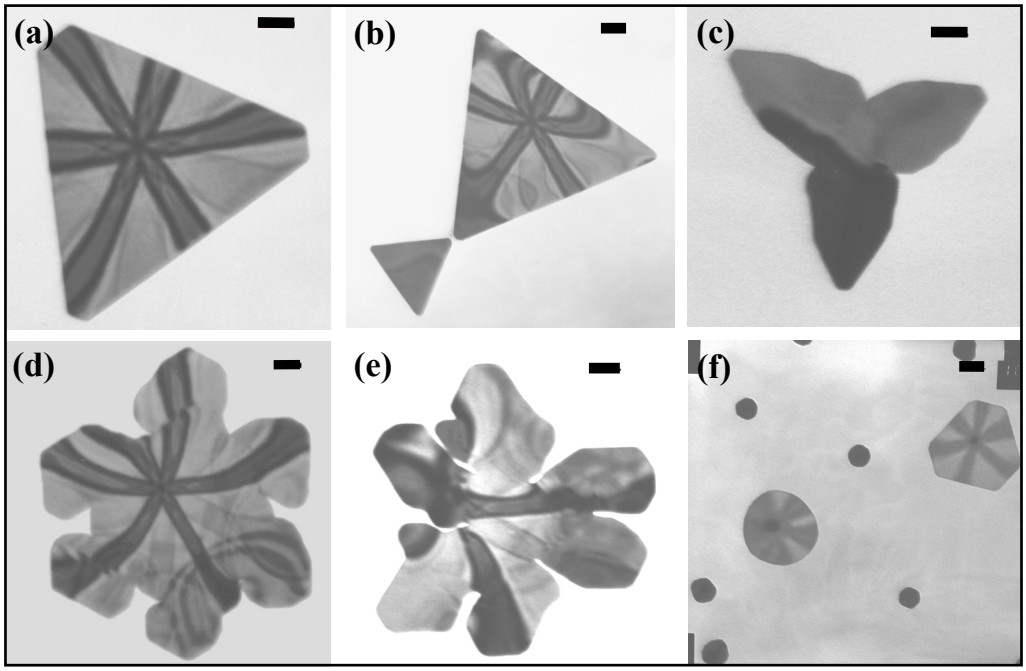

Figure 3.6. *TEM images of gold nanoplates in PVA films, formed with stress patterns (scale bar = 50 nm). The fabrication conditions corresponding to each image is given in Table 3.2.*

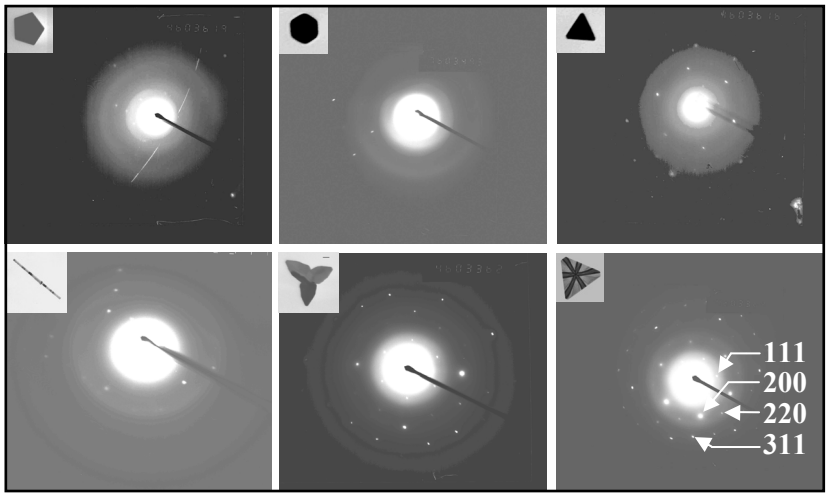

Figure 3.7. *Electron diffraction patterns (the specific nanoplate on which the ED is recorded is shown in the inset); indexing of the diffraction spots is shown on one of the patterns.*

3.3. Chemistry inside the Polymer Matrix

As noted in the previous section and in our earlier discussions, no specific reducing agents, other than the polymer itself is employed in our method of fabricating metal nanoparticle-embedded polymer films. In the present experiments, PVA alone is available for the reduction of the $AuCl_4^-$ ions. The polyol process is a popular method for the synthesis of metal nanoparticles. Ethylene glycol is often employed for the reduction of metal ions to form the nanoparticles; examples include silver,[19-21] platinum[22] and ruthenium.[23] PVA has been used as the reducing agent in the synthesis of silver[13, 24] and gold[25] nanoparticles; reduction of $AuCl_4^-$ to gold nanoparticles has been reported to occur slowly at room temperature.[25] We have examined the chemical changes occurring in the spin-cast films during the thermally induced metal reduction by the polymer.

FT-IR spectra of the free-standing films provide insight into the reaction process. The films were prepared by spin-coating at 1,000 RPM for 10 sec. Two layers of PS were coated as usual, followed by three or five layers of $HAuCl_4$-PVA. The higher values of x = 0.18 and 0.36 were chosen to ensure that clear spectral signatures were obtained. Spectra were recorded in transmission mode, from 4000 - 600 cm^{-1}. The general characteristics were found to be reproducible in the spectra of films with different thickness and gold content. The spectra for PS, PVA/PS (before and after heating) and $HAuCl_4$-PVA/PS (before and after heating, the latter corresponding to Au-PVA/PS), are provided in Fig. 3.8; the latter correspond to the cases having 5-layer $HAuCl_4$-PVA and x = 0.36. The heat treatment was carried out at T = 100^oC, for t = 60 min (a free-standing film was cut into two portions and only one part was subjected to the heat treatment, while the other one was retained at room temperature). Significant changes, if any, are observed only in the region 4000 - 1000 cm^{-1}; hence only this part is shown in Fig. 3.8, with the relevant peaks indicated. PVA/PS film showed characteristic absorptions at 3347 cm^{-1} and 1732 cm^{-1} assignable to hydroxy and carbonyl groups stretching vibrations respectively; the latter arises due to the remnant acetyl groups present in the PVA. It is significant to note that the spectrum of PVA/PS is unchanged on heating; this indicates that the broad peak at 3347 cm^{-1} is primarily due to the alcohol groups and not water. The unheated $HAuCl_4$-PVA/PS film shows a considerably reduced carbonyl peak, possibly as a result of the interaction with the acid

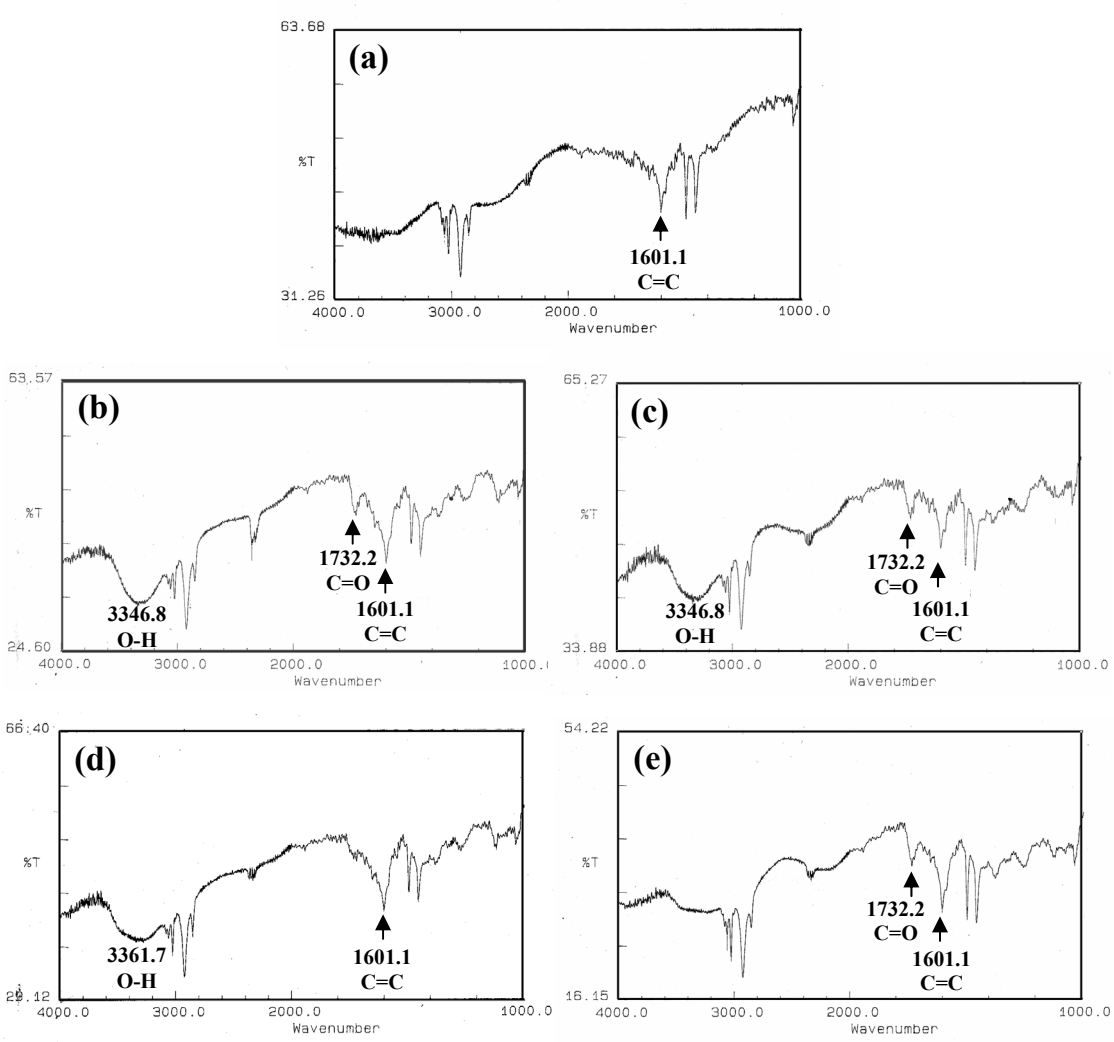

Figure 3.8. *FT-IR spectra of free-standing films of* ***(a)*** *PS; PVA/PS* ***(b)*** *before and* ***(c)*** *after heating; $HAuCl_4$-PVA/PS* ***(d)*** *before and* ***(e)*** *after heating.*

protons.[26] Most significantly, on heating the film, the carbonyl peak appears with an intensity higher than that in PVA/PS, accompanied by a marked reduction of the hydroxy peak absorption; the aromatic C=C stretch due to the PS layer at 1601 cm^{-1} could be used as a convenient internal standard to monitor peak intensity variations. A semi-quantitative assessment of the peak intensities was carried out by measuring the peak height from a baseline drawn connecting the beginning and end of each peak. The intensity is estimated by normalizing with respect to the intensity of the C=C stretch vibration from the aromatic ring of PS which remains unaffected by the heating and

chemical reactions in the film. The relevant values of C=O peak intensities listed in Table 3.1 provide a basis for the observations described above.

Table 3.1. *The values of C=O peak intensities for different samples.*

Sample film	**Intensity of C=O stretch normalized w.r.t. that of C=C stretch vibration**
PVA/PS (before heating)	0.38
PVA/PS (after heating)	0.38
$HAuCl_4$-PVA/PS (before heating)	0.27
$HAuCl_4$-PVA/PS (after heating) i.e. Au-PVA/PS	0.51

From the spectral changes observed, we infer that the following steps occur during the process of formation of the Au nanoparticles : (i) when $HAuCl_4$ is added to PVA, the acid protons coordinate to the carbonyl groups of the remnant acetyl groups of PVA (note that the PVA used is only 86% hydrolyzed), (ii) on heating, the alcohol groups of PVA reduce the $AuCl_4^-$ ion to Au; HCl is the byproduct, and (iii) the keto groups formed from the oxidation of the alcohol as well as the original carbonyl groups on PVA are coordinated by protons from the by-product HCl. So the mechanism for gold nanoparticle formation based on the IR spectral changes together with the appearance of the gold nanoparticle SPR peak indicate that the alcohol groups of the PVA reduce the metal ions, themselves getting oxidized to ketones in the process. HCl is the by-product and the protons are likely to interact with the keto groups; however, their larger population leads to the improved intensity.

The chemical reactions occurring in the PVA film matrix during the thermal annealing process might be complex, involving several side reactions. However based on the infra-red spectroscopy studies describe above and the mechanism proposed earlier[19] for the formation of metal nanoparticles using ethylene glycol as the reducing agent ('polyol route'), the chemical reactions involving the secondary alcohol group on the polymer may be written as:

$$3\ R_2CHOH\ +\ 2\ HAuCl_4\ \rightarrow\ 3\ R_2CO\ +\ 8\ HCl\ +\ 2\ Au$$

Similar chemical reactions may be envisaged for the formation of other metals such as silver and palladium discussed in this thesis.

3.4. Optical Limiting

We have carried out some preliminary examination of the optical limiting capability of Au-PVA films. The strong linear absorption of gold nanoplates at ~ 530 nm (Fig. 3.2), leads to low damage threshold with 532 nm wavelength nanosecond pulse laser. Therefore we have investigated the optical limiting capability of the films using Ti:Sapphire laser (800 nm, ~110 fs) as the excitation sources. The general setup used in the experiments has been described in Sec. 2.4.1. Optical limiting studies used f/40 geometry with input fluences in the range 0.15 - 1.40 J cm^{-2} i.e. intensities in the range, 1.36 - 12.73 TW cm^{-2}. Polystyrene showed damage with the femtosecond pulses even at low intensities, most probably because of strong multiphoton absorption, as it has strong linear absorption at 270 nm. We have employed Au-PVA coated directly on glass/quartz substrates for the optical limiting studies. PVA/glass showed ~ 10% nonlinear absorption as noted earlier (Sec 2.4.2). Z-scan study of the Au-PVA films clearly revealed RSA (Fig. 3.9); most probably, this arises due to two-photon absorption or excited state absorption by the gold nanoparticles. Result of the optical limiting

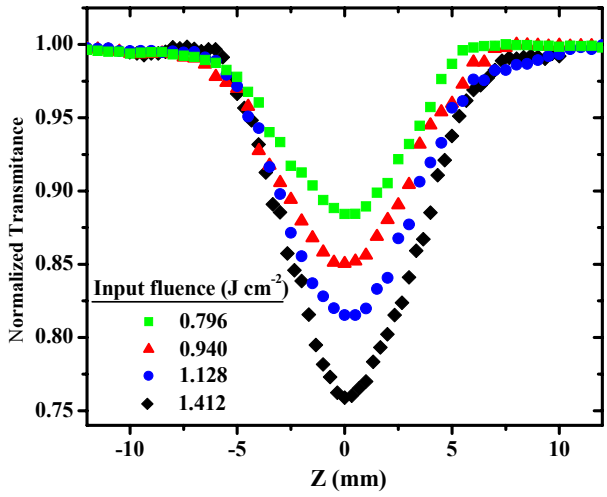

Figure 3.9. *Open aperture Z-scan traces of Au-PVA film (x = 0.24, T = 130°C, t = 60 min) at different input fluences.*

study is presented in Fig. 3.10. It is seen that the films showing appreciable linear transmission of ~ 89% exhibit a limiting threshold of ~ 0.7 J cm^{-2}; these characteristics are comparable to or better than that of some similar materials studied at such high laser powers earlier.[27] The current nonlinear optical studies are carried out on Au-PVA film with a relatively high value of x. Optimization of the composition and thermal treatment parameters could lead to improved responses. The dependence of the optical limiting efficiency on the specific type of gold nanostructures will be an important problem for future investigations.

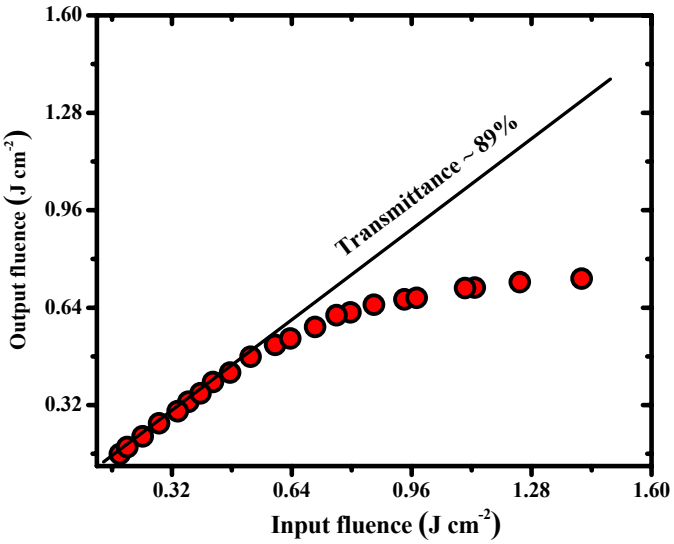

Figure 3.10. *Output versus input fluence plot of Au-PVA film (x = 0.24, T = 130^{o}C, t = 60 min) on glass substrate for femtosecond laser pulses.*

3.5. Gold Nanopyramids and Nanodomes in Polymer Films and 'Green' Synthesis of Gold Nanocrystals

During our investigations of gold nanoplates generated inside PVA films described in the previous sections, we have encountered some further interesting structures and phenomena. In addition, we have also considered novel approaches to the 'green' synthesis of gold nanocrystals. We would like to note that these explorations are quite preliminary and further studies are required to establish the details.

3.5.1. *Nanopyramids in Polymer Films*

Significant variations of nanostructures by slight changes in the synthesis parameters or protocols are interesting not only from the point of view of fundamental growth mechanism, but also for several applications. There are relatively few reports on nanopyramids compared to other 3-dimensional architectures generated through soft chemical and solution routes; this is particularly so in the case of metal nanoparticles. Most popular and common methods for the preparation of nanopyramids are chemical vapour deposition (CVD)[28] or physical evaporation.[29] Pyramidal nanostructures of gold have been fabricated on a sputtered gold surface by electrochemical deposition, leading to super-amphiphobic surfaces exhibiting both water and oil repellent properties.[30]

We have observed the formation of gold nanopyramids within PVA films under suitable conditions of thermal treatment. In the synthesis of gold nanoplates described earlier (Sec 3.2), the thermal treatment of the $HAuCl_4$-PVA film coated glass substrates was carried out in a closed stainless steel chamber with small volume (radius = 6.5 cm and height = 5 cm) placed in an oil bath. When similar films were heated by placing at the bottom of a furnace with large volume (width = 21 cm, depth = 24 cm and height = 11 cm), we observed frequent occurrence of gold nanopyramids inside the polymer film. Pyramids with a triangular base are observed in the images shown in Fig. 3.11 and 3.12. The mechanism leading to the morphology changes are not fully clear; different thermal gradients present in the two cases could be a relevant factor. In both cases, heating is carried out from the bottom. In the small volume stainless steel chamber, the temperature variations/gradient in different directions are likely to be negligible. In the relatively large volume furnace, however, larger thermal gradient may occur, especially in vertical direction. In a control experiment, we have placed the films inside the stainless steel container which in term was placed on the bottom of the furnace. On thermal annealing; it was observed that the film contained preliminary gold nanoplates. This supports the above suggestion about the role of anisotropic thermal gradient. A larger vertical gradient may cause uneven accumulation of gold in that direction, leading to the pyramid formation. The geometry of the base parallels the concentration (x) dependence seen in the case of nanoplates. The present observation need to be further validated by experiments employing carefully controlled thermal gradient; it is possible

perhaps to generate desired 3-dimensional morphologies by precise crafting of the thermal gradients in different directions.

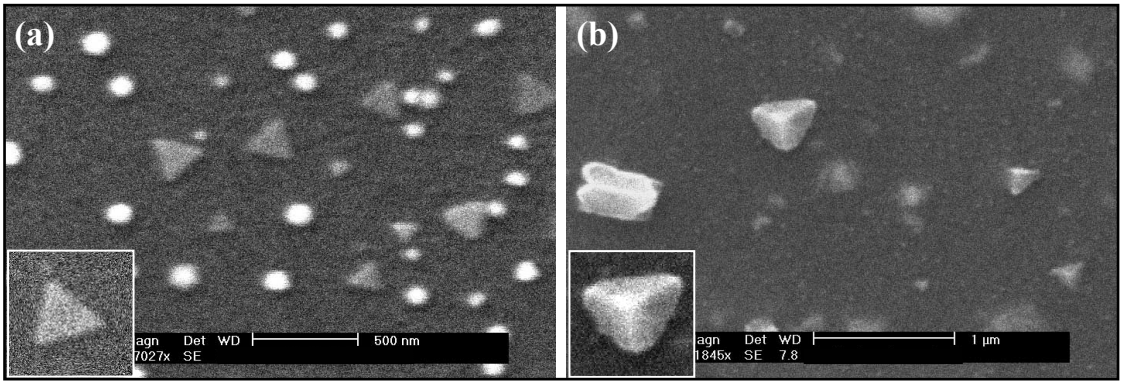

Figure 3.11. *SEM images of the Au-PVA films (x = 0.12, T = 100°C, t = 30 min) fabricated inside* ***(a)*** *small volume steel container* ***(b)*** *large volume furnace. Inset shows enlarged view of a single nanoplate/nanopyramid in each case.*

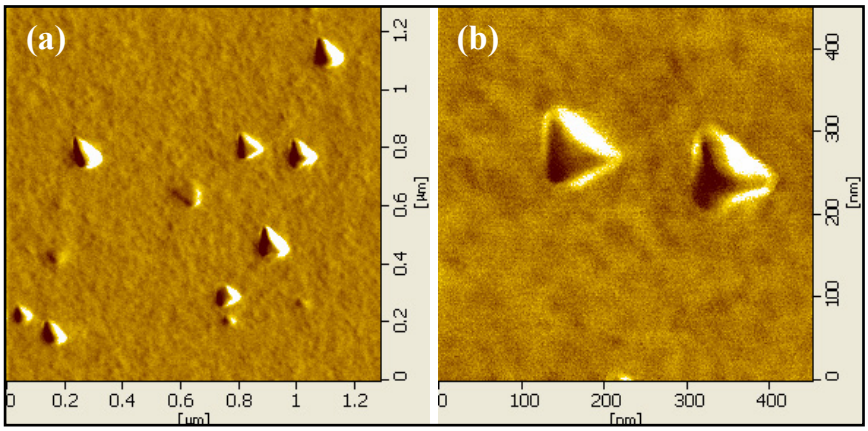

Figure 3.12. *AFM images of the Au-PVA films (x = 0.12, T = 100°C, t = 30 min) fabricated inside large volume furnace.*

3.5.2. *Real-time Monitoring of In situ Growth of Gold Nanodomes in Polymer Film*

The real-time monitoring of the nucleation and growth of nanoparticles using various techniques including spectroscopy and microscopy provides insight into the kinetics and mechanism of nanocrystal formation.[31, 32, 33] STM and AFM are the most

frequently used microscopy tools for this purpose. Imaging of the nucleation and growth of nanoparticles is usually carried out in presence of stimuli, such as chemical and thermal treatments applied *in situ*,[32] or by electrodeposition under potentiostatic control.[33] Monitoring the scanning induced growth caused by AFM tip itself has also been reported.[34]

All the Au-PVA films discussed in the earlier sections were characterized by microscopy imaging after considerable lapse of time after the fabrication. This is natural especially for TEM imaging, since sample preparation process is involved. When we examined some very thin $HAuCl_4$-PVA films coated on glass in the AFM, *immediately* after *brief* thermal treatment, we discovered that the features showed slow evolution in time. Therefore, we have carried out some systematic investigation of this aspect. Films with x = 0.02 - 0.10 were coated on cleaned glass plates in a two step process consisting of 500 RPM for 10 sec followed by 8,000 RPM for 10 sec. The films were heated at T = 100 - 130^{o}C for t = 2 - 15 min. The idea was to initiate the nucleation by thermal treatment for short time at relatively moderate temperatures and to immediately start monitoring the growth near the surface of the film by AFM in the differential force mode, at room temperature. Films with x > 0.08 and T = 130^{o}C, t = 10 min showed some growth of features, but the results were not very clear, since there was dense population of nucleation sites. When x < 0.04 or T < 130^{o}C or t < 10 min, the number of nucleation sites were very few and it became difficult to pick up growing features. After these optimization runs, we found that the combination, x = 0.04, T = 130^{o}C and t = 10 min, exhibited a time dependent growth of nanostructures on the film. The large area scans shown in Fig. 3.13 shows the real-time monitoring of the growth which saturates in about 6 h. Fig. 3.14 shows the AFM images of a single feature selected from the set shown in Fig. 3.13. The axes are rescaled in order to reveal the realistic shape of the feature. We called these features, nanodomes. We have recorded the absorption spectra of the film fabricated with x = 0.06, T = 130^{o}C, t = 10 min, immediately after fabrication and 6 h later when the growth is completed. The emergence of the SPR peak at ~ 550 nm (Fig. 3.15) provides support for the growth of the gold nanostructure at room temperature; the spectral change was less conspicuous in the film with x = 0.04.

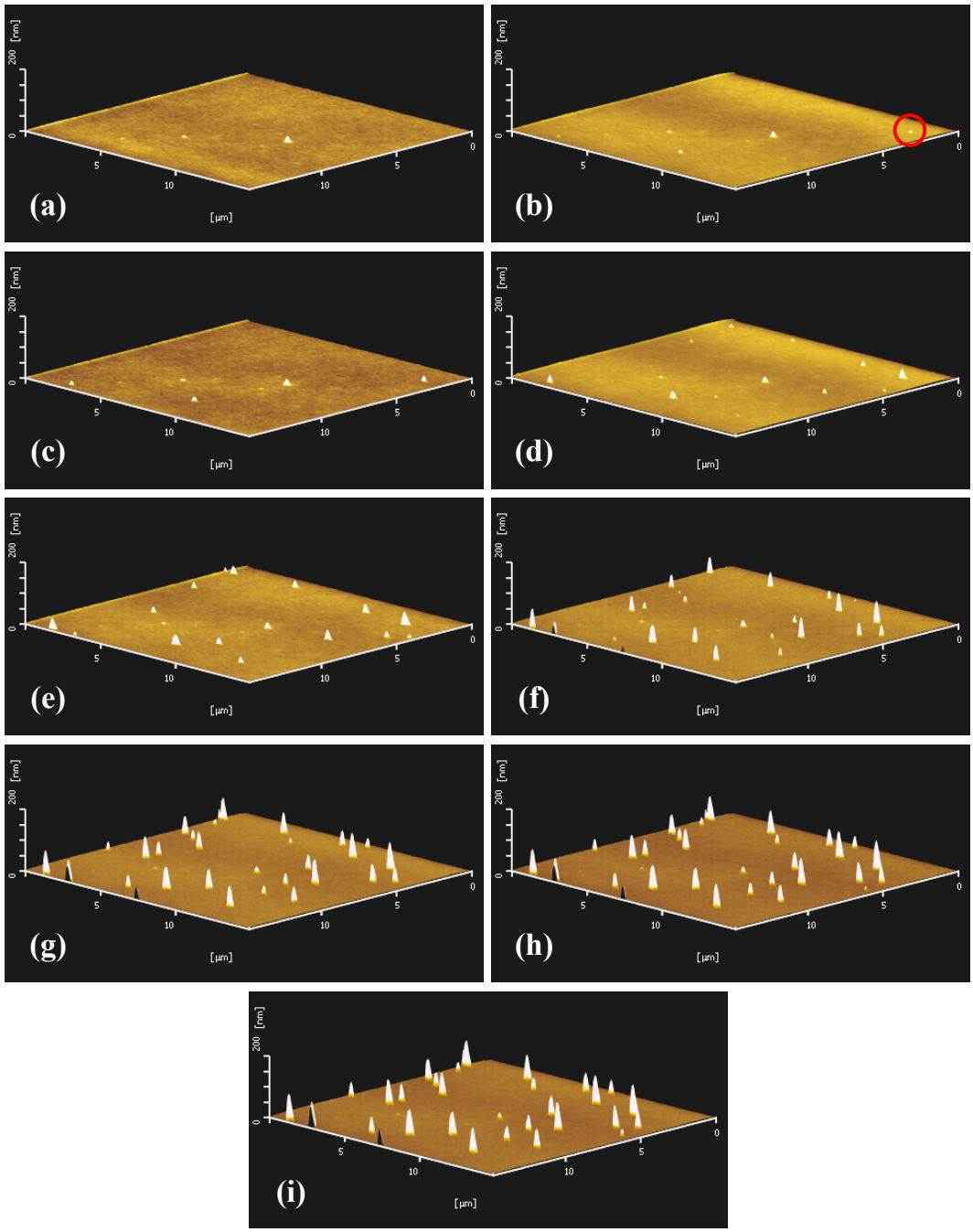

Figure 3.13. *AFM topography images (15 μm × 15 μm × 200 nm) of $HAuCl_4$-PVA films with x = 0.04, heated at T = 130°C and t = 10 min and brought to room temperature (25°C) immediately, monitored at room temperature as a function of time following the nucleation process :* ***(a)*** *10 min,* ***(b)*** *30 min,* ***(c)*** *1 h,* ***(d)*** *1.5 h,* ***(e)*** *2 h,* ***(f)*** *3 h,* ***(g)*** *4 h,* ***(h)*** *5 h and* ***(i)*** *6 h.*

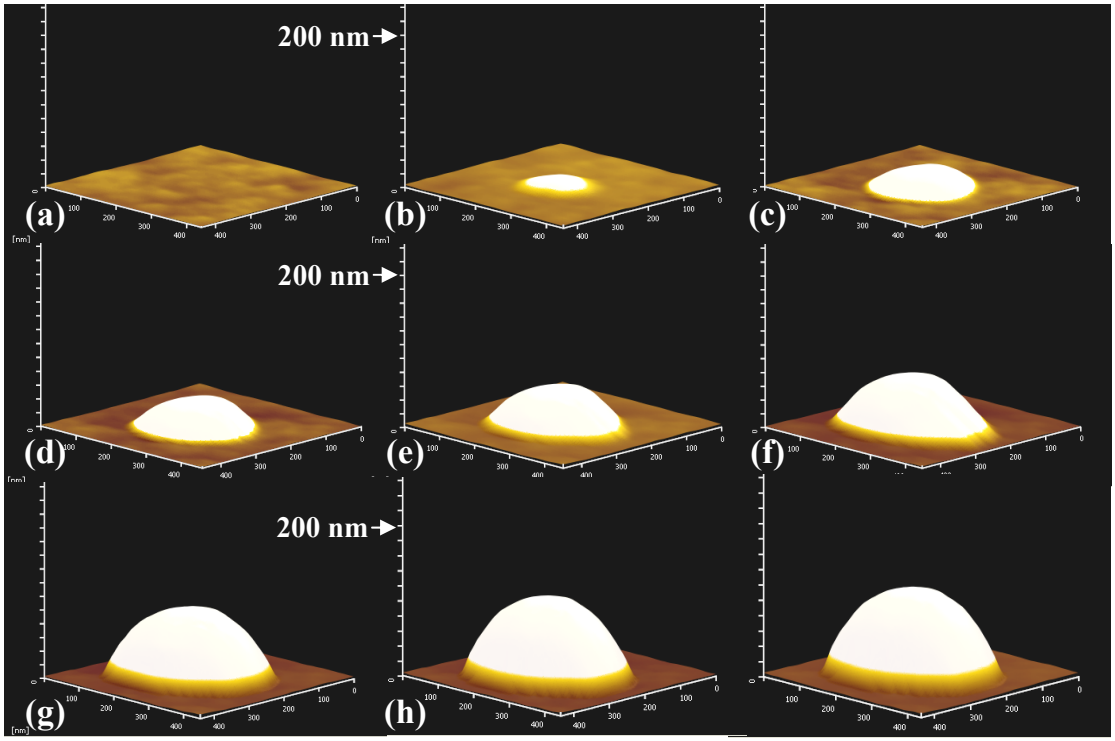

Figure 3.14. *AFM topography images (450 nm × 450 nm × 450 nm) of a single gold nanodome from Fig. 3.13. The time interval of the images after the nucleation process are* ***(a)*** *10 min,* ***(b)*** *30 min,* ***(c)*** *1 h,* ***(d)*** *1.5 h,* ***(e)*** *2 h,* ***(f)*** *3 h,* ***(g)*** *4 h,* ***(h)*** *5 h and* ***(i)*** *6 h.*

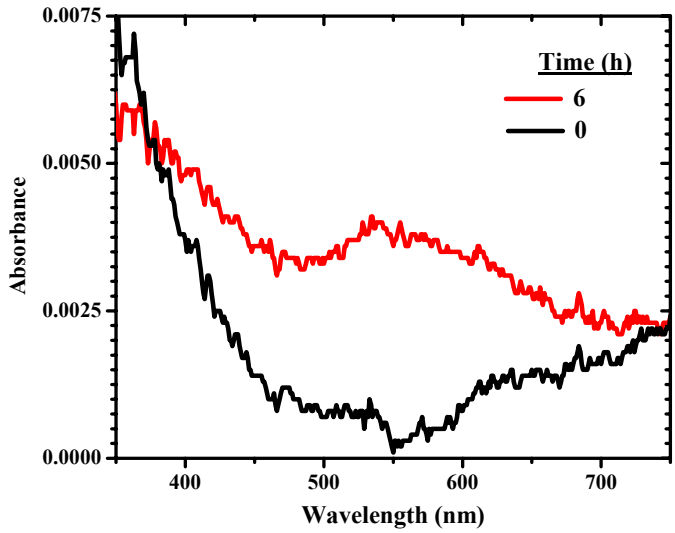

Figure 3.15. *The change in absorption spectrum with time after fabrication, for the $HAuCl_4$-PVA films with x = 0.06, T = 130°C and t = 10 min.*

The present experiments do not provide a full picture of the mechanism of growth of the nanodomes. Two obvious possibilities can be considered. The reduction of Au^{3+} to Au is completed during the short thermal treatment and the growth over the next 6 h at room temperature involves only the aggregation of the gold atoms to form the nanodomes. Alternatively, the short thermal treatment only creates some very small Au clusters and over the next 6 h, this cluster catalyses the reduction of more Au^{3+} to Au, causing the growth of the nanodome. Further experiments are required to clarify these issues.

3.5.3. *Green Synthesis of Gold Nanocrystals*

Synthesis of nanocrystals using biologically green technologies is one of the interesting issues in current nanotechnology/nanobiotechnology. Use of biological systems such as microorganisms[35] (bacteria, fungi, and yeast) for the synthesis of nanoparticles is a relatively new and exciting area of research with considerable potential for development. Another biosynthesis route involves the use of plant extracts, as a viable alternative to the chemical reducing/stabilizing agents and physical methods of synthesizing metal nanoparticles. There have been reports on the formation of gold and silver nanoparticles using extracts from geranium,[36] neem,[37] and tamarind leaves,[38] lemongrass,[39] Aloe vera[40] and several such sources. Usually the nanoparticles are synthesized by reaction of the extracted biomass with aqueous solutions of the precursor salts, the biomolecules acting both as the reducing agent and protective material. Detailed chemistry behind these processes and the role of biomolecules are currently under active exploration. In an interesting case, it has been shown that metal (Ag or Au) nanoparticles can be synthesized inside living plants.[41]

We have attempted a very different approach to 'green' (literally!) synthesis of gold nanocrystals, by spreading the aqueous solution of the precursor directly on the surface of 'green leaves'. In a typical experiment, a freshly plucked leaf is taken and its surface cleaned thoroughly by washing with Millipore water. A few drops of 10^{-7}-10^{-8} M aqueous solution of $HAuCl_4$ was spread on the leaf surface, the leaves were covered with petri plates to slow down the thermal evaporation of water, and kept in the dark to prevent photoreduction of the precursor. The reaction is completed in about 24 h and the gold nanocrystals formed on the leaf surface can be observed in a scanning electron

microscope. We have tried this experiment on a variety of leaves, and in most of the cases a mixture of different shapes of gold nanocrystals are observed. Tender leaves were found to give better yield of nanocrystals compared to more mature ones of the same kind. The Fig. 3.16a show SEM image of the gold nanocrystals formed on the surface of tender leaves of *Bauhinia purpurea* (Family name: Leguminosae); two distinct shapes are seen - spherical particles and hexagonal/truncated triangular nanoplates. The process by which the reduction of Au^{3+} to Au takes place would be interesting to investigate. We speculate that, some of the biomaterials on the surface of the leaf or close within get extracted into the solution of $HAuCl_4$, cause the reduction and the biomolecules (such as proteins or enzymes) present stabilize the gold nanocrystals formed. We have also experimented with transfer of the gold nanocrystals from the leaf surface onto a polymer film. A solution of poly(methyl methacrylate), (PMMA) in acetone was applied on the leaf surface bearing the nanocrystals and allowed to dry. The polymer film was then peeled off. Fig. 3.16b show nanocrystals transferred onto the PMMA film. It may be noted that fast evaporation of water after

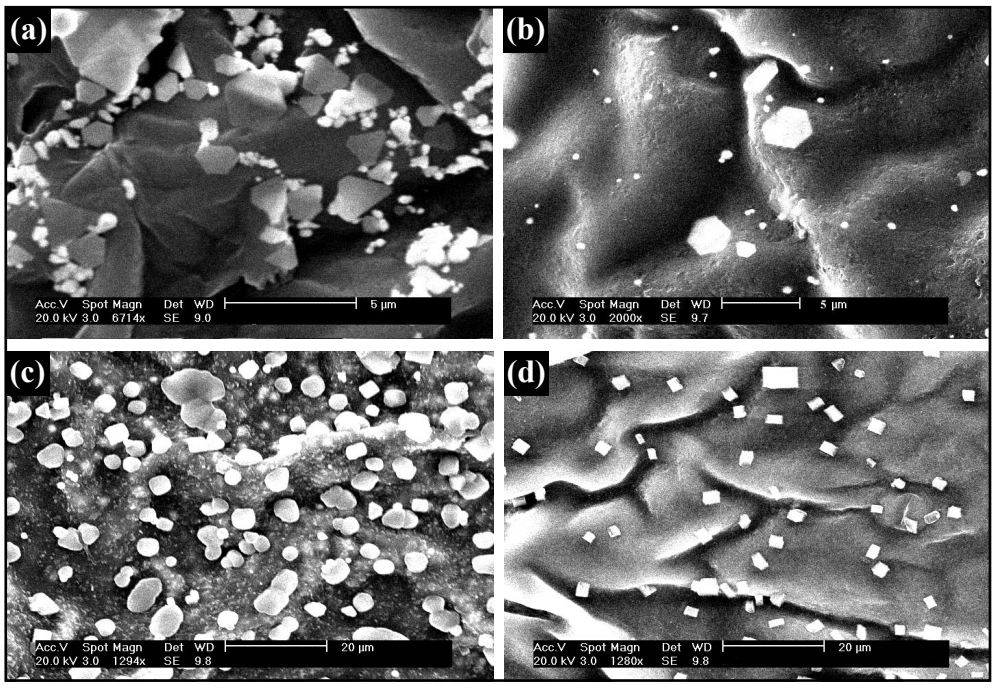

Figure 3.16. *SEM images of the gold nanocrystals:* ***(a)*** *grown on tender Bauhinia leaf surface and* ***(b)*** *transferred onto a PMMA film;* ***(c)*** *$HAuCl_4$ precipitated by fast evaporation of solution on Bauhinia leaf and* ***(d)*** *transferred onto a PMMA film.*

spreading the $HAuCl_4$ solution on leaf surface led to precipitation of $HAuCl_4$ which could be observed as microcrystals with a variety of shapes in the SEM image (Fig. 3.16c). On transfer to PMMA film, cuboid microcrystals are obtained (Fig. 3.16d) suggesting that the $HAuCl_4$ crystals are recrystallized through dissolution in acetone. Fig 3.17 shows a collection of overlap growth of gold nanoplates on the surface of *Bauhinia* leaf. We believe this truly 'green' synthesis methodology can be fine-tuned to generate gold nanocrystals of desired shapes in an extremely clean and environment-friendly way.

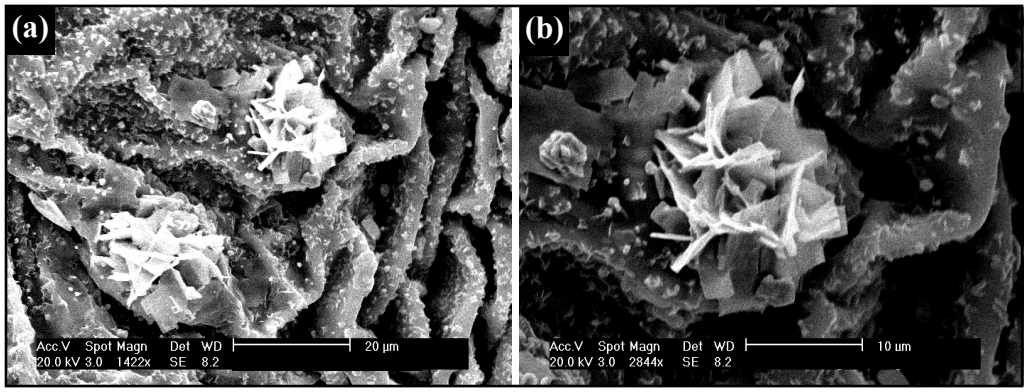

Figure 3.17. *SEM images showing overlap growth of gold nanoplates on the surface of tender Bauhinia leaf.*

3.6. Summary

We have demonstrated the *in situ* generation of gold nanocrystals in PVA films using the polymer as the only reagent, leading to films with embedded particles of different shapes. Appreciable orientational ordering of polygonal nanoplates is observed without the help of special templates or linker molecules, possibly arising due to the anisotropic nature of the polymer thin film. The gold nanoparticle-polymer composite thin film shows appreciable optical limiting response for femtosecond laser pulses. Preliminary experiments suggest that temperature gradients on the film can lead to further variations in the morphology and assembly of nanoparticles, and that in very thin films fabricated under appropriate conditions, the growth of gold nanostructures can be monitored in real time. Finally, we have also presented a simple approach to the 'green' synthesis of gold nanocrystals on the surface of green leaves.

References

1. (a) Lim, M. H.; Ast, D. G. *Adv. Mater.* **2001**, *13*, 718; (b) Jiang, C. Y.; Markutsya, S.; Tsukruk, V. V. *Adv. Mater.* **2004**, *15*, 157.
2. Matsuda, S.; Ando, S. *Polym. Adv. Tech.* **2003**, *14*, 458.
3. Warheit, D. B.; Laurence, B. R.; Reed, K. L.; Roach, D. H.; Reynolds, G. A. M.; Webb, T. R. *Toxicol. Sci.* **2004**, *77*, 117.
4. Raveendran, P.; Fu, J.; Wallen, S. L. *J. Am. Chem. Soc.* **2003**, *125*, 13940.
5. (a) Chen, S.; Wang, Z. L.; Ballato, J.; Foulger, S. H.; Carroll, D. L. *J. Am. Chem. Soc.* **2003**, *125*, 16186; (b) Métraux, G. S.; Cao, Y. C.; Jin, R.; Mirkin, C. A. *Nano Lett.* **2003**, *3*, 519.
6. (a) Sun, Y.; Xia, Y. *Science* **2002**, *298*, 2176; (b) Kim, F.; Connor, S.; Song, H.; Kuykendall, T.; Yang, P. *Angew. Chem. Int. Ed.* **2004**, *43*, 3673; (c) Seo, D.; Park, J. C.; Song, H. *J. Am. Chem. Soc.* **2006**, *128*, 14863.
7. (a) Sau, T. K.; Murphy, C. J. *J. Am. Chem. Soc.* **2004**, *126*, 8648; (b) Chu, H.-C.; Kuo, C.-H.; Huang, M. H. *Inorg. Chem.* **2006**, *45*, 808.
8. (a) Jana, N. R. *Angew. Chem. Int. Ed.* **2004**, *43*, 1536; (b) Gole, A.; Murphy, C. J. *Chem. Mater.* **2004**, *16*, 3633; (c) Alekseeva, A. V.; Bogatyrev, V. A.; Khlebtsov, B. N.; Mel'nikov, A. G.; Dykman, L. A.; Khlebtsov, N. G. *Colloid Journal* **2006**, *68*, 661; (d) Wu, H.-Y.; Huang, W.-L.; Huang, M.H. *Crystal Growth & Design* **2007**, *7*, 831.
9. Hu, J.; Zhang, Y.; Liu, B.; Liu, J.; Zhou, H.; Xu, Y.; Jiang, Y.; Yang, Z.; Tian, Z. *J. Am. Chem. Soc.* **2004**, *126*, 9470.
10. Kuo, C.; Chiang, T.; Chen, L.; Huang, M. H. *Langmuir* **2004**, *28*, 7820.
11. Daniel, M.-C.; Astruc, D. *Chem. Rev.* **2004**, *104*, 293.
12. (a) van der Zande, B. M. I.; Böhmer, M. R.; Fokkink, L. G. J.; Schönenberger, C. *J. Phys. Chem. B* **1997**, *101*, 852; (b) Hornyak, G. L.; Patrissin, C. J.; Martin, C. R. *J. Phys. Chem. B* **1997**, *101*, 1548; (c) Mohamed, M. B.; Ismael, K. Z.; Link, S.; El-Sayed, M. A. *J. Phys. Chem. B* **1998**, *102*, 9370.
13. (a) Porel, S.; Singh, S.; Harsha, S. S.; Rao, D. N.; Radhakrishnan, T. P. *Chem. Mater.* **2005**, *17*, 9; (b) Anthony, S. P.; Porel, S.; Rao, D. N.; Radhakrishnan, T. P. *Pramana* **2005**, *65*, 871.
14. Jain, P. K.; El-Sayed, I. H.; El-Sayed, M. A. *Nanotoday* **2007**, *2*, 18.
15. (a) Chen, S.; Sommers, J. M. *J. Phys. Chem. B* **2001**, *105*, 8816; (b) Choo, H. P.; Liew, K. Y.; Mahmood, W. A. K.; Liu, H. *J. Mater. Chem.* **2001**, *11*, 2906.
16. (a) Xu B.; Tanak, S. *Nanostr. Mater.* **1998**, *8*, 1131; (b) Hanyuan, C.; Yan, G.; Huairou, Z.; Libao, L.; Hongchun, Y.; Huanfang, T.; Sishen, X.; Jianqi, L. *J. Phys. Chem. B* **2004**, *108*, 12038.
17. Sun, Y.; Mayers, B.; Herricks, T.; Xia, Y. *Nano Lett.* **2003**, *3*, 955.
18. Shao, Y.; Jin, Y.; Dong, S. *Chem. Commun.* **2004**, 1104.
19. Sun, Y.; Yin, Y.; Mayers, B. T.; Herricks, T.; Xia, Y. *Chem. Mater.* **2002**, *14*, 4736.

20. Sun, Y.; Gates, B.; Mayers, B.; Xia, Y. *Nano Lett.* **2002**, *2*, 165.
21. Wiley, B.; Herricks, T.; Sun, Y.; Xia, Y. *Nano Lett.* **2004**, *4*, 1733.
22. Herricks, T.; Chen, J.; Xia, Y. *Nano Lett.* **2004**, *4*, 2367.
23. Li, H.; Wang, R.; Hong, Q.; Chen, L.; Zhong, Z.; Koltypin, Y.; Calderon-Moreno, J.; Gedanken, A. *Langmuir* **2004**, *20*, 8452.
24. Fritzsche, W.; Porwol, H.; Wiegand, A.; Bornmann, S.; Köhler, J. M.; *Nanostruct. Mater.* **1998**, *10*, 89.
25. Longenberger, L.; Mills, G. *J. Phys. Chem.* **1995**, *99*, 475.
26. Chandra, A. K.; Nguyen, M. T.; Zeegers-Huyskens, T. *Chem. Phys.* **2000**, *255*, 149.
27. (a) Samoc, M.; Samoc, A.; Luther-Davies, B.; Bao, Z.; Yu, L.; Hsieh, B.; Scherf, U. *J. Opt. Soc. Am. B* **1998**, *15*, 817; (b) Elim, H. I.; Yang, J.; Lee, J-Y.; Mi, J.; Ji, W. *Appl. Phys. Lett.* **2006**, *88*, 083107.
28. (a) Riedel, M.; Müller, B.; Wintermantel, E. *Biomaterials* **2001,** *22*, 2307; (b) Lue, F.; Cao, P.; Zhang, H. Tian, J; Xiao, C.; Shen, C.; Li, J.; Gao, H. *Adv. Mater.* **2005**, *17*, 1893; (c) Gruzintsev, A. N.; Redkin, A. N.; Emelchenko, G. A.; Barthou, C.; Benalloul, P. *J. Opt. A: Pure Appl. Opt.* **2006**, *8***,** S148.
29. Guha, P.; Kar, S.; Chaudhuri, S. *Appl. Phys. Lett.* **2004***, 85*, 3851.
30. (a) Tian, Y.; Liu, H.; Zhao, G.; Tatsuma, T. *J. Phys. Chem. B* **2006**, *110,* 23478; (b) Tian, Y.; Liu, H.; Deng, Z. *Chem. Mater.* **2006**, *18,* 5820.
31. (a) Qu, L.; Yu, W. W.; Peng, X. *Nano Lett.* **2004***, 4*, 465; (b) Rodríguez-Fernández, J.; Pérez-Juste, J.; García de Abajo, F. J.; Liz-Marzán, L. M. *Langmuir* **2006**, *22,* 7007.
32. Kolmakov, A.; Goodman, D. W. *Chem. Record* **2002**, *2*, 446.
33. Simm, A. O.; Ji, X.; Banks, C. E.; Hyde, M. E.; Compton, R. G. *ChemPhysChem* **2006**, *7*, 704.
34. McEvoy, A. L.; Stevens, F.; Langford, S. C.; Dickinson, J. T. *Langmuir* **2006**, *22,* 6931.
35. (a) Mukherjee, P.; Senapati, S.; Mandal, D.; Ahmad, A., Khan, M. I.; Kumar, R.; Sastry, M. *ChemBioChem* **2002**, *3*, 461; (b) Sastry, M.; Ahmad, A.; Khan, M. I.; Kumar, R. *Curr. Sci.* **2003**, *85*, 162; (c) Ahmad, A.; Mukherjee, P.; Senapati, S.; Mandal, D.; Khan, M. I.; Kumar, R.; Sastry, M. *Colloids Surf. B* **2003**, *28*, 313; (d) Ahmad, A.; Senapati, S.; Khan, M. I.; Kumar, R.; Sastry, M. *J. Biomed. Nanotechnol.* **2005**, *1*, 47; (e) Mandal, D.; Bolander, M. E.; Mukhopadhyay, D.; Sarkar, G.; Mukherjee, P. *Appl. Microbiol. Biotechnol.* **2006**, *69*, 485; (f) Bhainsa, K. C.; D'Souza, S. F. *Colloids and Surfaces B: Biointerfaces* **2006**, *47*, 160; (g) Shahverdi, A. R.; Minaeian, S.; Shahverdi, H. R.; Jamalifar, H.; Nohi, A.-A. *Process Biochemistry* **2007**, *42*, 919.
36. (a) Shankar, S. S.; Ahmad, A.; Pasricha, R.; Sastry, M. *J. Mater. Chem.* **2003**, *13***,** 1822; (b) Shankar, S. S.; Ahmad, A.; Sastry, M. *Biotechnol. Prog.* **2003**, *19*, 1627.
37. Shankar, S. S.; Rai, A.; Ahmad, A.; Sastry, M. *J. Colloid Interface Sci.* **2004**, *275*, 496.
38. Ankamwar, B.; Chaudhary, M.; Sastry, M. *Synth. React. Inorg. Met.-Org. Nano-Metal Chem.* **2005**, *35*, 19.
39. Shankar, S. S.; Rai, A.; Ankamwar, B.; Singh, A.; Ahmad, A.; Sastry, M. *Nat. Mater.* **2004**, *3*, 482.

40. Chandran, S. P.; Chaudhary, M.; Pasricha, R.; Ahmad, A.; Sastry, M. *Biotechnol. Prog.* **2006**, *22*, 577.

41. (a) Gardea-Torresdey, J. L.; Parsons, J. G.; Dokken, K; Peralta-Videa, J; Troiani, H. E.; Santiago, P.; Jose-Yacaman, M. *Nano Lett.* **2002**, *2*, 397; (b) Gardea-Torresdey, J. L.; Gomez, E.; Peralta-Videa, J.; Parsons, J. G.; Troiani, H.; Jose-Yacaman, M. *Langmuir* **2003**, *19*, 1357.

Scope

Assembly of nanoparticles and construction of organized nanostructures are challenging problems in nanotechnology with specific application in the area of nanoscale devices. We have discovered a novel methodology to produce palladium nanowires embedded inside poly(vinyl alcohol) film by first crystallizing precursor nanowires of potassium palladium (II) chloride inside the film and then reducing them by the polymer itself under mild thermal annealing. The chemical reaction occurring in situ inside the polymer film, including byproduct formation can be monitored through spectroscopy and microscopy. The overall process can be described as a crystal-to-crystal transformation at the nanoscopic level. Optical limiting capability of the Pd-PVA films is examined. The fabrication procedure developed, involving chemistry inside a polymer matrix mediated by the polymer, opens up a convenient route to the fabrication of free-standing metal nanowire-embedded polymer thin films. The generality of our methodology to nanowires fabrication is probed by preliminary studies on gold.

4.1. Introduction

Fabrication of nanomaterials generally follows one of the 'top-down' or 'bottom-up' approaches. For example, metal nanowires which are of great current interest in applications ranging from chemical sensors[1, 2] to lasers,[3] are sculpted through lithographic techniques[4] or synthesized by templating[5] and self-assembly[6] processes. Crystal-to-crystal transformation of precursor nanostructures of metal salts to the corresponding metal nanostructures via direct reduction in a suitable environment would add a new dimension to this scenario. Polymers with appropriate functional groups can provide such an environment. Crystal growth in solution is known to be influenced by the presence of polymers;[7,8] crystallization inside diffusion-limited media like gels or thin polymer films often leads to fibrous and dendritic morphologies.[9] Since a solid polymer matrix can impose morphological integrity during the conversion of the precursor to the metal, this opens up a simple route to the fabrication of metal nanowires embedded in polymer films; the possibility of dendritic structures enhancing the electrical conductivity in nanowires[10] is notable in this context. As noted in earlier chapters, *in situ* formation of nanomaterials inside polymer matrices have additional benefits such as the preclusion of potential health hazards of inhalable nanoparticles,[11]

the feasibility of employing simple, efficient and environmentally benign synthesis conditions[12] and the facilitation of further mechanical or optical manipulations of the nanoparticle-polymer composite films.[13] Following our studies on Ag-PVA (Chapter 2)[12,14] and Au-PVA (Chapter 3)[15] films, we explored the possibility of creating palladium nanostructures inside poly(vinyl alcohol) films, using similar methodology.

Palladium based nanomaterials have applications ranging from catalysis[16] to sensors[1] and hydrogen storage.[17] In this chapter, we describe first, the fabrication of palladium nanostructures in PVA film and the detailed characterizations of the process involved in transformation of nanowires of the precursor, potassium palladium(II) chloride (K_2PdCl_4), to palladium nanowires. Metal reduction occurring via the polyol route, but carried out in this instance inside a solid polymer matrix, shows concomitant formation of microcrystals of the byproduct, KCl. Crystal-to-crystal transformation through solid state chemical reactions at the bulk level are known. Such processes at the nanocrystal level are rare; two examples involve photodimerization and photopolymerization reactions.[18] To the best of our knowledge, such a phenomenon occurring at the nanoscopic level in a polymer matrix has not been demonstrated earlier. We explore also, the nonlinear optical application of the Pd nanowire-embedded polymer film and the generality of the fabrication procedure we have developed for nanowire-embedded polymer films.

4.2. Fabrication of Films and Morphology of Precursor Nanostructures

The general fabrication procedure is already discussed in detail in Sec. 2.2. Here we describe the steps involved and the specific details related to palladium in PVA. The first step is the preparation of a mixture of aqueous solutions of K_2PdCl_4 and PVA, with different weight ratios, x (0.01 - 0.10) of Pd to PVA. The required weight of K_2PdCl_4 dissolved in 1.25 ml water was mixed with 0.3 ml of a solution of PVA (average molecular weight = 13 - 23 kDa, % hydrolysis = 86) in water (2.4 g PVA in 8 ml water) to prepare different compositions (for example, 24.9 mg of K_2PdCl_4 gives x = 0.09). In the second step, the K_2PdCl_4-PVA solution was spin-coated on a suitable substrate (glass, quartz or glass pre-coated with a sacrificial layer of polystyrene, PS), by spinning at 8,000 RPM for 10 sec. In the final step, the film-coated plates were heated in a hot

air oven at temperatures, T = 110 - 150°C, for different times, t = 15 - 120 min, to generate the palladium nanostructures within the polymer matrix. As shown later, the reduction of Pd^{2+} to Pd is not complete in the case of most of the films. In the following discussions, the general term PPVA denotes PVA films containing K_2PdCl_4, Pd or a mixture of both. The thickness of the PPVA and PS layers are ~ 400 nm and 4 μm respectively as measured using a profilometer. PPVA/PS can be peeled off the glass substrates as free-standing film (Fig. 4.1a); alternately the sacrificial layer of PS can be dissolved out in toluene to obtain the film of PPVA alone (Fig. 4.1b).

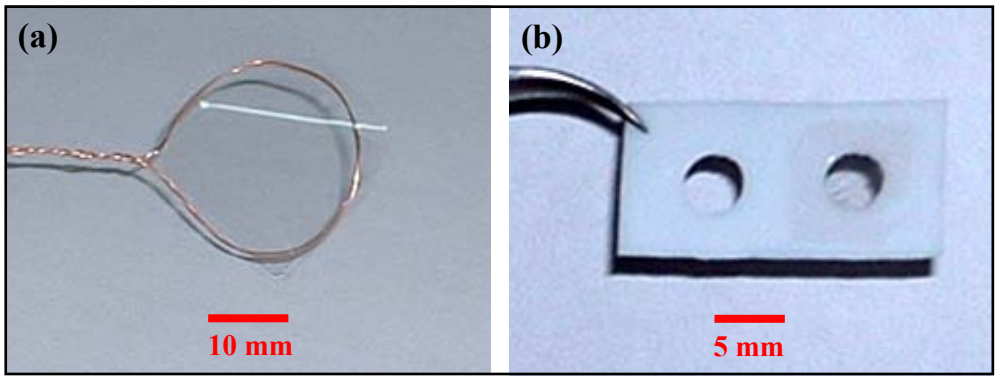

Figure 4.1. *Photographs of* ***(a)*** *PPVA/PS film supported on a copper wire and* ***(b)*** *PPVA film placed on a teflon support; the empty hole on the left shows the contrast.*

The morphologies of the K_2PdCl_4 nanostructures in the spin-cast films are found to be very sensitive to the value of x used. Only spherical structures were obtained when x < 0.06. Dendritic structures with increasing density are obtained when x = 0.07 - 0.08 and long nanowires, when x = 0.09 - 0.10 (Fig. 4.2). PVA appears to play an important role in the formation of these structures as seen from control experiments with similar concentrations of K_2PdCl_4 but using a polymer possessing considerably less hydroxy groups and using no polymer at all, which produced very different morphologies. For example, spin coating of DMSO solution containing K_2PdCl_4 and poly(vinyl alcohol-*co*-ethylene (5:4)) gave rod-like nanocrystals typically a few microns long and several hundred nanometers thick (Fig. 4.3) very different from those obtained in PVA. When aqueous solution of K_2PdCl_4 without any added polymer is evaporated on glass substrates while spinning, needle-like crystals several microns thick are obtained (Fig. 4.4). The specific chemical structure of PVA and physical properties

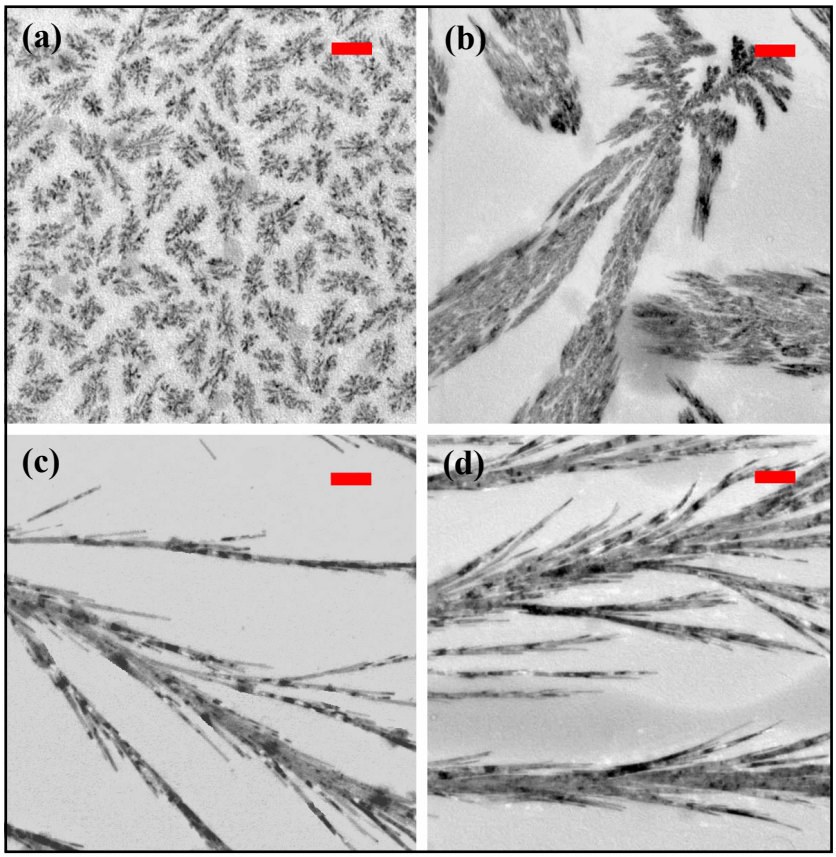

Figure 4.2. *TEM images of unheated PPVA films with different values of x :* ***(a)*** *0.07,* ***(b)*** *0.08,* ***(c)*** *0.09 and* ***(d)*** *0.10 (scale bar = 1 μm).*

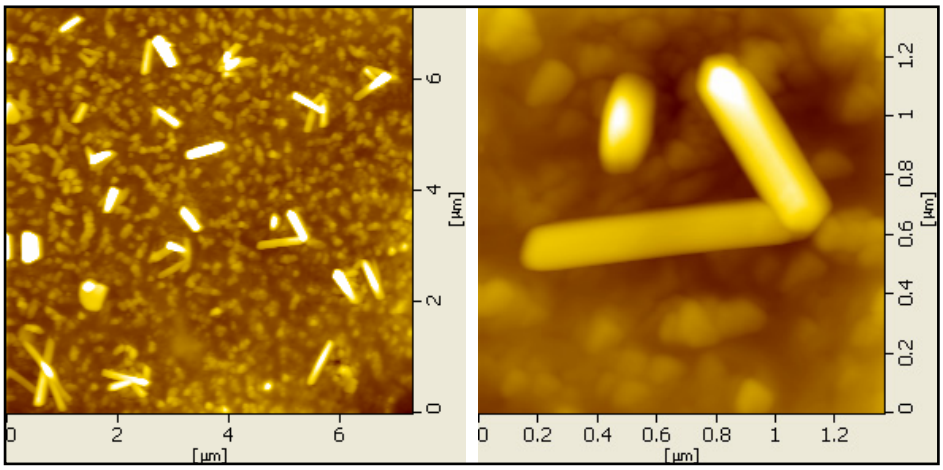

Figure 4.3. *AFM topography images of unheated K_2PdCl_4-poly(vinyl alcohol-co-ethylene (5:4)) films with x = 0.09 coated on glass with different magnifications.*

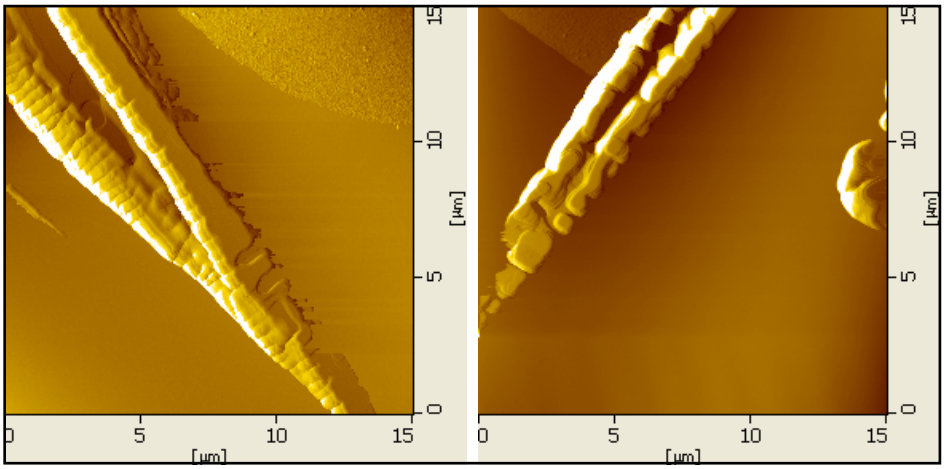

Figure 4.4. *AFM topography images of K_2PdCl_4 evaporated on glass.*

such as viscosity of its solution, appears to be relevant for the formation of the nanowire structures of K_2PdCl_4.

4.3. Transformation of Precursor to Palladium Nanostructure

The limits of temperature, T and time, t for the thermal treatment of the K_2PdCl_4-PVA films were selected based on the formation of palladium nanostructures. The structure of the precursor in the PVA film is largely maintained during the reduction carried out at T = 130°C and t ≤ 120 min, but is accompanied by some size reduction. Higher temperatures and longer heating times lead to aggregation of nanostructures and/or polymer degradation. The focus of the following discussion will be on the nanowire structures obtained when x = 0.09. The transformation of K_2PdCl_4 to Pd in PVA films was investigated using different spectroscopy and microscopy techniques.

The PPVA films coated on quartz substrates were used to record the absorption spectra. Preliminary evidence for the chemical reaction occurring when the PVA film containing K_2PdCl_4 is heated, comes from the absorption spectra. Fig. 4.5a shows the spectra of the film with x = 0.09, heated at T = 130°C, for different periods of time. The unheated film shows absorption peaks characteristic of Pd^{2+} with small shifts due to environment effects; on heating, a broad absorption typical of nanoscopic palladium

structures emerges.[19] Notably, the spectral signature of Pd^{2+} does not vanish even after heating for 120 min. Fig. 4.5b shows that the reduction progresses much more when x is smaller and Fig. 4.5c shows the reaction is almost complete when in addition, temperature is higher. More definitive evidence of the chemical reduction on heating is obtained from X-ray photoelectron spectra (XPS), recorded using free-standing PPVA/PS films. Fig. 4.6a shows the XPS spectrum for the film with x = 0.09 before heating; palladium is exclusively in the +2 state.[20] Fig. 4.6b and 4.6c show clear signature of neutral palladium formed in the films heated for 30 and 120 min respectively. Once again the film with low x, shows considerably larger proportion of Pd^0 (Fig. 4.6d).

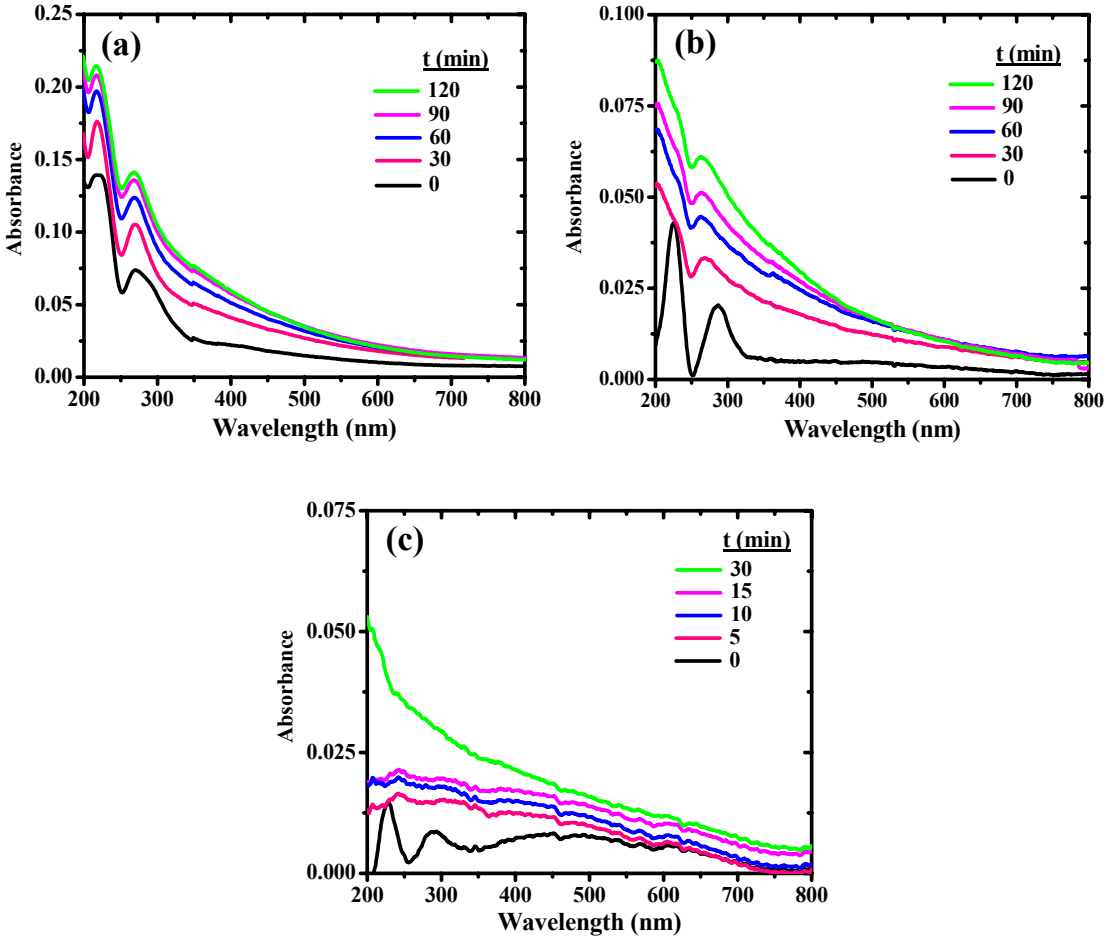

Figure 4.5. *Absorption spectra of PPVA films :* ***(a)*** *x = 0.09, T =130°C,* ***(b)*** *x = 0.015, T =130°C* ***(c)*** *x = 0.015, T =150°C heated for different periods of time, t.*

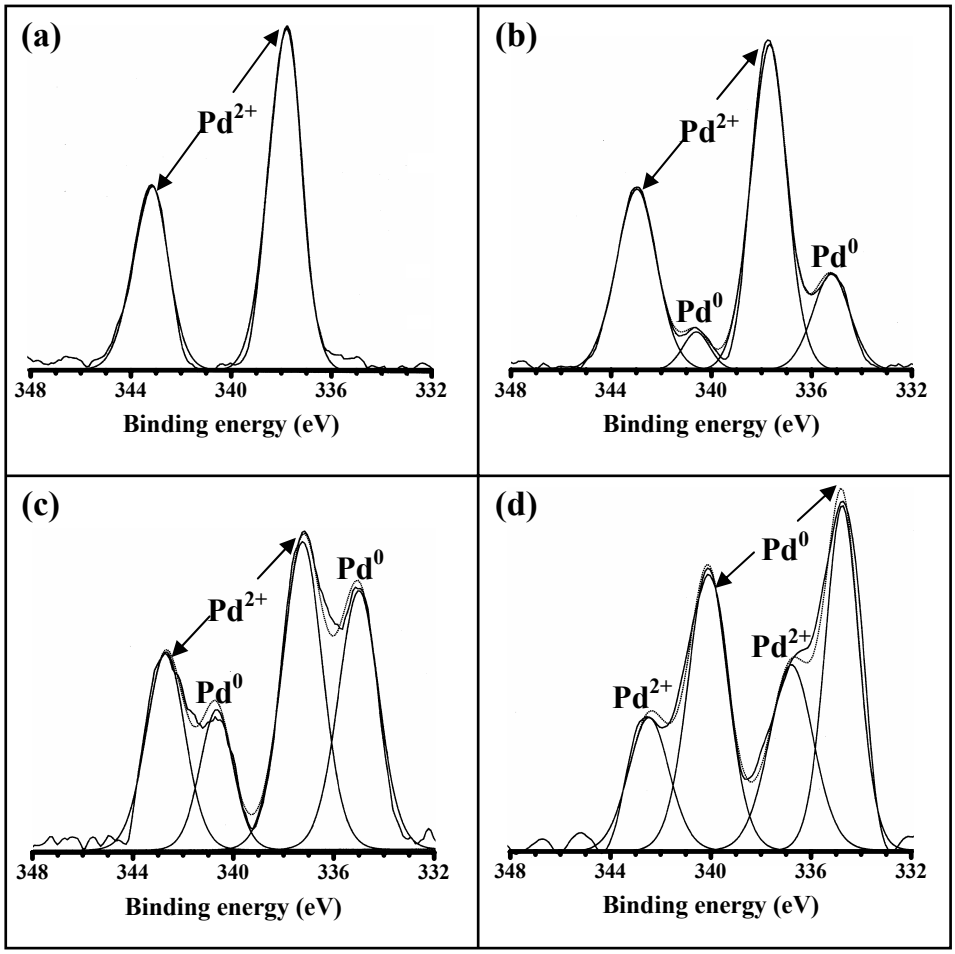

Figure 4.6. *XPS spectra of PPVA films :* ***(a)*** *x = 0.09, before heating,* ***(b)*** *x = 0.09, T =130^{o}C, t = 30 min,* ***(c)*** *x = 0.09, T =130^{o}C, t = 120 min, and* ***(d)*** *x = 0.015, T =130^{o}C, t = 60 min. Deconvolution of each spectrum is indicated.*

Atomic force microscopy images in Fig. 4.7 provide a view of the surface of the films with x = 0.09, before and after heating. Based on the spectral evidences above, it can be inferred that the structures observed before heating are due to the crystallization of K_2PdCl_4 in the polymer matrix; the thinness of the polymer film enables the observation of the embedded nanostructures. The apparent heights and widths are approximately 30 - 50 and 350 - 450 nm respectively (Fig. 4.8) indicating that these are likely to be either tape-like formations or collections of wires; they extend up to several microns in length. Heating causes small but definite changes in the dimensions, the overall morphology being largely preserved; the structures form shorter segments and

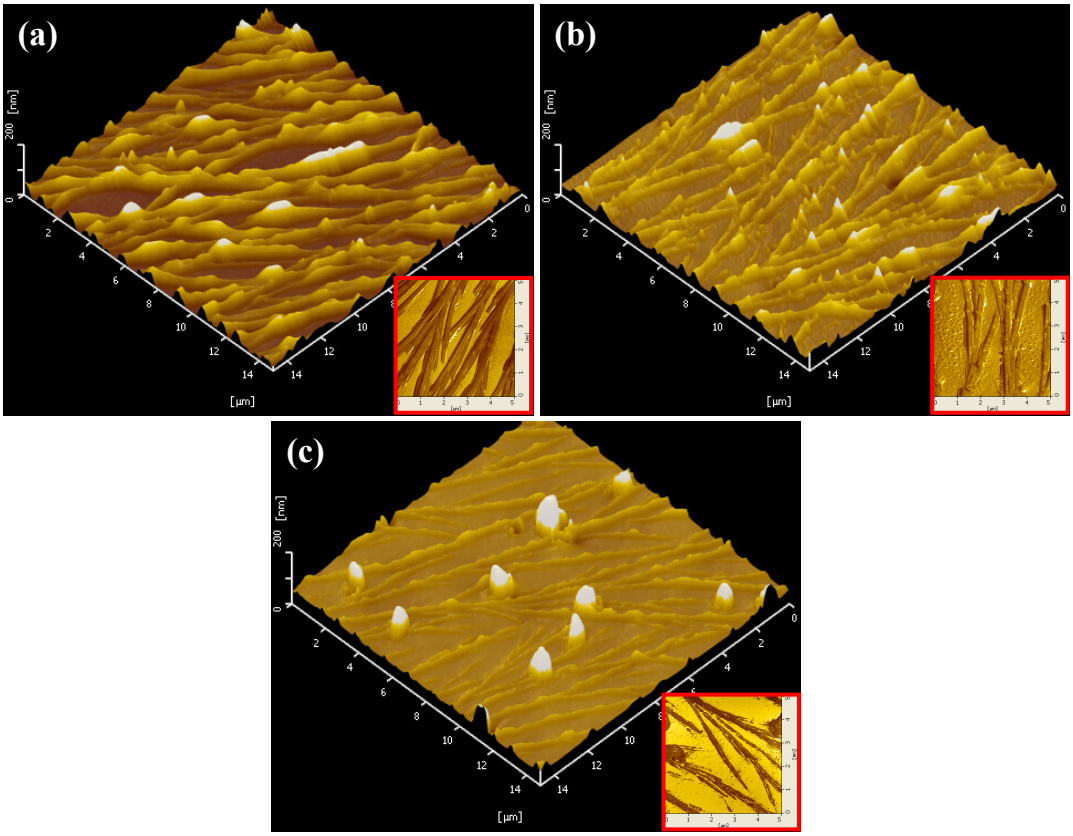

Figure 4.7. *AFM topography images (15 µm x 15 µm x 200 nm) of PPVA films with x = 0.09,* ***(a)*** *before heating, and heated at T =130°C for* ***(b)*** *t = 30 min and* ***(c)*** *t = 120 min. The corresponding phase images (5 µm x 5 µm) are shown in the inset. The apparent sharpness of features is due to the expanded scale of the z-axis.*

there is a reduction in the height and width to about 15 - 25 and 150 - 250 nm respectively. The AFM phase images in the insets of Fig. 4.7 reveal significant changes on heating, suggesting the likelihood of composition variation between the samples. Another significant feature revealed in the AFM images is the formation of relatively large plate-like structures in the heated films; electron microscopy studies discussed below probe their origin.

The field emission scanning electron microscopy (FESEM) images in Fig. 4.9 reveal the nanowire structures in the PPVA/PS films and their fibrous growth patterns. The tendency of these wires to shrink on heating is evident once again. The large area images show the concomitant growth of nearly micron-sized square plates. Energy

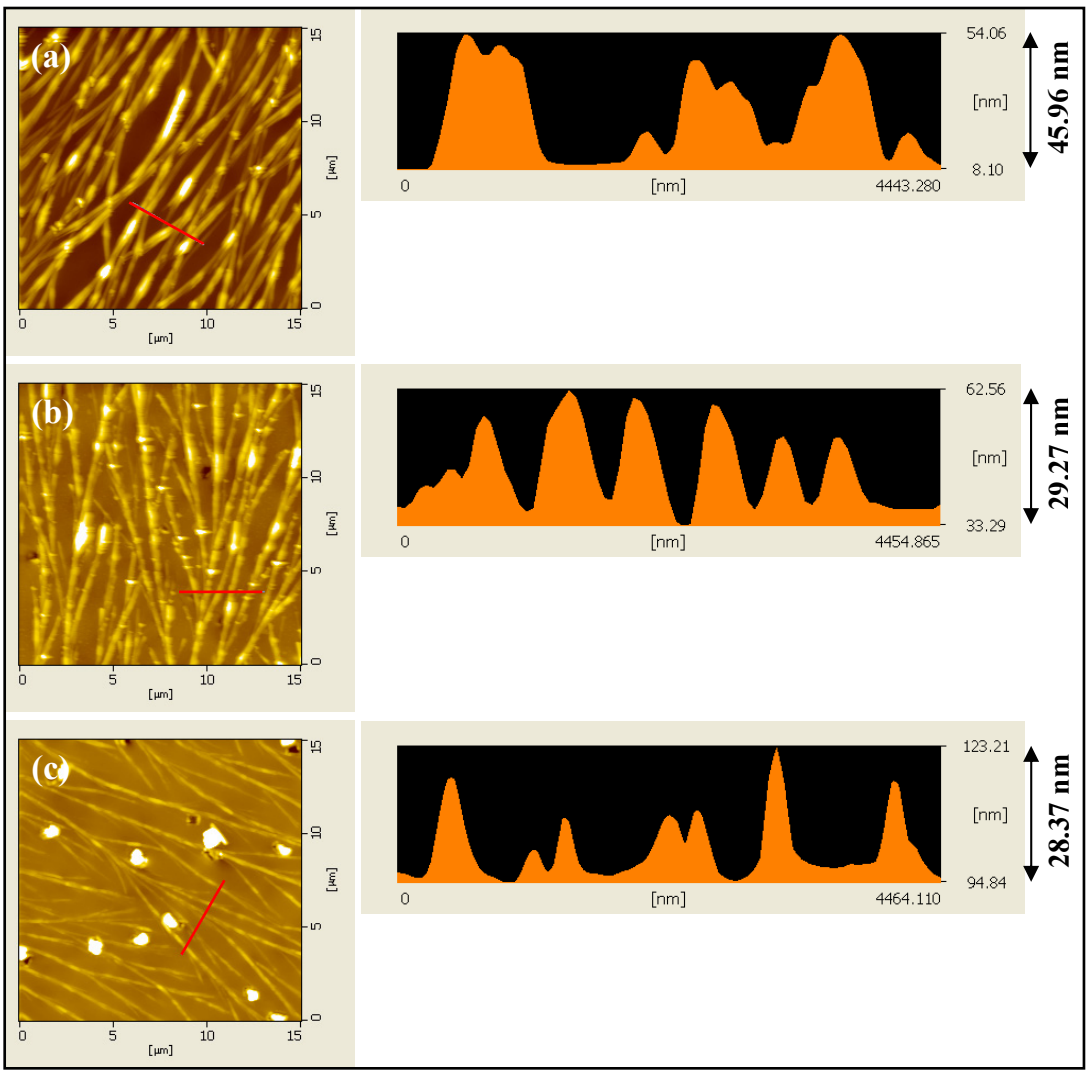

Figure 4.8. *AFM topography images (15 µm x 15 µm) of PPVA films with x = 0.09,* ***(a)*** *before heating and heated at T =130°C for* ***(b)*** *t = 30 min and* ***(c)*** *t = 120 min. The corresponding line profile analysis of the AFM images is also shown.*

dispersive X-ray (EDX) analysis of the different films showed the presence of potassium, palladium and chlorine; quantitative assignments to specific compositions in different regions are precluded, since only the surface region of the polymer film is probed. Fig. 4.10 shows the area maps corresponding to a selected region of the PPVA/PS film. It may be noted that higher or longer electron beam irradiation leads to polymer damage, limiting the possibility of improving the detection sensitivity. Within the short time periods of recording (~ 30 min), the mapping for oxygen is rather uniform,

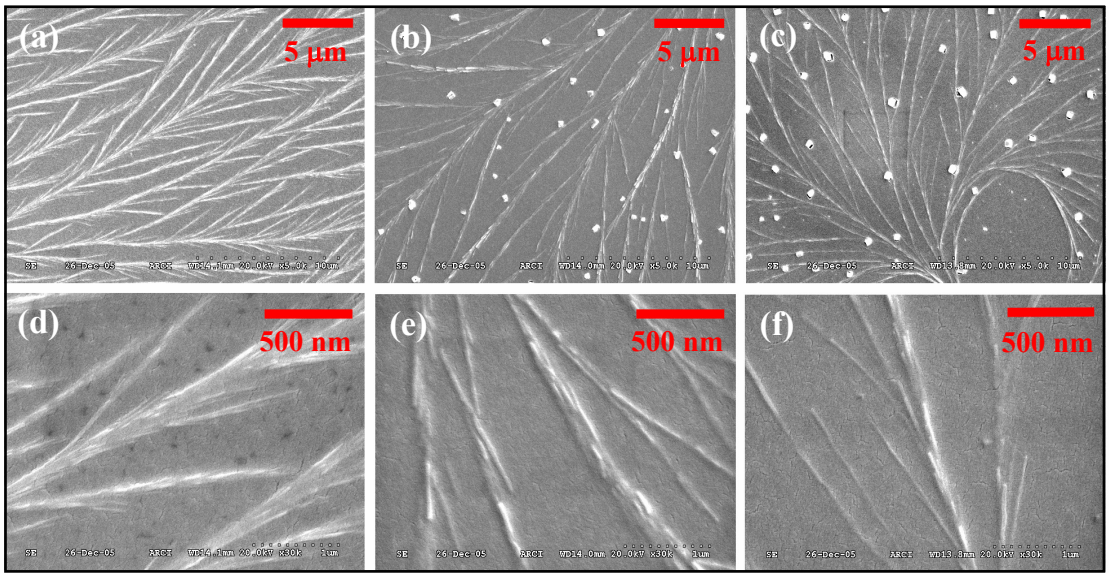

Figure 4.9. *FESEM images of PPVA films with x = 0.09,* ***(a)*** *before heating and heated at T =130°C for* ***(b)*** *t = 30 min and* ***(c)*** *t = 120 min. Higher magnification images of the wire structures in the same films are shown in* ***(d)****,* ***(e)*** *and* ***(f)*** *respectively.*

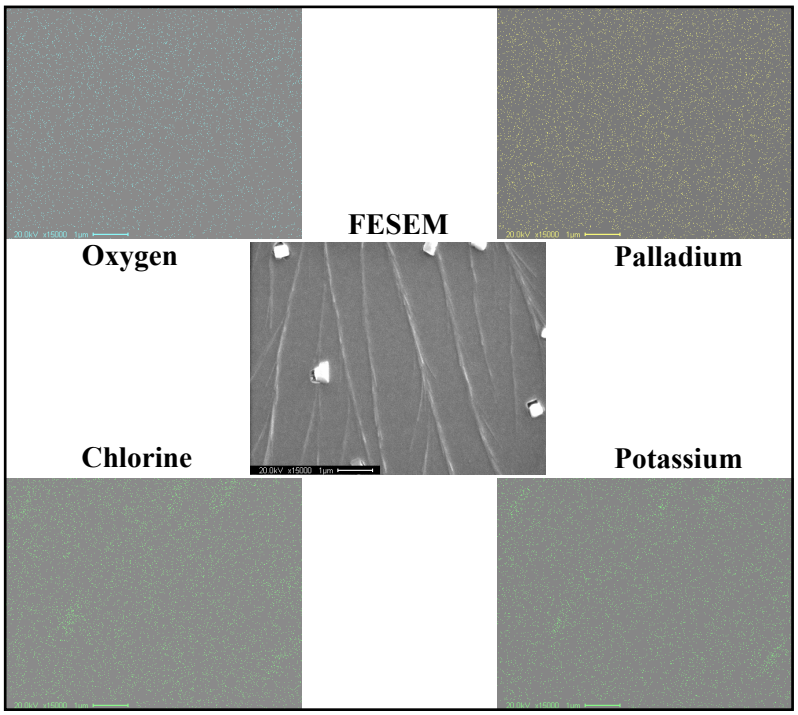

Figure 4.10. *EDX area maps of different elements for the FESEM image (in the centre) of PPVA/PS film (x = 0.09, T = 130°C, t = 120 min).*

as it comes from the polymer. Even though wire structures are present in the film area imaged, some palladium is possibly distributed elsewhere in the film as well, in the neutral and cationic states; this most likely leads to the distribution seen in the area map. Further, the palladium is mostly buried in the polymer film, leading to relatively lower sensitivity in its detection by EDX. Since the square-plate structures are prominent and protruding out on the film surface, their elemental composition is visible in the mapping, indicating that they are primarily constituted of potassium and chlorine. The likelihood of these being KCl crystals, a byproduct of the reduction of K_2PdCl_4, is supported by their complete disappearance from films which were washed briefly with water (Fig. 4.11). Comparison of the absorption spectra showed that the palladium content of these films is largely preserved in this washing process, and that there is some decrease in the peaks corresponding to the precursor salt possibly resulting from its dissolution (Fig. 4.12). We believe that this procedure can be fine-tuned if required, to fabricate PVA films containing only palladium.

Final evidence for the nanowire formation and transformation come from TEM imaging together with electron diffraction. Fig. 4.13 shows the TEM images of films with x = 0.09, before heating and after heating at 130^{o}C for 30 and 120 min. ED pattern recorded on any of the wires in the unheated film (Fig. 4.13a) can be indexed satisfactorily to the crystal structure of K_2PdCl_4 belonging to the tetragonal space group, *P*4/*mmm* (No. 123)[21]. The indexing is shown in Fig 4.14a and the comparison of the calculated and observed d values are collected in Table 4.1. Fig. 4.13b and 4.13c show the formation of square plates on heating. The ED from the thin wires (typically with

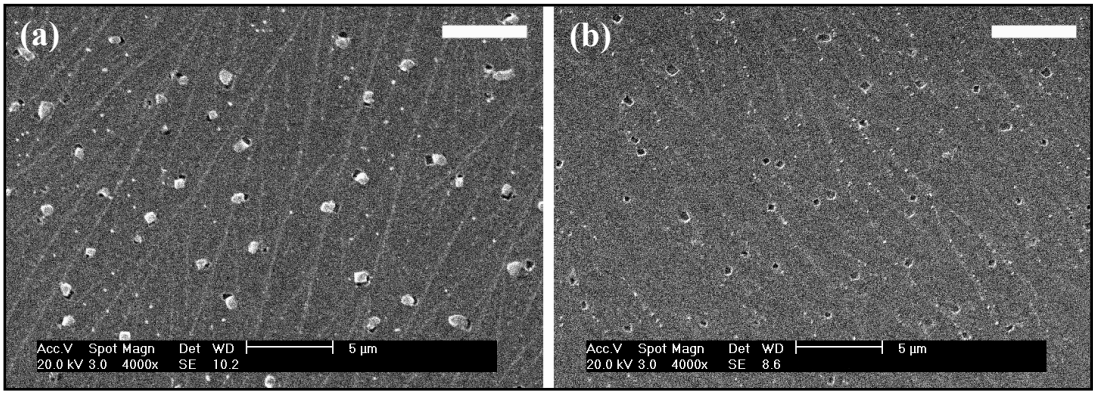

Figure 4.11. *SEM images of PPVA film (x = 0.09, T = 130^{o}C, t = 120 min)* ***(a)*** *before and* ***(b)*** *the same film after washing in water for 15 sec (Scale bar = 5 µm).*

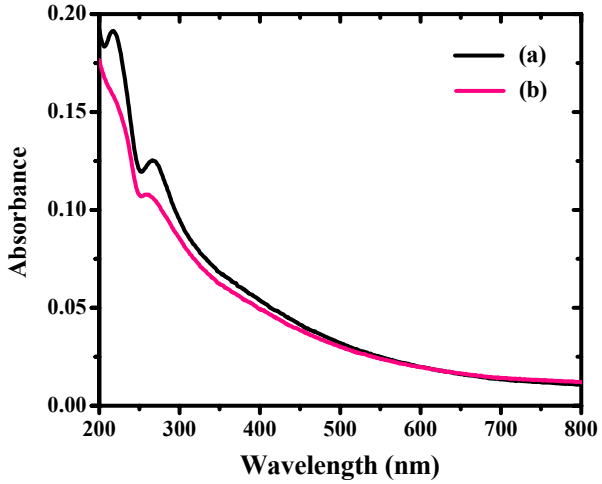

Figure 4.12. *Absorption spectra of PPVA film (x = 0.09, T = 130°C, t = 120 min)* ***(a)*** *before and* ***(b)*** *the same film after washing in water for 15 sec.*

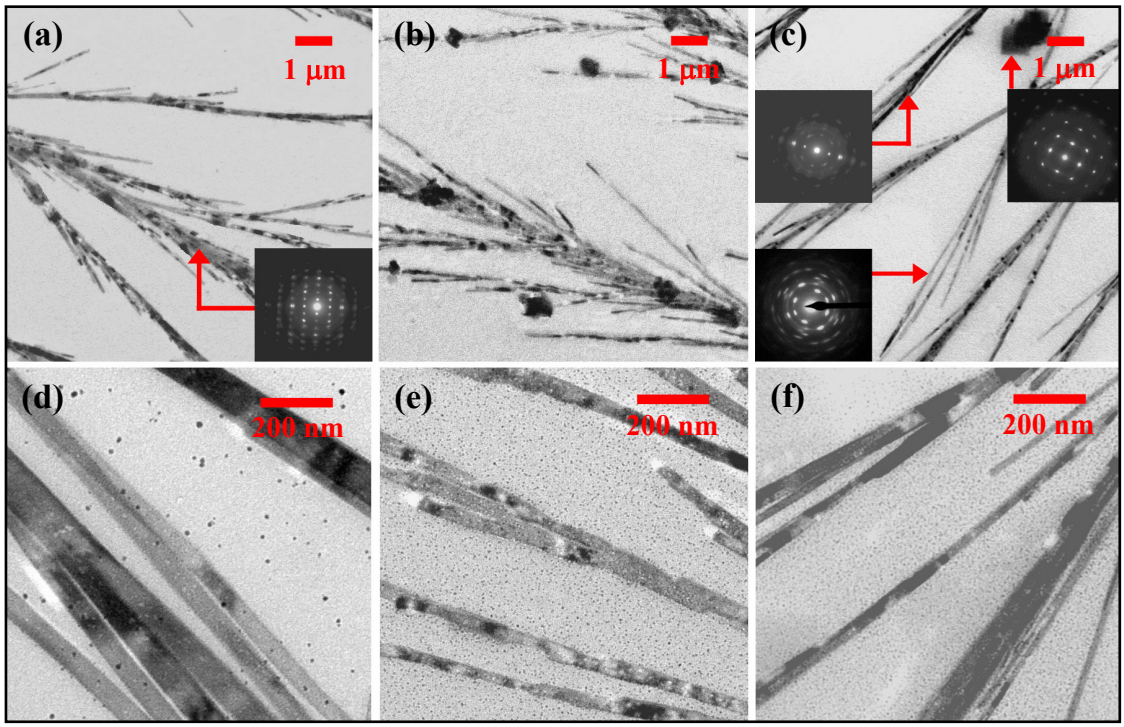

Figure 4.13. *TEM images of PPVA films with x = 0.09 :* ***(a)*** *before heating, and heated at T =130°C for* ***(b)*** *t = 30 min and* ***(c)*** *t = 120 min; higher magnification images are shown in* ***(d)***, ***(e)*** *and* ***(f)*** *respectively. Insets in* ***(a)*** *and* ***(c)*** *show ED pattern of selected regions.*

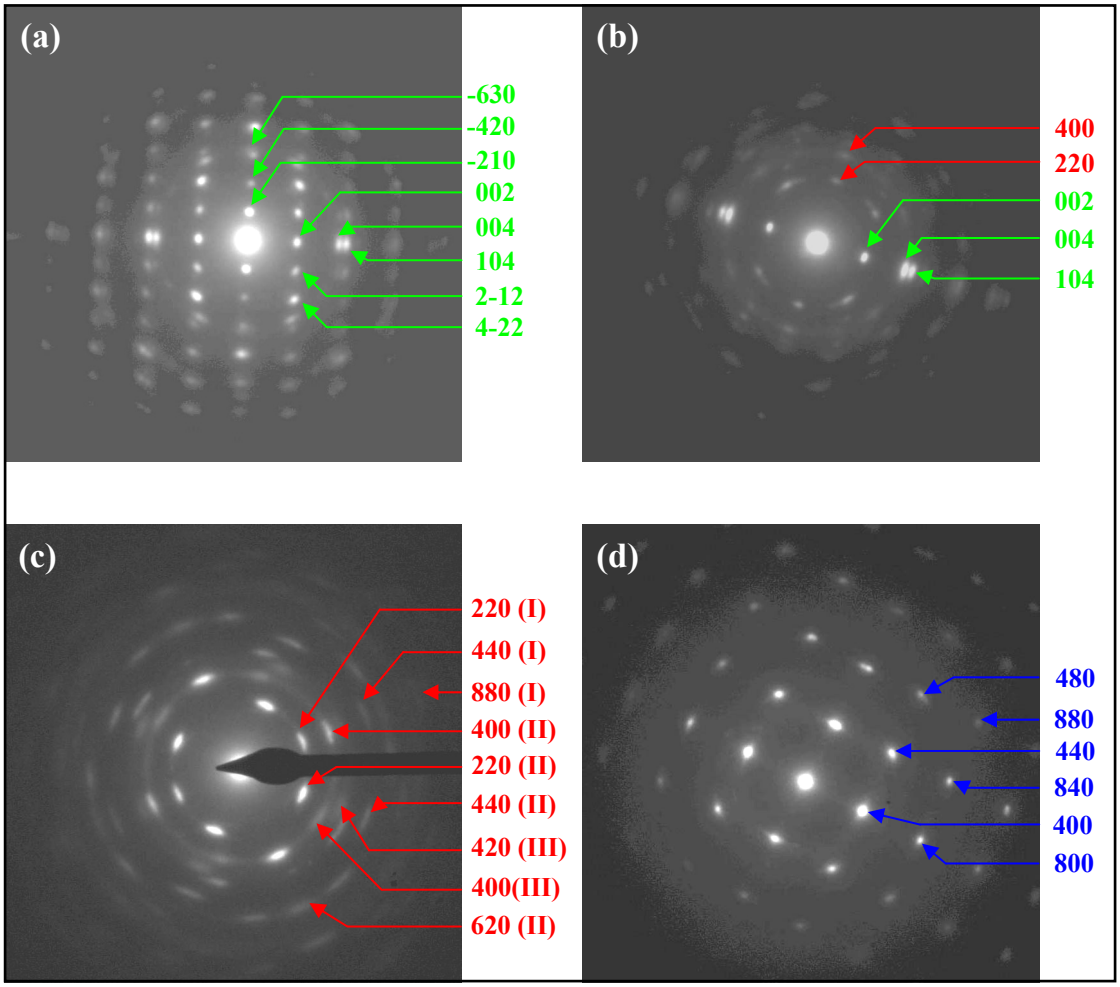

Figure 4.14. *Electron diffraction patterns of PPVA films showing the indexing :* ***(a)*** *pattern shown in Fig. 4.13a (for wire in unheated sample) and (b) – (d) patterns shown in Fig. 4.13c for films with x = 0.09, T = 130°C, t = 120 min :* ***(b)*** *on thick wire (>100nm),* ***(c)*** *on thin wire (<100nm) and* ***(d)*** *on square plate.*

Color code for the indexing

Green : K_2PdCl_4 (a = 7.0750 Å, c = 4.1158 Å, Space group no. 123)

Red* : Pd (a = 3.8907 Å, Space group no. 225)

Blue : KCl (a = 6.2931 Å, Space group no. 225)

*(I), (II) and (III) represent crystallites with different orientations, (I) having a preferred growth direction

Table 4.1. *Details of indexing the electron diffraction patterns shown in Fig. 4.14.*

Crystal (Space group)	h k l	d (Å) (Cal-culated)	d (Å) (Experimental)					
			Un-heated	t = 30 min, T = 130°C		t = 120 min, T = 130°C		
				Thick wire	Thin wire	Thick wire	Thin wire	Square plate
K_2PdCl_4 (No. 123)	-2 1 0	3.164	3.151	3.151	-	-	-	-
	0 0 2	2.058	2.035	2.035	2.035	2.035	-	-
	-2 1 2	1.725	1.714	1.714	-	-	-	-
	-4 2 0	1.582	1.575	-	-	-	-	-
	-4 2 2	1.254	1.252	1.252	-	-	-	-
	-6 3 0	1.055	1.050	-	-	-	-	-
	0 0 4	1.029	1.028	1.028	1.028	1.028	-	-
	1 0 4	1.018	0.967	0.967	0.967	0.967	-	-
Pd (No. 225)	2 2 0	1.376	-	-	-	1.376	1.376	-
	4 0 0	0.973	-	-	-	0.977	0.977	-
	4 2 0	0.867	-	-	0.872	-	0.872	-
	4 2 2	0.794	-	-	0.794	-	0.794	-
	4 4 0	0.688	-	0.688	-	-	0.688	-
	6 2 0	0.615	-	-	-	-	0.614	-
	8 8 0	0.344	-	-	-	-	0.343	-
KCl (No. 225)	4 0 0	1.573	-	-	-	-	-	1.576
	4 4 0	1.113	-	-	-	-	-	1.113
	8 0 0	0.787	-	-	-	-	-	0.788
	8 4 0	0.704	-	-	-	-	-	0.702
	8 8 0	0.556	-	-	-	-	-	0.557

diameters < 100 nm) and square plate structures in Fig. 4.13c can be indexed respectively to crystals of Pd and KCl, both belonging to the cubic $Fm\bar{3}m$ space group (No. 225) (Fig. 4.14c and 4.14d and Table 4.1). The Pd wires appear to have crystallites with more than one orientation, some of them exhibiting preferential growth direction. The ED pattern of the thicker wires (diameters > 100 nm) in Fig. 4.13c is complex with diffraction spots assignable to Pd as well as K_2PdCl_4 (Fig. 4.14b and Table 4.1); similar is the case with the wires in Fig. 4.13b. None of the ED patterns correspond to $PdCl_2$ ruling out its formation by decomposition of K_2PdCl_4. The magnified images in Fig. 4.13d - 4.13f reveal clearly the individual wire strands and demonstrate the shrinkage during the transformation of the precursor to palladium. The diameter of individual nanowires decrease from ~ 50 - 150 nm to ~ 20 - 70 nm upon heating. The porous structure of palladium wires, possibly resulting from the thermal transformation is shown in the magnified image in Fig. 4.15. The SEM and TEM observations suggest that the features in the AFM images (Fig. 4.7) possibly correspond to collections of such wires together with a polymer sheath. The electron diffraction study (supported by the XPS and absorption spectra) demonstrates the gradual change of K_2PdCl_4 nanowires to Pd nanowires upon heating, along with the concomitant formation of microcrystals of the byproduct KCl; the thin nanowires in the films heated for 120 min result from the crystal-to-crystal transformation.

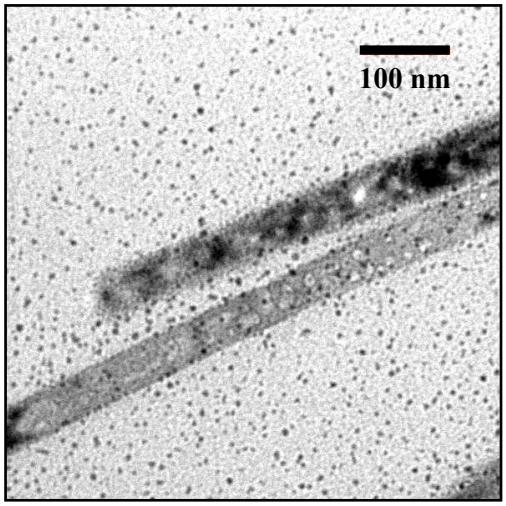

Figure 4.15. *Magnified TEM image of nanowires present in PPVA film (x = 0.09, T = 130^{o}C, t = 120 min) showing the porous structure.*

4.4. Optical Limiting

Palladium nanoparticles are known to possess optical limiting characteristics.[22] We have carried out Z-scan experiments to investigate the nonlinear absorption and optical limiting capability of the PPVA film. Second harmonic (532 nm) of an Nd:YAG laser (10 Hz, 6 ns) with peak intensities in the range 4.5 - 30.0 × 10^7 W cm^{-2} was used in f/24 geometry;[23] PPVA/PS film with x = 0.09 was studied. The details of experimental set up have been already discussed in Sec. 2.4.1. A weak reverse saturable absorption (comparable to that of plain PS film) is observed in the unheated PPVA/PS film (Fig. 4.16a), indicating that the effect arises due to the PS layer. The film heated at T = 130°C for t = 120 min showed a considerably enhanced effect (Fig. 4.16b) due to

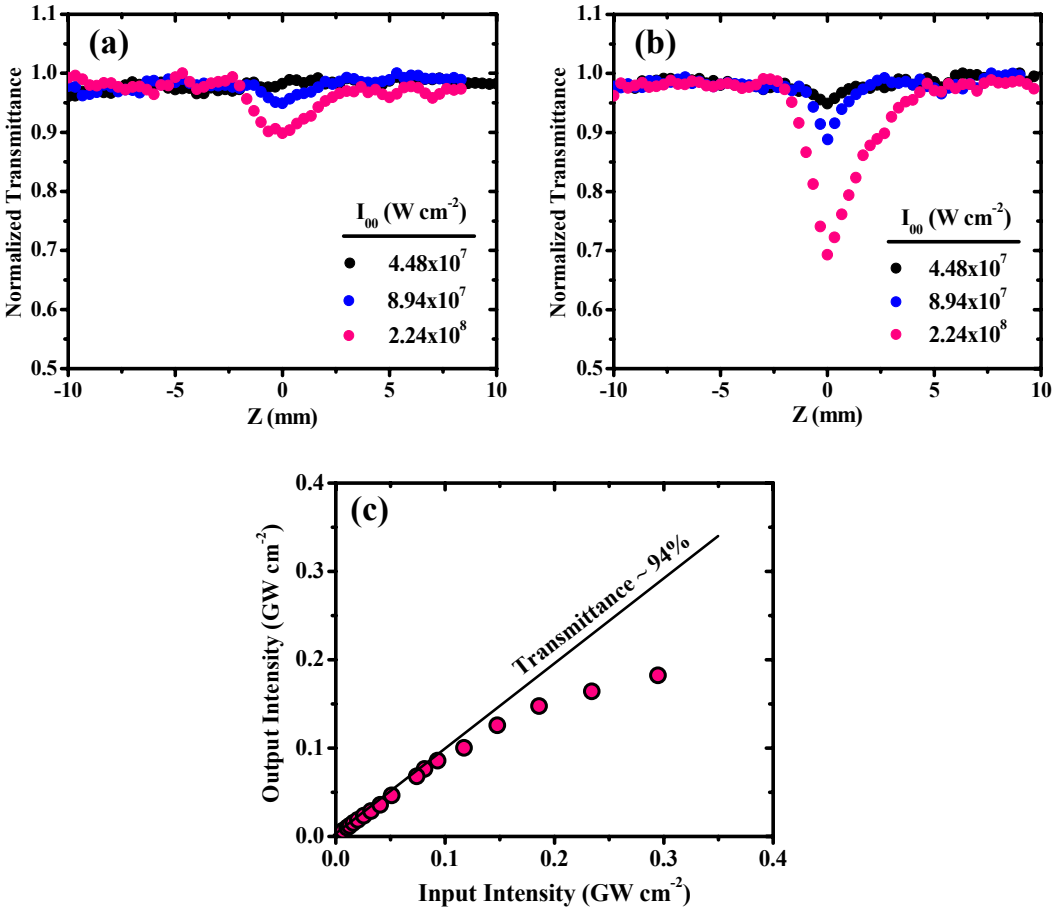

Figure 4.16. *Open aperture Z-scan traces at different input intensities for PPVA/PS film (x = 0.09) on glass,* ***(a)*** *unheated and* ***(b)*** *heated at T = 130°C for t = 120 min;* ***(c)*** *output versus input intensity plots of the film in* ***(b)*** *for nanosecond laser pulses.*

the palladium nanowires formed. Plot of the output power versus input power (Fig. 4.16c) shows the optical limiting behavior of the heated PPVA/PS film; the linear transmittance is ~ 94% at low laser intensities and the output is clamped at ~ 0.18 GW cm^{-2} at higher intensities. The high linear transmittance and appreciable optical limiting are promising features of the new composite material.

4.5. Extension of the Fabrication Methodology to Gold

We have explored the general utility of the approach developed for the fabrication of palladium nanowire by carrying out some preliminary studies with gold. Our earlier experiments on gold[15] (Sec. 3.2) have shown that when x = 0.04 - 0.18, nanoplates are obtained with no extended structures. In the current study, we have investigated films with compositions, x = 0.12 - 0.22, fabricated under different conditions from that used previously. The main variations tested are the dilution of the solutions and the spin-coating conditions. With x = 0.12 and 0.18, more dilute solutions and slower spinning rates, the films showed the formation of dendritic morphologies. However, organized structures could be realized by further modification of the composition and fabrication conditions. Films with x = 0.18 and 0.22 were prepared as follows. Required amount of $HAuCl_4$ dissolved in 1.25 ml water was mixed with 0.3 ml of a solution of PVA (Aldrich, average molecular weight = 13 - 23 kDa, % hydrolysis = 86) in water (2.4 g PVA in 8 ml water). The solution was spin coated on top of the polystyrene layer at 500 rpm/10sec followed by 8000 rpm/10sec. AFM images of the unheated films revealed structures aggregated into linear arrays several microns long with widths ~ 50 - 100 nm and heights ~ 5 - 15 nm (Fig. 4.17) with fair degree of organization. As observed in the case of palladium, heating causes distinct shrinkage of the structures so that the widths become ~ 30 - 40 nm and heights ~ 1 - 3 nm; the morphology is reminiscent of the nanowires reported earlier for gold[24] and palladium.[1,25] The absorption spectra of the heated film shows the emergence of plasmon peaks at 530 and 810 nm (Fig. 4.18), the latter possibly arising due to the high aspect ratio gold nanostructures that are formed. XPS spectra provide further evidence for reduction of $HAuCl_4$ to Au upon heating the film[26] (Fig. 4.19). The unheated film shows predominantly, the presence Au^{3+}; a small proportion of Au^0 is observed, possibly arising from slight reduction during storage and measurement. The heated film

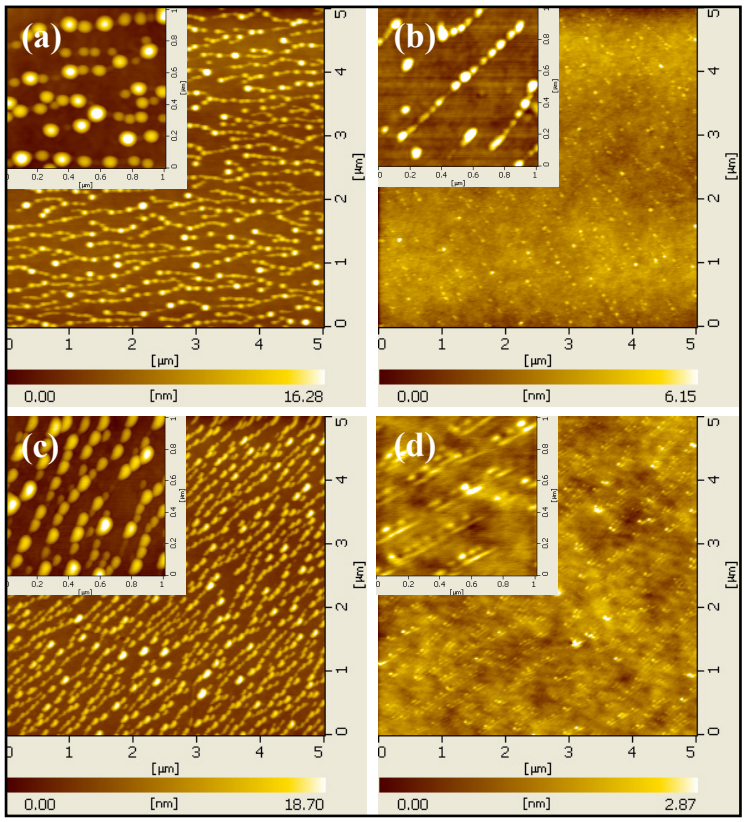

Figure 4.17. *AFM topography images (5 µm x 5 µm) of* $HAuCl_4$-PVA *films with x = 0.18,* ***(a)*** *before heating and* ***(b)*** *heated at T =130°C, t = 60 min, and with x = 0.22,* ***(c)*** *before heating and* ***(d)*** *heated at T =130°C, t = 60 min. Higher magnification images are shown in the inset in each case.*

contains exclusively Au^0. Since the byproduct in the reduction of $HAuCl_4$ is HCl, the microscopy images of heated films show only the gold nanostructures; this may be contrasted with the case of palladium which showed micrometer-sized crystals of KCl from the reduction of K_2PdCl_4.

In conjunction with our earlier investigations on silver and gold, the present observations suggest that a range of morphologies of metal nanostructures from spherical particles to nanoplates to nanowires can be realized *in situ* inside PVA films by fine-tuning the composition and fabrication conditions. The general observation is that, increasing the metal/polymer ratio and optimizing the spin-coating conditions (to reduce the film thickness) leads to the formation of extended structures.

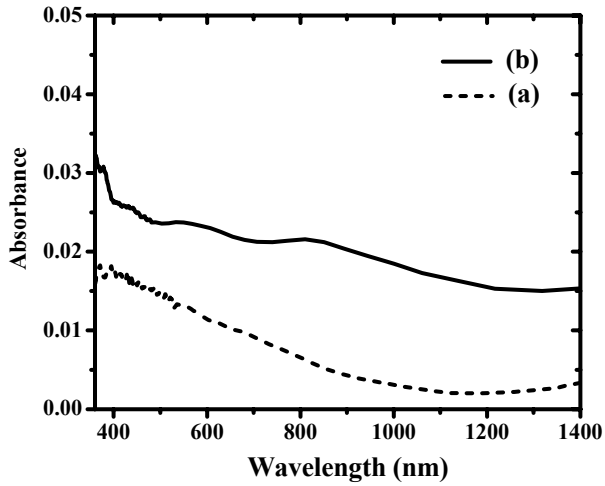

Figure 4.18. *Absorption spectra of Au-PVA films with x = 0.22,* ***(a)*** *before heating, and* ***(b)*** *heated at T =130^{o}C, t = 60 min.*

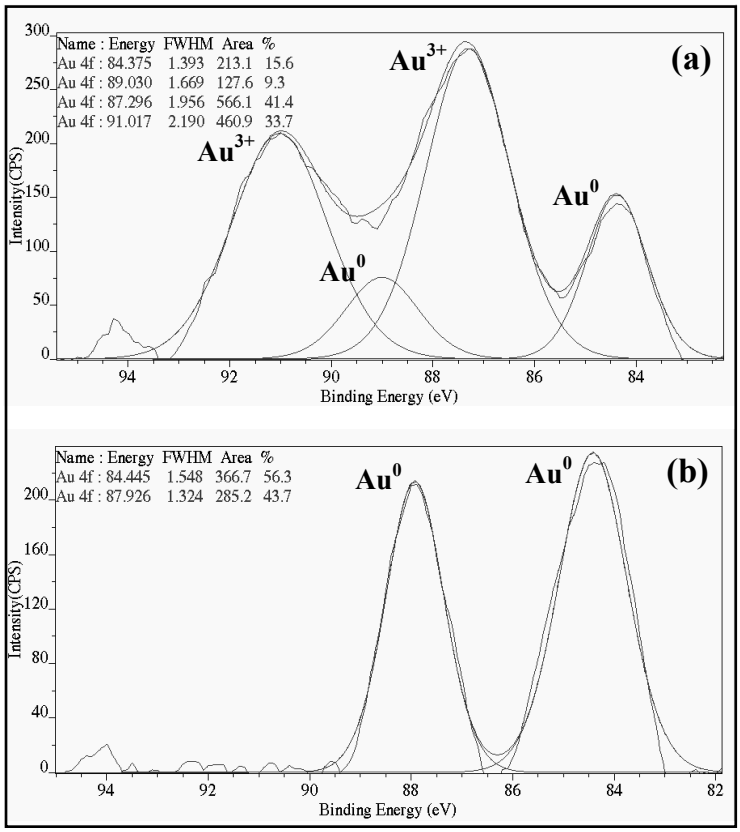

Figure 4.19. *XPS spectra of Au-PVA films with x = 0.22,* ***(a)*** *before heating, and* ***(b)*** *heated at T =130^{o}C, t = 60 min. Deconvolution of each spectrum is indicated.*

4.6. Summary

The *in situ* formation of palladium nanowires in PVA films and the preliminary studies on gold illustrate that the crystallization of metal salts in appropriate concentrations inside polymer matrices followed by their reduction to the corresponding metal through the participation of the polymer matrix, offers a convenient route to the fabrication of free-standing or supported, metal nanowire-embedded polymer thin films. The reaction occurring inside the polymer matrix, including byproduct formation, could be monitored using microscopy and spectroscopy; it is shown to be a nanometric crystal-to-crystal transformation. The Z-scan studies indicated that the palladium nanowire-embedded polymer films show appreciable nonlinear absorption which is of potential interest in optical limiting applications.

The protocol adopted in this work uses thermal annealing. The methodology is amenable to other approaches such as microwave heating or laser irradiation, the latter being of interest in patterning applications. Another important aspect of the nanowire-embedded polymer films is the partial conversion of the precursor salt leading to a mixture of palladium in neutral and dicationic states; relevance of such materials to catalytic applications are being investigated in our laboratory currently.

References

1. Favier, F.; Walter, E. C.; Zach, M. P.; Benter, T.; Penner, R. M. *Science* **2001**, *293*, 2227.
2. (a) Hahm, J.; Lieber, C. M.; *Nano Lett.* **2004**, *4*, 51; (b) Liu, H. Q.; Kameoka, J.; Czaplewski, D. A.; Craighead, H. G. *Nano Lett.* **2004**, *4*, 671; (c) Murray, B. J.; Newberg, J. T.; Walter, E. C.; Li, Q.; Hemminger, J. C.; Penner, R. M. *Anal. Chem.* **2005**, *77*, 5205.
3. (a) Huang, M. H.; Mao, S.; Feick, H.; Yan, H.; Wu, Y.; Kind, H.; Weber, E.; Russo, R.; Yang, P. *Science* **2001**, *292*, 1897; (b) Yan, H.; He, R.; Johnson, J.; Law, M.; Saykally, R. J.; Yang, P. *J. Am. Chem. Soc.* **2003**, *125*, 4728.
4. (a) Hu, S.; Hamidi, A.; Altmeyer, S.; Köster, T.; Spangenberg, B.; Kurz, H. *J. Vac. Sci. Technol. B* **1998**, *16*, 2822; (b) Natelson, D. in *Recent Developments in Vacuum Science and Technology*, (Ed.) Dabrowski, J.; Research Signpost, Kerala, India; 2003, p.157.
5. (a) Zach, M. P.; Ng, K. H.; Penner, R. M. *Science* **2000**, *290*, 2120; (b) Yin, A. J.; Li, J.; Jian, W.; Bennett, A. J.; Xu, J. M. *Appl. Phys. Lett.* **2001**, *79*, 1039; (c) Thompson, M. A.; Menke, E. J.; Martens, C. C.; Penner, R. M. *J. Phys. Chem. B* **2006**, *110*, 36.
6. (a) Scheibel, T.; Parthasarathy, R.; Sawicki, G.; Lin, X-M.; Jaeger, H.; Lindquist, S. L. *Proc. Natl. Acad. Sci. USA* **2003**, *100*, 4527; (b) Cheng, C.; Haynie, D. T. *Appl. Phys. Lett.* **2005**, *87*, 263112; (c) Cheng, C.; Gonela, R. K.; Gu, Q.; Haynie, D. T. *Nano Lett.* **2005**, *5*, 175.
7. Wang, C. Y.; Zhou, Y.; Chen, Z. Y.; Lu, Q. Y.; Mo, X. *J. Nanoparticle Res.* **1999**, *1*, 479.
8. (a) Hosoda, N.; Kato, T. *Chem. Mater.* **2001**, *13*, 688; (b) Taubert, A.; Kübel, C.; Martin, D. C. *J. Phys. Chem. B* **2003**, *107*, 2660; (c) Xie, Q.; Liu, Z.; Shao, M.; Kong, L.; Yu, W.; Qian, Y. *J. Cryst. Growth* **2003**, *252*, 570; (d) Yang, J.; Qi, L.; Zhang, D.; Ma, J.; Cheng, H. *Cryst. Growth Des.* **2004**, *4*, 1371.
9. (a) Oaki, Y.; Imai, H. *Cryst. Growth Des.* **2003**, *3*, 711; (b) Gránásy, L.; Pusztai, T.; Warren, J. A.; Douglas, J. F.; Börzsönyi, T.; Ferreiro, V. *Nature Mater.* **2003**, *2*, 92; (c) Gránásy, L.; Pusztai, T.; Börzsönyi, T.; Warren, J. A.; Douglas, J. F. *Nature Mater.* **2004**, *3*, 645.
10. Kalyanaraman, C.; Evans, D. G. *Nano Lett.* **2002**, *2*, 437.
11. Warheit, D. B.; Laurence, B. R.; Reed, K. L.; Roach, D. H.; Reynolds, G. A. M.; Webb, T. R. *Toxicol. Sci.* **2004**, *77*, 117.
12. Porel, S.; Singh, S.; Harsha, S. S.; Rao, D. N.; Radhakrishnan, T. P. *Chem. Mater.* **2005**, *17*, 9.
13. Matsuda, S.; Ando, S. *Polym. Adv. Tech.* **2003**, *14*, 458.
14. Anthony, S. P.; Porel, S.; Rao, D. N.; Radhakrishnan, T. P. *Pramana* **2005**, *65*, 871.
15. Porel, S.; Singh, S.; Radhakrishnan, T. P. *Chem. Commun.* **2005**, 2387.
16. (a) Astruc, D.; Lu, F.; Aranzaes, J. R. *Angew. Chem. Int. Ed.* **2005**, *44*, 7852; (b) Wilson, O. M.; Knecht, M. R.; Garcia-Martinez, J. C.; Crooks, R. M. *J. Am. Chem. Soc.* **2006**, *128*, 4510.
17. (a) Kishore, S.; Nelson, J. A.; Adair, J. H.; Eklund, P. C. *J. Alloys Comp.* **2005**, *389*, 234;

(b) Horinouchi, S.; Yamanoi, Y.; Yonezawa, T.; Mouri, T.; Nishihara, H. *Langmuir* **2006**, *22*, 1880.

18. Takahashi, S.; Miura, H.; Kasai, H.; Okada, S.; Oikawa, H.; Nakanishi, H. *J. Am. Chem. Soc.* **2002**, *124*, 10944.; (b) Bučar, D.; MacGillivray, L. R. *J. Am. Chem. Soc.* **2006**, *129*, 32.
19. (a) Garcia-Martinez, J. C.; Scott, R. W. J.; Crooks, R. M. *J. Am. Chem. Soc.* **2003**, *125*, 11190; (b) Scott, R. W. J.; Ye, H.; Henriquez, R. R.; Crooks, R. M. *Chem. Mater.* **2003**, *15*, 3873; (c) Shifrina, Z. B.; Rajadurai, M. S.; Firsova, N. V.; Bronstein, L. M.; Huang, X.; Rusanov, A. L.; Muellen, K. *Macromolecules* **2005**, *38*, 9920; (d) Chen, M.; Falkner, J.; Guo, W.-H.; Zhang, J.-Y.; Sayes, C.; Colvin, V. L. *J. Colloid Interface Sci.* **2005**, *287*, 146.
20. Kidambi, S.; Bruening, M. L. *Chem. Mater.* **2005**, *17*, 301.
21. Hester, J. R.; Maslen, E. N.; Spadaccini, N.; Ishizawa, N.; Satow, Y. *Acta Cryst.* **1993**, *B49*, 842.
22. (a) Gao, Y.; Song, Y.; Li, Y.; Wang, Y.; Liu, H.; Zhu, D. *Appl. Phys. B* **2003**, *76*, 761; (b) Zeng, H.; Yang, Y.; Jiang, X.; Chen, G.; Qiu, J.; Gan, F. *J. Cryst. Growth* **2005**, *280*, 516; (c) Pan, H.; Chen, W.; Feng, Y. P.; Ji, W.; Lin, J. *Appl. Phys. Lett.* **2006**, *88*, 223016.
23. Kiran, P. P.; De, G.; D. N. Rao, *IEE Proc. Circuits Devices Syst.* **2003**, *150*, 559.
24. (a) Patolsky, F.; Weizmann, Y.; Lioubashevski, O.; Willner, I. *Angew. Chem. Int. Ed.* **2002**, *41*, 2323; (b) Fullam, S.; Cottell, D.; Rensmo, H.; Fitzmaurice, D. *Adv. Mater.* **2000**, *12*, 1430.
25. Atashbar, M. Z.; Banerji, D.; Singamaneni, S.; Bliznyuk, V. *Nanotechnology* **2004**, *15*, 374.
26. Abdou, M. S. A.; Holdcroft, S. *Chem. Mater.* **1996**, *8*, 26.

5.1. Overview of the Present Work

The design and fabrication of nanomaterials, their characteristics and functions, and finally applications, are closely linked problems. Currently, there is enormous interest and activity in each of these areas – developing new synthesis protocols, predicting and realizing novel properties and exploring potential applications in a wide range of fields. Development of novel nanomaterials requires the knowledge and control of the structure and organization at the nanometer level. Properties of nanomaterials depend sensitively on the size, shape and organization of nanoparticles as well as the interactions between themselves and with the medium in which they exist. These continue to be challenging problems to understand and control precisely. Nanomaterials are finding application in almost every discipline and many facets of daily life. An approach which allows (i) the generation of nanoparticles within a medium, (ii) characterization of the properties without further isolation steps and finally (iii) direct utilization of the nanoparticle-matrix composite in desired applications will be highly desirable and useful. Polymers are particularly interesting candidates for use as the matrix materials. Many of the polymers are easy to process and water soluble ones are specially useful from the point of view of ease of handling. Attributes such as flexibility, transparency and permeability are advantageous for specific applications. Polymers with conducting, semiconducting or insulating characteristics can be chosen to tailor the fabrication of new generation nanodevices and 'smart' materials.

Polymers are often used as the stabilizer for nanoparticles in colloidal state. Composites of metal/semiconductor nanoparticles with polymers are also popular. However, generation of metal nanoparticles within a polymer matrix (using the matrix itself as the only reagent to reduce the precursor materials) coupled with direct characterization and application of the nanoparticle-embedded solid polymer films has not been investigated prior to our work. We have presented in this thesis, the fabrication of silver, gold and palladium nanoparticles using the polymer, primarily poly(vinyl alcohol), as a multifunctional medium for their controlled generation. PVA is a bio-compatible and bio-degradable polymer and acts as the reducing and/or stabilizing agent for the metal nanoparticles. It facilitates the formation of supported and free-standing nanoparticle-embedded films. The synthesis scheme we have developed is simple to implement and efficient; the use of the aqueous medium makes it

an 'environment-friendly' process. The *in situ* nature of the particle generation eliminates potential health hazard from inhalable nanoparticles. The free-standing composite thin films can be characterized directly in TEM without the need for sample processing such as microtoming. We believe that this is very significant not only in terms of avoiding sophisticated sample preparation, but also because it provides a direct visualization of the nanostructures that will be involved in the applications. This may be contrasted with the regularly used procedure wherein colloidal drops containing the nanoparticles are placed on a TEM grid and allowed to dry before imaging, in which case artifacts could arise in the drying process. Based on the different metal-polymer systems we have studied, we have observed that the metal/polymer ratio plays an important role in controlling the nanostructures. Increasing concentration leads to increased size of nanoparticles in the case of silver, but significant changes in the nanoplates geometry in the case of gold. The composition also influences the morphology (particles, dendrites or wires) of the precursor salt (as shown clearly in the case of palladium) and hence that of the final metal nanostructure. Temperature and time of thermal treatment provide another convenient control parameter. These factors affect the extent of reaction as well as the size and shape of the nanostructures. The influence of the thermal treatment is likely to be two-fold; softening the polymer matrix and accelerating the diffusion of ions and atoms as well as enhancing the chemical reduction process. We do not have a clear picture of the relative roles of these different effects at the moment. These are relevant issues to be addressed in future explorations.

The fabrication methodology we have developed for the metal-polymer nanocomposites presents some further advantages. It allows convenient monitoring of the reaction occurring inside the polymer thin films, including byproduct formation, through spectroscopy and microscopy. In the case of formation of gold nanoplates, we were able to examine the role of polymer and in case of palladium, the formation of microcrystalline byproduct. The thin film form of the polymer composite can be exploited to obtain preferred orientation of anisotropic nanostructure, as seen in the case of gold nanoplates. However, the full potential of the thin films to achieve tailored organization of nanostructures remains to be demonstrated.

At the application front, all the three kinds of nanoparticle-polymer composite films we have fabricated display appreciable optical limiting capability. The fact that

thin films typically a few microns thick, show responses comparable to colloids with path lengths of a few millimeters, is highly encouraging from the point of view of developing novel 'smart materials'. The possibility of fabricating free-standing metal nanoparticles-embedded polymer films allowed us to make unambiguous estimation of the nonlinear refractive index and susceptibility of the nanoparticles. This is a significant contribution towards fundamental understanding of the nonlinear optics of metal nanoparticles. The efficient bactericidal application of silver nanoparticle-polymer composite films is another important development. The reusability of the polymer films is an important consideration from the economics perspective. From the technical point of view, the facility afforded by the thin film nature of the bactericide to scrutinize it between action cycles is highly relevant.

We believe that the studies presented in this thesis on the fabrication, characterization and application of metal nanoparticle-embedded polymer films represent a new direction in the science and technology of nanomaterials. Further optimization of the methodology is likely to open up a powerful route to achieve enhanced control of nanostructures in polymer films with implications for the fabrication of nanoscale devices.

5.2. Future Prospects

The basic idea of environment-friendly synthesis of metal nanoparticle in a dielectric environment has been demonstrated in the studies we have presented. The current protocol can be used for the synthesis of a wide range of other metal nanoparticles as well, in the form of embedding in polymer films. Based on redox potential consideration and some preliminary experiments, we have found that nanoparticles of metals such as ruthenium and platinum also can be generated in PVA films. The methodology can also be extended with minor modifications, to generate semiconductor nanoparticles inside polymer films. Another interesting avenue to explore is the fabrication of alloys and core-shell structures inside polymer films, using our methodology. Some experiments in this direction have been reported recently.[1, 2] We have discussed preliminary observations related to the fabrication of gold nanopyramids, real-time monitoring of the *in situ* growth of gold nanodomes and the

'green' synthesis of gold nanocrystals. In addition to more detailed characterization, some specialized studies are likely to be rewarding. It would be interesting to explore the possibility of sculpting desired 3-dimentional nanostructures inside the polymer films by tuning the temperature gradients and the thickness of the films. The kinetics of growth of the nanostructures inside polymer film and dependence on factors such as the precursor concentration and polymer viscosity are fundamental issues to be investigated. The molecular basis of the 'green' synthesis, the relevance of the type of leaf used and development of an efficient procedure to harvest the fabricated nanocrystals are points to be addressed in further studies.

Investigation of several variations on the fabrication methodology we have developed, could prove interesting. In all the studies reported in this thesis, we have used thermal treatment of the precursor-polymer films to generate the metal nanoparticles. Alternate procedures such as photoirradiation (at a suitable wavelength in the UV, visible or IR regions), laser irradiation or microwave heating can be attempted. Preliminary explorations we have carried out indicate that microwave heating can be quite effective. In the case of irradiation with light, masking or interference effects can be attempted to generate patterned structures; a study along these lines has been reported.[3] It is well known that seeding protocol is very useful for the colloidal synthesis of nanorods with different aspect ratios. Parallel studies can be carried out inside matrices as well. A simple approach to the organization of metal nanoparticles could be the incorporation of organic linker molecules in the polymer films.

Several characteristics of metal nanoparticles-polymer films remain to be investigated. A significant property that may be assessed is the conductivity or dielectric behavior with extreme cases of metal/polymer compositions. Surface-enhanced Raman scattering (SERS) of these films could be interesting to explore because of the application potential in sensing. Modeling the electronic absorption and investigation of electroabsorption properties of these composite films, taking into account the distinct size and shape factors would be interesting exercises to take up. We have focused attention on the metal nanoparticles and their properties, the polymer serving only as the matrix. In a different approach, focus can be placed on the modification of the polymer properties as a result of the incorporation of metal

nanoparticles. Such studies reported for composites prepared from preformed nanoparticles,[4] can now be extended to the kind of metal-polymer films we have fabricated.

A series of further explorations can be envisaged from the point of view of applications of the metal nanoparticles-embedded polymer films. Detailed mechanism of the optical limiting in gold and palladium nanostructure-embedded films remains to be studied. The shape dependent behavior in the case of gold nanoplates will be a particularly interesting problem to pursue. The wavelength dependence of optical limiting phenomena in these materials need to be examined. Another feature that would be interesting to explore is the microwave absorption of metal nanoparticle-embedded polymer thin films. We have demonstrated the antibacterial property of silver nanoparticle-PVA composite thin films only towards gram-negative bacteria, specifically *E. coli*. These films appear to be effective against other gram-negative and gram-positive bacteria and for a wide spectrum of microbes. Experimental confirmation of these preliminary observations would be critical to establish the nanocomposite films as an effective agent for water purification and related applications. Another important area for potential application of the metal nanoparticle-polymer films is in catalysis. Systems like Pd-PVA could be efficient reusable catalyst for a number of organic reactions. Semiconductor nanoparticle-polymer composite films can be considered for photocatalytic applications. It is also possible to envisage the development of photoluminescent thin films through our methodology. Candidate systems will include polymer films with *in situ* fabricated semiconductor nanoparticles and organic dye-metal nanoparticle combinations.

Several of the new directions listed above, covering various aspects of fabrication of nanoparticle-embedded polymer films, their characterizations and applications are currently being actively pursued in our laboratory. It is heartening to note that our fabrication methodology has been applied fruitfully by other researchers in the field.[1, 2, 5-8] We believe that the novel developments in the field of nanomaterials presented in this thesis and the extension of these ideas into further avenues, will pave the way for further exciting research in future.

References

1. Karthikeyan, B.; Anija, M.; Philip, R. *Appl. Phys. Lett.* **2006**, *88*, 053104.
2. Sakamoto, M.; Tachikawa, T.; Fujitsuka, M.; Majima, T. *Adv. Funct. Mater*. **2007**, *17*, 857.
3. (a) Korchev, A. S.; Bozack, M. J.; Slaten, B. L.; Mills, G. *J. Am. Chem. Soc.* **2004**, *126*, 10; (b) Pérez-Juste, J.; Rodríguez-González, B.; Mulvaney, P.; Liz-Marzán, L. M. *Adv. Funct. Mater.* **2005**, *15*, 1065.
4. (a) Mbhele, Z. H.; Salemane, M. G.; van Sittert, C. G. C. E.; Nedeljkovic´, J. M.; Djokovic´, V.; Luyt, A. S. *Chem. Mater.* **2003**, *15*, 5019; (b) Feng, Q.; Dang, Z.; Li, N.; Cao, X. *Mater. Sci. Eng.* **2003**, *B99*, 325.
5. (a) Karthikeyan, B. *Physica B: Conden. Matt.* **2005**, *364*, 328; (b) Karthikeyan, B. *Chem. Phys. Lett.* **2006**, *432*, 513.
6. Clemenson, S.; Alcouffe, P.; David, L.; Espuche, E. *Desalination* **2006**, *200*, 437.
7. Yu, D.-G.; Lin, W.-C.; Lin, C.-H.; Chang, L.-M.; Yang, M.-C. *Mater. Chem. Phys.* **2007**, *101*, 93.
8. Oates, T. W. H.; Christalle, E. *J. Phys. Chem. C* **2007**, *111*, 182.

Materials and Instrumentation

Materials

Silver nitrate	Aldrich, 99+%
Hydrogen tetrachloroaurate(III) trihydrate	Aldrich, 99.9+%
Potassium palladium (II) chloride	Aldrich, 99.99%
poly(vinyl alcohol)	Fluka, M_w = 15 kDa, % of hydrolysis = 87-89 Aldrich, M_w = 16 kDa, % of hydrolysis = 98 Aldrich, M_w = 31-50 kDa, % of hydrolysis = 98-99 Aldrich, M_w = 87-146 kDa, % of hydrolysis = 99+
Polystyrene	Aldrich, M_w = 280 kDa
Ultrapure water	Millipore MilliQ water (Resistivity = 18 MΩ cm)
LB broth	Himedia
LB agar media	Himedia

Instrumentation

Spin-coating

Laurell Technologies Corporation Model WS-400B-6NPP/LITE/8K or custom-built standard photoresist spinner was used for the fabrication of the polymer films.

Film Thickness Measurements

Thickness of the films was measured using an Ambios Technology XP-1 profilometer.

Differential Scanning Calorimetry

Thermal properties of the polymers were examined using Perkin Elmer PYRIS Diamond DSC.

Absorption spectroscopy

Absorption spectra of the polymer films coated on quartz/glass substrates were recorded on a Shimadzu Model UV-3101 UV-Vis Spectrometer.

Infra-red spectroscopy

FT-IR spectra of free-standing films were recorded on a Jasco5300 FTIR spectrometer in transmission mode.

X-ray photoelectron spectroscopy

XPS analysis of free-standing films was carried out on a Kratos Axis 165 Spectrometer with a Mg K_α X-ray source (1253.6 eV). The X-ray power supply was run at 15 kV and 5 mA. The pressure in the analysis chamber during the scans was, ~10^{-9} Torr. Spectra were calibrated using the C1s peak at 284.6 eV.

Atomic force microscopy

AFM images of the nanoparticle – polymer composite films on glass substrate were recorded on a SEIKO Model SPA 400 atomic force microscope in the dynamic force (non-contact) mode using a tip having a force constant of 12 N/m. Generally, topography and phase images were recorded. Line profiles were analyzed using the software supplied by the microscope manufacturer.

Scanning electron microscopy

SEM and FESEM images of free-standing films were recorded on a Philips XL 30 ESEM and a HITACHI S-4300SE/N FESEM respectively using beam voltages of 20 kV. The samples were fixed on aluminum platforms using carbon tapes and given a very thin (3 - 5 nm) coating of gold.

Transmission electron microscopy and Electron diffraction

The samples were examined in a JEOL 100CX TEM or TECNAI G^2 FEI F12 TEM at an accelerating voltage of 100 kV or 120 kV using a 20 μm aperture. Electron diffraction data from selected features was collected at 100 kV accelerating voltage at a camera length of 46, 66 or 76 cm. The patterns were photographed using beam stoppers for 4 sec. The beam stopper was placed especially for those samples where it was critical to verify if any spots appear close to the beam center, so that they are not lost by overlap of the beam brightness.

Optical Limiting studies

532 nm wavelength beam from a ns-pulsed (6 ns, 10 Hz) Nd-YAG laser (Spectra physics, Model INDI 40) and 800 nm wavelength beam from a fs-pulsed (~110 fs, 1 kHz) Ti:Sapphire laser (Mai Tai, Spitfire) were used. The input intensity could be

varied using calibrated neutral density filters. The transmitted output was collected using appropriate optics, calibrated fast photodiode (EG & G, FND 100) and processed using a data acquisition system consisting of a lock-in amplifier (Princeton Applied Research, Model No. 121) or boxcar averager (Stanford Research Systems Model SR250), ADC and computer.

Antibacterial studies

Luria-Bertani broth was prepared by mixing 20 g of the solid with 1.0 l sterilized double distilled water and autoclaving for 15 min at 15 psi pressure. LB agar plate was prepared by autoclaving the LB broth with 1.5% agar, cool it to ~ 50-60°C, pouring into petriplates and allowing the agar to solidify. *Escherichia coli* (ATCC No. 25922) was procured from National Chemical Laboratory, Pune grown and stored as glycerol stock. The culture from the glycerol stock was grown in the LB broth at 37°C overnight. It was spread on to LB agar plate and incubated at 37°C overnight. From the bacterial colony obtained, a single one was used for inoculating 10 ml LB culture which was then grown at 37°C for 12 h and used for experiments. The culture was serially diluted to the appropriate density using sterile double distilled water and the bacterial counts (CFU/ml) were made. The final experiments were conducted in one of the following ways: (i) 100 µl of 10^8-10^9 CFU/ml was introduced in 15 ml LB broth or (ii) 1 ml of bacteria culture was serially diluted and 10^5 CFU/ml was introduced in 14 ml Millipore water. Ag-PVA film was immersed in the above media and shaken at 170 rpm inside the incubator at 37^{o}C for 30 or 15 min respectively. In the case of (i), the bacterial growth was monitored at different time periods up to 12 h by measuring the optical density at 600 nm and for (ii), the water sample was plated on LB agar plates and incubated for 12 h at 37^{o}C and the colonies were counted.

All the experiments mentioned above and those in the Sec 2.5, were done under standard laminar air flow systems. The glassware and other equipment were sterilized in an autoclave and by UV irradiation. Bacteria are potentially hazardous; so adequate care was taken while working with them. Standard biosafety laboratory techniques were followed while handling bacteria, and various media. The work area was sterilized with 70% ethanol/water and UV irradiation after completion of the work. Unused media and bacterial suspensions were first deactivated with commercial bleach for 1 h before disposing off in biosafety bags. All materials that had come in contact with

bacteria (e.g., pipette tips, tubes, agar plates etc.) were disposed off using biosafety bags in tightly closed bins. Biosafety bags were autoclaved for 2 h before final disposal.

PUBLICATIONS

1. **Porel**, **S.**; Singh, S.; Harsha, S. S.; Rao, D. N.; Radhakrishnan, T. P. *Chem. Mater.* (Communication) **2005**, *17*, 9.
Nanoparticle-Embedded Polymer: *In situ* Synthesis, Free-standing Films with Highly Monodisperse Silver Nanoparticles and Optical Limiting.

2. **Porel**, **S.**; Singh, S.; Radhakrishnan, T. P. *Chem. Commun.* **2005**, 2387.
Polygonal Gold Nanoplates in a Polymer Matrix.

3. Anthony, S. P.; **Porel**, **S.**; Rao, D. N.; Radhakrishnan, T. P. *Pramana* **2005**, *65*, 871.
Thin Films of Metal-Organic Compounds and Metal Nanoparticle-Embedded Polymers for Nonlinear Optical Applications.

4. **Porel**, **S.**; Venkatram, N.; Rao, D. N.; Radhakrishnan, T. P. *J. Nanosci. Nanotechnol.* **2007**, *7*, 1887.
In situ Synthesis of Metal Nanoparticles in Polymer Matrix and Their Optical Limiting Application.

5. **Porel**, **S.**; Hebalkar, N.; Sreedhar, B.; Radhakrishnan, T. P. *Adv. Funct. Mater.* **2007** (*In press*).
Palladium Nanowire from Precursor Nanowire : Crystal-to-crystal Transformation via *In situ* Reduction by Polymer Matrix.

6. **Porel**, **S.**; Venkatram, N.; Rao, D. N.; Radhakrishnan, T. P. *J. Appl. Phys.* **2007** (*Accepted*).
Optical Power Limiting in the Femtosecond Regime by Silver Nanoparticle-Embedded Polymer Film.

---

i. Publication 1 above was the **5th most-accessed** publication in *Chemistry of Materials* during the year **2005** and highlighted in
(a) Trohalaki, S. *MRS Bulletin*, **2005**, *30*, 77. (www.mrs.org/publication/bulletin)
(b) Dellow, N. *High Performance Plastics*, May **2005**, 12. (www.performance-materials.net)

ii. **Porel**, **S.**; Ramakrishna, D.; Dutta Gupta A.; Radhakrishnan, T. P.
(Indian patent application under process)
Reusable Silver Nanoparticle-Embedded Polymer Film for Antibacterial Applications.

PRESENTATIONS

1. **Porel**, **S.**; Harsha, S. S.; Kiran, P. P.; Radhakrishnan, T. P.; Rao, D. N.
Photonics-2004 (7th International Conference on Optoelectronics, Fiber Optics & Photonics), Cochin, India, 9-11 December 2004.
Optical Limiting Properties of Silver Nanoparticles-Embedded Polymer Films.

2. **Porel**, **S.**; Radhakrishnan, T. P.
ICONSAT-2006 (International Conference on Nanoscience & Technology), New Delhi, India, 16-18 March 2006.
In situ Synthesis of Metal Nanoparticles in Polymer Matrices and Optical Limiting applications
(Received "*Outstanding Poster Award*")

3. **Porel**, **S.**
Dr. K. V. Rao 6th Annual Research Award, Hyderabad, April 2006.
Metal Nanoparticle-Embedded Polymer Films: Fabrication and Applications.
(Received "*Winner trophy*")

4. **Porel**, **S.**; Venkatram, N.; Rao, D. N.; Radhakrishnan, T. P.
Photonics-2006 (8th International Conference on Optoelectronics, Fiber Optics & Photonics), Hyderabad, India, 13-16 December, 2006.
Optical Limiting Properties of Metal Nanoparticle-Embedded Polymer Thin Films.
(Received "*Best Poster Award*")

5. **Porel**, **S.**
National Review and Coordination Meeting on Nanoscience and Nanotechnology, Hyderabad, 21- 23 February, 2007.
In situ Synthesis of Silver Nanoparticles/Gold Nanoplates/Palladium Nanowires in Polymer Matrix and Application in Optical Power Limiting.